Optimal trajectory designs and systems engineering analyses
of reusable launch vehicles

by

Hung-i Bruce Tsai

A dissertation submitted to the graduate faculty

in partial fulfillment of the requirements for the degree of

DOCTOR OF PHILOSOPHY

Major: Aerospace Engineering

Program of Study Committee:
Ping Lu, Major Professor
Julie A. Dickerson
James H. Oliver
Darryl J. Trulin
Jerald M. Vogel

Iowa State University

Ames, Iowa

2003

UMI Number: 3118261

INFORMATION TO USERS

The quality of this reproduction is dependent upon the quality of the copy submitted. Broken or indistinct print, colored or poor quality illustrations and photographs, print bleed-through, substandard margins, and improper alignment can adversely affect reproduction.

In the unlikely event that the author did not send a complete manuscript and there are missing pages, these will be noted. Also, if unauthorized copyright material had to be removed, a note will indicate the deletion.

UMI®

Graduate College
Iowa State University

This is to certify that the doctoral dissertation of

Hung-i Bruce Tsai

has met the dissertation requirements of Iowa State University

Committee Member

Committee Member

Committee Member

Committee Member

Major Professor

For the Major Program

To the men and women who faithfully departed on February 1, 2003

aboard the ill-fated Space Shuttle Columbia (STS-107),

your courage and gallantry have brought

"us closer to our home in space."
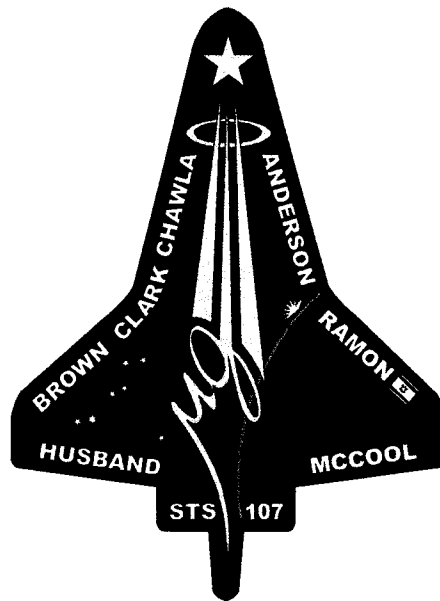
We will never forget who we work for!

TABLE OF CONTENTS

LIST OF FIGURES

LIST OF TABLES

NOMENCLATURE

Most of the fundamental ideas of science are essentially simple,
and may, as a rule, be expressed in a [mathematical] language
comprehensible to everyone.

— Dr. Albert Einstein [1]

ALL variables with subscript "i" denote the initial value of that variable whereas "f" denotes the final value. Every variable with subscript "u" denotes the upper bound value of that variable while "ℓ" denotes the lower bound value. All variables with superscript * denote terminal value or optimal value. All bold faced variables refer to vectors and non bold faced are scalars. "Standard" aerospace and optimal control notations will be used whenever possible. Some notations have deviated from the standard notations in order to avoid repeating the same notation for two different variables.

Lower Case

$\mathbf{1}_b = \mathbf{1}_x$	unit vector defining the vehicle body longitudinal axis
$\mathbf{1}_h$	unit vector defining the direction normal to the plane of r_f and $\mathbf{1}_{HAC}$
$\mathbf{1}_n = -\mathbf{1}_z$	unit vector defining the vehicle body normal axis

$\mathbf{1}_y$	unit vector defining the vehicle body axial axis
$\mathbf{1}_z$	unit vector completes right hand system $(\mathbf{1}_x \times \mathbf{1}_y)$
$\mathbf{1}_{\text{HAC}}$	unit vector defining the heading alignment direction
$\alpha,\ \dot{\alpha},\ \ddot{\alpha}$	angle-of-attack angle (deg), rate (deg/s), acceleration (deg/s^2)
β	side-slip-angle (deg)
η	engine throttle setting (%)
δ	perturbation size
ϵ	error in the gradient of the Lagrangian
γ	flight-path-angle (deg)
κ	scalar step length
λ	multiplier
ω	rotation rate of the Earth (deg/sec)
$\boldsymbol{\omega}_E$	rotation rate of the Earth in $X_I Y_I Z_I$ (deg/sec)
$\phi,\ \dot{\phi}$	roll angle (deg), rate (deg/s)
$\psi,\ \dot{\psi}$	yaw angle (deg), rate (deg/s)
ρ	atmospheric density (kg/m^3)
$\sigma,\ \dot{\sigma},\ \ddot{\sigma}$	bank angle (deg), rate (deg/s), acceleration (deg/s^2)
τ_s	time segment in trapezoidal discretization
$\theta,\ \dot{\theta}$	pitch angle (deg), rate (deg/s)

$\boldsymbol{v}$	trapezoidal discretization NLP variables
φ_k	step size
ϱ_1, ϱ_2	actual and predicted reduction
a_a	axial acceleration limit (g)
b	scale height
$\boldsymbol{c}$	NLP constraints
f_k	right hand side of differential equations
g_o	gravitational constant $\left(g_o = 9.806 \text{ m/s}^2\right)$
$\boldsymbol{g}$	gravitational acceleration vector $\left(\text{m/s}^2\right)$
i	orbit inclination (deg)
$m(t)$	mass of the vehicle at the current time (kg)
n_a	normal acceleration limit (g)
n	proportional constant to the atmospheric density
$\boldsymbol{o}$	unit vector in the direction of perturbation
q	dynamic pressure $\left(\text{N/m}^2\right)$
$\boldsymbol{r}$	position vector in guidance frame (km)
r	altitude measured from Earth surface (km)
$\hat{\boldsymbol{r}}$	position vector in inertial frame (km)
r_c	altitude measured from center of Earth to spacecraft (km)

r_{HAC}	range-to-HAC (km)
r_{togo}	range-to-go (km)
s	slack variable
x	state vector
u	control vector

Upper Case

$\mathcal{G}$	gradient vector
$\mathcal{H}$	Hessian matrix
$\mathcal{I}$	initial conditions
$\mathcal{J}$	Jacobian matrix
$\mathcal{L}$	Lagrange problem, $J = \int\limits_0^{t_f} \mathcal{L}\left(x, u, t\right) dt$
$\mathcal{M}$	Mayer problem, $J = \mathcal{M}\left[x\left(t_f\right)\right]$
$\mathcal{O}$	merit function
$\mathcal{P}$	path constraint
$\mathcal{T}$	terminal condition
χ	step length
Δ	perturbation direction
ΔT	thrust loss inside the atmosphere due to back pressure (Newton)

Ω	argument of ascending node (deg)
Θ	longitude (deg)
Φ, Φ_c	geodetic latitude, geocentric latitude (deg)
Ψ	velocity azimuth angle (deg)
Ψ_{LOS}	velocity azimuth angle from line-of-sight (deg)
$\boldsymbol{A}$	aerodynamic forces in the body axial direction (g)
A_z	launch azimuth angle (deg)
C_A, C_N	axial/normal aerodynamic coefficient (dimensionless)
C_ℓ, C_d	lift/drag coefficient (dimensionless)
D	drag acceleration (g)
I_{SP}	specific impulse of the engine (sec)
J	performance index in optimization
L	lift acceleration (g)
$\boldsymbol{N}$	aerodynamic forces in the body normal direction (g)
$\dot{Q}$	heat rate (W/m^2)
R_0	radius of Earth (m)
S_{ref}	vehicle reference area (m^2)
T	current thrust magnitude (Newton)
$\boldsymbol{T}_{EP}$	coordinate transformation matrix

T_{vac}	full vacuum thrust magnitude (Newton)
U	nondimensional velocity
V	inertial velocity (m/s)
V_r	relative velocity (m/s)
$\boldsymbol{V}_r$	magnitude of the Earth-relative velocity vector (m/s)
$\boldsymbol{V}_w$	wind velocity (m/s)
$X_B Y_B Z_B$	body coordinate system
$X_I Y_I Z_I$	initial launch plumbline coordinate system
$X_G Y_G Z_G$	guidance coordinate system
$\boldsymbol{Y}$	first derivative

Acronyms

A/L	approach and landing
AB	Air Base
ABS	absolute
AerE	Aerospace Engineering (Department of)
AFB	Air Force Base
AIAA	American Institute of Aeronautics and Astronautics
AOA	abort-once-around

ARC	Ames Research Center, Moffett Field, California
ARF	Assembly and Refurbishment Facility
ARMOR	adaptable, robust, metallic, operable, reusable
ASEE	American Society for Engineering Education
ASME	American Society of Mechanical Engineers
ATD	advanced technology demonstrator
ATO	abort-to-orbit
BC	burn-coast
BCB	burn-coast-burn
BIT	built in test
BITE	built in test equipment
C/C	carbon/carbon
CALS	continuous acquisition and life-cycle support
CBF	cheaper, better and faster
CCB	configuration control board
CDR	critical design review
CI	configuration item
CL	closed-loop
CM	configuration management

CML	configuration management librarian
CR/DR	crossrange / downrange
CSA	configuration status accounting
CST	central standard time
CVA	configuration verification audit
DBTC	design, build, test and commercialize
DFRC	Dryden Flight Research Center, Edwards, California
DI	data item
DLR	Deutsches Zentrum für Luft- und Raumfahrt
DoD	Department of Defense
DOF	degree-of-freedom
DOT	Department of Transportation
DR	downrange
ECEF	Earth-centered Earth-fixed
ECI	Earth-centered inertial
ECP	engineering change proposal
ECprE	Electrical and Computer Engineering (Department of)
EDI	electronic data interchange
EG	entry guidance

EGC	equilibrium glide condition
EI	entry interface
ELV	expendable launch vehicle
EOM	end of mission
EOM	equation of motion
ET	external tank
EQ	equality
FAA	Federal Aviation and Administration
FBD	functional block diagram
FMECA	failure mode, effects, and criticality analysis
FSSR	functional subsystem software requirement
FTA	fault-tree analysis
FTP	file transfer protocol
G&C	guidance and control
G&N	guidance and navigation
GIF	graphics interchange format
GLOW	gross lift-off weight
GPMC	Governing Program/Project Management Council
GRC	Glenn Research Center, Cleveland, Ohio

GN&C	guidance navigation and guidance
H/W	hardware
HAC	heading alignment circle or heading alignment cone
HCF	high cycle fatigue
HL	horizontal landing
HMF	Hypergolic Maintenance Facility
HP	Hewlett-Packard
HSF	human space flight
HTML	hypertext markup language
IAF	International Aeronautical Federation
IBM	International Business Machine
IEEE	Institute of Electrical and Electronics Engineers
IFB	invitation for bid
IMSE	Industrial, Manufacturing and Systems Engineering (Dept. of)
INEQ	inequality
ISS	International Space Station
ISU	Iowa State University
IVHM	integrated vehicle health management
JPEG/JPG	joint photographic experts group

JPL	Jet Propulsion Laboratory, Pasadena, California
JSC	Johnson Space Center, Houston, Texas
KKT	Karush-Kuhn-Tucker
KSC	Kennedy Space Center, Cape Canaveral, Florida
L/G	landing gear
LaRC	Langley Research Center, Hampton, Virginia
LAI	Lean Aerospace Initiative
LARE	linear aerospike rocket engine
LCC	life-cycle cost
LCF	low cycle fatigue
LEO	low Earth orbit
LFD	logic flow diagram
LH_2	liquid hydrogen
LOV	loss of vehicle
LOX	liquid oxygen
LP	linear programming
LQR	linear quadratic regulator
MAVERIC	Marshall Aerospace Vehicle Representation in C
MCC	Mission Control Center

ME	Mechanical Engineering (Dept. of)
MEA-LR	Mathematics and Engineering Analysis, Library Report
MECO	main-engine-cut-off
MGMT	management
MIL-HDBK	military handbook
MIL-STD	military standard
MIPS	millions of instructions per second
MIT	Massachusetts Institute of Technology
MLP	mobile launch platform (also known as the crawler)
MM	major mode
MPG/MPEG	motion picture experts group
MPG	Marshall procedures and guidelines
MRc	mission reliability
MTBF	mean time between failure
MTBM	mean time between maintenance
MWI	Marshall work instruction
N/A	not applicable or not available
NASA	National Aeronautics and Space Administration
NASA/CR	NASA contractor report

NASA/TM	NASA technical memorandum
NASA/TP	NASA technical publication
NATO	North Atlantic Treaty Organization
NEP	nominal entry point or nominal entry profile
NGLT	Next Generation Launch Technology
NLP	nonlinear programming
NPG	NASA procedure & guideline
NRA	NASA Research Announcement
NSTP	National Space Transportation Policy
NSTS	National Space Transportation System
NTDI	non-developmental test item
OCP	optimal control problem
OL	open loop
OMDP	orbiter maintenance down period
OMM	orbiter major modifications
OMS	orbital maneuvering system
OPF	Orbiter Processing Facility
OPS	operations
PBVP	point boundary value problem

PC	personal computer
PCA	propulsion controlled aircraft
PDF	portable document file
PDR	preliminary design review
PI	performance index
PI	principal investigator
PL	payload
PM	project manager
PPA	powered pitch-around
PPD	powered pitch-down
PRA	probabilistic risk assessment
PRR	project requirements review
PWBS	program work breakdown structure
QP	quadratic programming
QR	quarterly review
QRAS	quantitative risk assessment system
RCS	reaction control system
RFP	request for proposal
RK4	Runge-Kutta 4th order polynomial curve fit

RLV	reusable launch vehicle
RPSF	Rotation, Processing, and Surge Facility
RSRM	reusable solid rocket motor
RTLS	return-to-launch-site
SAE	Society of Automotive Engineers
SCA	shuttle carrier aircraft
SE	system engineering
SEMP	system engineering management plan
SGI	Silicon Graphic Inc.
SIAM	Society for Industrial & Applied Mathematics
SiC	silicone carbide
SL	sea level
SLF	Shuttle Landing Facility
SLI	Space Launch Initiative
SMART	Simulation & Modeling for Acquisition, Requirements, & Training
SOCS	Sparse Optimization Control Software
SOL	solicitation
SQP	sequential quadratic programming
SRB	solid rocket booster

SRM	solid rocket motor
SSME	Space Shuttle main engine
SSTO	single-stage-to-orbit
SSV	Space Shuttle vehicle
STA	shuttle training aircraft
STS	Space Transportation System
TA	technology area
TAEM	terminal area energy management
TAL	transoceanic-abort-landing
TEPP	test and evaluation program plan
TIF/TIFF	tagged image file format
TIG	time of ignition
TM	trademark
TOC	theory of constraint
TPM	technical performance measure
TPS	thermal protection system
TRL	technology readiness level
TSTO	two-stage-to-orbit
TVC	thrust vector control

US	United States
USA	United Space Alliance, Houston, Texas
USA	United States of America
USAF	United States Air Force
USL	Universal Space Lines, Newport, California
V&V	verification and validation
VAB	Vehicle Assembly Building
WBS	work breakdown structure
WT	weight

Unit Symbols

BTU	British thermal unit
ft	foot
J	Joules $(N \cdot m)$
kg	kilogram
km	kilometer
km/hr	kilometer per hour
lbf	pound force
lbm	pound mass

M   mega $(\times 10^6)$

m   meter

m/s   meter per second

mph   miles per hour

N   Newton $\left(\text{kg} \cdot \text{m/s}^2\right)$

nm   nautical miles (1 nm = 1.1508 miles)

Pa   Pascal $\left(\text{N/m}^2\right)$

psf   pound per square foot $\left(\text{lbf/ft}^2\right)$

sec   second

Conversion Factors

1 BTU/ft$^2\cdot$ sec   11,349 Watt/m^2 $\left(\text{N} \cdot \frac{\text{m}}{\text{s}} / \text{m}^2\right)$

1 deg (on map) $\approx$ 111 km or 60 nm

1 ft   0.3048 m

1 ft^2 0.0929 m^2

1 ft/s   0.3048 m/s

1 lbf   4.4482 N

1 lbm   0.4536 kg

1 Mach   331 m/s, 1,193 km/hr, 1,087 ft/s, or 741 mph (all at SL)

1 nm	1.852 km
1 psf	47.8803 N/m^2 (Pa)
1 rad	57.2958 deg

1

ACKNOWLEDGEMENT

Being a graduate student is like becoming all of the Seven Dwarves.
In the beginning you're Dopey and Bashful.
In the middle, you are usually sick (Sneezy), tired (Sleepy), and irritable (Grumpy).
But at the end, they call you Doc, and then you're Happy.

— Dr. Ronald T. Azuma [2]

END of the tunnel at last! First and foremost, I would like to express my sincere gratitude to my major professor Dr. Ping Lu for all of his help, guidance and support during the undertaking of this research. He has introduced me to a most interesting and leading edge technology research field in the area of optimal trajectory analysis applied to the next generation reusable launch vehicles. His enthusiasm, encouragement, inspiration and challenges have made this project an enjoyable and valuable experience. I would also like to thank Drs. Julie A. Dickerson (ECprE), Douglas D. Gemmill (IMSE), James H. Oliver (ME), Darryl J. Trulin (AerE) and Jerald M. Vogel (AerE) for their invaluable interdisciplinary contributions and serving as members on my program of study committee.

Many thanks to my research teammates Hongsheng Sun and Dr. Zuojun Shen for the discussions on ascent and entry trajectories. Special acknowledgement to the Department of Aerospace Engineering for the wonderful and valuable teaching experience and financial support.

I have greatly enjoyed my time at Iowa State, due in no small part to the many fantastic people that I have met over the years. They have made my stay at Iowa State a mesmerizing experience. I count myself fortunate that there is not enough room here to mention them all because the complete list may exceed the length of this dissertation. Thank you all for helping me achieving this milestone!!! You know who you are! Because of you, I have became more than just a "GN&C engineer" (gone nuts and crazy engi*nerd*) who just got a "PhD" (permanent head damage), but also a better artist, athlete, aviator, chef, comedian, musician and person.

Finally, I would like to thank my family, especially my parents, for all their unwavering support in my endeavors, even if they never quite worked out what my research is about.

Thank You!

謝謝, *obrigado, danke, gracias, merci* !

H. Bruce Tsai
Veni, vidi, vici on August 20, 2003

ABSTRACT

Every great advance in science has issued from
a new audacity... of imagination.

— John Dewey [3]

REALIZING a reusable launch vehicle (RLV) that is low cost with highly effective launch capability has become the "Holy Grail" within the aerospace community world-wide. Clear understanding of the vehicle's operational limitations and flight characteristics in all phases of the flight are preponderant components in developing such a launch system. This dissertation focuses on characterizing and designing the RLV optimal trajectories in order to aid in strategic decision making during mission planning in four areas: ① nominal ascent phase, ② abort scenarios and trajectories during ascent phase including abort-to-orbit (ATO), transoceanic-abort-landing (TAL) and return-to-launch-site (RTLS), ③ entry phase (including footprint), and ④ systems engineering aspects of such flight trajectory design. The vehicle chosen for this study is the Lockheed Martin X-33 lifting-body design that lifts off vertically with two linear aerospike rocket engines and lands horizontally. An in-depth investigation of the optimal endo-atmospheric ascent guidance parameters such as earliest abort time, engine throttle setting, number of flight phases, flight characteristics and structural design limitations will be performed and analyzed to establish a set of benchmarks for making better trade-off decisions. Parametric analysis of the entry guidance will also be inves-

tigated to allow the trajectory designer to pinpoint relevant parameters and to generate optimal constrained trajectories. Optimal ascent and entry trajectories will be generated using a direct transcription method to cast the optimal control problem as a nonlinear programming problem. The solution to the sparse nonlinear programming problem is then solved using sequential quadratic programming. Finally, guidance system hierarchy studies such as work breakdown structure, functional analysis, fault-tree analysis, and configuration management will be developed to ensure that the guidance system meets the definition of vehicle design requirements and constraints.

CHAPTER 1   INTRODUCTION

The United States Government is committed to encouraging a viable commercial U.S. space transportation industry.

The United States space program is critical to achieving U.S. national security, scientific, technical, commercial, and foreign policy goals.

The Department of Defense (DoD) will be the lead agency for improvement and evolution of the current U.S. expendable launch vehicle (ELV) fleet, including appropriate technology development.

The National Aeronautics and Space Administration (NASA) will provide for the improvement of the Space Shuttle system, focusing on reliability, safety, and cost-effectiveness.

> US National Space Transportation Policy [4]
> August 5, 1994

ONCE John Glenn first manned an orbital mission in Mercury-Atlas 6 and Neil Armstrong first stepped on the Moon in Apollo 11, humankind has been fascinated with the endless prospects of space exploration. These possibilities range from as simple as exploring the unknown, to military operations, to commercial applications. Although the current systems meet the needs of the US space program, the systems lack affordability, reliability, responsiveness, operability and safety. The current launch price tag is approximately $470 million dollars with a payload capacity of 26,786 kg

(59,053 lb) [5, 6]. Table 1.1 shows the typical expendable and reusable launch vehicles performance data in terms of gross lift-off weight (GLOW), vehicle dry weight (DRY WT), low Earth orbit payload (LEO PL), mission reliability (MRc) and launch operations cost per payload weight ($/PL).

Table 1.1   Expendable vs reusable launch vehicle performance data [5–9]

	GLOW (ton)	DRY WT (ton)	LEO PL (ton)	MRc (%)	$/PL kg
Expendable					
Pegasus	19.05	1.72	0.36	50.0	$6,804
Delta II	229.52	19.05	4.98	97.0	$1,860
Atlas III	187.34	10.89	6.75	100.0	$2,436
LM-3	201.85	15.42	4.99	92.0	$1,651
Ariane IV	471.74	26.76	9.53	87.5	$2,483
Zenit	459.04	45.81	13.74	92.3	$1,123
Titan III	680.40	50.35	14.52	93.0	$2,127
Titan IV	861.84	51.26	17.69	93.0	$2,502
Ariane V	712.15	51.26	18.01	N/A	$1,200
Proton	703.08	52.16	19.96	87.7	$826
Reusable					
Energia	2,404.08	127.01	87.99	N/A	N/A
Space Shuttle	2,041.20	282.59	26.79	97.4	$4,545
Proposed RLV					
X-33[‡]	129.25	34.01	N/A	N/A	N/A
VentureStar[TM‡]	1,168.00	117.00	22.68	N/A	$454

A more affordable "highway to space" is highly desired to compete in the world-wide space launch market. NASA has issued a report entitled "Access to Space Study" [10] in 1990 recommending directions for future space transportation development, especially focusing on improving reliability, safety and operational cost (please refer to Appendix A starting on page 266 for more detail). Upon the completion of the study, a fully reusable

---

[‡] These are the initial X-33/VentureStar[TM] prototype specifications. Some of these values have changed as the program progressed.

VentureStar is a trademark of Lockheed Martin Corporation.

launch vehicle (RLV) was determined to be a feasible solution that can achieve all the above mentioned improvements [11–20]. To summarize, the development of the RLV is to [21–23]:

☆ balance efforts to modernize existing space transportation capabilities and invest in the development of improved future capabilities

☆ maintain a strong transportation capability and technology base

☆ reduce the cost of current space transportation systems, while improving reliability, operability, responsiveness, and safety

☆ foster technology development and demonstration to support future decisions on the development of the next-generation RLV

☆ encourage, to the fullest extent feasible, the cost-effective use of commercially provided U.S. products and services

☆ foster the international competitiveness of the U.S. commercial space transportation industry, actively considering commercial needs and factoring them into decisions on improvements to launch facilities and vehicles

1.1   Reusable Launch Vehicle Project Goals and Requirements

In the effort to study possible designs for the next generation of launch vehicles, several goals and expectations were given by DoD and NASA. The top five goals stated in the National Space Transportation Policy (NSTP) are [22–27]:

① Affordability: reduced space transportation operational (recurring) cost for both the existing and replacement system

② Reliability: improved dependability/reliability of existing and replacement system and also improves availability

③ Responsiveness: improved supportability, maintainability and launch on demand availability

④ Operability: improved operability-simplicity

⑤ Safety: improved vehicle and personnel safety

Specific technology objectives expected to be achieved for the RLV space vehicle include [26–28]:

☆ demonstrate a reusable cryogenic tank system, including the tanks for liquid hydrogen (LH_2) and liquid oxygen (LOX), cryogenic insulation, and an integrated thermal protection system (TPS)

☆ verify TPS durability, low maintenance, and performance at both low and high temperatures

☞ **demonstrate guidance, navigation, and control systems, including autonomous flight control of checkout, takeoff, ascent, flight, reentry, and landing for an autonomously controlled space vehicle**

☆ achieve hypersonic flight speeds (speeds up to Mach 15 or 18,000 km/hr (11,000 mph))

☆ demonstrate composite primary space vehicle structures integrated with TPS

☆ demonstrate ability to perform 7-day turnarounds between
   three consecutive flights

☆ demonstrate ability to perform a 2-day turnaround between
   two consecutive flights

☆ demonstrate that a maximum of 50 personnel performing hands-
   on vehicle operations, maintenance, and refueling can success-
   fully accomplish flight readiness for two flights

1.2   Proposed Reusable Launch Vehicle Designs

With the project goals and requirements defined by DoD and NASA, three compa-
nies took the challenge in participating the concept definition and design (Phase I) of the
next generation reusable launch vehicle. They were Rockwell International[1] Space Trans-
portation Systems Division in Downey, California, McDonnell Douglas[2] Space Defense
Systems Division in Huntington Beach, California, and Lockheed Martin Skunk Works
in Palmdale, California. Upon completion of the concept definition and design phase,
these three companies also submitted the Phase II proposals to NASA on May 13, 1996
to compete for the technology demonstration of the X-33 [29].

On July 2, 1996, Vice President Al Gore and NASA Administrator Daniel S. Goldin
unveiled the winning design at a Jet Propulsion Laboratory (JPL) press conference in
Pasadena, California. Vice President Al Gore announced that Lockheed Martin has been
selected as the linchpin of NASA's RLV program. Lockheed was awarded US$941 million
to build the X-33 test vehicle and to demonstrate the technology necessary to produce
an operational RLV [32, 33].

---

[1] North American Rockwell became part of Rockwell International on February 15, 1973, and the
Space and Defense divisions of Rockwell International was acquired by Boeing on December 5, 1996.
Rockwell International is now known as Rockwell Collins [30].

[2] McDonnell Douglas merged with Boeing on August 1, 1997 [31].

The Lockheed Martin Skunk Works concept for the X-33 (shown in Figure 1.1) advanced technology demonstrator (ATD) vehicle is based on the lifting body shape with two ground-breaking linear aerospike rocket engines (LAREs). The vehicle takes off vertically like rockets and lands horizontally like airplanes. The lifting body (no wing) shape was chosen because it derives the lift solely from the shape of the body and has the unique advantage of volumetric efficiency. The lifting body shape also provides better aerodynamic efficiency at high angles of attack and hypersonic speeds while maintaining lower re-entry temperatures and landing speeds. Other lifting body experimental vehicles studied by NASA in the 1960s and 1970s include Martin Marietta X-24A, Northrop HL-10, and Northrop M2-F2 [33, 34].

Figure 1.1 Artist rendition of Lockheed Martin X-33 RLV
concept, courtesy NASA [35]

1.3 X-33 Characteristics

The vehicle model used for this research is the Lockheed Martin X-33 prototype vehicle (one-half scale model of the full size VentureStar™). The X-33 configuration and dimensions are illustrated in Figure 1.2 and other specifications are itemized in Table 1.2. X-33 is a futuristic triangular shaped spacecraft that derives its lift solely from the shape of its body. It has two vertical rudders found in most modern fighter aircraft for yaw motion. It also has two body flaps similar to those flaps found on conventional aircraft wings for pitch maneuver and to create additional lift or drag. There are two elevons (a combination of elevators and ailerons found in most aircraft as shown in Figure 1.3) used for pitch and roll control to maintain a controlled flight. Finally, X-33 is powered by two linear aerospike rocket engines (LAREs) with thrust vector control (TVC) capability. Refer to Appendix B starting on page 274 for more information about LARE and its specifications [33, 36].
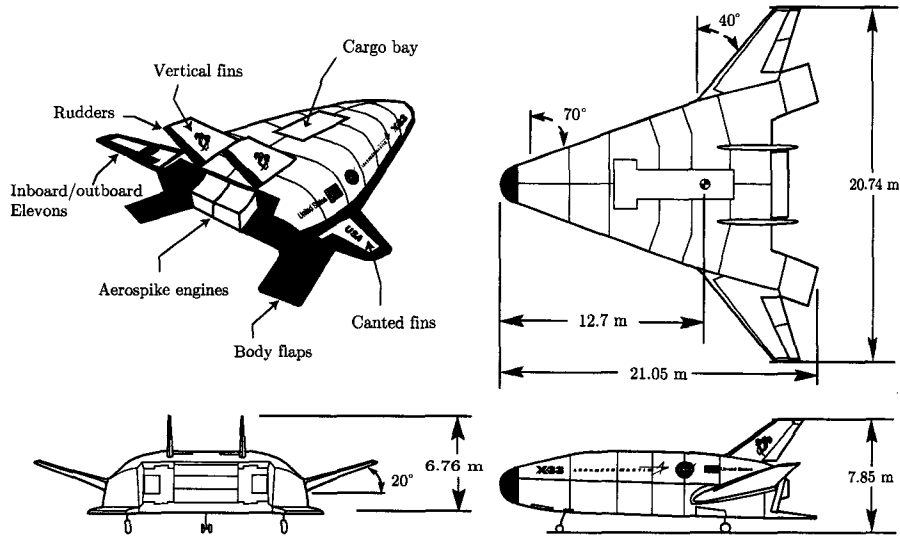
Figure 1.2   Lockheed Martin X-33 prototype geometry and configuration[‡], adapted from Ref. [36]
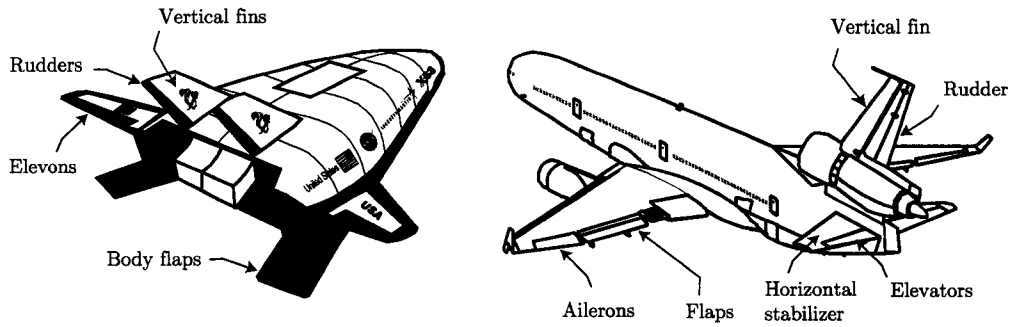
Figure 1.3   Flight control surfaces of X-33 and of a conventional aircraft.   Notice X-33 has a special control surface called the "elevons"

Table 1.2   Lockheed Martin X-33 prototype specifications[‡] [36, 37]

Dimensions		
Length:	21.05 m	69 ft
Wingspan:	20.74 m	68 ft
Height:	6.76 m	22.17 ft
Wing Area:	198 m^2	2,125 ft^2
Weight		
Empty:	28,440 kg	62,700 lb
Total Fuel:	95,255 kg	210,000 lb
Max Take-off:	124,000 kg	273,300 lb
Propulsion		
Engines:	2 XRS-2200	
Total Thrust:	1,832 kN (SL)	410,000 lb
	2,384 kN (vacuum)	536,000 lb
Performance		
Max Speed:	17,690 km/hr	11,000 mph
Service Ceiling:	76,270 m	250,000 ft
Range:	1,530 km	825 nm

[‡] These are the initial X-33 prototype specifications. Some of these values have changed since the program started.

1.4 Current Status of RLV Development

Even though NASA announced the cancellation of the X-33 project on March 1, 2001, the technology resulting from this project will undoubtedly serve as the corner-stone for the development of future reusable launch vehicles. This includes the three two-stage-to-orbit (TSTO) configurations by Boeing, Lockheed Martin and Northrop Grumman that NASA is currently studying under the Space Launch Initiative (SLI), more specifically the Next Generation Launch Technology (NGLT) program. A typical TSTO configuration consists of a booster and an orbiter as portrayed in Figure 1.4. The booster flies back and lands on a runway after burn out and jettison from the orbiter, thus making it fully reusable [38–41].

orbiter
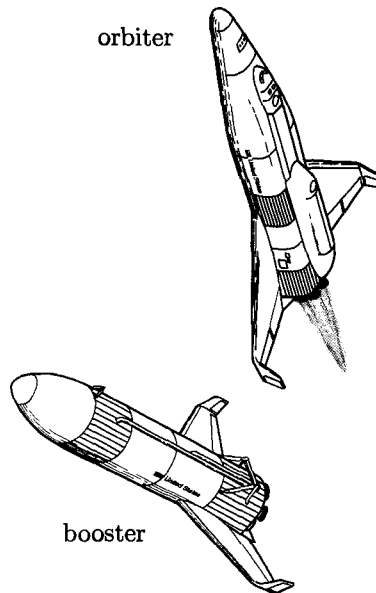
booster

Figure 1.4 Generic bimese TSTO RLV configuration with booster fly-back capability, adapted from Ref. [42]

Furthermore, since Lockheed Martin was announced as the primary contractor of the X-33 competition on July 2, 1996, the development of a "cheaper, better and faster (CBF)" RLV has become the modern "Holy Grail" within the aerospace community. These phenomena can be seen in the many highly publicized RLV activities currently under development. The X-Prize competition is one example of this world-wide endeavor to design, build, test and commercialize (DBTC) a CBF RLV system. There are currently 19 companies from five countries seeking to win the US $10 million dollar prize for building a privately funded vehicle to fly three people into space, return and repeat within two weeks. In addition to the X-Prize, other designs such as Kistler's SSTO Rotary's Roton (USA), Pioneer's TSTO Pathfinder (USA), Vela Technology's TSTO Space Cruiser (USA), Kelly's TSTO Eclipse Astroliner (USA), DLR's TSTO Astra (Germany), Daimler Benz Aerospace's TSTO Sänger (Germany), Japan's HOPE-X and several European Space Agency's SSTO/TSTO systems are also participating in this venture [43–47].

1.5 Proposed Doctoral Study

According to the Department of Transportation Federal Aviation Administration (DOT FAA) report [48], autonomous guidance and control technologies are recognized as critical to the long term goal of achieving reliable, safe, low-cost, aircraft-like operations into space. Guidance schemes such as open-loop [49], closed-loop [50], and hybrid [51] approachs are being explored in attempts to find the best suitable guidance system for the future RLV.

The passage to safe, reliable, and affordable access to space has been stymied by technical and business challenges. Comprehension of the vehicle's operational limitations and flight characteristics are preponderant components in developing such a launch system. The proposed research will focus on characterizing and understanding the RLV

optimal trajectories in order to aid in strategic decision making during mission planning in four areas:

① nominal ascent phase,

② abort scenarios and trajectories during ascent phase including abort-to-orbit (ATO), transoceanic-abort-landing (TAL) and return-to-launch-site (RTLS),

③ entry phase (including footprint), and

④ systems engineering aspects of such flight trajectory design.

The vehicle chosen for this study is the Lockheed Martin X-33 as described in Section 1.3. A thorough investigation of the X-33 optimal ascent flight characteristics such as earliest abort time, engine throttle setting, control angle profiles, structural design limitations will be performed and analyzed to establish a set of benchmarks for making better trade-off decisions. An in-depth parametric analyses of the entry flight characteristics such as bank reversal logic and sensitivity of the entry flight corridor will be investigated to allow the trajectory designer to pinpoint relevant parameters and to generate optimal constrained entry trajectories. Finally, guidance system hierarchy studies such as work breakdown structure, functional analysis, fault-tree analysis, and configuration management will be developed to ensure that the guidance system meets the definition of vehicle design requirements and constraints. A system engineering management plan will also make certain there is a proper procedure to report failures, document results and keep the project up to date.

1.6   Dissertation Overview

This dissertation is organized in 9 chapters and 5 supporting appendices.

☆ **Chapter 1   Introduction:** The introduction presents the background and motivation leading to the objectives and scope for this research.

☆ **Chapter 2   Mission Profile Synopsis:** A general overview of spacecraft mission profile from launch to re-entry.

☆ **Chapter 3   Numerical Optimization Method:** This chapter outlines the numerical technique used to generate these optimal trajectories.

☆ **Chapter 4   Optimal Ascent and Abort Trajectory Designs:** Formulation, results and discussions of nominal and different abort trajectories.

☆ **Chapter 5   Optimal Entry Trajectory Designs:** Formulation, results and discussions of different entry scenarios as well as footprint determination.

☆ **Chapter 6   Loh's Theory for Entry Trajectories:** Formulation, results and discussions of Loh's analytical results vs those obtained from numerical integration.

☆ **Chapter 7   System Engineering Management Plan:** This chapter focuses on the project management and system engineering development process for a methodical top-down approach to identify the areas of concentration for the flight mechanics team.

☆ **Chapter 8   Summaries and Conclusions:** Summarize the conclusions of the work presented in this dissertation.

☆ **Chapter 9   Recommendations for Future Work:** Discuss the prospects for the future development of some of the ideas presented.

CHAPTER 2 MISSION PROFILE SYNOPSIS

> *A scientist discovers that which exists.*
> *An engineer creates that which never was.*
>
> — *Dr. Theodore von Kármán* [52]

S TATE-OF-THE-ART components and systems are part of the next generation reusable launch vehicle (RLV) designs. One of the specific technology objectives expected to be achieved is to "demonstrate guidance, navigation, and control systems, including autonomous flight control of checkout, takeoff, ascent, flight, reentry, and landing for an autonomously controlled space vehicle." Familiarization with the spacecraft mission profile is a must in order to achieve such objective.

According to NASA [53–55], an RLV mission profile is composed of six main flight phases: *ascent, orbit insertion, orbit, deorbit, re-entry* and *abort.* The purpose of *ascent guidance* is to maneuver the vehicle to the intended orbit after the spacecraft has lifted off from the launch pad. In a nominal mission, the vehicle flies mostly at full power until the orbital insertion point (also referred to as the main-engine-cut-off, MECO). After MECO, *in-orbit guidance* will steer the spacecraft to the desired orbital operations location by using small reaction control systems (RCS) to provide attitude control of the spacecraft as well as any minor translation maneuvers along a given axis on orbit. The orbital maneuvering system (OMS) on the other hand is used for velocity change if necessary. Nominal mission flight phases are portrayed in Figure 2.1.
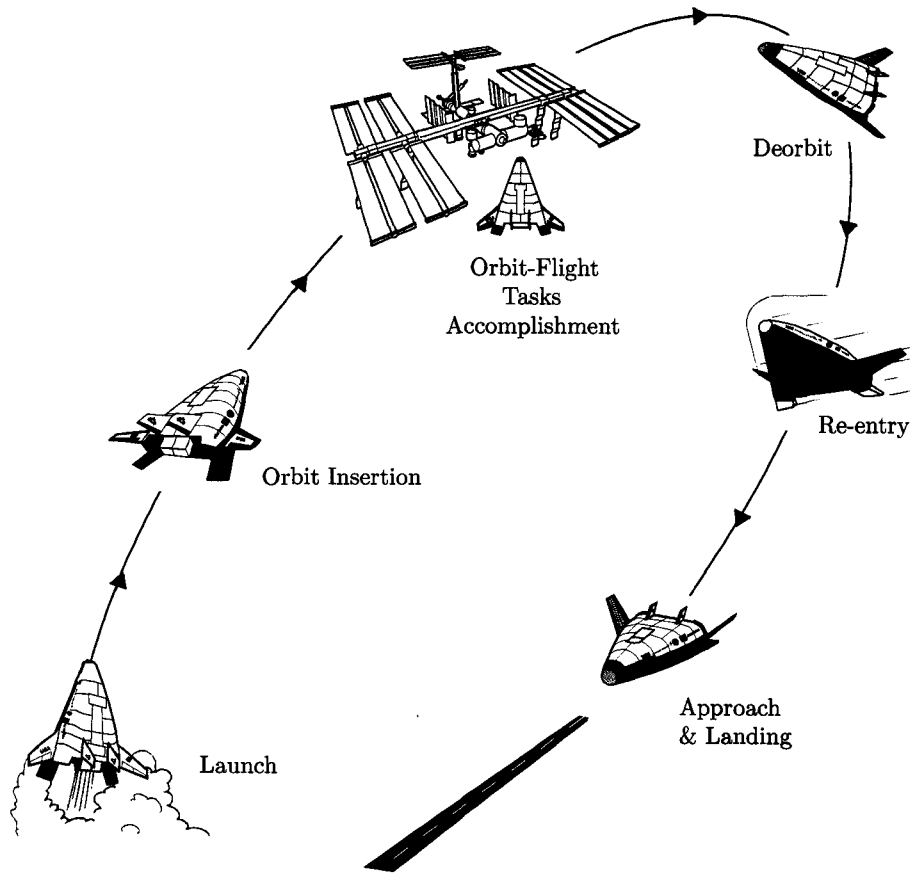
Figure 2.1   Nominal RLV flight phases from launch to landing

Upon completing orbital operations, *deorbit guidance* will orient the spacecraft in a tail first attitude by RCS, and OMS engines are commanded to slow the vehicle for deorbit. RCS then turns the vehicle's nose forward in preparation for re-entry. RCS is used for direction control (banking) until atmospheric density is sufficient for the aerodynamic control surfaces to become effective. This typically starts at altitudes of 75~80 km where atmospheric density becomes prominent.

During re-entry, *entry guidance* must dissipate the tremendous amount of vehicle energy when it enters the Earth's atmosphere to assure that the vehicle does not either burn up (entry angle too steep) or skip out of the atmosphere (entry angle too shallow). Entry trajectory must be inside of a very narrow "entry flight corridor." It must also ensure that the vehicle is properly positioned and aligned with the terminal area energy management (TAEM, pronounced "tame") point towards the end of entry trajectory. Entry guidance uses drag to control velocity (kinetic energy) in order to achieve the proper range requirement. This is accomplished by banking the vehicle to modulate the drag profile.

Finally upon TAEM point, *TAEM guidance* steers the vehicle to the heading alignment circle/cone (HAC) before commencing final approach and landing (A/L). More detail about TAEM will be discussed in Section 2.4.

2.1 Ascent Abort Modes

Ascent abort may be necessary if the vehicle performance is significantly affected by failures such as engine malfunction, mechanical defect or cabin depressurization. The timing and cause of the failure will determine which abort mode to choose. The abort mode chosen must be the safest or improves mission success with the remaining vehicle performance. If the failure is due to loss of vehicle performance (i.e., engine failure), then the order of preferable abort modes would be abort-to-orbit (ATO), abort-once-around (AOA), transoceanic-abort-landing (TAL), then return-to-launch-site (RTLS) as rendered in Figure 2.2. On the other hand, if the failure is due to the malfunctioning of support systems (i.e., cabin depressurization), then TAL or RTLS may be more desirable than ATO since getting the crew (if present) down will be the number one priority [56, 57].
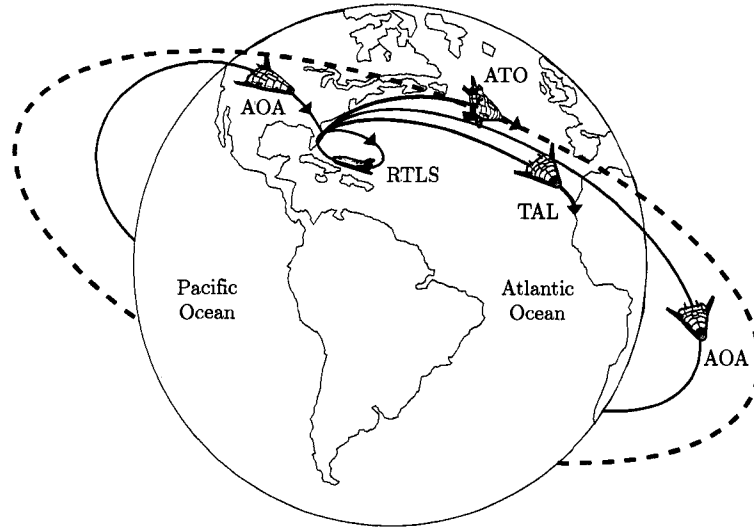
Figure 2.2   Possible intact abort scenarios during ascent phase

2.1.1   Abort-to-Orbit Mode

The abort-to-orbit, ATO, mode is designed to permit the vehicle to reach the desired orbit (or a lower orbit followed by an OMS maneuver to raise the orbit) and continue with the planned mission activities. ATO is the most favorable option because it resembles the nominal ascent trajectory. Furthermore, ATO does not require the abrupt maneuvers involved in other abort modes. This option is only commenced when the vehicle has gained proper altitude and velocity for orbital insertion. Otherwise, transoceanic-abort-landing or return-to-launch-site mode may be selected [57–59].

2.1.2   Transoceanic-Abort-Landing Mode

As its name suggests, the transoceanic-abort-landing (TAL) mode is an abort procedure where the vehicle continues to fly across the Atlantic Ocean and then will glide to a NASA approved TAL landing site in Africa or Europe. TAL is selected if failure occurs before the ATO option is available, and after the last opportunity for a safe

return-to-launch-site is possible. After TAL abort mode is selected by the flight computer (autocommander), the vehicle continues flying across the Atlantic Ocean to reach the proper altitude, velocity and heading alignment with the TAEM point at a selected TAL landing site before commencing MECO.

NASA approved TAL landing sites include Banjul International Airport (Banjul, Gambia), Ben Guerir Air Base (Ben Guerir, Morocco), Lajes Air Base (Açores, Portugal), Morón Air Base (Morón, Spain), and Zaragoza Air Base (Zaragoza, Spain) as limned in Figure 2.3. These sites are chosen in part as they are near the nominal ascent ground track (depending on the launch inclination), therefore allowing the optimum use of propellant and crossrange/downrange requirements. Furthermore, these TAL sites are equipped with orbiter-unique landing aids, and they are staffed with contractors, NASA and DoD personnel during launch [57–59].
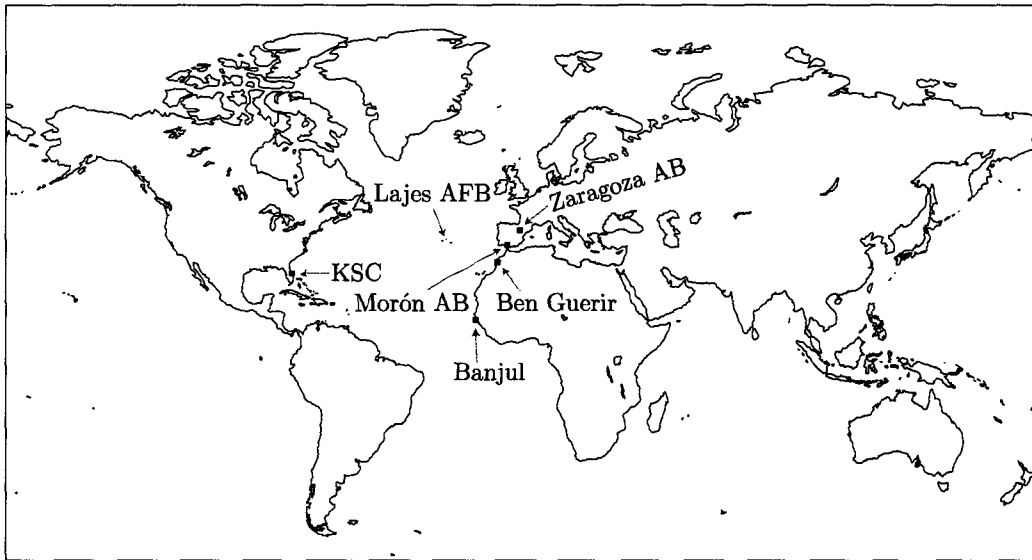
Figure 2.3   NASA approved TAL landing sites

2.1.3 Return-to-Launch-Site Mode

The return-to-launch-site, RTLS, abort mode is designed to allow the safe return of the launch vehicle, crew (if present), and payload back to the launch site, Kennedy Space Center (KSC).

RTLS is the least desirable abort mode since it is considered by the engineers to be the most difficult and dangerous maneuver because of the large abrupt turnings (especially the large pitch maneuver) required to turn the spacecraft around. However, until the vehicle has reached an appropriate altitude and velocity where it can make a TAL landing, this is the only intact abort option (intact abort allows the spacecraft to safely return to a planned site whereas contingency abort permits the survival of the crew, but not the spacecraft).

After RTLS abort mode is selected by the autocommander, the vehicle continues flying downrange to dissipate excess propellant (dumping fuel option may not be available), gain enough altitude and velocity as delineated in Figure 2.4 before the vehicle reverses its course and flies back to launch site.
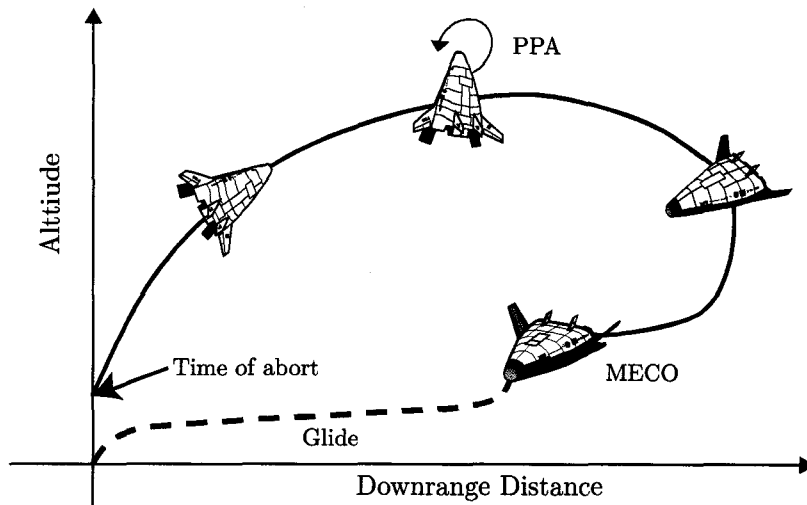
Figure 2.4 Typical RTLS profile from time of abort to MECO, adapted from Ref. [60]

The course reversal is done by a powered pitch-around (PPA) maneuver that flips the vehicle over and points it back to the landing site. PPA is a drastic maneuver for the X-33 (also for the current Space Shuttle), hence the flight software is programmed to fly PPA at a maximum pitch rate $\left(\dot{\theta}\right)$ of ± 10 deg/sec to prevent the vehicle from gaining too much altitude while performing the maneuver. Structural constraints must not be violated while performing PPA to avoid structural catastrophe. The goal of RTLS is to gain enough altitude and velocity while leaving only enough propellant to allow the spacecraft to turn around, align with HAC at KSC, and achieve MECO conditions so that the vehicle can glide back to KSC for a safe landing [57, 58, 60].

2.2 Nominal Entry Trajectory

Coming home from space is as important, unforgiving and challenging as reaching the orbit. This was re-confirmed around 8:00A.M. CST on February 1, 2003 when the Space Shuttle Columbia (STS-107) disintegrated during re-entry at an altitude of 63 km (207,000 ft) and speed of Mach 18.3 (17,000 mph or 28,000 km/hr) [61].

The primary entry profile encompasses from post de-orbit entry initiation to the acquisition of TAEM interface. Shortly after the atmospheric penetration, the orbiter will hit air molecules and build up extreme heat from friction at such high speed. This makes the design of a trajectory within the heat rate constraint a critical task in addition to a reliable thermal protection system (TPS). A combination of regulating angle-of-attack and bank angle maneuvers will be used to achieve guidance objectives — achieve the range requirements by a controlled unpowered flight trajectory [57].

General entry guidance objectives are divided into five phases as described in United Space Alliance's (USA) "Entry Through Landing Guidance" for the Space Shuttle [62] and an illustration is exhibited in Figure 2.5:

① Pre-entry: Pre-entry is an attitude hold mode prior to atmospheric entry.

② Temperature control: The temperature control phase defines an entry profile shape consistent with the TPS constraints during the highheating part of entry.

③ Equilibrium glide: The equilibrium glide phase provides an entry profile that has the fundamental shape of equilibrium flight. It is used during the intermediate velocity region of entry.

④ Constant drag: The constant drag phase provides a profile shape consistent with control system limits.

⑤ Transition: The transition phase provides a profile shape consistent with the control system limits and guides the vehicle to the proper TAEM interface conditions.

The current shuttle entry trajectory is calculated based on these five phases mainly due to its computing power. According to NASA [63], the Space Shuttle uses an IBM AP-101F computer with an average speed of 0.48 millions of instructions per second (MIPS). This speed is approximately an equivalent of an Intel 286 computer. The current Pentium 4 computers have an average speed of 1,500 MIPS [64]. Hence it is possible to enforce every constraint at all times with the advancement in technology and the plan of installing faster computer processors on the next generation RLV.

IBM is a trademark of International Business Machines Corporation. Intel and Pentium are trademarks of Intel Corporation.
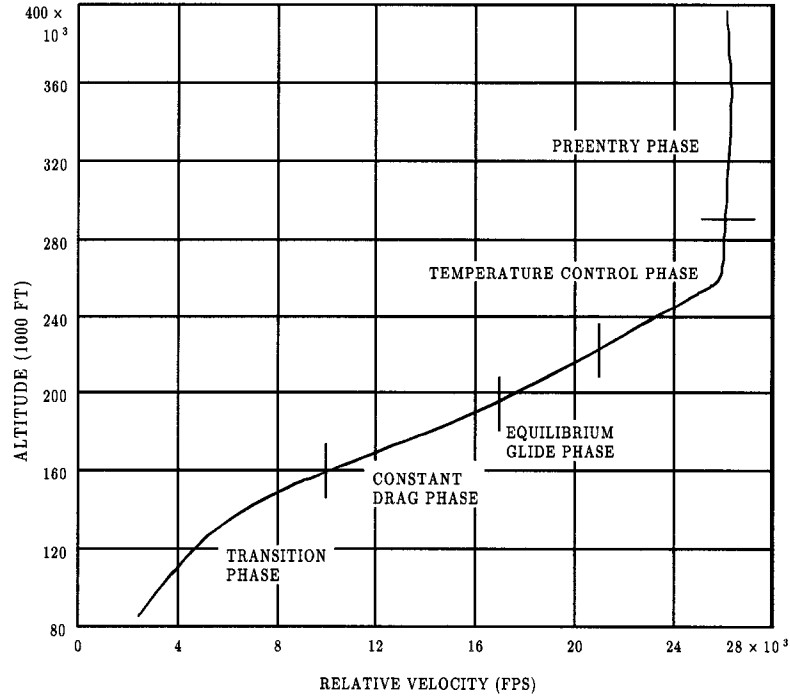
Figure 2.5   General entry guidance phases, courtesy of Ref. [62]

2.3   Thermal Protection System

The primary function of an entry analysis is to generate a trajectory that allows for ranging capabilities in both downrange and crossrange in order to achieve the entry-TAEM conditions as well as to satisfy the thermal, load and structural constraints. The entry vehicle is essentially a glider; therefore, the only achievable means to accomplish the range requirement is through the modulation of vehicle's aerodynamic forces. While the vehicle's aerodynamic lifting capability determines the range, it also presents an entry aerothermal problem, namely how this affects the reusability of the thermal protection system (TPS). Thus, there are two interrelated aspects of TPS design: ① optimize the entry trajectory to minimize internal structure temperature; and ② test of new durable, reusable and lightweight TPS materials [65–69].

Each type of TPS material has its own distinctive thermal features. As an example, metallic TPS can resist oxidization to approximately 980°C (1,800°F) compared to that of ceramic TPS that has a maximum temperature of approximately 1,430°C (2,600°F) [70]. While metallic TPS has the advantage of low maintenance, its lower maximum temperature will undesirably constrain its flight envelope to avoid excessive heating. Consequently this may increase the overall heat (heat load) absorbed by the vehicle throughout the entire entry flight because the trajectory may have be lofted so the flight time is longer. A new experimental metallic TPS called ARMOR (adaptable, robust, metallic, operable, reusable TPS) developed at NASA's Langley Research Center (LaRC) is undergoing extensive laboratory testing. The sandwiched panel ARMOR is designed to re-radiate the heat absorbed by TPS during the entry aerothermal environment. ARMOR is also designed to be able to fly through rain. This is an improvement from the ceramic tiles currently used on the Space Shuttles. Figure 2.6 illustrates the different types of TPS proposed to be used on the X-33/VentureStar [69, 71].
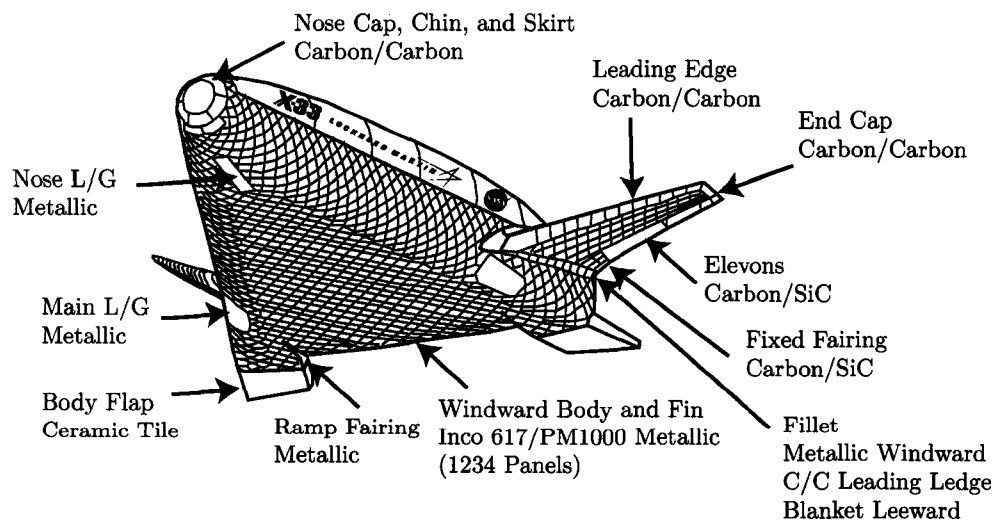
Figure 2.6 X-33 shown with different types of thermal protection system tiles, courtesy of Ref. [72]

Lastly, the selection of TPS for a commercially viable RLV must be based on durability, be lightweight, have lower maintenance, and lower life-cycle costs since 400,000 man hours (approximately 60-day turnaround) are spent currently inspecting and refurbishing the TPS tiles between flights for the shuttle [65].

2.4 Terminal Area Energy Management Guidance

The "entry phase" ends and the terminal area entry management (TAEM, pronounced "tame") phase starts when the vehicle reaches relatively low altitude and velocity. For the X-33, the TAEM phase begins around 30.5 km (100,000 feet) in altitude, approximately 55.5 km (30 nm) from the runway, and a velocity of Mach 3 (993 m/s or 3,300 ft/s) [73]. The purposes of TAEM are:

☆ to maintain proper energy while approaching the landing site

☆ to align vehicle with the runway centerline for the final approach & landing phase

The *TAEM guidance* steers the vehicle to a predicted virtual heading alignment circle (HAC), which radius is approximately 5.5 km (18,000 feet) and height is approximately 3 km (10,000 feet). HAC is located tangent to the runway centerline for a straight in final approach. Excess energy is dissipated between TAEM and HAC with an S-turn. The speed brake may also be used to modify drag, lift-to-drag ratio and flight-path-angle to allow a normal A/L. Figure 2.7 displays a sample flight path of the landing sequence from TAEM to HAC based on the Space Shuttle's entry ground track [58, 74, 75].

The heading alignment circle, or heading alignment cone (HAC) as it is sometimes called, is a virtual heading alignment guideline used for the spacecraft to align itself for a straight final A/L. Since the spacecraft is essentially a glider at this point, it is extremely important for it to have suitable energy (adequate altitude and speed) and

align properly with the runway centerline at the nominal entry point (NEP) as shown in Figure 2.7 after the spacecraft has circled around the cone. HAC is predicted based on the spacecraft's altitude and speed at the entry point. HAC can be on either end of the runway depending upon which direction of the runway is chosen for landing.

TAEM phase starts:
    55.5 km (30 mi) away from HAC
    30.5 km (100K ft) altitude

A

Ground Track

Predicted Virtual HAC:
    5.5 km (18K ft) radii
    3 km (10K ft) altitude

A

Runway:
    4,572 m × 91.4 m
    (15,000 ft × 300 ft)

B

D

C

C

A = TAEM interface
B = Begin heading alignment
    subphase
C = NEP and begin pre-final
    subphase
D = Runway threshold

B
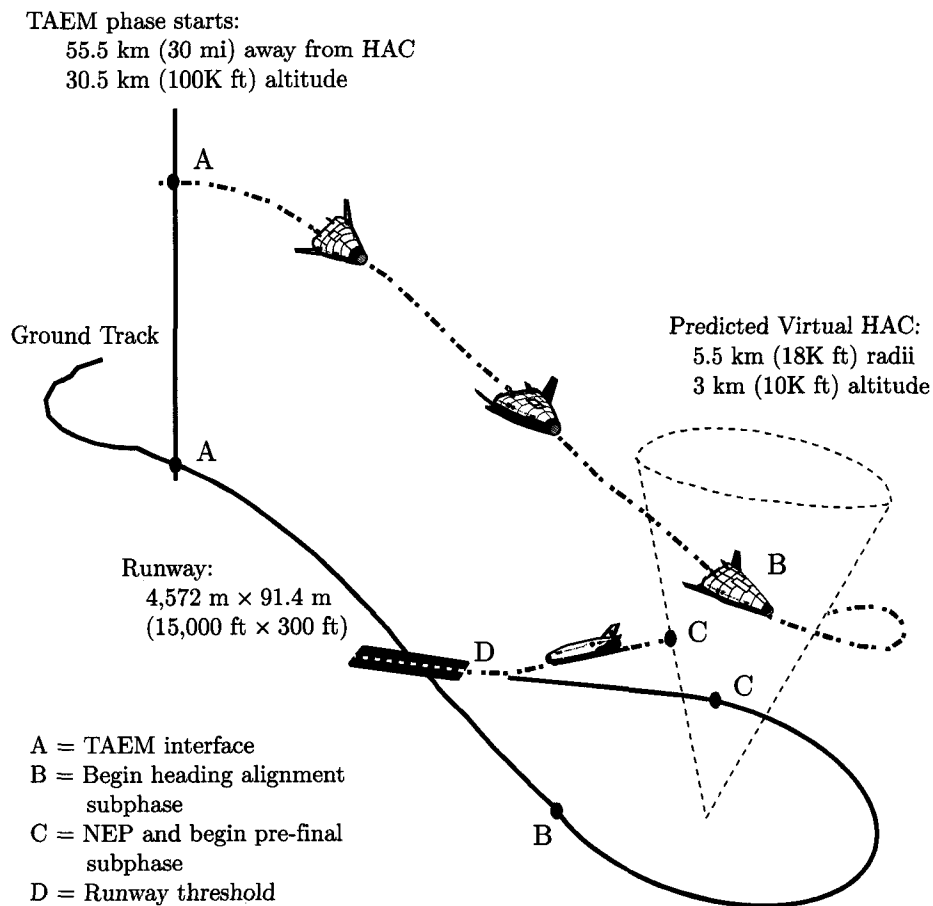
Figure 2.7   Flight profile of RLV landing sequence from TAEM to
runway, adapted from Ref. [75]

CHAPTER 3   NUMERICAL OPTIMIZATION METHOD

Computers are useless.
They can only give you answers.

— Pablo Picasso [3]

PERFORMING the computation of ascent [50] and entry [76–78] trajectories have been a challenge since the days of Mercury space exploration era. Trajectory generation involves numerical integration of the state equations subject to common path constraints and terminal conditions. The major challenge in optimal ascent trajectory generation is the presence of aerodynamic forces inside atmosphere while the major obstacle in optimal entry trajectory generation is the heating constraint. This chapter details the numerical optimization technique used to generate the optimal ascent and entry trajectories.

Numerical integration is used to solve for optimal ascent and entry trajectories since there are no exact analytical solutions. The fundamental rationale of all effective numerical optimization methods is to simplify a difficult problem such as ascent trajectory into a set of simpler subproblems to solve.

Note: In order to avoid repeating the same notation for two different variables, some notations have deviated from the standard optimal control notations.

3.1 Optimal Control Problem

Optimization is the process of determining the state $x(t)$ and control $u(t)$ time histories for a given dynamic system in a finite period of time that minimizes a performance index J without violating a set of constraints [79, 80].

The basic optimal control problem (OCP) is to determine $u(t)$ that maximizes or minimizes J in terms of a Mayer problem $(\mathcal{M})$, Lagrange problem $(\mathcal{L})$, or Bolza problem $(\mathcal{M} + \int \mathcal{L})$

$$J = \mathcal{M}\left[x\left(t_f\right)\right] + \int_0^{t_f} \mathcal{L}\left(x, u, t\right) dt \tag{3.1}$$

subject to the dynamic equations of motion (EOMs) defined by a set of ordinary differential equations (also referred to as the state equations)

$$\dot{x} = f\left(x, u, t\right) \tag{3.2}$$

and initial condition constraints

$$\mathcal{I}_\ell \leq \mathcal{I}\left[x\left(t_0\right)\right] \leq \mathcal{I}_u \tag{3.3}$$

and algebraic path constraints (inequality constraint) in the form of

$$\mathcal{P}_\ell \leq \mathcal{P}\left[x\left(t\right)\right] \leq \mathcal{P}_u \tag{3.4}$$

and terminal state constraints

$$\mathcal{T}_\ell \leq \mathcal{T}\left[x\left(t_f\right)\right] \leq \mathcal{T}_u \tag{3.5}$$

and control variables

$$u_\ell \leq u(t) \leq u_u \qquad (3.6)$$

Note that equality constraints can be imposed if the upper and lower bounds are equal.

3.2 Transcription Formulation

The basic approach for solving an OCP by transcription (discretization) is to [81]

T1. transcribe the dynamic system into a problem with a <u>finite</u> set of variables, then,

T2. solve the finite dimensional problem using a parameter optimization method (i.e. the nonlinear programming [NLP] subproblem), then,

T3. assess the accuracy of the finite dimensional approximation and, if necessary, repeat the transcription and optimization steps.

Transcription methods such as Hermite-Sympson discretization [82], 4th order Runge-Kutta discretization [83], or trapezoidal discretization [81, 83] all divide the time interval in τ_s segments

$$t_0 < t_1 < t_2 < \ldots < t_f = t_{\tau_s}$$

where these points are referred to as grid, mesh or node points.

Let $x_k \equiv x(t_k)$ denotes the value of the state variable at a node point and $u_k \equiv u(t_k)$ to denote the control at a node point. The trapezoidal discretization used in this research has the NLP variables of

$$v = [x_0, \ u_0, \ x_1, \ u_1, \ \ldots, \ x_f, \ u_f, \ t_0, \ t_f]^T \qquad (3.7)$$

and the state equations are approximately satisfied by setting

$$\zeta_k = x_k - x_{k-1} - \frac{\varphi_k}{2}\left(f_k + f_{k-1}\right) = 0 \tag{3.8}$$

for $k = 1, \ldots, \tau_s$, $\varphi_k \equiv t_k - t_{k-1}$ is the step size, and $f_k \equiv f\left[x\left(t_k\right), u\left(t_k\right), t_k\right]$ is the right hand side of the differential equations.

The optimal control constraints are also replaced with the NLP constraints

$$\boldsymbol{c}_\ell \leq \boldsymbol{c}\left(v\right) \leq \boldsymbol{c}_u \tag{3.9}$$

where

$$\boldsymbol{c}\left(v\right) = \left[\zeta_1,\ \zeta_2,\ \ldots,\ \zeta_f,\ \mathcal{I},\ \mathcal{T},\ \mathcal{P}_0,\ \mathcal{P}_1,\ \ldots,\ \mathcal{P}_f\right]^T \tag{3.10}$$

and

$$\boldsymbol{c}_\ell = \left[0,\ \ldots,\ 0,\ \mathcal{I}_\ell,\ \mathcal{T}_\ell,\ \mathcal{P}_\ell\right]^T \tag{3.11}$$

and a comparable definition of $\boldsymbol{c}_u$ can be derived.

In the same fashion that the state and control variable bounds become simple bounds on the NLP variables, the path constraints and variable bounds are also imposed at the grid points [84]. Figure 3.1 shows a simple 11-grid point discretization example. Notice that using transcription method, the change in grid point #6 will only affect the functions connecting #5 & #6 and #6 & #7. The remaining portions of the curve will not be impacted. The reduced sensitivity in the boundary value problem means sparsity in the construction of Jacobian matrix.
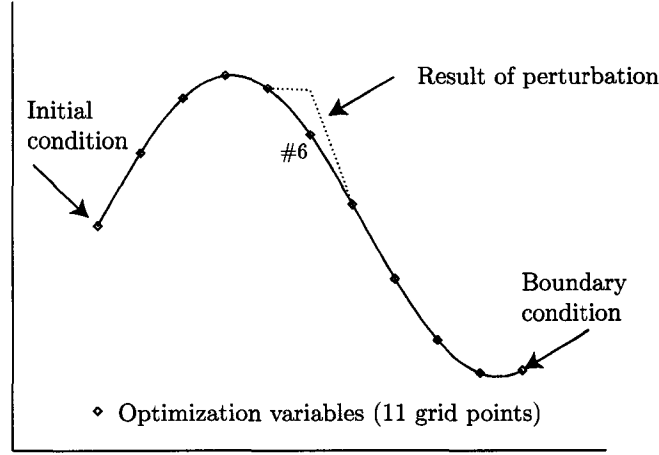
Figure 3.1   Transcription method used for solving
optimal problems, courtesy of Ref. [81]

3.3   Large Sparse Nonlinear Programming

Calculating Jacobian and Hessian information using Newton based methods rely on
the accessibility of first and second derivative information. However, a single finite differ-
ence gradient evaluation of first derivative can require z additional function evaluations.
These extra function evaluations are computationally costly when z is large ($z \leq 10^6$).
Furthermore, computing second derivative is just as tedious. Current research has fo-
cused on pointwise quasi-Newton updates [85] or sparse finite differences [86, 87] to help
overcome these computational burdens.

The concept of sparse finite differencing was first introduced by Curtis *et al.* [88] in
1974. They proposed to partition the columns of first derivative Y into subsets (Γ^k)
such that each subset has at most one nonzero element per row.

$$
\boldsymbol{Y} =
\begin{bmatrix}
(\nabla e_1)^T \\
(\nabla e_2)^T \\
\vdots \\
(\nabla e_w)^T
\end{bmatrix}
= \frac{\partial \boldsymbol{e}}{\partial \boldsymbol{v}}
\tag{3.12}
$$

A perturbation direction vector is introduced as

$$
\boldsymbol{\Delta}^k = \sum_{j \in \Gamma^k} \delta_j \boldsymbol{o}_j
\tag{3.13}
$$

where δ_j is the perturbation size and $\boldsymbol{o}_j$ is a unit vector in direction of j. Using the partition technique, the first derivatives can be estimated by

$$
\boldsymbol{Y}_{ij} \approx \frac{1}{2\delta_j} \left[e_i \left(\boldsymbol{v} + \boldsymbol{\Delta}^k \right) - e_i \left(\boldsymbol{v} - \boldsymbol{\Delta}^k \right) \right]
\tag{3.14}
$$

Similarly, second derivatives can be obtained. The estimation technique has proven to be efficient and accurate for well scaled functions [87, 89, 90]. This technique can now be used to obtain the Jacobian matrix.

The computation savings observed by Betts led to exploring the benefit of grouping terms and isolating the linear terms. That is to say,

$$
\begin{aligned}
0 &= \boldsymbol{x}_{k+1} - \boldsymbol{x}_k - \frac{\kappa_k}{2} \left(\boldsymbol{f}_{k+1} + \boldsymbol{f} \right) \\
&= \left(\boldsymbol{f}_{k+1} - \boldsymbol{f} \right) - \frac{1}{2}\tau_k \left(t_f \boldsymbol{f}_{k+1} \right) - \frac{1}{2}\tau_k \left(t_f \boldsymbol{f}_k \right)
\end{aligned}
\tag{3.15}
$$

where $\kappa_k = \tau_k \left(t_f - t_i \right) = \tau_k \Delta t$ with $0 < \tau_k < 1$. In this formation, the NLP constraints become

$$c(x) = Ax + Bw(x) \tag{3.16}$$

where A and B are given by

$$A = \begin{bmatrix} 0 & -I & 0 & I & \\ & & -I & 0 & I \\ \vdots & & & & \ddots \end{bmatrix} \tag{3.17}$$

$$B = -\frac{1}{2} \begin{bmatrix} \tau_1 I & \tau_1 I & & & & \\ & & \tau_2 I & \tau_2 I & & \\ & & & & \ddots & \\ & & & & & \tau_{M-1} I & \tau_{M-1} I \end{bmatrix} \tag{3.18}$$

with the isolated linear terms

$$w = \begin{bmatrix} \Delta t f_1 \\ \Delta t f_2 \\ \vdots \\ \Delta t f_M \end{bmatrix} \tag{3.19}$$

Now the sparse finite difference can be constructed to estimate the matrix

$$Y \equiv \begin{bmatrix} \frac{\partial}{\partial t_f} (\Delta t f_1) & \Delta t \frac{\partial f_1}{\partial x_1} & & & \\ \frac{\partial}{\partial t_f} (\Delta t f_2) & & \Delta t \frac{\partial f_2}{\partial x_2} & & \\ \vdots & & & \ddots & \\ \frac{\partial}{\partial t_f} (\Delta t f_M) & & & & \Delta t \frac{\partial f_M}{\partial x_M} \end{bmatrix} \tag{3.20}$$

and then Jacobian becomes

$$\mathcal{J} = A + BY \tag{3.21}$$

The advantage of this type of construction is now clear. Equation (3.20) calls for the partial derivatives of state and control all evaluated at the same grid point. Using a 4 states and 1 control example, matrix Y now becomes

$$struct \left(\frac{\partial f}{\partial x} \middle| \frac{\partial f}{\partial u} \right) = \begin{bmatrix} 0 & 0 & x & 0 & 0 \\ 0 & 0 & 0 & x & 0 \\ 0 & 0 & 0 & 0 & x \\ 0 & 0 & 0 & 0 & x \end{bmatrix} \tag{3.22}$$

The nonzero pattern defined by the structured sparsity template appears repeatedly in Y at every grid point introduced by the discretization method. Betts [81] has documented that this method can reduce the computation time of evaluating $\mathcal{J}$ and $\mathcal{H}$ by as much as 93%.

3.4 Sequential Quadratic Programming

Sequential quadratic programming (SQP) is one of the most widely used optimization algorithm for solving general nonlinear problems. The following is the variation implemented in the SOCS [81, 87, 91] software.

A summarized sparse SQP algorithm starts with an iteration at a point

$$v = v_0 + \kappa p \tag{3.23}$$

where κ is a scalar step length and must be grater than 0. The algorithm proceeds as follows [81]:

SQP 1. **Gradient Evaluation:** Evaluate gradient and Jacobian information by computing $\boldsymbol{p}$ to minimize a quadratic approximation to the Lagrangian

$$\boldsymbol{\mathcal{G}}^T \boldsymbol{p} + \frac{1}{2}\boldsymbol{p}^T \boldsymbol{\mathcal{H}} \boldsymbol{p} \tag{3.24}$$

where $\boldsymbol{\mathcal{G}}$ is the gradient vector, $\boldsymbol{\mathcal{J}}$ is the Jacobian matrix of the constraint gradients and $\boldsymbol{\mathcal{H}}$ is the Hessian matrix. Equation (3.24) is subject to the linear approximation to the constraints

$$\boldsymbol{b}_\ell \leq \begin{bmatrix} \boldsymbol{\mathcal{J}} \boldsymbol{p} \\ \boldsymbol{p} \end{bmatrix} \leq \boldsymbol{b}_u \tag{3.25}$$

with bound vectors given by

$$\boldsymbol{b}_\ell = \begin{bmatrix} \boldsymbol{c}_\ell - \boldsymbol{c} \\ \boldsymbol{x}_\ell - \boldsymbol{x} \end{bmatrix} \qquad \boldsymbol{b}_u = \begin{bmatrix} \boldsymbol{c}_u - \boldsymbol{c} \\ \boldsymbol{x}_u - \boldsymbol{x} \end{bmatrix} \tag{3.26}$$

(a) evaluate the error in the gradient of Equation (3.24)

$$\epsilon = \boldsymbol{\mathcal{G}} - \boldsymbol{\mathcal{J}}^T \boldsymbol{\lambda} - \boldsymbol{\nu} \tag{3.27}$$

where $\boldsymbol{\lambda}$ and $\boldsymbol{\nu}$ are used to define search directions for the Lagrange multipliers $\hat{\boldsymbol{\lambda}}$ and $\hat{\boldsymbol{\nu}}$ in

$$\Delta\boldsymbol{\lambda} \equiv \hat{\boldsymbol{\lambda}} - \boldsymbol{\lambda} \tag{3.28}$$

$$\Delta\boldsymbol{\nu} \equiv \hat{\boldsymbol{\nu}} - \boldsymbol{\nu} \tag{3.29}$$

(b) terminate if the Karush-Kuhn-Tucker (KKT) conditions are satisfied. That is to say

☆ $\boldsymbol{x}^*$ is feasible when Equations (3.30) and (3.31) must be satisfied

$$\boldsymbol{c}_\ell \leq \boldsymbol{c}(\boldsymbol{x}) \leq \boldsymbol{c}_u \tag{3.30}$$

$$\boldsymbol{x}_\ell \leq \boldsymbol{x} \leq \boldsymbol{x}_u \tag{3.31}$$

☆ the Lagrange multipliers λ for Equation (3.30) and ν for Equation (3.31) must satisfy

$$G = \mathcal{J}^T \lambda + \nu \tag{3.32}$$

☆ and the $\tilde{\mathcal{J}}$ corresponding to the active constraints has full row rank

(c) compute $\mathcal{H}_\ell$ from

$$\mathcal{H}_\ell = \nabla_x^2 F - \sum_{i=1}^{j} \lambda_i \nabla_x^2 c_i \tag{3.33}$$

SQP 2. **Search Direction:** Construct the optimization search direction;

(a) compute p by solving Equations (3.24) and (3.25)

(b) compute the direction of slack variable, Δs

$$\Delta s \equiv \mathcal{J} p + (c - s) \tag{3.34}$$

(c) compute the multipliers search direction from Equations (3.28) and (3.29)

(d) compute penalty parameters to satisfy the directional derivative of the merit function $\mathcal{O}_0'$

$$\mathcal{O}_0' \leq \frac{1}{2} p^T \mathcal{H} p \tag{3.35}$$

(e) and initialize, $\chi = 1$.

SQP 3. **Prediction:** Compute the predicted point for

(a) the variables, multiplier and slack from

$$\begin{bmatrix} \bar{v} \\ \bar{\lambda} \\ \bar{s} \end{bmatrix} = \begin{bmatrix} v \\ \lambda \\ s \end{bmatrix} + \chi \begin{bmatrix} p \\ \Delta \lambda \\ \Delta s \end{bmatrix} \tag{3.36}$$

(b) evaluate the constraints $c = c(\bar{v})$ at the predicted point.

SQP 4. **Line Search:** Evaluate the merit function

(a) if the merit function $\bar{\mathcal{O}}$ is "sufficiently" less than $\mathcal{O}$, then $\bar{v}$ is an improved point — terminate the line search and go to Step 5.

(b) else change the step length χ to reduce $\mathcal{O}$ and return to Step 3

SQP 5. **Update:** Update all quantities, set $k = k + 1$

(a) compute the actual reduction from

$$\varrho_1 = \mathcal{O}^{(k-1)} - \mathcal{O}^{(k)} \tag{3.37}$$

(b) compute the predicted reduction from

$$\varrho_2 = \mathcal{O}^{(k-1)} - \tilde{\mathcal{O}}^{(k)} = -\mathcal{O}'_o - \frac{1}{2}p^T \mathcal{H}p \tag{3.38}$$

where $\tilde{\mathcal{O}}^{(k)}$ is the predicted value of the merit function

(c) return to Step 1

CHAPTER 4   OPTIMAL ASCENT AND ABORT

TRAJECTORY DESIGNS

It was a thunderingly beautiful experience —
[...], dangerous, and expensive as hell.

— Kurt Vonnegut, Jr. [52]

ASCENT trajectory is dictated by payload performance, orbital insertion requirements, and constraints which limit the acceptable trajectories to those satisfying assumed system limitations such as maximum dynamic pressure, maximum structural load and orbital insertion targets (or abort targets).

4.1   Equations of Motion for Ascent Flight

The nondimensional point mass and windless equations of motion (EOMs) of the reusable launch vehicle (RLV) in an inertial coordinate system are (bold faced variables are vectors and non-bold faced are scalars) [51, 92, 93]

$$\dot{\boldsymbol{r}} = \boldsymbol{V} \tag{4.1}$$

$$\dot{\boldsymbol{V}} = \boldsymbol{g}(\boldsymbol{r}) + \frac{\boldsymbol{A}}{m(t)} + \frac{T\boldsymbol{1}_b}{m(t)} + \frac{\boldsymbol{N}}{m(t)} \tag{4.2}$$

$$\dot{m} = -\frac{\eta T_{vac}}{g_0 I_{SP}} \tag{4.3}$$

where r and V are the inertial positions and velocity vectors; $g(r)$ is the gravitational acceleration as a function of r; T is the current thrust magnitude including thrust lost due to back pressure; 1_b is the unit vector that defines the RLV body longitudinal body axis; A and N are the axial and normal aerodynamic forces; $m(t)$ is the current mass; η is the engine throttle setting; T_{vac} is the full vacuum thrust magnitude; g_0 is the gravitational constant; and I_{SP} is the specific impulse of the engine. All distance related terms have been normalized by R_0, velocity related terms by $\sqrt{R_0 g_0}$, and time related terms by $\sqrt{R_0/g_0}$ where R_0 is the radius of Earth and g_0 is the gravitational constant. The reason for using the dimensionless form is for better numerical conditioning of the trajectory optimization problem.

The axial (A) and normal (N) aerodynamic forces in g in Equation (4.2) are defined by

$$A = \frac{1}{2}\frac{\rho V_r^2 S_{ref} C_A R_0}{m(t)} \tag{4.4}$$

$$N = \frac{1}{2}\frac{\rho V_r^2 S_{ref} C_N R_0}{m(t)} \tag{4.5}$$

where ρ is density at the current altitude, V_r is relative velocity, S_{ref} is vehicle reference surface area, C_A is axial aerodynamic force coefficient, and C_N is normal aerodynamic force coefficient. These coefficients are computed as follow:

$$C_A = C_{A0} + C_{A1}\alpha + C_{A2}\alpha^2 \tag{4.6}$$

$$C_N = C_{N0} + C_{N1}\alpha + C_{N2}\alpha^2 \tag{4.7}$$

where C_{Ai} and C_{Ni} are functions of Mach number.

The thrust magnitudes shown in Equation (4.2) is given by

$$T = \frac{\eta T_{vac} + \Delta T}{m(t)g_0} \tag{4.8}$$

where ΔT is the thrust loss inside the atmosphere due to back pressure.

There are three coordinate systems used in this dissertation — Earth-centered inertial (ECI), guidance, and body coordinate systems. The ECI launch plumbline coordinate system is limned in Figure 4.1. The X_I points to the direction of Greenwich Meridian at launch, Z_I points in the direction of the North Pole while the Y_I completes the right-hand triad.
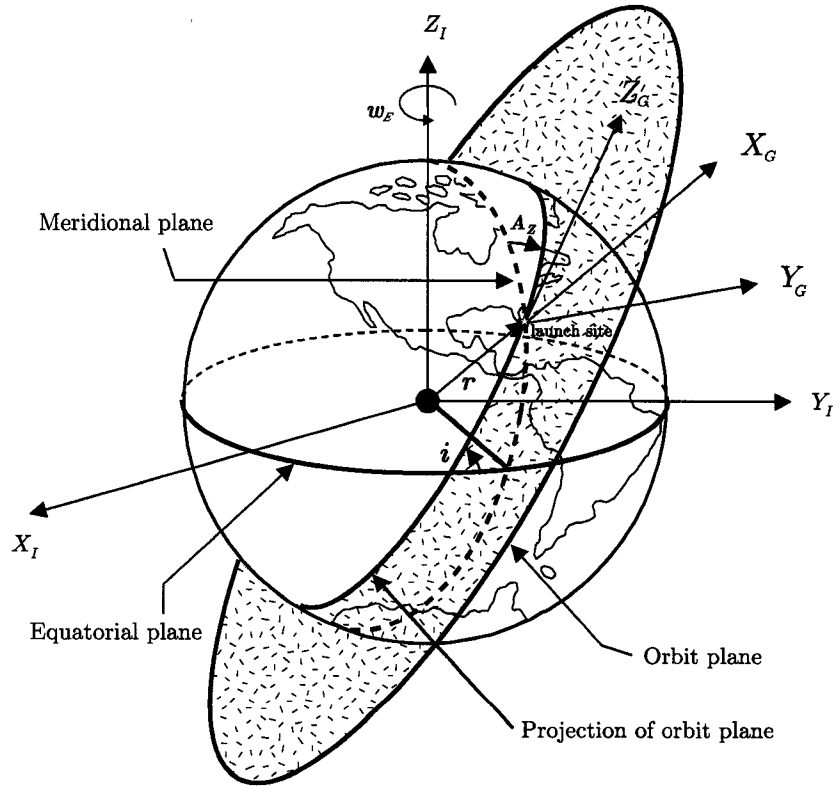
Figure 4.1 Earth-centered inertial $(X_I Y_I Z_I)$ and guidance $(X_G Y_G Z_G)$ coordinate systems

The guidance coordinate system is also portrayed in Figure 4.1. The X_G is defined from the center of the Earth, parallel to the gravity direction at the launch site. The Z_G is the downrange along the launch azimuth, and the Y_G completes the right-hand system (crossrange). The longitude and geocentric latitude of the launch site is defined by (Θ, Φ_c), respectively.

The body coordinate system is defined with X_B aligned with body longitudinal axis; Y_B aligned with body lateral axis; and Z_B completes the right-hand triad as illustrated in Figure 4.2. It is worth mentioning that guidance and body coordinate systems are the same when the vehicle is sitting on the launch pad.
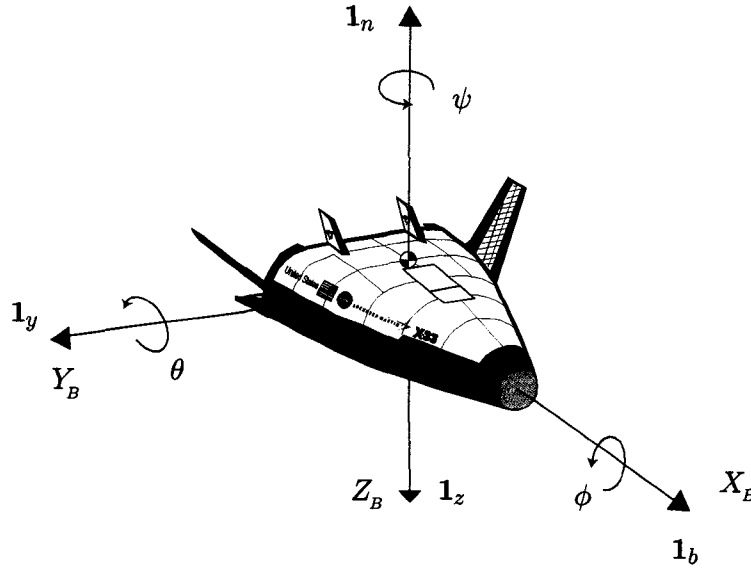
Figure 4.2   Body coordinate system showing Euler angles

The unit vector that defines the RLV body longitudinal axis in body frame is specified by three Euler angles as rendered in Figure 4.2. $\mathbf{1}_b$ defines the vehicle body axis; $\mathbf{1}_y$ defines the vehicle lateral axis; and $\mathbf{1}_z$ completes the right-hand rules.

The X-33 is at $\psi = 0°$, $\theta = 0°$ and $\phi = 0°$ when sitting on the launch pad in a vertical position. Yawing (ψ) to the left (counterclockwise) from neutral position is defined as "negative" yaw; pitching (θ) down from neutral position is defined as "negative" pitch; and rolling (ϕ) to the right from neutral position is defined as "negative" roll. An illustration of Euler angles sign conversion is depicted in Figure 4.3. Neutral position refers to 0°.

(a) Yaw angle: from neutral to negative

(b) Pitch angle: from neutral to negative

(c) Roll angle: from neutral to negative
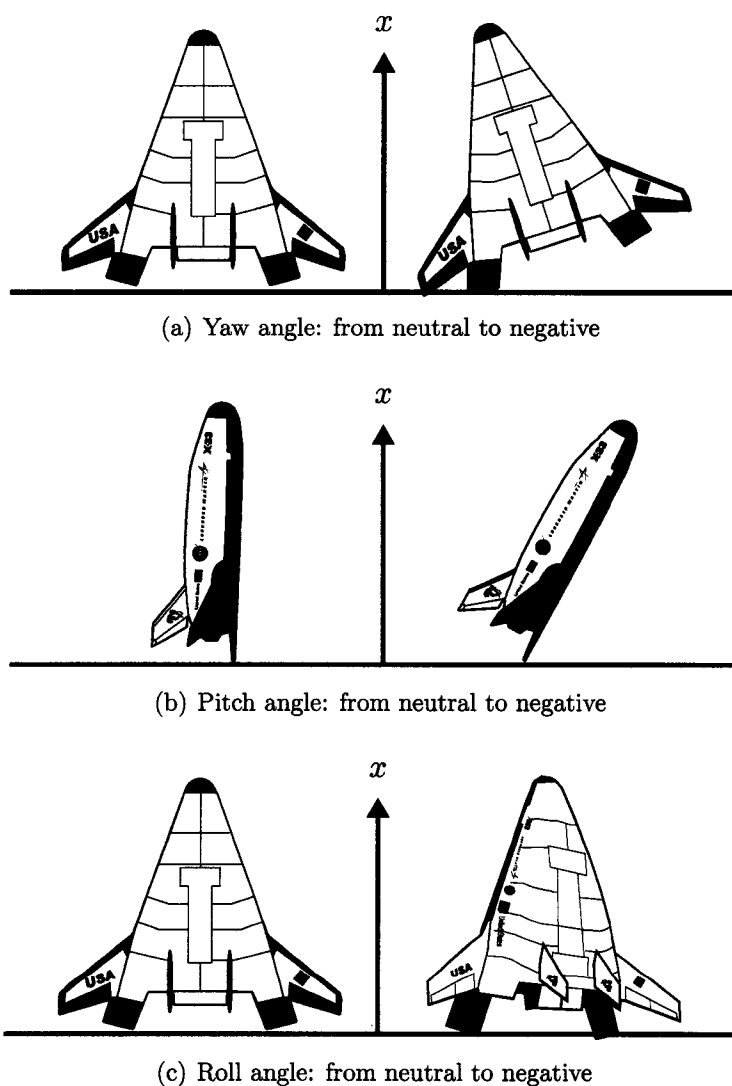
Figure 4.3   Euler angles sign convention

Use rotation sequence of yaw-pitch-roll (also referred to as 3-2-1 rotation), the unit vector of the body x-axis, $\mathbf{1}_b$ in ECI frame, is defined as

$$\mathbf{1}_b = \begin{bmatrix} \cos\psi\sin\theta \\ \sin\psi\cos\theta \\ -\sin\theta \end{bmatrix} = \mathbf{1}_x \tag{4.9}$$

The unit vector of the body y-axis in ECI frame is given by

$$\mathbf{1}_y = \begin{bmatrix} \cos\psi\sin\theta\sin\phi - \sin\psi\cos\phi \\ \cos\psi\cos\theta + \sin\psi\sin\theta\sin\phi \\ \cos\theta\sin\phi \end{bmatrix} \tag{4.10}$$

To complete the right-hand system, the body z-axis $\mathbf{1}_z$ is

$$\mathbf{1}_z = \mathbf{1}_b \times \mathbf{1}_y = -\mathbf{1}_n \tag{4.11}$$

Let T_{EP} be the coordinate transformation matrix from ECI inertial coordinate system $(X_I Y_I Z_I)$ to the guidance coordinate system $(X_G Y_G Z_G)$.

$$T_{EP} = \begin{bmatrix} \cos\Theta\cos\Phi & \sin\Theta\cos\Phi & \sin\Phi \\ -\sin\Theta\cos A_z + \cos\Theta\sin\Phi\sin A_z & \cos\Theta\cos A_z + \sin\Theta\sin\Phi\sin A_z & -\cos\Phi\sin A_z \\ -\sin\Theta\sin A_z - \cos\Theta\sin\Phi\cos A_z & \cos\Theta\sin A_z - \sin\Theta\sin\Phi\cos A_z & \cos\Phi\cos A_z \end{bmatrix} \tag{4.12}$$

where Φ is longitude, Θ is geodetic latitude, and A_z is launch azimuth angle. The launch azimuth for an ascending orbit is defined by

$$A_z = \sin^{-1}\left(\frac{\cos i}{\cos\Phi_c}\right) \tag{4.13}$$

where i is the target orbit inclination.

The Earth relative velocity is then defined as

$$V_r = V - \omega \times r - V_w \qquad (4.14)$$

where V_w is the wind velocity vector (ignored in this research) and ω is defined as

$$\omega = T_{EP}\, \omega_E \qquad (4.15)$$

where ω_E is the rotation of the Earth. Since the Earth rotates, it is necessary to take into account the rotation of the Earth in EOMs. Let the rotation rate vector of the Earth in $X_I Y_I Z_I$ (Earth centered, Z_I-axis pointing to the North) be

$$\omega_E = \begin{bmatrix} 0 \\ 0 \\ \omega \end{bmatrix} \qquad (4.16)$$

where ω is the Earth rotation rate. A sidereal day is the time it takes the Earth to rotate 360° (measured relative to the stars) and is equal to 23 hours, 56 minutes and 4 seconds [94], thus

$$\omega = \frac{2\pi}{23\text{hr }56\text{min }4\text{sec}} \qquad (4.17)$$

The angle-of-attack (α), side-slip-angle (β) and flight-path-angle (γ) are defined by

$$\alpha = \tan^{-1}\left(\frac{\mathbf{1}_z^T V_r}{\mathbf{1}_x^T V_r}\right) \qquad (4.18)$$

$$\beta = \sin^{-1}\left(\frac{\mathbf{1}_y^T V_r}{\|V_r\|}\right) \qquad (4.19)$$

$$\gamma = 90° - \cos^{-1}\left(\frac{r^T V_r}{\|r\|\,\|V_r\|}\right) \qquad (4.20)$$

Finally, it is necessary to convert the position vector from guidance frame (r) back to ECI frame ($\hat{r}$) in order to calculate longitude and geodetic latitude (Θ, Φ). Let

$$\hat{r} = T_{EP} \cdot r \tag{4.21}$$

then,

$$\Theta = \tan^{-1}\left(\frac{\hat{r}_y}{\hat{r}_x}\right) \tag{4.22}$$

$$\Phi = \tan^{-1}\left(\frac{\hat{r}_z}{\sqrt{\hat{r}_x^2 + \hat{r}_y^2}}\right) \tag{4.23}$$

4.2 Equality Constraints for Ascent Flight

Equality constraints are usually applied at a point (i.e., terminal condition). The four commonly used equality constraints in ascent trajectory include orbital insertion radius (r_f^*), velocity (V_f^*), flight-path-angle (γ_f^*) and orbital inclination (i^*) as shown in Equations (4.24) through (4.27)

$$\frac{1}{2}r_f^T r_f - \frac{1}{2}r_f^{*2} = 0 \tag{4.24}$$

$$\frac{1}{2}V_f^T V_f - \frac{1}{2}V_f^{*2} = 0 \tag{4.25}$$

$$1_n^T(r_f \times V_f) - \|r_f \times V_f\|\cos i^* = 0 \tag{4.26}$$

$$r_f^T V_f - \|r_f\|\|V_f\|\sin\gamma_f^* = 0 \tag{4.27}$$

where 1_n is a unit vector parallel to the polar axis of the Earth and pointing to the north. For orbital insertion cases in this dissertation, the target orbit is a circular orbit with $r_f^* = 185.2$ km (100 nm), $V_f^* = 7{,}793.6$ m/s, and $\gamma_f^* = 0°$. The two orbital inclinations used for this research are $i^* = 51.6°$ (the orbital inclination of the International Space Station, ISS), and $i^* = 28.5°$ (the minimum orbital inclination achievable from Kennedy

Space Center, KSC). Equation (4.24) guarantees that the difference between $\|r_f\|$ and the specified r_f^* is zero, thus the final orbital insertion altitude (MECO altitude) will be exactly as defined by r_f^*. Equation (4.25) ensures the final orbital velocity is exactly as specified by V_f^*. Equation (4.26) defines the angle from the polar axis of the Earth ($\mathbf{1}_n$) to the angular momentum vector ($r_f \times V_f$) is the final orbital inclination angle. Finally, Equation (4.27) defines the angle between r and V is indeed the flight-path-angle.

For abort cases such as transoceanic-abort-landing and return-to-launch-site, the terminal constraints are such that the ascent trajectory merges tangentially onto a nominal entry profile (NEP) instead of at a specific point. The NEP was numerically generated and are shown in Figures 4.4 through 4.6 in solid line. These histories are then curve-fitted by 4th order polynomials of range-to-go (r_{togo}) as

$$r_f^* = -2.2989e^{-14}r_{\text{togo}}^4 + 1.2741e^{-9}r_{\text{togo}}^3 - 1.0343e^{-5}r_{\text{togo}}^2 + 0.0321r_{\text{togo}} + 38.2061 \qquad (4.28)$$

$$V_f^* = -1.3355e^{-11}r_{\text{togo}}^4 + 2.1716e^{-7}r_{\text{togo}}^3 - 0.00138r_{\text{togo}}^2 + 4.477r_{\text{togo}} + 917.9185 \qquad (4.29)$$

$$\gamma_f^* = -1.7514e^{-14}r_{\text{togo}}^4 + 2.7468e^{-10}r_{\text{togo}}^3 - 1.6003e^{-6}r_{\text{togo}}^2 + 0.00386r_{\text{togo}} - 3.4089 \qquad (4.30)$$

where r_{togo} is in km, r_f^* in km, V_f^* in m/s and γ_f^* in degrees. Note: $e^{-14} = 10^{-14}$.
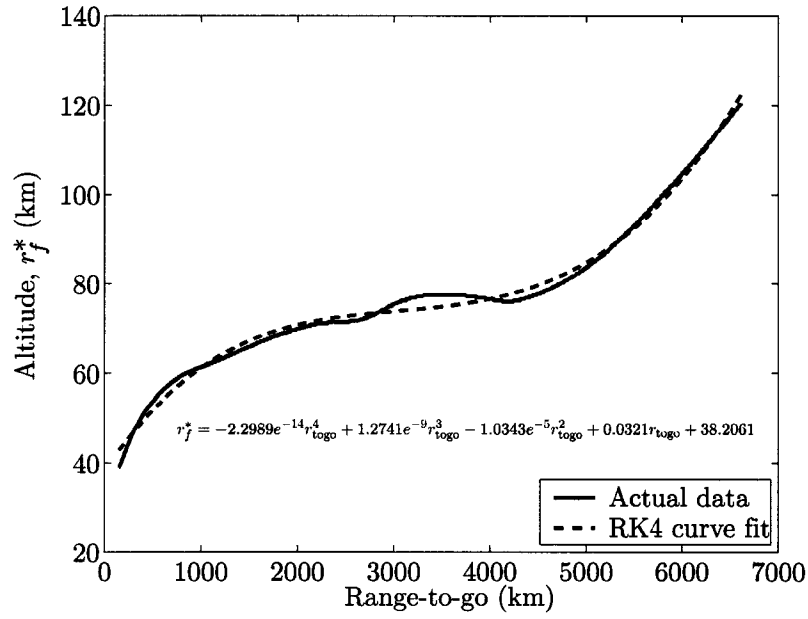
Figure 4.4 X-33 altitude vs. range-to-go nominal entry profiles and RK4 curve fit

$$r_f^* = -2.2989e^{-14}r_{togo}^4 + 1.2741e^{-9}r_{togo}^3 - 1.0343e^{-5}r_{togo}^2 + 0.0321r_{togo} + 38.2061$$
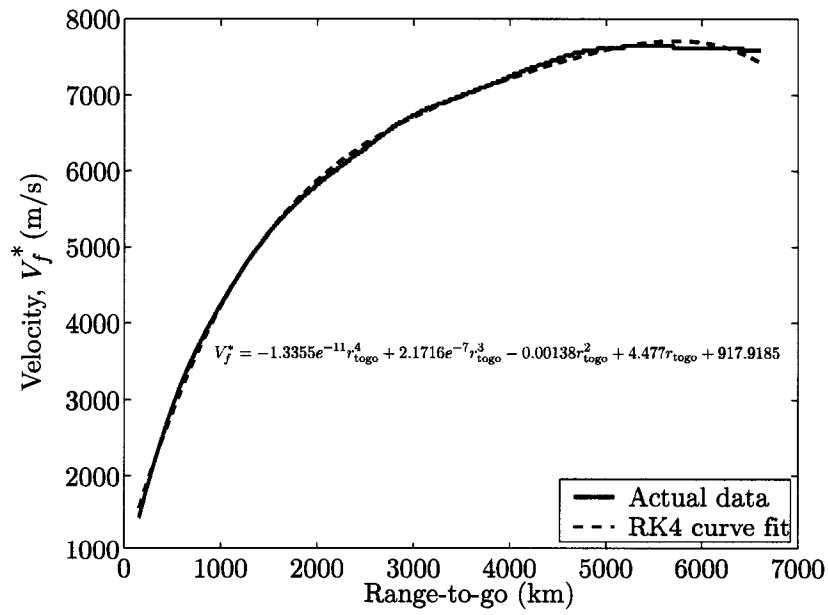
Figure 4.5 X-33 velocity vs. range-to-go nominal entry profiles and RK4 curve fit

$$V_f^* = -1.3355e^{-11}r_{togo}^4 + 2.1716e^{-7}r_{togo}^3 - 0.00138r_{togo}^2 + 4.477r_{togo} + 917.9185$$
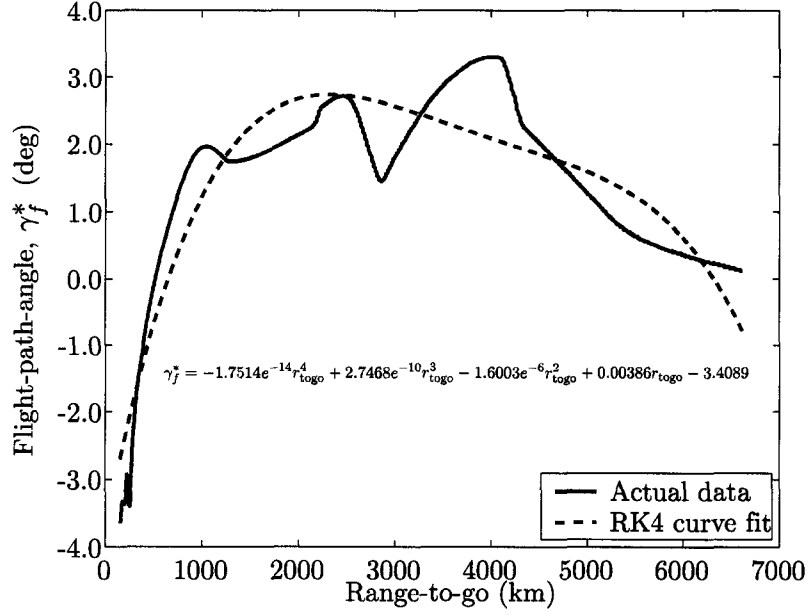
Figure 4.6 X-33 flight-path-angle vs. range-to-go nominal
entry profiles and RK4 curve fit

Range-to-go normalized by radius of the Earth is the angle from current location to
the target location. It is defined as

$$r_{\text{togo}} = \cos^{-1}\left(\frac{r_f 1_{\text{HAC}}}{\|r_f\|}\right) \tag{4.31}$$

where unit vector 1_{HAC} is the direction of the heading alignment cone (HAC) and it is
defined in the inertial frame by

$$1_{\text{HAC}} = \begin{bmatrix} \cos \Phi_{\text{HAC}} \cos \Theta_{\text{HAC}} \\ \cos \Phi_{\text{HAC}} \sin \Theta_{\text{HAC}} \\ \sin \Phi_{\text{HAC}} \end{bmatrix} \tag{4.32}$$

where Φ_{HAC} and Θ_{HAC} are longitude and geodetic latitude of the corresponding landing
site.

The formulation for return-to-launch-site (RTLS) is a little different from the previously described. This is because RTLS requires taking into account that the spacecraft has to fly downrange to dissipate excess propellant followed by the abrupt maneuver to turn the vehicle around to point back to KSC. For RTLS, the five terminal constraints are

$$\frac{1}{2}r_f^T r_f - \frac{1}{2}r_f^{*2} = 0 \tag{4.33}$$

$$\frac{1}{2}V_f^T V_f - \frac{1}{2}V_f^{*2} = 0 \tag{4.34}$$

$$1_{\mathrm{HAC}}^T r_f - \|r_f\| \cos r_{\mathrm{togo}} = 0 \tag{4.35}$$

$$V_f^T 1_h = 0 \tag{4.36}$$

$$1_{\mathrm{HAC}}^T V_f - \|V_f\| \cos\left(\frac{\pi}{2} - r_{\mathrm{togo}} - \gamma_f^*\right) = 0 \tag{4.37}$$

where unit vector 1_h specifies the direction normal to the plane of r_f and 1_{HAC}, and it is defined as

$$1_h = \frac{r_f \times 1_{\mathrm{HAC}}}{\| r_f \times 1_{\mathrm{HAC}} \|} \tag{4.38}$$

Again, Equations (4.33) and (4.34) ensure that final altitude and velocity are exactly as specified. Equation (4.35) defines the distance between the end of entry phase (beginning of TAEM interface) to the approach threshold on the target runway, thus, range-to-go. Equation (4.36) ensures that the velocity vector is in plane with HAC. Lastly, Equation (4.37) guarantees that the vehicle turns back to align itself with KSC.

It is often difficult for a numerical program to determine "when" to turn around; thus, RTLS problem are solved in two phases: downrange and return-to-launch-site. For the downrange phase, altitude, range and flight-path-angle are specified by educated guesses. Adequate altitude and distance away from KSC should be considered to allow

for a powered pitch-around (PPA) maneuver. Since a PPA maneuver is used to turn the orbiter around, a final γ_f^* for the downrange phase must be positive (else the spacecraft may perform a nose dive maneuver). Equation (4.39) is used to compute γ_f^* for the downrange portion of the flight.

$$r_f^T V_f - \|r_f\| \|V_f\| \sin\gamma_f^* = 0 \tag{4.39}$$

As for the fly-back phase, r_f^*, V_f^* and γ_f^* are to be intersected with a NEP similar to TAL cases. Intersecting a NEP instead of a specific point is beneficial because this eliminates the need to impose those inequality constraints typically associated with entry flight (to ensure that MECO condition is within the confinement of entry flight corridor). Detailed discussion on the inequality constraints associated with entry flight will be given in Section 5.3. Further discussion on entry flight corridor will be presented in Section 5.4.

4.3 Inequality Constraints for Ascent Flight

An inequality path constraint refers to a constraint that has a lower and upper limit throughout the entire trajectory. The three types of inequality path constraints generally imposed on the ascent trajectory include structural constraints, axial acceleration and throttle setting limits.

4.3.1 Structural Constraints

According to Tartabini *et al.* [70, 95], parameters such as the dynamic pressure (q) must be constrained between $0 \leq q \leq 18.2$ KPa (380 psf), and $q\alpha$ and $q\beta$ must both be constrained at ±71.8 KPa-deg (1,500 psf-deg) for the X-33 in the nominal ascent trajectory to satisfy structural design limits and prevent structural failures. Parameters

$q\alpha$ and $q\beta$ are products of dynamic pressure and angle-of-attack, and dynamics pressure and side-slip-angle. Since this research does not take into account of wind effect, $q\alpha$ and $q\beta$ limits are further reduced to ± 35.9 KPa-deg (750 psf-deg) to leave some margins. The angle-of-attack is limited to $-4° \leq \alpha \leq 12°$ up to 11 km (inside of atmosphere) to avoid exceeding structural design limits. Although increasing $q\alpha$ limits means increasing payload capacity as shown in Figure 4.7, the gain is considered minimum [70, 93, 95].
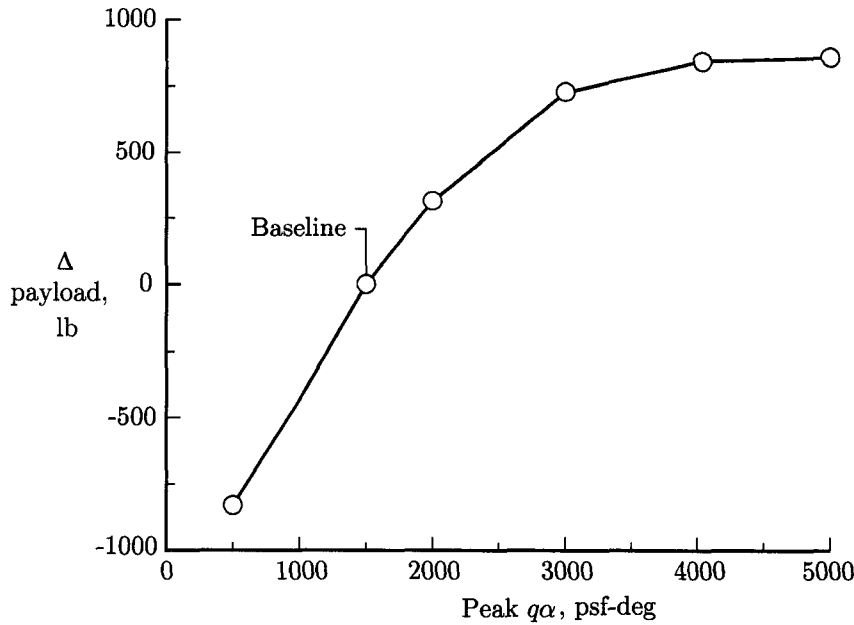
Figure 4.7   Effect of $q\alpha$ structural constraint on vehicle
payload capacity, courtesy of Ref. [70]

4.3.2   Axial Acceleration Limits

A study done by Tartabini *et al.* [70, 95] delineated in Figure 4.8 illustrates how axial acceleration during ascent affects the payload capacity and engine power level. Increasing the axial acceleration (a_a) limit from $3g$'s to $5g$'s had a reduction of approximately 454 kg (1,000 lbs) of payload capacity. While increasing a_a typically reduces payload

capacity, the power level increases and the burn time decreases. This is advantageous from engine design point of view since it enables higher thrust usage at MECO and results in shorter engine burn times (longer engine life-cycle). A compromised axial acceleration limit of $4g$'s was chosen for this research to balance the reduction in payload capacity and the increase in thrust usage. The axial acceleration limit is imposed according to Equation (4.8).
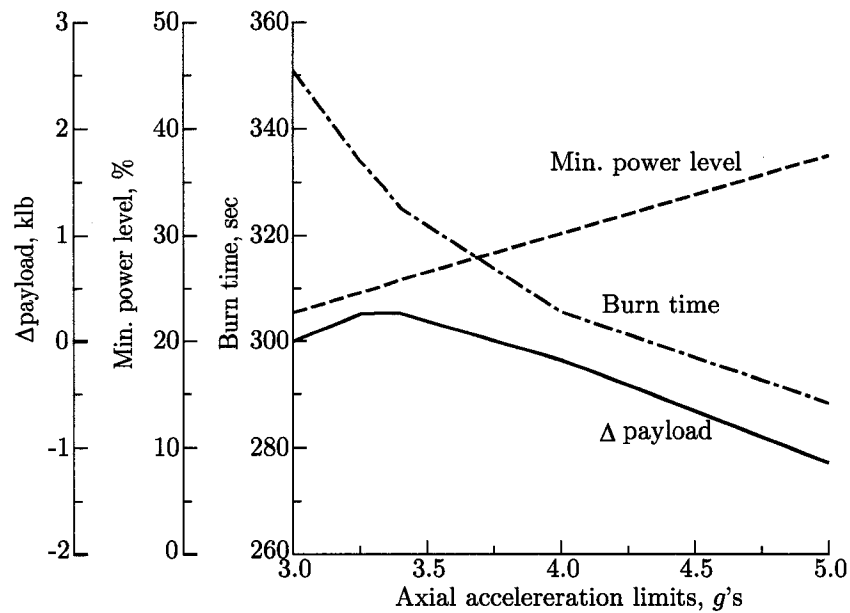
Figure 4.8 Effect of axial acceleration on vehicle payload capacity, courtesy of Ref. [70]

4.3.3 Throttle Settings

Throttle settings can be used for tasks as simple as controlling the vehicle speed to more sophisticated tasks such as emergency flight control of multi-engine vehicles (known as propulsion controlled aircraft, PCA). In this research, throttle setting is used to control the vehicle speed in order to stay within the structural design limits,

particularly to ensure that dynamic pressure stays within $0 \leq q \leq 18.2$ KPa (380 psf) and axial acceleration stays within $4g$'s. Engine is throttled back accordingly once the maximum dynamic pressure or axial acceleration is reached. The relationship between throttle setting (η) and velocity (V) is shown in Equations (4.2) and (4.3). The XRS-2200 engine used for the X-33, has a throttle setting of $50\% \leq \eta < 100\%$ and no re-start capability according to Boeing Rocketdyne [96].

4.4 Objective of Ascent Trajectory

The main objective of the ascent guidance problem is to find the best body orientation that will satisfy all the equality and inequality constraints along with the optimization performance index. Therefore the controls for ascent guidance are throttle setting, yaw angle, pitch angle and roll angle. More specifically, the controls are throttle setting, yaw rate, pitch rate and roll rate. Using rates as the controls instead of angles will result in smoother yaw, pitch and roll angle profiles.

4.5 Nominal Ascent Results

Nominal ascent analysis is the first step in determining the baseline performance of the X-33. Optimal nominal ascent trajectory is used as the baseline to predict the propellant usage for a maximum allowable payload. The design reference mission of the X-33 is to deliver a payload of 11,345 kg (25,000 lb) into an orbit with inclination angle ranging from 28.5° to 51.6° from Kennedy Space Center (KSC). For this research, ascent trajectory starts after clearing the launch tower (5 seconds after time of ignition) and stops at the main-engine-cut-off (MECO) point. This means when the final mass is equal to 37,600 kg for $J = \min t_f$ cases (nominal and all abort cases).

4.5.1 Nominal Ascent with $i = 51.6°$

Optimal ascent trajectories of the X-33 are computed based on targeting the orbital insertion conditions by minimizing final time (t_f) with full power. In this case, the launch inclination of 51.6° is the orbital inclination of the International Space Station (ISS). The trajectory is optimized by adjusting throttle setting and yaw/pitch/roll commands. These parameters are further constrained to make the problem more realistic. Table 4.1 lists a set of initial conditions used for all nominal trajectories with $i = 51.6°$ and Table 4.2 enumerates the constraints imposed on the flight parameters. Again, the initial flight time of $t = 0$ second corresponds to that of the X-33 after clearing the tower. **Thus, an extra 5 seconds must be added to all flight times.** The first five seconds of the flight are purely vertical ascent because any maneuvering during this period may hit the tower.

Table 4.1   Initial conditions for all nominal trajectories with $i = 51.6°$

$J = \min\ t_f$			
time =	0.00 sec	# of engines =	2
$x =$	6,373,379.80 m	$i =$	51.60°
$y =$	868.70 m	yaw (ψ) =	0.00°
$z =$	865.50 m	pitch (θ) =	−1.00°
$V_x =$	25.57 m/s	roll (ϕ) =	0.00°
$V_y =$	290.10 m/s	mass (m) =	122,176.39 kg
$V_z =$	289.98 m/s	throttle setting (η) =	100%

The major flight characteristics of the X-33 nominal ascent trajectory are delineated in Figures 4.9 through 4.12 (without q constraint) and Figures 4.13 through 4.16 (with q constraint). Figure 4.9 shows MECO occurred near the perigee of the transfer orbit ($r_f^* = 185.2$ km) with $V_f^* = 7,793.6$ m/s and $t_f = 320.99$ seconds. The angle-of-attack is indeed within the constraint in the first 11 km where aerodynamic forces are significant. Figure 4.10 depicts the dynamic pressure peaking at $q = 24,323$ N/m² (508 psf) at

Table 4.2 Constraints imposed on nominal and ATO ascent trajectories

Constraints:	Values:
Final orbit, r_f^*	185.2 km
Final velocity, V_f^*	7,793.6 m/s
Final flight-path-angle, γ_f^*	0.0°
Axial acceleration limit, a_a	$a_a \leq 4g$
Dynamic pressure limit, q	$0 \leq q \leq 18,194.4$ N/m^2 (380 psf)
$q\alpha$ limit	$\pm 35,910$ N/m^2-deg (750 psf-deg)
Angle-of-attack, α	$-4° \leq \alpha \leq 12°$ (up to 11 km)
Engine throttle setting, η	$50\% \leq \eta \leq 100\%$

$V = 628$ m/s when q constraint is not imposed. The engine throttle is flown at 100% from launch to 230 seconds where axial acceleration of $4g$'s is reached. The throttle setting is gradually reduced back to 65% in order to maintain the $4g$'s limit. The $q\alpha$ constraint in this case is limited to $\pm 35,910$ N/m^2-deg (750 psf-deg) which lasted for 46 seconds. Figure 4.11 illustrates the Euler angles required in order to yield the optimal trajectory. Pitch is the most contributing maneuver in the nominal ascent trajectory as it started with $-1°$ and ended with $-121°$ (pitching down). Small yaw and roll maneuvers are also used to achieve the target orbit (note: it is possible to achieve the orbit without roll). Figure 4.12 shows the flight-path (γ) and side-slip (β) angles. The flight-path-angle ended with 0° at MECO as constrained (flying straight and level). The side-slip-angle is small in nominal ascent.
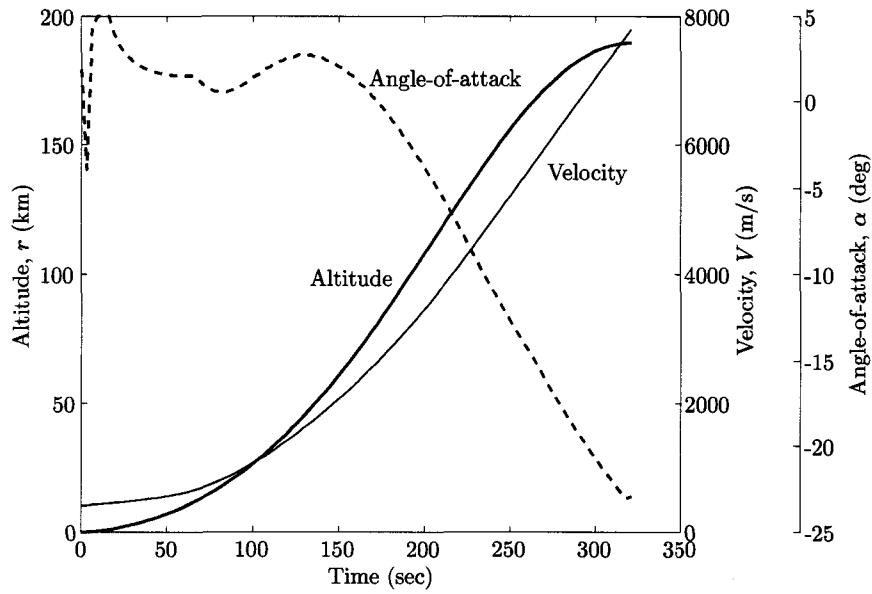
Figure 4.9   Nominal ascent altitude, velocity and angle-of-attack profiles for $i = 51.6°$ without q constraint based on conditions in Table 4.1 and Table 4.2
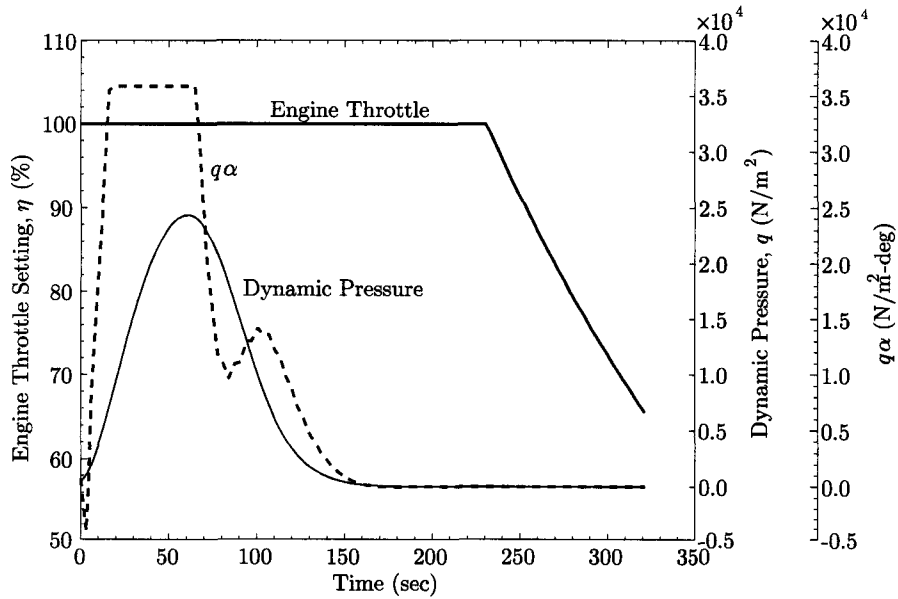
Figure 4.10   Nominal ascent throttle setting, dynamic pressure and $q\alpha$ profiles for $i = 51.6°$ without q constraint based on conditions in Table 4.1 and Table 4.2
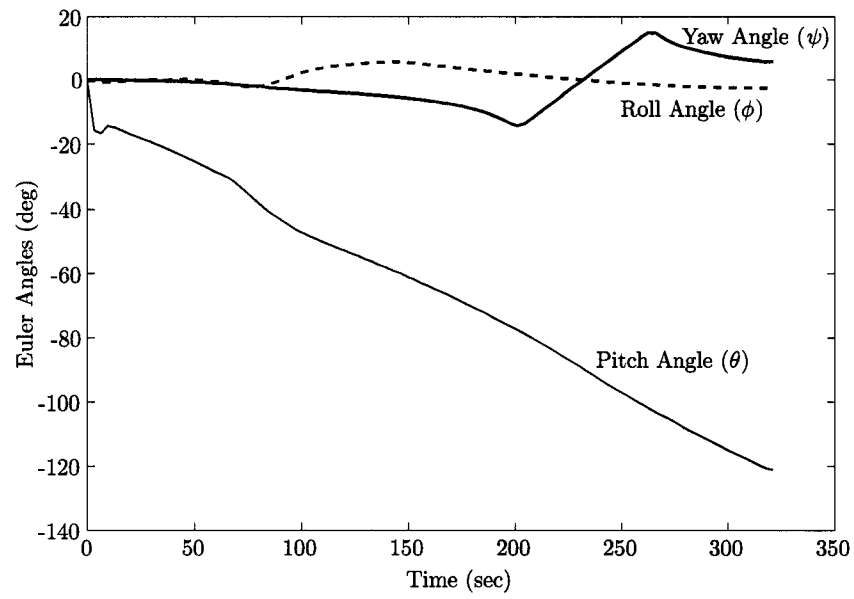
Figure 4.11   Nominal ascent Euler angle profiles for $i = 51.6°$ without q constraint based on conditions in Table 4.1 and Table 4.2
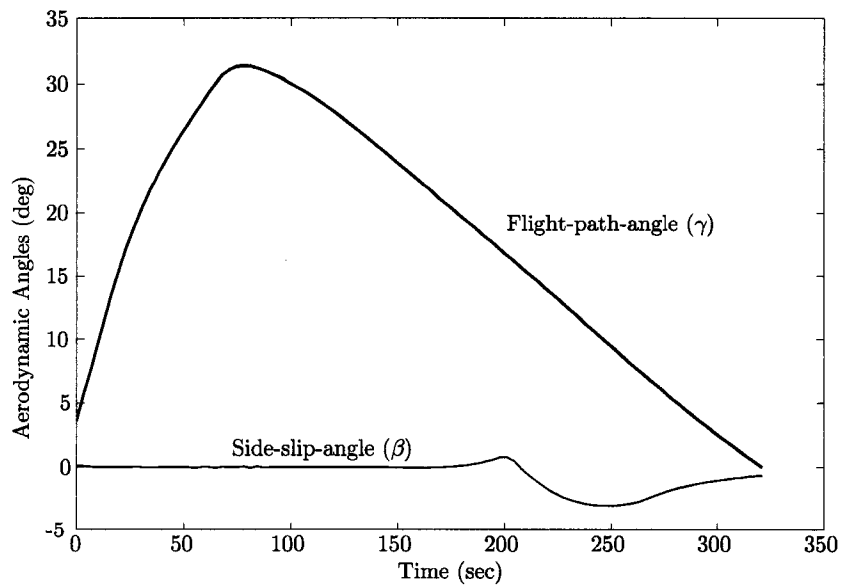
Figure 4.12   Nominal ascent aerodynamic angle profiles for $i = 51.6°$ without q constraint based on conditions in Table 4.1 and Table 4.2

The next four figures show the nominal 51.6° orbit with the addition of the dynamic pressure constraint. Figure 4.13 displays that MECO occurred near the perigee of the transfer orbit ($r_f^* = 185.2$ km) with $V_f^* = 7,793.6$ m/s and $t_f = 323.14$ seconds. The angle-of-attack again is within the specified bound of $-4° \leq \alpha \leq 12°$ for the first 11 km where aerodynamic forces are large.

Figure 4.14 depicts the dynamic pressure peaking at the upper bound of 18,194 N/m² (380 psf) for 16 seconds with velocity ranging from 478 m/s to 524 m/s. The engine throttle setting is flown at 100% from launch to 231 seconds where axial acceleration of $4g$'s is reached. The throttle drops from $46 \leq t \leq 59$ seconds are due to the fact that maximum dynamic pressure has been reached, thus throttle setting is reduced to uphold $q = 18,194$ N/m². As a result, the vehicle's pitch attitude oscillated and caused small dips in the angle-of-attack profile as shown in Figure 4.13. The engine is throttled back after $t = 231$ sec gradually to 65% in order to maintain the $4g$'s limit. The $q\alpha$ constraint reached both ±35,910 N/m²-deg (750 psf-deg) in this case because of α oscillation.

Figure 4.15 illustrates the Euler angles mustered in order to yield the optimal trajectory. Large pitch angle is observed as it is the most contributing maneuver in the nominal ascent trajectory. It started with $-1°$ and ended with $-121°$. These flight histories are similar to those without q constraint, but smoother. Figure 4.16 shows the flight-path-angle (γ) and side-slip-angle (β) profiles. The flight-path-angle ended with $0°$ at MECO again and the side-slip-angle is small.

The total flight time for this configuration is 328.14 seconds. Detailed MECO conditions can be found in Appendix C, Section C.1 starting on page 276.
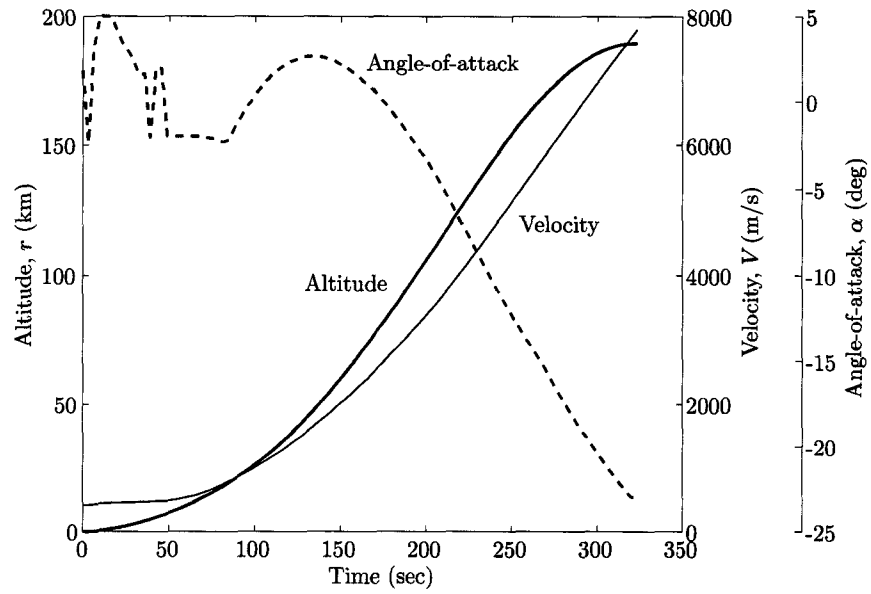
Figure 4.13   Nominal ascent altitude, velocity and angle-of-attack profiles for $i = 51.6°$ with q constraint based on conditions in Table 4.1 and Table 4.2
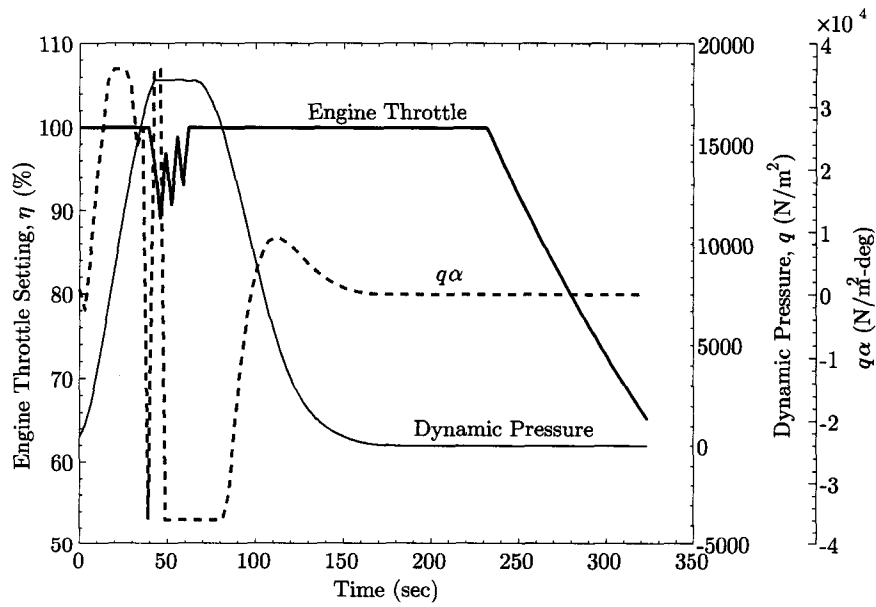
Figure 4.14   Nominal ascent throttle setting, dynamic pressure and $q\alpha$ profiles for $i = 51.6°$ with q constraint based on conditions in Table 4.1 and Table 4.2
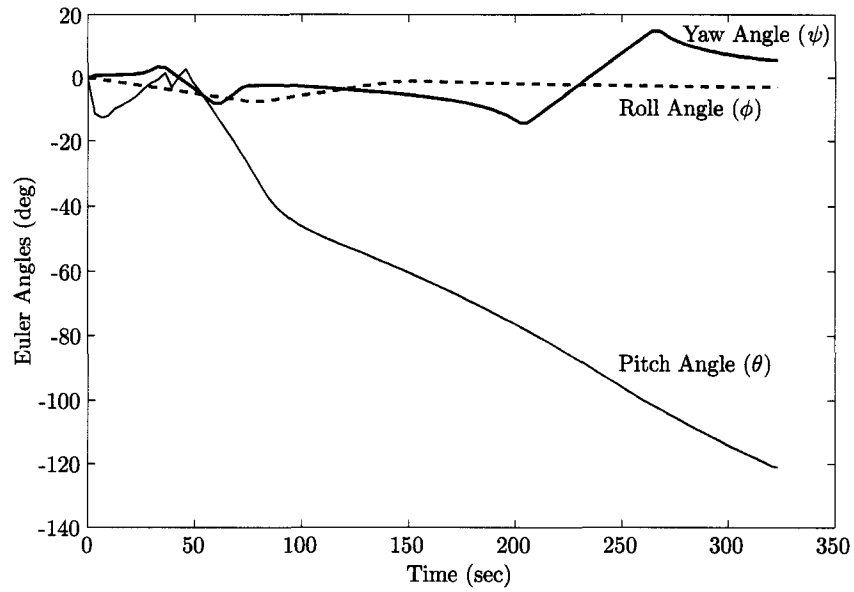
Figure 4.15 Nominal ascent Euler angle profiles for $i = 51.6°$ with q constraint based on conditions in Table 4.1 and Table 4.2
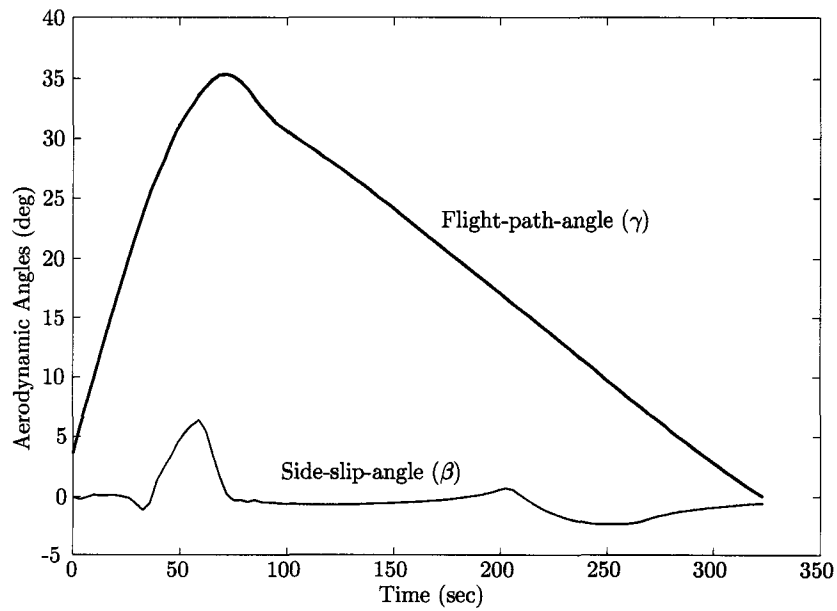
Figure 4.16 Nominal ascent aerodynamic angle profiles for $i = 51.6°$ with q constraint based on conditions in Table 4.1 and Table 4.2

4.5.2 Nominal Ascent with $i = 28.5°$

A launch inclination of 28.5° is the minimum orbital inclination that can be achieved from KSC. The performance index here is minimizing t_f again with initial conditions itemized in Table 4.3 and constraints in Table 4.2 (same equality, inequality constraints and orbital insertion conditions are used for both $i = 28.5°$ and $i = 51.6°$). The initial flight time of $t = 0$ second corresponds to that of the X-33 after clearing the tower. All profiles shown from Figures 4.17 to 4.20 resembled closely to those of $i = 51.6°$ with q constraint in the previous subsection. The total flight time for this configuration is 320.24 seconds. Even though not presented here, the flight profiles for $i = 28.5°$ without q constraint also resembled closely to those of $i = 51.6°$ without q. Detailed MECO conditions can be found in Appendix C, Section C.1 starting on page 276. Finally, a comparison of ascent trajectories and ground tracks with $i = 51.6°$ and $i = 28.5°$ (both with q constraint) is illustrated in Figure 4.21

Table 4.3   Initial conditions for all nominal ascent trajectory with $i = 28.5°$

$J = \min\ t_f$		
time =	0.00 sec	# of engines =	2
$x =$	6,373,380.26 m	$i =$	28.50°
$y =$	26.75 m	yaw $(\psi) =$	0.00°
$z =$	1,229.46 m	pitch $(\theta) =$	−1.00°
$V_x =$	25.57 m/s	roll $(\phi) =$	0.00°
$V_y =$	25.85 m/s	mass $(m) =$	122,176.39 kg
$V_z =$	409.72 m/s	throttle setting $(\eta) =$	100%
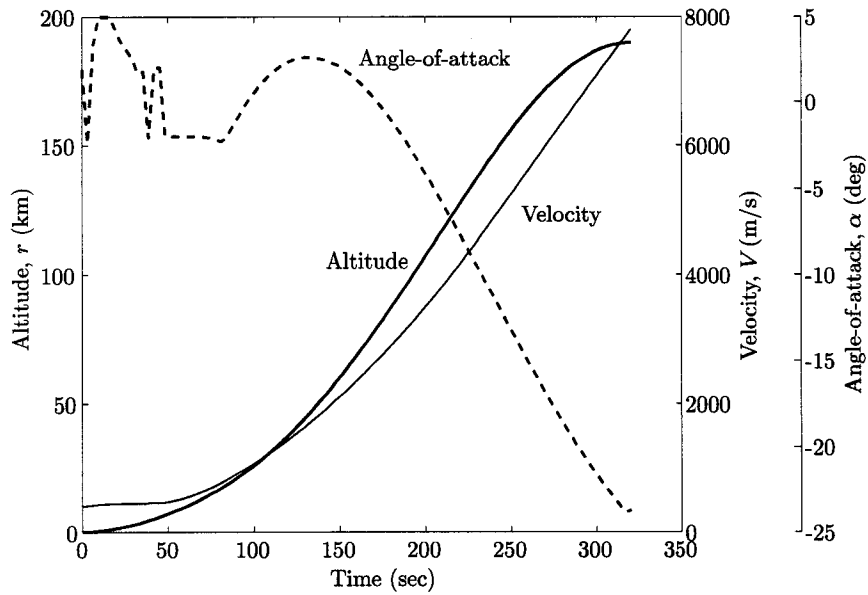
Figure 4.17 Nominal ascent altitude, velocity and angle-of-attack profiles for $i = 28.5°$ based on conditions in Table 4.3 and Table 4.2
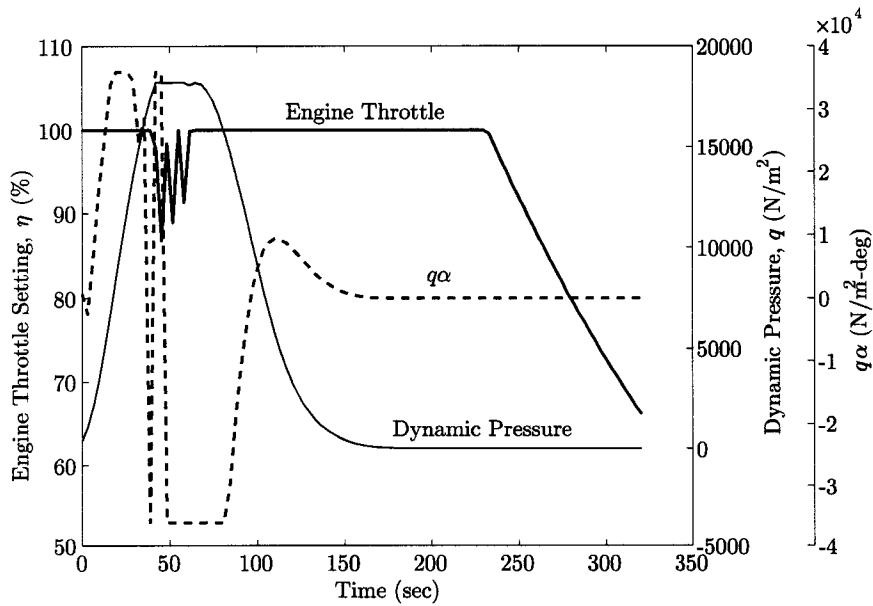
Figure 4.18 Nominal ascent throttle setting, dynamic pressure and $q\alpha$ profiles for $i = 28.5°$ based on conditions in Table 4.3 and Table 4.2
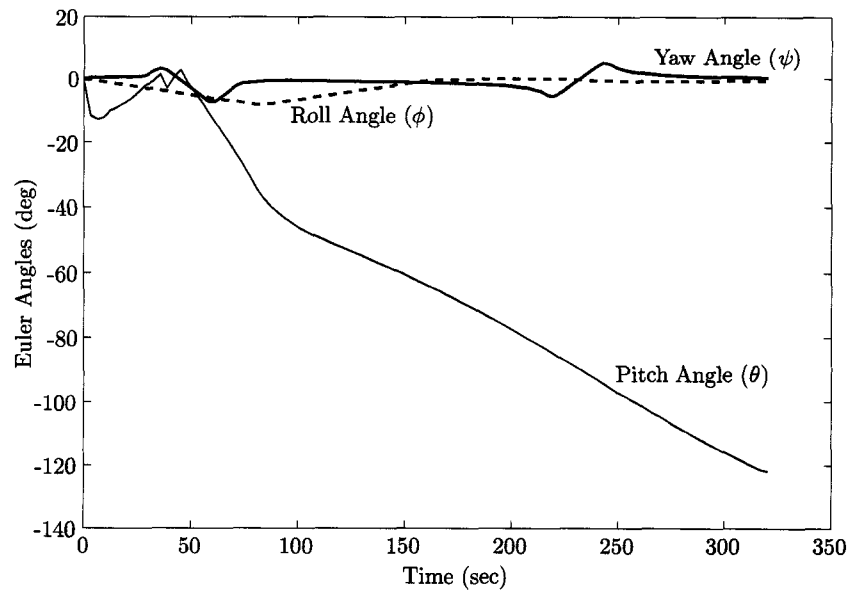
Figure 4.19 Nominal ascent Euler angle profiles for $i = 28.5°$ based on conditions in Table 4.3 and Table 4.2
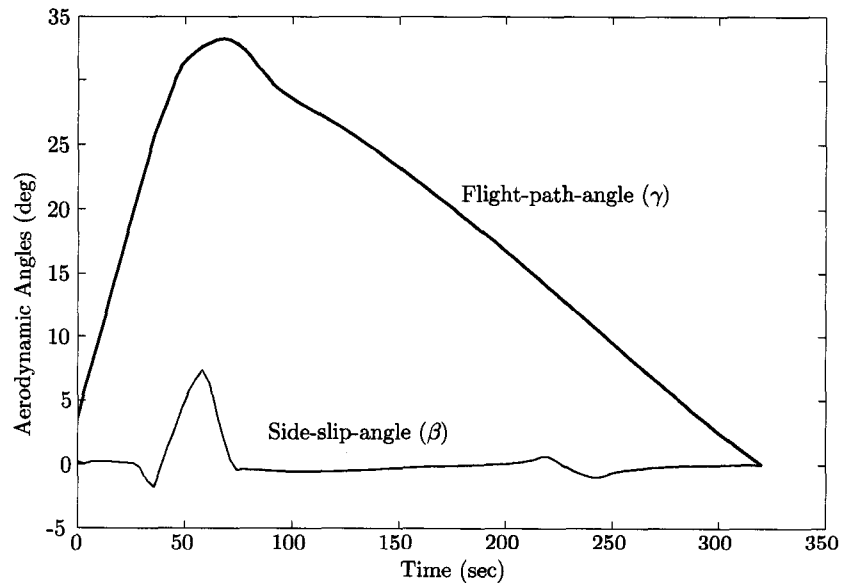
Figure 4.20 Nominal ascent aerodynamics angle profiles for $i = 28.5°$ based on conditions in Table 4.3 and Table 4.2
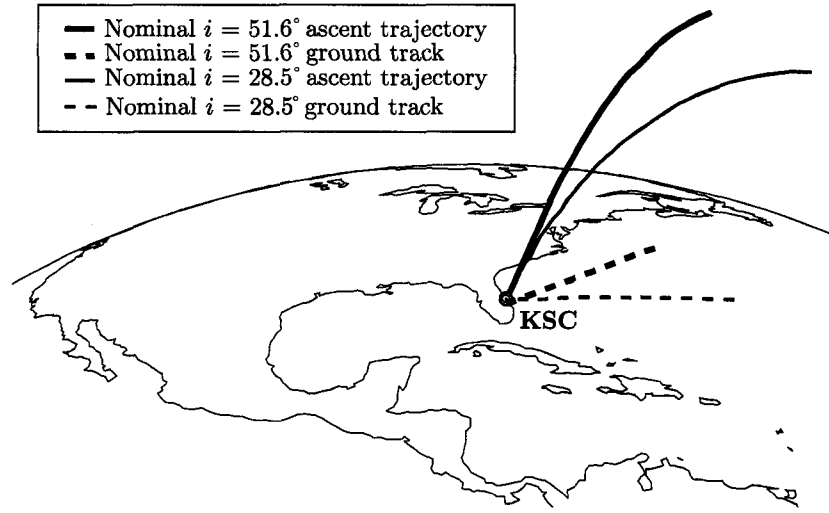
Figure 4.21   Nominal ascent trajectories and ground tracks for
$i = 51.6°$ and $i = 28.5°$ both with q constraint

4.5.3   Nominal Ascent with Different Performance Indices

Choosing the right performance index (PI) is very important for a trajectory optimization designer since a "wrong" PI may yield different results, poor results, or no results at all. The four typical ascent trajectory optimization PI's are: ① maximize final energy, ② maximize final mass, ③ maximize final velocity and ④ minimize final time. Table 4.4 shows the equality and inequality constraints imposed on each PI in nominal ascent.

The "specified" values in Table 4.4 are itemized in Table 4.5 and the *free* values are to be determined by the optimizer for a given PI. In addition to the imposed eight constraints listed in Table 4.4, a_a and α are also constrained as before.

Table 4.4 Constraints imposed on nominal ascent trajectory for each performance index with $i = 51.6°$

	q	$q\alpha$	$q\beta$	η
Max Final Energy $(\mathscr{E}_f)$	specified	specified	specified	specified
Max Final Mass (m_f)	specified	specified	specified	specified
Max Final Velocity (V_f)	specified	specified	specified	specified
Min Final Time (t_f)	specified	specified	specified	specified

	r_f^*	V_f^*	γ_f^*	m_f
Max Final Energy $(\mathscr{E}_f)$	free	free	specified	specified
Max Final Mass (m_f)	specified	specified	specified	free
Max Final Velocity (V_f)	specified	free	specified	specified
Min Final Time (t_f)	specified	specified	specified	specified

Table 4.5 Constraints values used for testing different performance indices

Constraints:	Values:
Dynamic pressure limit, q	$0 \leq q \leq 18,194.4$ N/m² (380 psf)
$q\alpha$ limit	$\pm35,910$ N/m²-deg (750 psf-deg)
$q\beta$ limit	$\pm35,910$ N/m²-deg (750 psf-deg)
Engine throttle setting, η	$50\% \leq \eta \leq 100\%$
Final orbit, r_f^*	185.2 km
Final velocity, V_f^*	7,793.6 m/s
Final flight-path-angle, γ_f^*	0.0°
Final mass, m_f	37,600 kg

Different PI indeed yielded different results. The minimizing final time PI resulted the shortest ground track as expected (Figure 4.22). The maximizing final mass PI had a long ground track because reducing throttle setting or coasting is a must in order to minimize propellant usage. Even though the maximizing energy PI had a farther range compared to the minimizing time PI as portrayed in Figure 4.22, they both had the same flight time. The maximizing energy PI accomplished this by having a lower final orbit (r_f^*) with higher velocity (V_f^*) as exhibited in Figures 4.23 and 4.24 and Table 4.6. Maximize final mass, velocity and minimize time all had the same orbit altitude as specified, but the flight times are different depending on the PI.
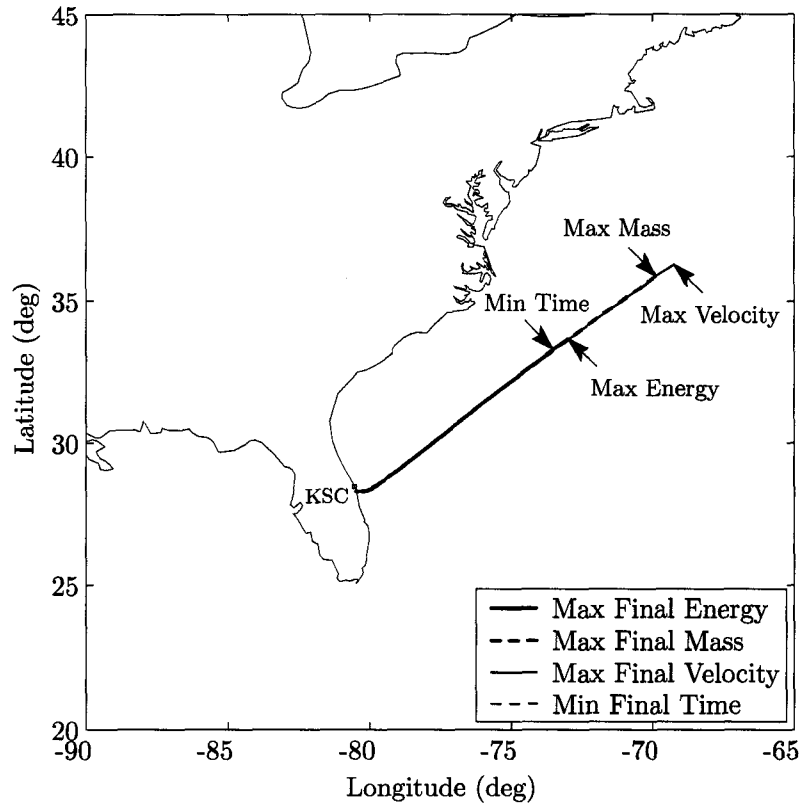
Figure 4.22   Nominal ascent ground tracks with different performance indices for $i = 51.6°$

Table 4.6   Summary of nominal ascent with different performance indices for $i = 51.6°$

	r_f^* (km)	V_f^* (m/s)	Mass (kg)	Flight Time (sec)
Max Final Energy ($\mathscr{E}_f$)	**158.12**	**8,079.33**	37,600.00	326.99
Max Final Mass (m_f)	185.07	7,793.66	**39,146.88**	403.86
Max Final Velocity (V_f)	185.07	**8,137.95**	37,600.00	411.16
Min Final Time (t_f)	185.07	7,793.64	37,600.00	326.99
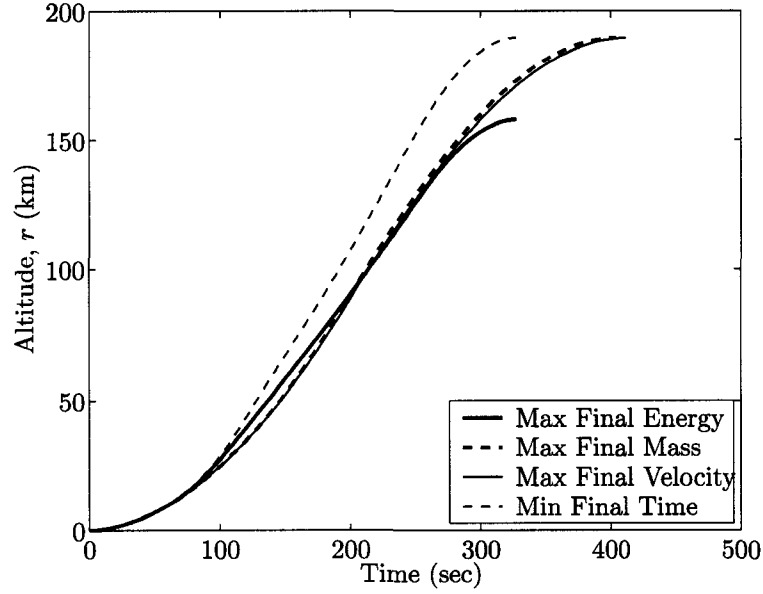
Figure 4.23 Nominal ascent altitude profile for $i = 51.6°$ based
on conditions in Table 4.1 and Table 4.5

The velocity profile rendered in Figure 4.24 can be separated into two categories based on their similarities: ① maximize final energy and minimize final time; and ② maximize final mass and maximize final velocity. It took longer to achieve the same orbital velocity in the maximize final mass case because throttle setting was reduced to minimize propellant usage (Figure 4.26). As for the maximize final velocity case, it is necessary to reduce throttle setting for a period of time in preparation for the final "boost" at the end in order to achieve the highest orbital velocity. The reduced throttle setting and the boost phenomena are due to the highly constrained settings.

The dynamic pressure in Figure 4.27 and $q\alpha$ in Figure 4.28 show all four PI's yielded similar profiles. Since all of them had similar altitude and velocity profiles, thus dynamic pressure profiles are similar.

The Euler angle profiles (Figures 4.29 through 4.31) for all four PI's are similar. The flight-path and side-slip angle profiles are also similar (Figures 4.32 and 4.33). Lastly, all flight-path-angle profiles ended with $\gamma_f^* = 0°$ as specified.
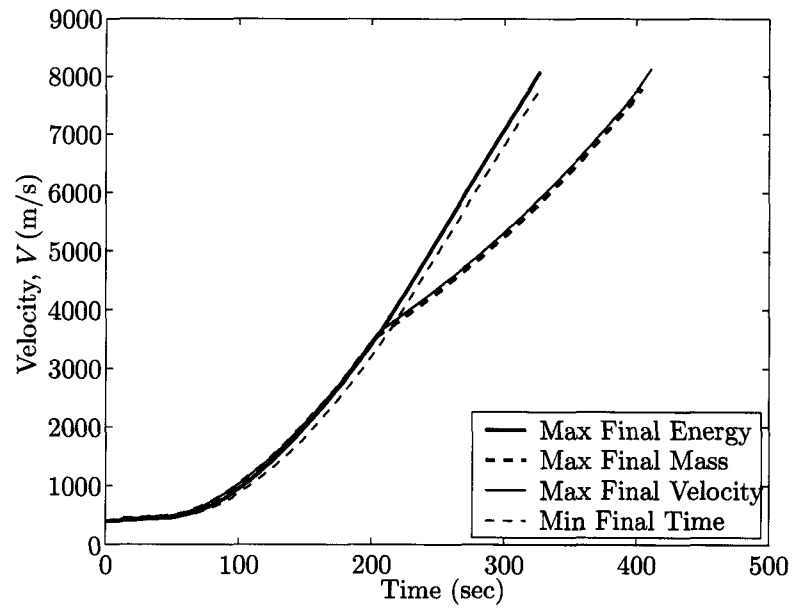
Figure 4.24 Nominal ascent velocity profile for $i = 51.6°$ based on conditions in Table 4.1 and Table 4.5
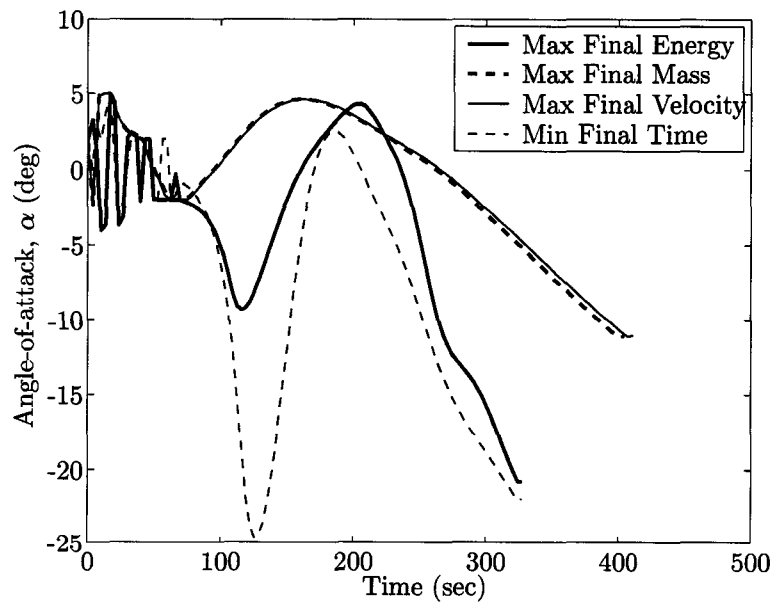
Figure 4.25 Nominal angle-of-attack altitude profile for $i = 51.6°$ based on conditions in Table 4.1 and Table 4.5
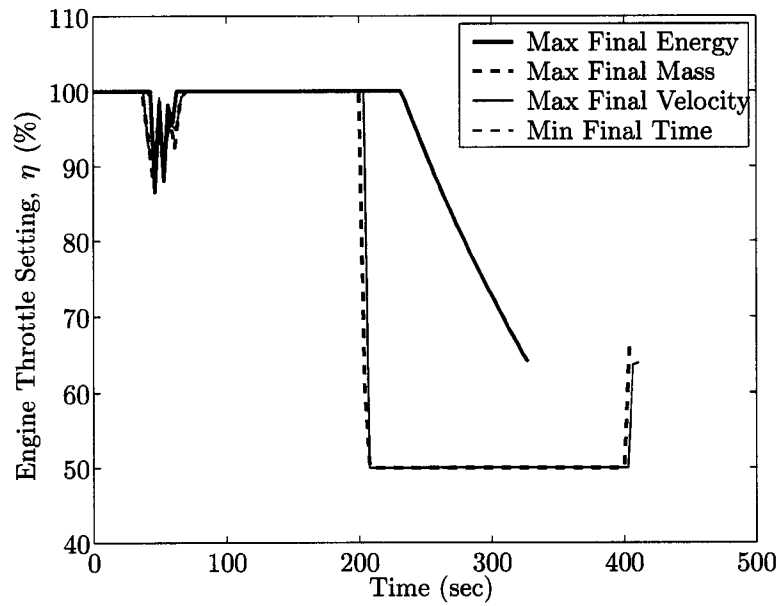
Figure 4.26 Nominal throttle setting altitude profile for $i = 51.6°$ based on conditions in Table 4.1 and Table 4.5
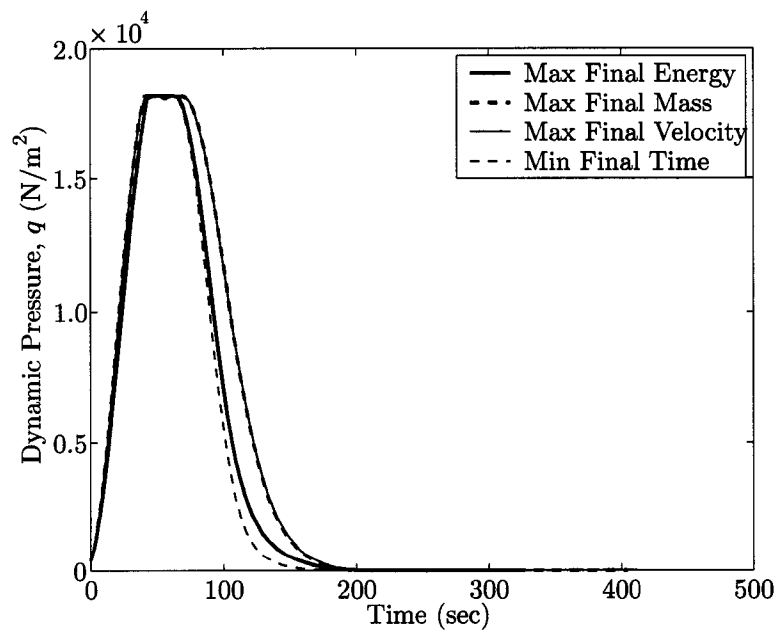
Figure 4.27 Nominal ascent dynamic pressure profile for $i = 51.6°$ based on conditions in Table 4.1 and Table 4.5
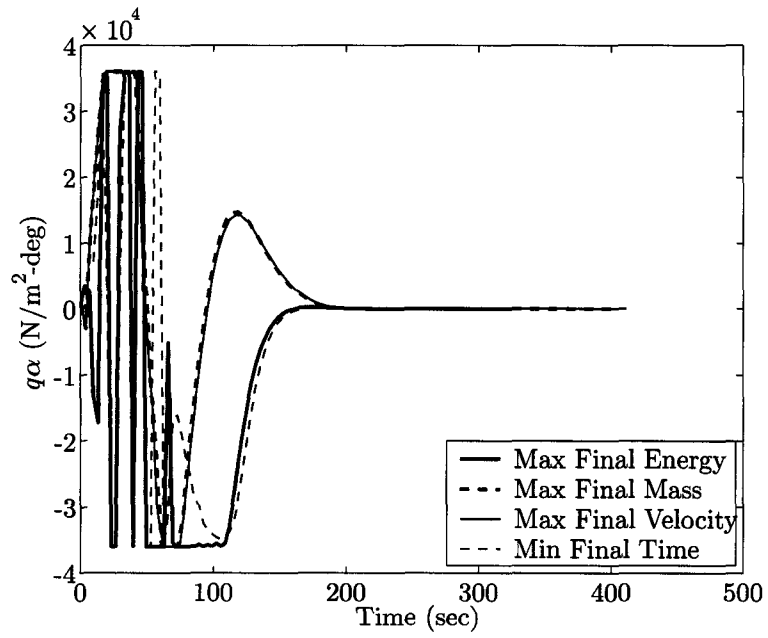
Figure 4.28 Nominal ascent $q\alpha$ profile for $i = 51.6°$ based on conditions in Table 4.1 and Table 4.5
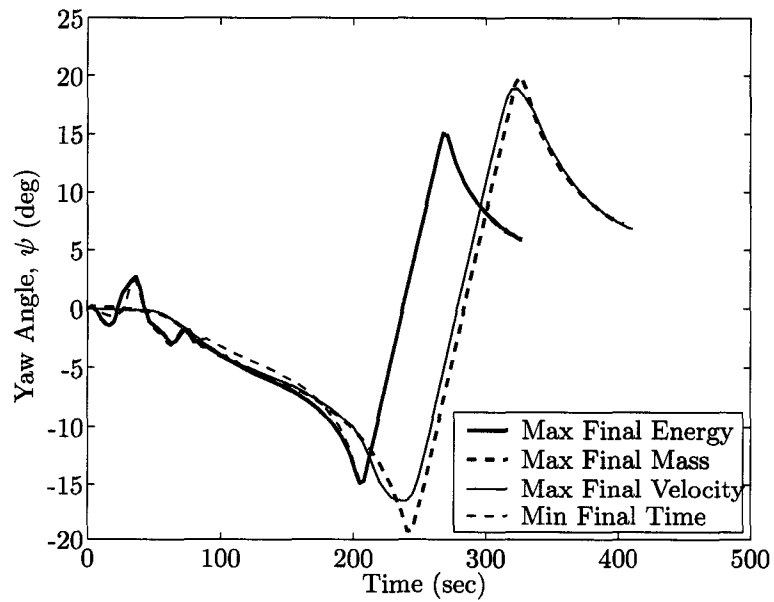
Figure 4.29 Nominal ascent yaw angle profile for $i = 51.6°$ based on conditions in Table 4.1 and Table 4.5
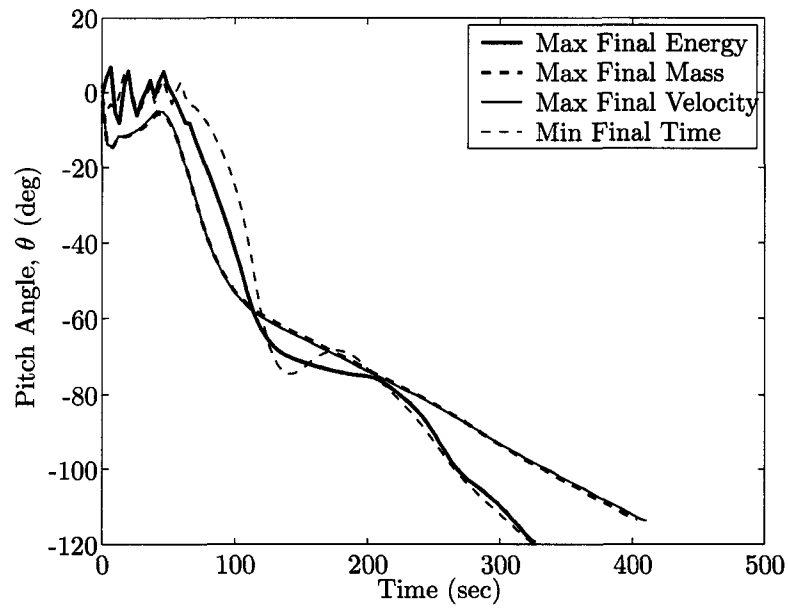
Figure 4.30   Nominal ascent pitch angle profile for i = 51.6°
based on conditions in Table 4.1 and Table 4.5
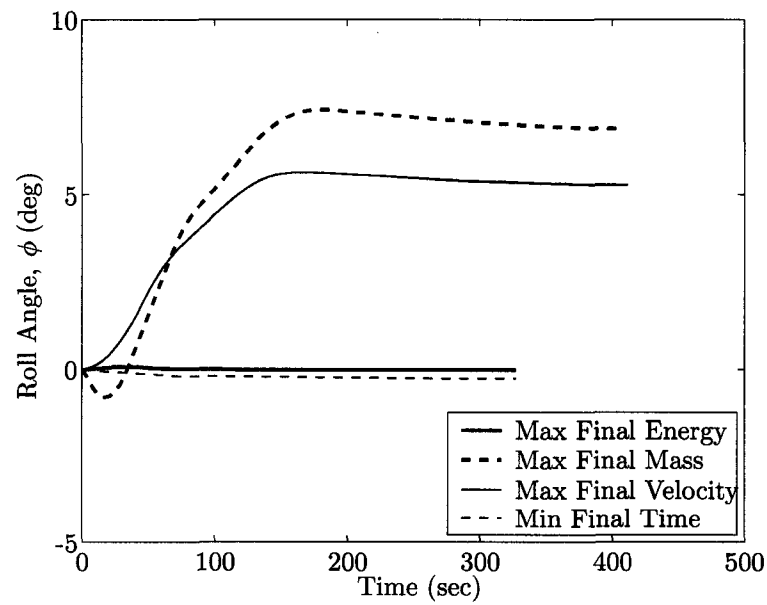
Figure 4.31   Nominal ascent roll angle profile for i = 51.6°
based on conditions in Table 4.1 and Table 4.5
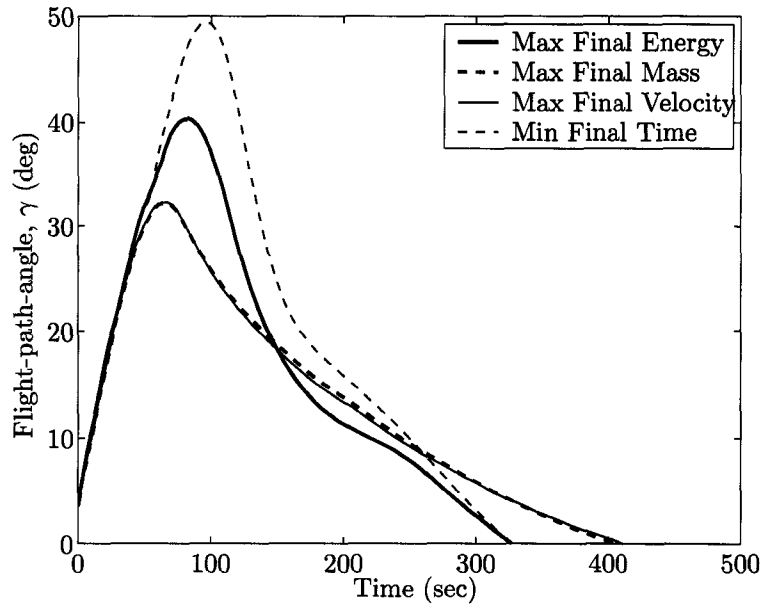
Figure 4.32   Nominal   ascent   flight-path-angle   profile   for
$i = 51.6°$ based on conditions in Table 4.1 and
Table 4.5
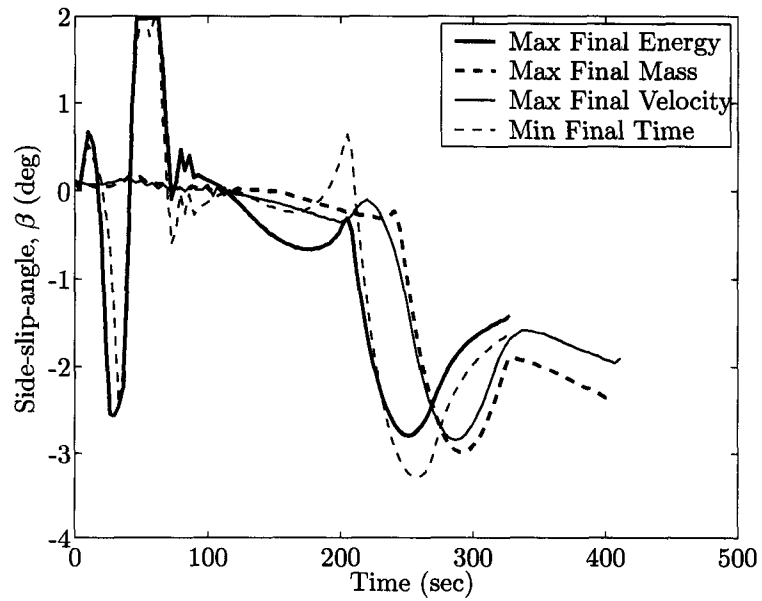
Figure 4.33   Nominal ascent side-slip-angle profile for $i = 51.6°$
based on conditions in Table 4.1 and Table 4.5

4.6 Abort-to-Orbit Results

Abort-to-orbit (ATO) is said to be the most preferable abort mode amongst all the abort modes because ATO flight profile deviates the least from a nominal ascent trajectory. ATO mode avoids the excessive vehicle movement that may inherently affect the structural integrity of the spacecraft. Furthermore, this abort mode does not require the drastic pitch change required in the return-to-launch-site (RTLS) mode or the large yaw needed in the transoceanic-abort-landing (TAL) mode. The Mission Control Center (MCC) always want the safest choice for the crew and the spacecraft. The abort mode chosen by MCC (for the shuttle) or autocommander (for the X-33) is the safest mode that can be accomplished with the remaining vehicle performance.

The initial conditions used for the ATO ascent trajectory are listed in Table 4.7 and the same equality and inequalities constraints are imposed as the nominal ascent trajectories (Table 4.2). The earliest time possible to commence ATO with $i = 51.6°$ is determined to be 110.23 sec after clearing the tower. The reason for the initiation of ATO is due to the loss of an engine for this research. The engine throttle setting (η) parameter refers to the operational usage of the remaining good engine.

Table 4.7   Initial conditions for ATO ascent trajectory
with $i = 51.6°$ at $t = 110.23$ sec

$J = $ min t_f			
abort time $=$	110.23 sec	# of engines $=$	1
$x =$	6,405,297.47 m	$i =$	51.60°
$y =$	31,436.96 m	yaw (ψ) $=$	$-3.55°$
$z =$	58,568.47 m	pitch (θ) $=$	$-50.17°$
$V_x =$	589.79 m/s	roll (ϕ) $=$	$-3.55°$
$V_y =$	246.47 m/s	mass (m) $=$	91,864.16 kg
$V_z =$	1,058.90 m/s	throttle setting (η) $=$	100%

A three-dimensional (3D) ATO and nominal flight profiles along with their respective ground tracks are pictured in Figure 4.34. Both ATO and nominal trajectories have the same imposed equality and inequality constraints. The nominal case reached the MECO point in 323.14 sec while the ATO case reached it in 511.67 sec because it was operating with only one good engine. The resemblance of these two scenarios is best illustrated in the ground track comparison.
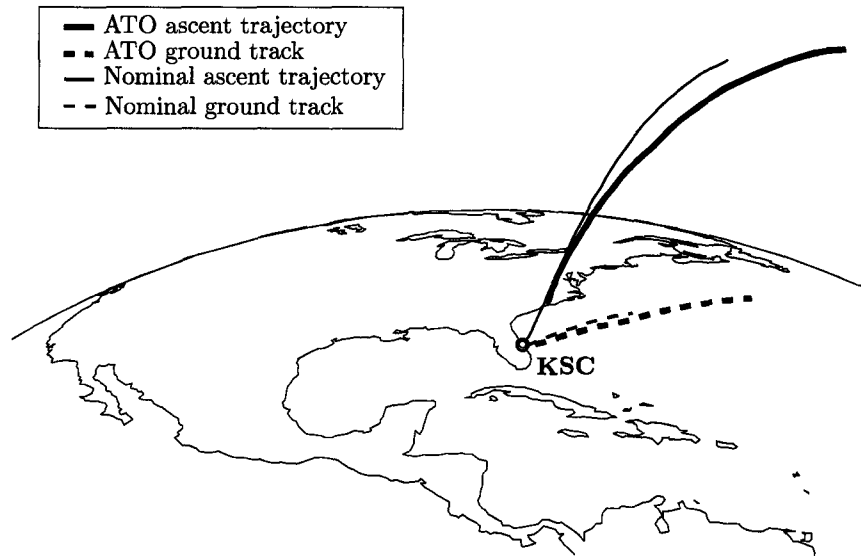
Figure 4.34   ATO ascent trajectory and ground track based on
              conditions in Tables 4.8 and 4.9 compared to those
              of nominal with q constraint

The altitude (Figure 4.35) and velocity (Figure 4.36) profiles for ATO and nominal ascent are identical in history, except ATO took longer to reach the same values. Just as a reminder, the α constraint of $-4° \leq \alpha \leq 12°$ for up to altitude of 11 km is no longer applicable in ATO cases because 11 km corresponds to approximately 70 seconds into the flight. Thus, the spacecraft is no longer subjected to the aerodynamic forces

outside the atmosphere. The α profile (Figure 4.37) for ATO showed slower pitch down movement (spacecraft continued to fly upward for a longer period of time before pitching down).

With only one operational engine, the engine throttle setting profile in Figure 4.38 shows 100% usage throughout MECO point. The dynamic pressure (Figure 4.39) at high altitudes is almost zero as the density (ρ) term in $q = \frac{1}{2}\rho V^2$ is very small. Thus there is not much change in the q and $q\alpha$ profiles.

As for the Euler angles (Figures 4.41 through 4.43) and aerodynamic angle (Figures 4.44 and 4.45) profiles, the time history for each of these profiles is similar to those of the nominal case, but took longer to reach the same value. The roll angle (or the roll rate) is purposely set to zero to show that roll maneuver has little effect in ascent trajectories.
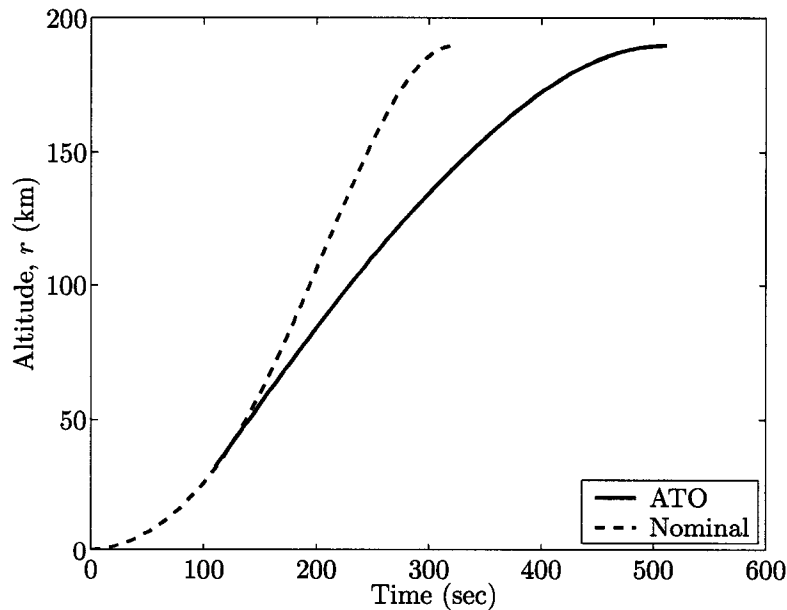
Figure 4.35   ATO altitude profile based on conditions in
Tables 4.8 and 4.9
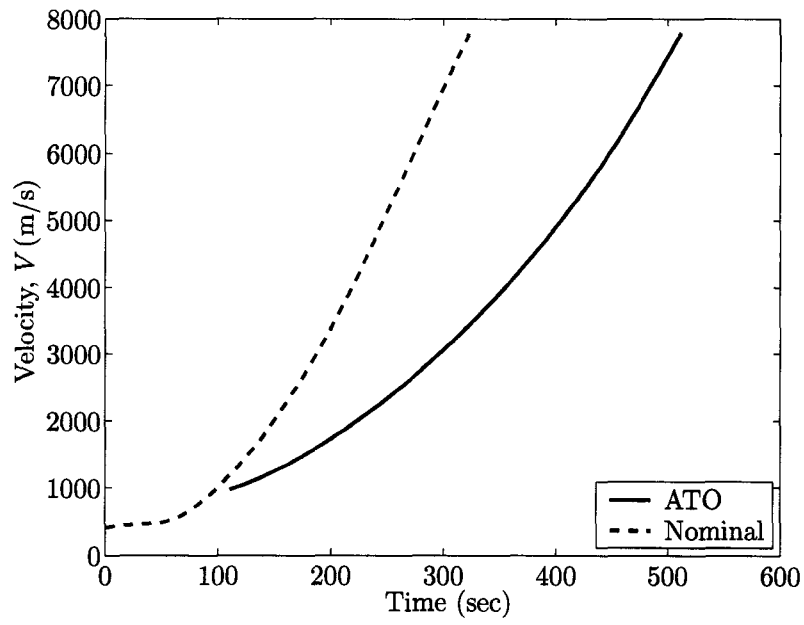
Figure 4.36   ATO velocity profile based on conditions in
Tables 4.8 and 4.9
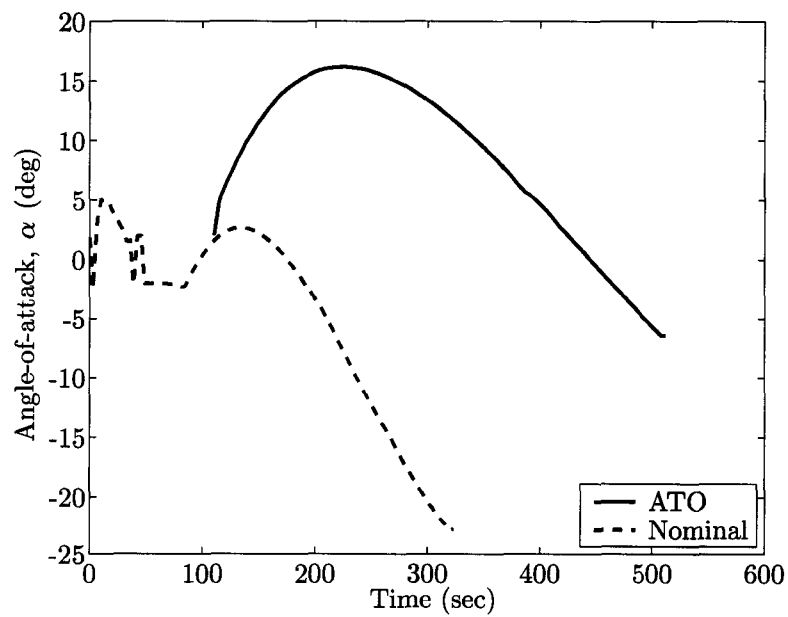
Figure 4.37   ATO angle-of-attack profile based on conditions
in Tables 4.8 and 4.9
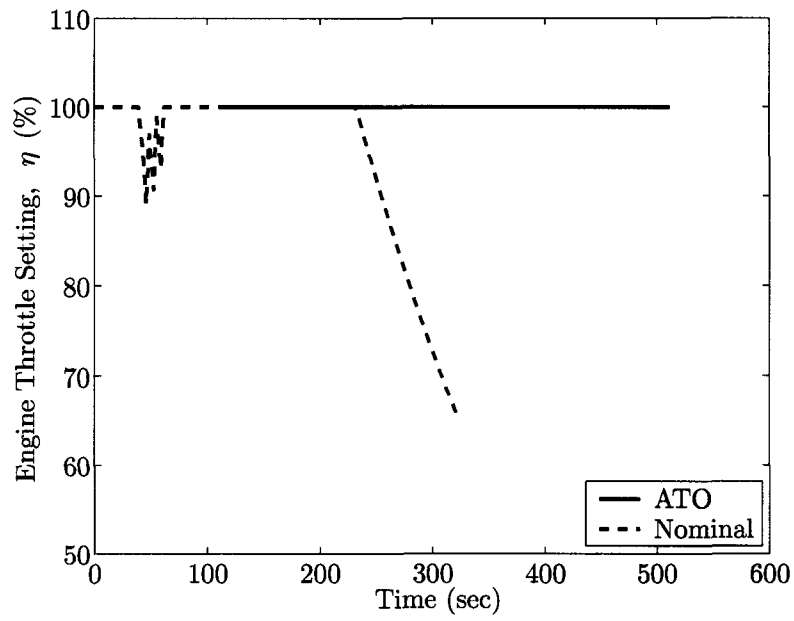
Figure 4.38   ATO throttle setting profile based on conditions in Tables 4.8 and 4.9
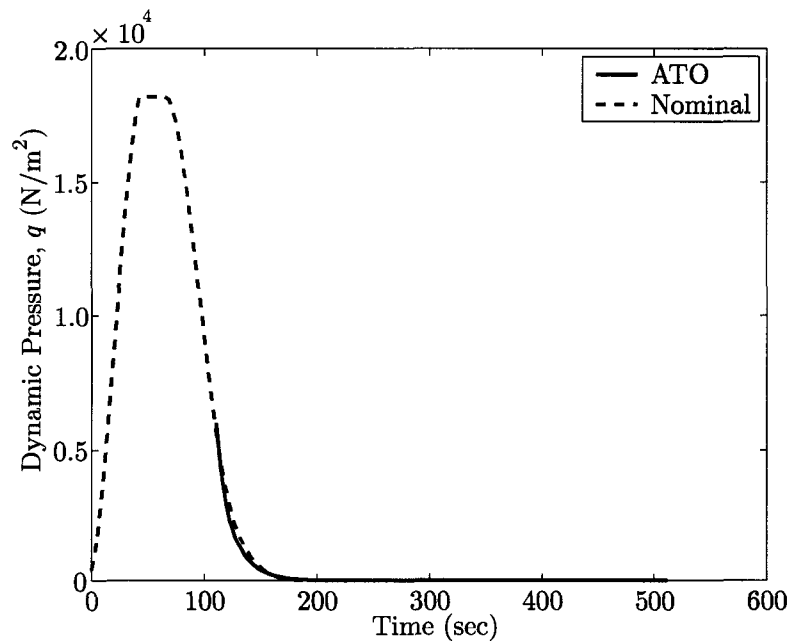
Figure 4.39   ATO dynamic pressure profile based on conditions in Tables 4.8 and 4.9
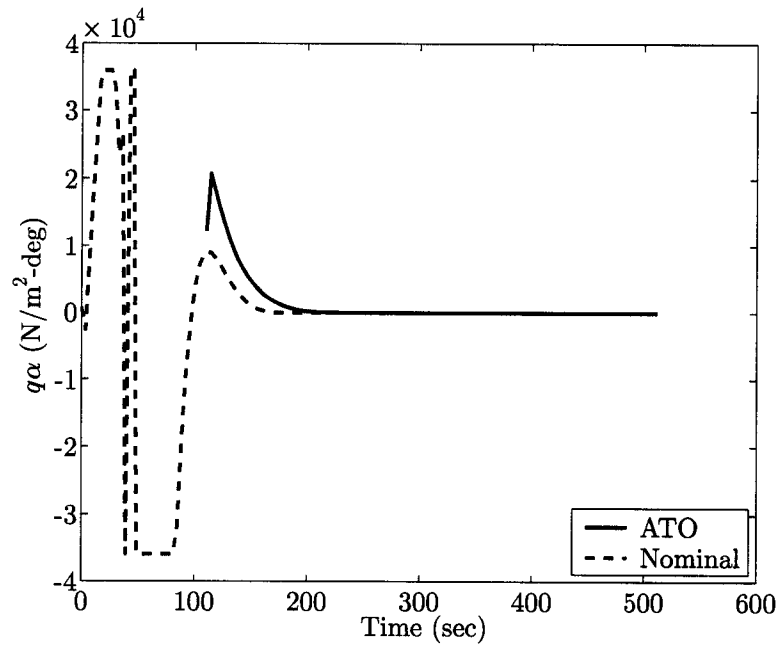
Figure 4.40 ATO $q\alpha$ profile based on conditions in Tables 4.8 and 4.9
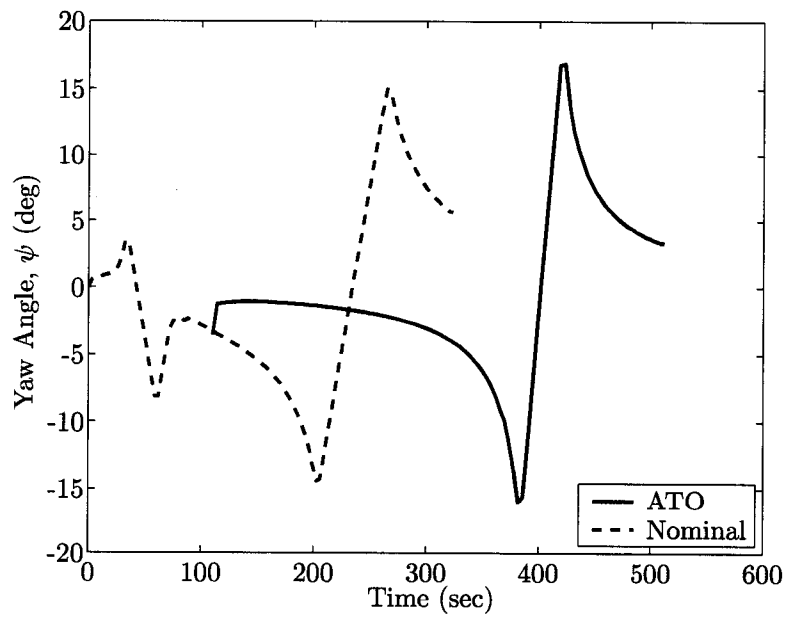
Figure 4.41 ATO yaw angle profile based on conditions in Tables 4.8 and 4.9
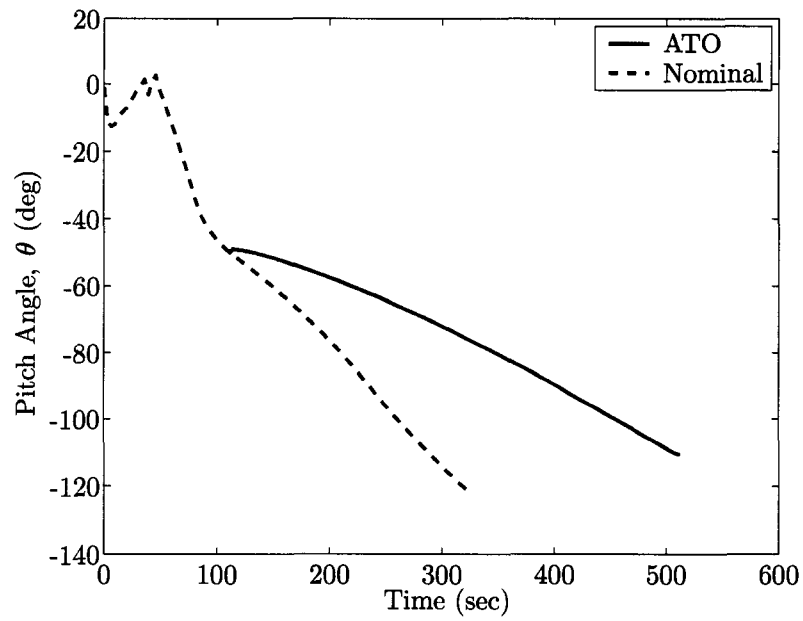
Figure 4.42   ATO pitch angle profile based on conditions in
Tables 4.8 and 4.9
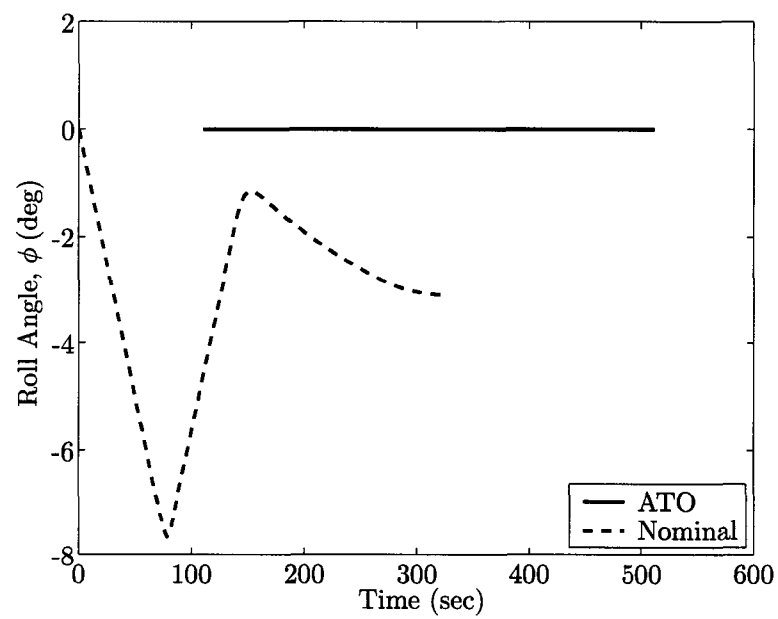
Figure 4.43   ATO roll angle profile based on conditions
in Tables 4.8 and 4.9
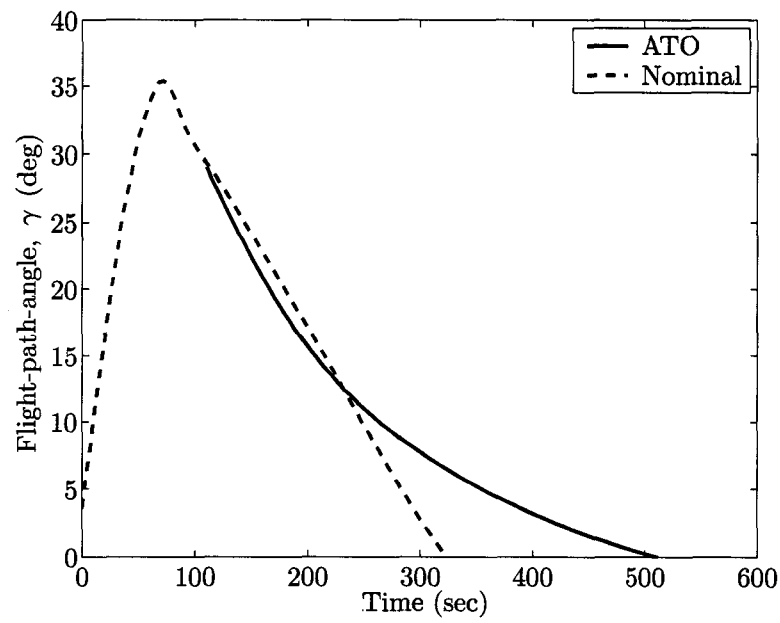
Figure 4.44 ATO flight-path-angle profile based on conditions in Tables 4.8 and 4.9
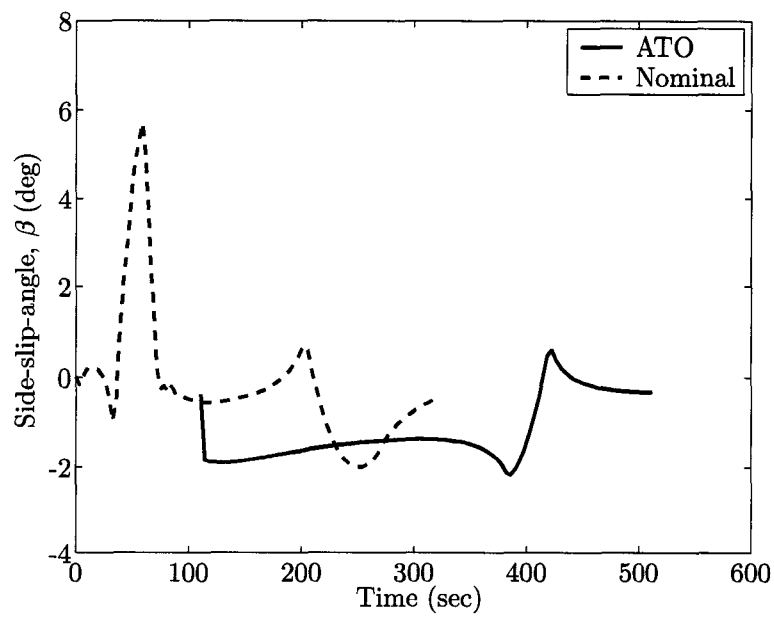
Figure 4.45 ATO side-slip-angle profile based on conditions in Tables 4.8 and 4.9

4.7 Transoceanic-Abort-Landing Results

The earliest abort time for a transoceanic-abort-landing (TAL) is determined to be 47.65 seconds after clearing the tower with intended orbital insertion condition of $i = 51.6°$. If an engine failure occurs before $t = 47.65$ sec, a return-to-launch-site mode may be selected by autocommander. Table 4.8 shows the initial conditions corresponding to the earliest TAL abort time with minimizing final time, t_f, as the optimal trajectory performance index. Table 4.9 lists the equality as well as the inequality constraints imposed on all TAL trajectories. The typical final altitude (r_f^*), velocity (V_f^*), and flight-path-angle (γ_f^*) used in nominal and ATO cases do not apply here. Instead, these variables are to be merged onto NEP using Equations (4.28) to (4.30) on page 45.

Table 4.8 Initial conditions for TAL trajectories with
$i = 51.6°$ at $t = 47.65$ sec

$J = \min t_f$			
abort time =	47.65 sec	# of engines =	1
$x =$	6,378,842.73 m	$i =$	51.60°
$y =$	13,269.56 m	yaw $(\psi) =$	0.22°
$z =$	13,330.21 m	pitch $(\theta) =$	−1.00°
$V_x =$	215.32 m/s	roll $(\phi) =$	N/A
$V_y =$	291.19 m/s	mass $(m) =$	110,586.10 kg
$V_z =$	294.09 m/s	throttle setting $(\eta) =$	100%

Table 4.9 Constraints imposed on all TAL trajectories

Dynamic pressure limit, q	$0 \leq q \leq 18,194.4$ N/m^2 (380 psf)
$q\alpha$ and $q\beta$ limits	$\pm35,910$ N/m^2-deg (750 psf-deg)
Angle-of-attack, α	$-4° \leq \alpha \leq 12°$ (up to 11 km)
Engine throttle setting, η [†]	$50\% \leq \eta \leq 100\%$

[†] except for multi-phase cases

4.7.1 Burn-Coast-Burn Maneuver for $i = 51.6°$

The chosen TAL landing sites for this research are the ones approved by NASA as stated in Section 2.1.2 on page 17 — Banjul, Ben Guerir, Lajes, Morón and Zaragoza. Figures 4.46 through 4.56 are based on the initial conditions summarized in Table 4.8. These cases all have three phases: burn, coast and burn (BCB) as shown later in the engine throttle setting profiles (Figure 4.56).

A TAL landing site is typically decided based on the orbital inclination (unless weather is a concern). Higher inclination launch aborts will land in the northern regions (i.e., Zaragoza or Morón) while lower inclination launch aborts will land in the southern regions (i.e., Banjul). This is due to its geographical location corresponding to the entry ground track. However, this is not the case for the X-33 Advanced Technology Demonstrator. Figure 4.46 shows the X-33 has much greater maneuverability compared to the current Space Shuttle. The combination of its powerful LAREs and aerodynamic efficient body shape allow the X-33 to make to any of the five NASA approved TAL site regardless of launch inclination.

Figures 4.47, 4.48 and 4.49 illustrate the histories of how altitude, velocity and flight-path-angle for different TAL destinations intersect with NEP as discussed in Section 4.2 on page 44. Notice that the intersecting portion of all three guidance parameters is very narrow and can even be approximated linearly. Figure 4.47 also shows that except for Lajes, the other four destinations will require flying to a higher altitude before intersecting NEP. This is due to the higher velocity needed in order to glide to these four destinations since they are further away compared to Lajes, as can be seen in Figure 2.3 on page 18.
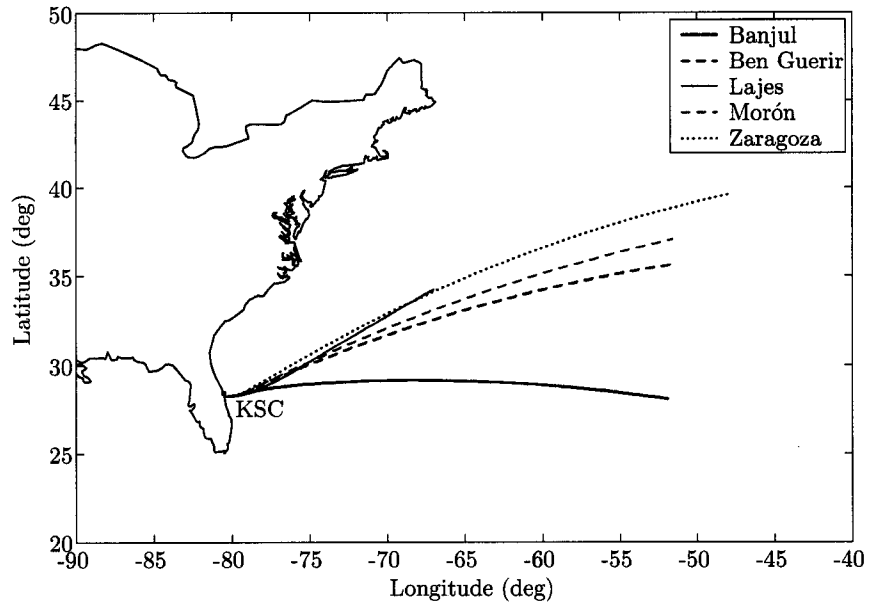
Figure 4.46   BCB TAL ground track profiles based on conditions in Tables 4.8 and 4.9
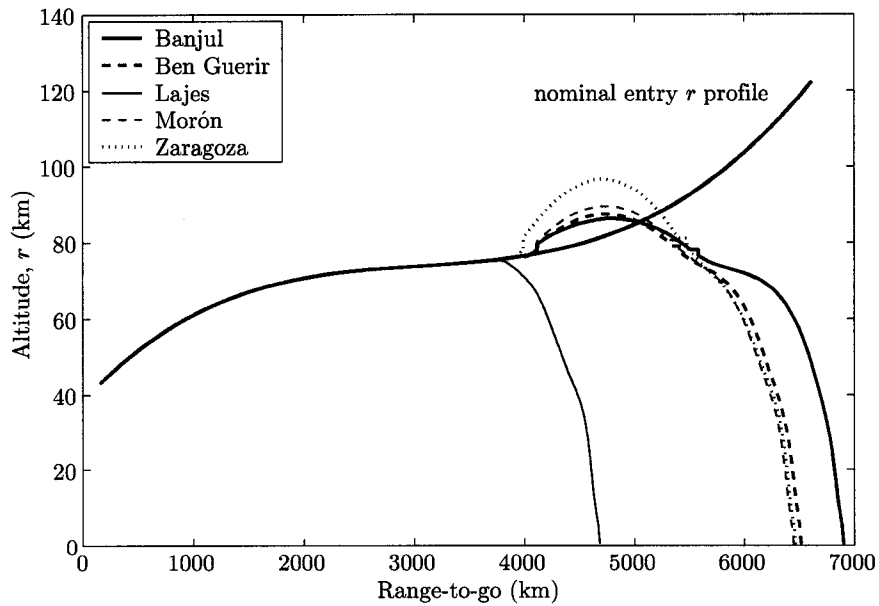
Figure 4.47   BCB TAL altitude trajectories intersecting NEP based on conditions in Tables 4.8 and 4.9

Figure 4.48 delineates Lajes intersecting at a lower velocity. Again, this is due to Lajes being closer compared to other four designations, thus, lower velocity is enough to reach the target. Figure 4.49 exhibits all five cases have similar final flight-path-angle $\left(-0.46° \leq \gamma_f^* \leq -0.36°\right)$. This is expected because the vehicle should be at a horizontal position ready for the gliding phase. Detailed MECO conditions can be found in Appendix C, Section C.3 starting on page 279.
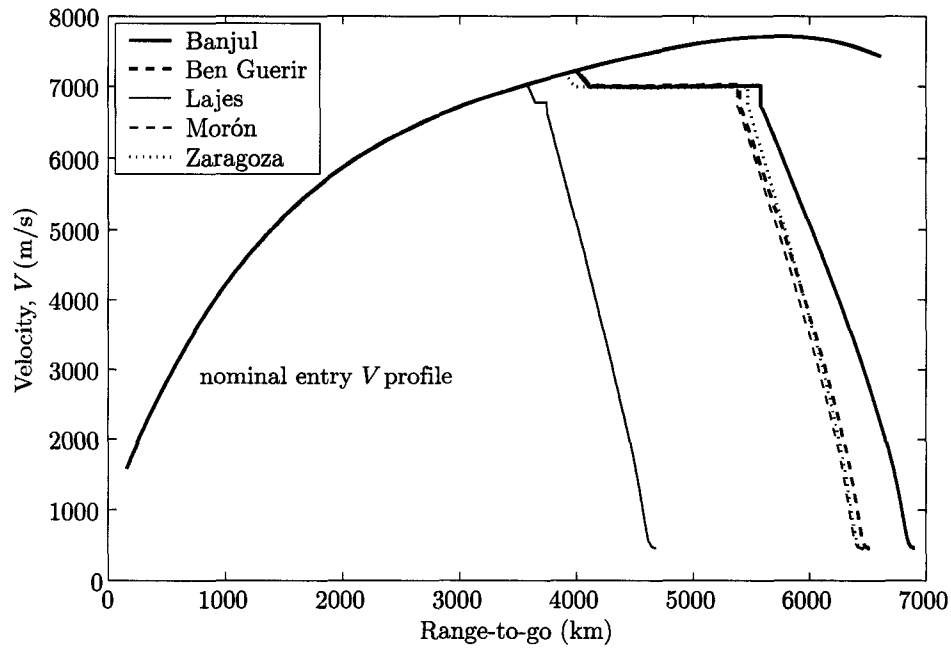
Figure 4.48   BCB TAL velocity trajectories intersecting NEP
based on conditions in Tables 4.8 and 4.9

Figures 4.50 through 4.52 depict the three Euler angle profiles. The end of yaw angle profile shows the last chance to re-align with landing site. The pitch angle profile shows all five trajectories have negative pitch angles at MECO. This makes sense because the spacecraft should be pointing down at the MECO point and be ready to glide to their respective destinations. Roll angle (or roll rate) is purposely set to zero. This is to show that roll angle has very little impact on ascent trajectory.
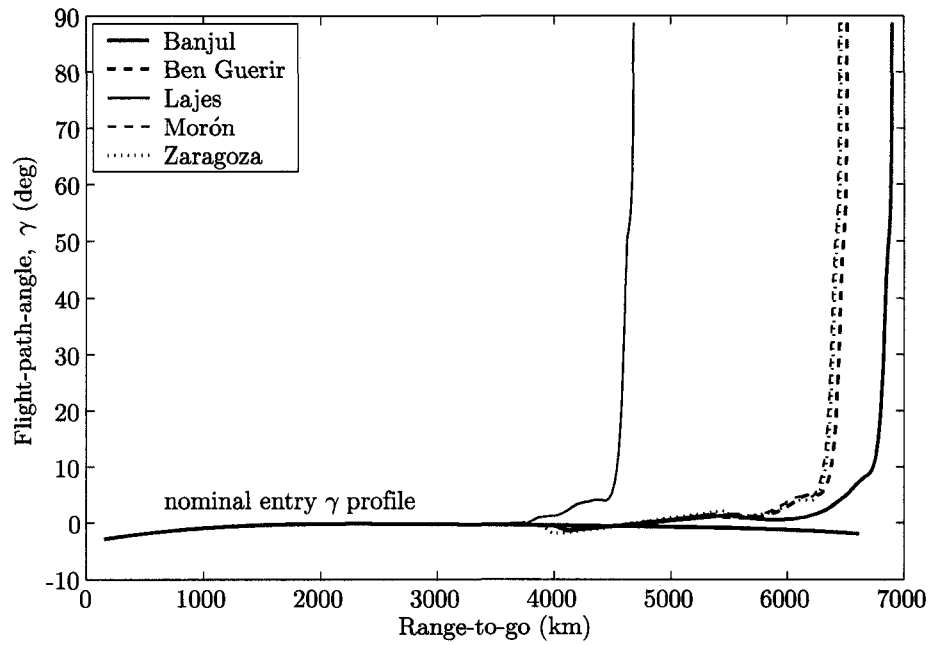
Figure 4.49   BCB TAL flight-path-angle trajectories intersecting NEP based on conditions in Tables 4.8 and 4.9
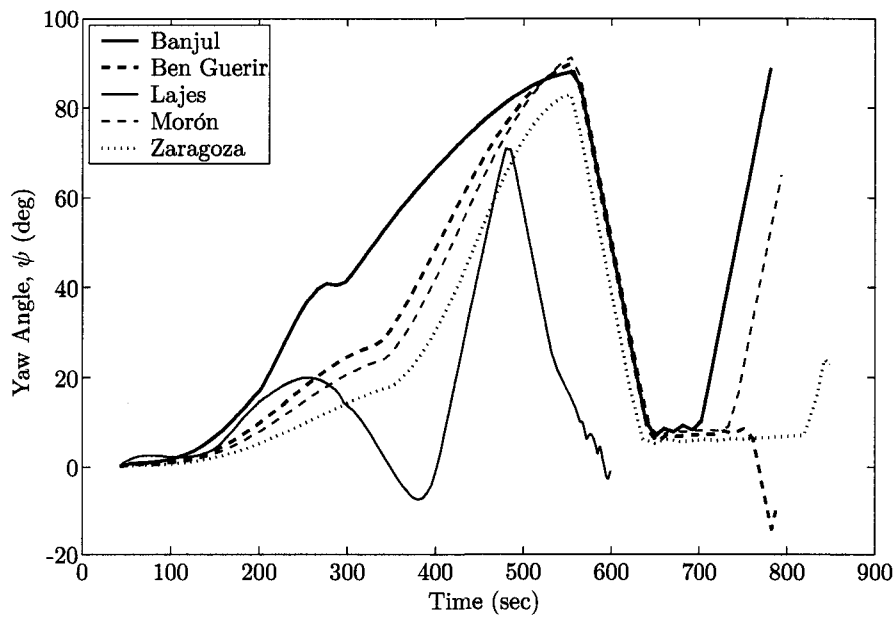
Figure 4.50   BCB TAL yaw angle profiles based on conditions in Tables 4.8 and 4.9
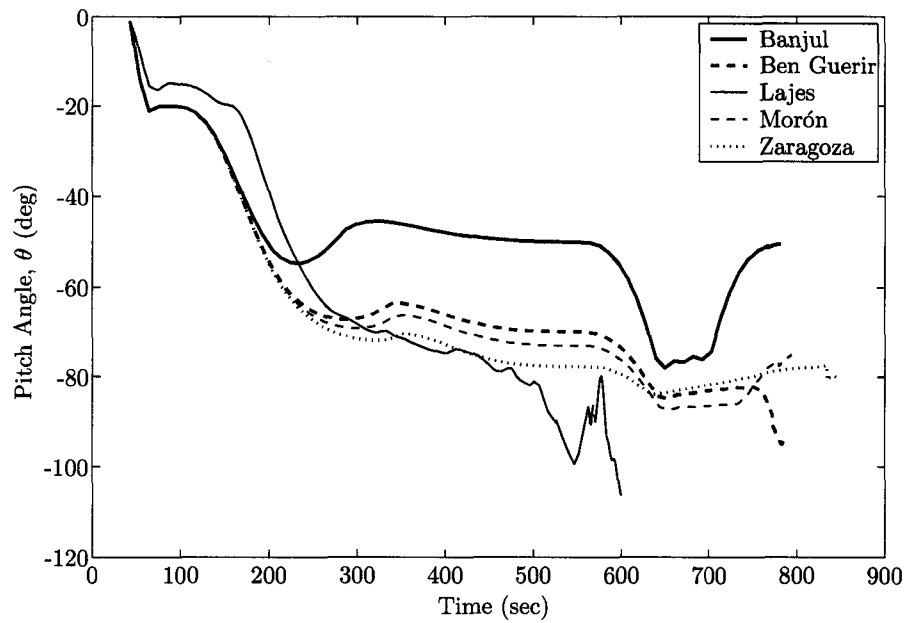
Figure 4.51 BCB TAL pitch angle profiles based on conditions in Tables 4.8 and 4.9
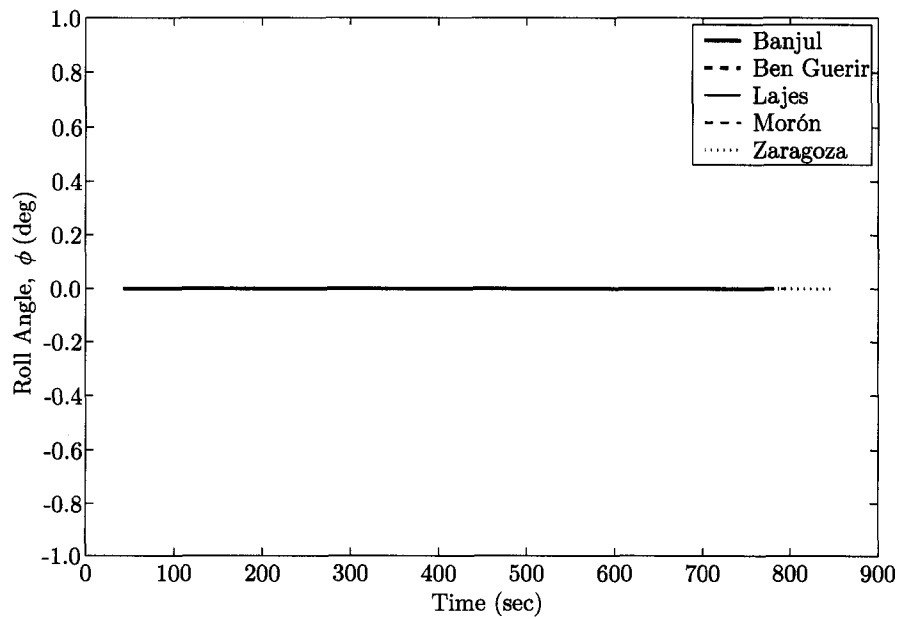
Figure 4.52 BCB TAL roll angle profiles based on conditions in Tables 4.8 and 4.9

Figures 4.53, 4.54 and 4.56 illustrate the histories of inequality constraints $q\alpha$ and

η, respectively. As discussed in Section 4.3 on page 49, the dynamic pressure term q

is a function of density and velocity. Since Banjul, Ben Guerir, Morón and Zaragoza

require reaching a higher altitude followed by a dive to achieve proper velocity, these four

cases have reached the maximum $q\alpha$ constraint as shown in Figure 4.54. Again, Lajes is

closer and does not require the high altitude and velocity compared to the other ones,

accordingly, maximum $q\alpha$ constraint is not attained. Referring back to Figure 4.46,

Banjul is the lowest destination amongst the five and Zaragoza is the highest. As a

result, Banjul's trajectory deviated the most from the nominal trajectory and Zaragoza

deviated the least.
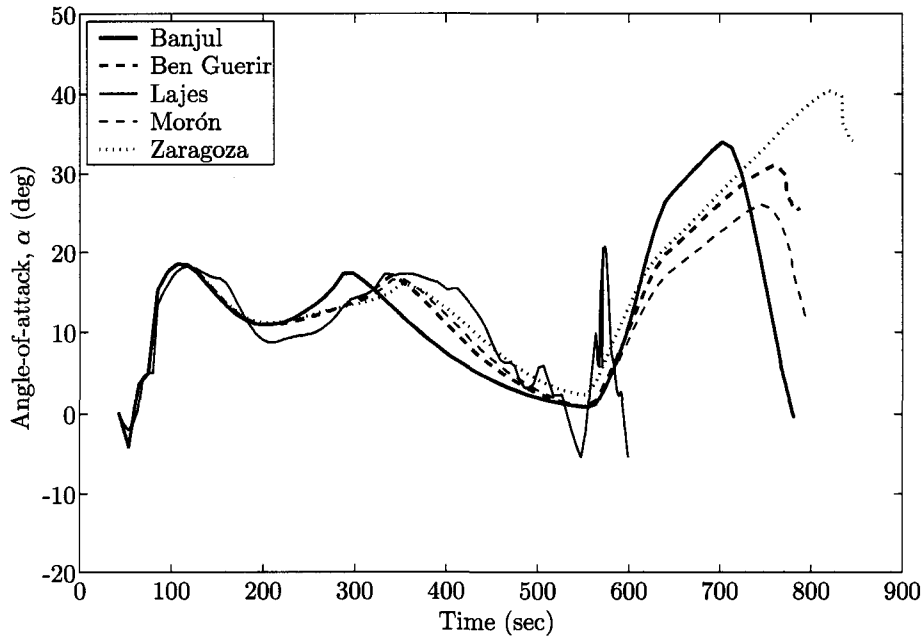
Figure 4.53 BCB TAL angle-of-attack inequality constraint
profiles based on conditions in Tables 4.8 and 4.9
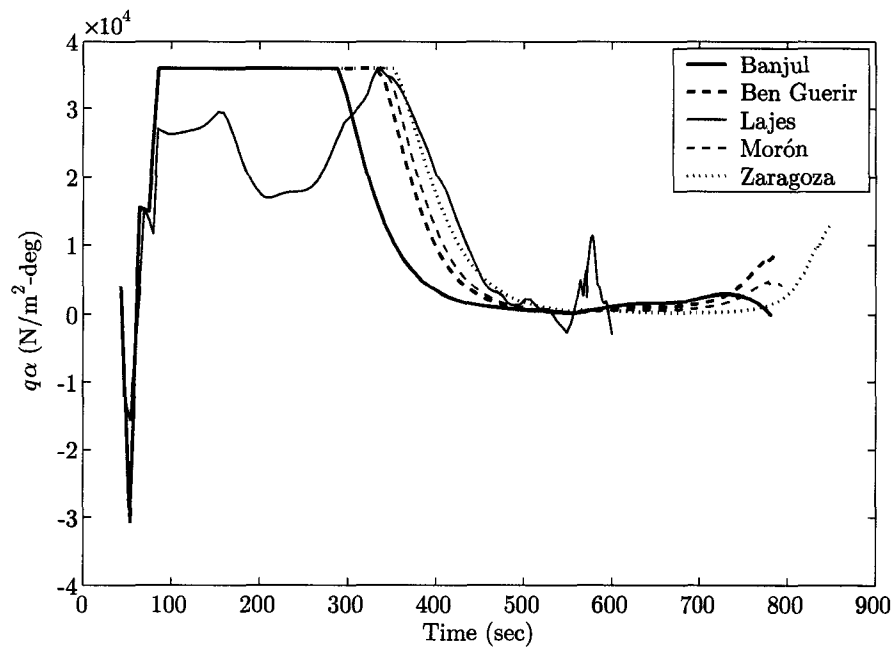
Figure 4.54   BCB TAL $q\alpha$ inequality constraint profiles based on conditions in Tables 4.8 and 4.9
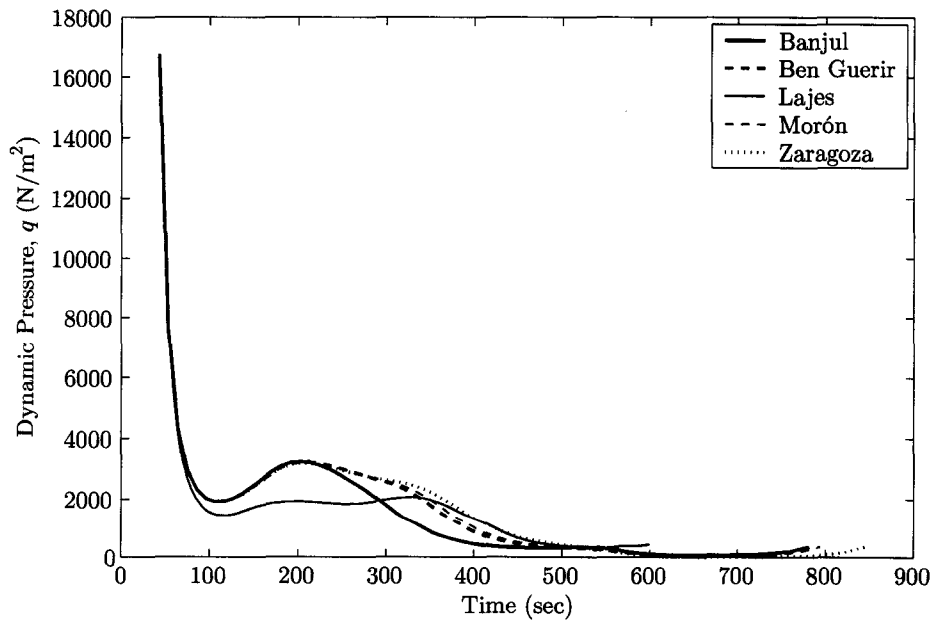
Figure 4.55   BCB TAL dynamic pressure inequality constraint profiles based on conditions in Tables 4.8 and 4.9

Even though the XRS-2200 linear aerospike rocket engine (LARE) does not have re-start capability, the burn-coast-burn (BCB) maneuver may still be used to analyze the feasibility of using such maneuver to intersect nominal entry profile. Figure 4.56 delineates all five cases have full engine throttle setting for the first phase, coasting in the second phase, and a short burn in the third phase to make final necessary course corrections. Full throttle in the first phase is expected because the performance index is minimizing final time, t_f.
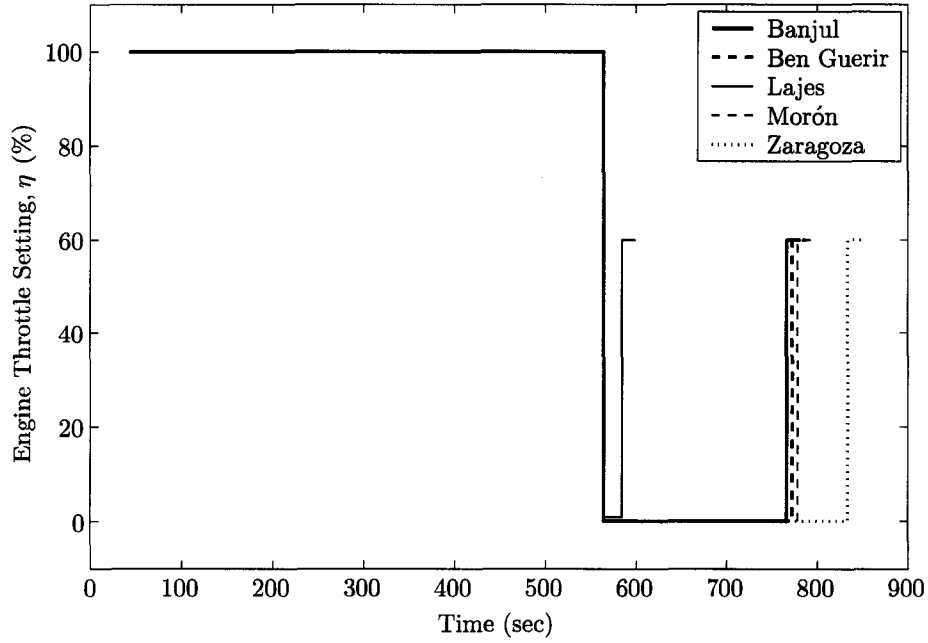
Figure 4.56 BCB TAL engine throttle setting inequality constraint profiles based on conditions in Tables 4.8 and 4.9

4.7.2 Burn-Coast Maneuver for $i = 51.6°$

Figures 4.57 through 4.67 are also based on the initial conditions specified in Table 4.8 and constraints in Table 4.9. These cases however all have two phases: a burn followed by a coast (BC) as shown later in the engine throttle setting profile (Figure 4.67). Even though the BC maneuver is possible as shown in this case, it is less desirable compared to the BCB maneuver because the lack of last course correction before MECO.
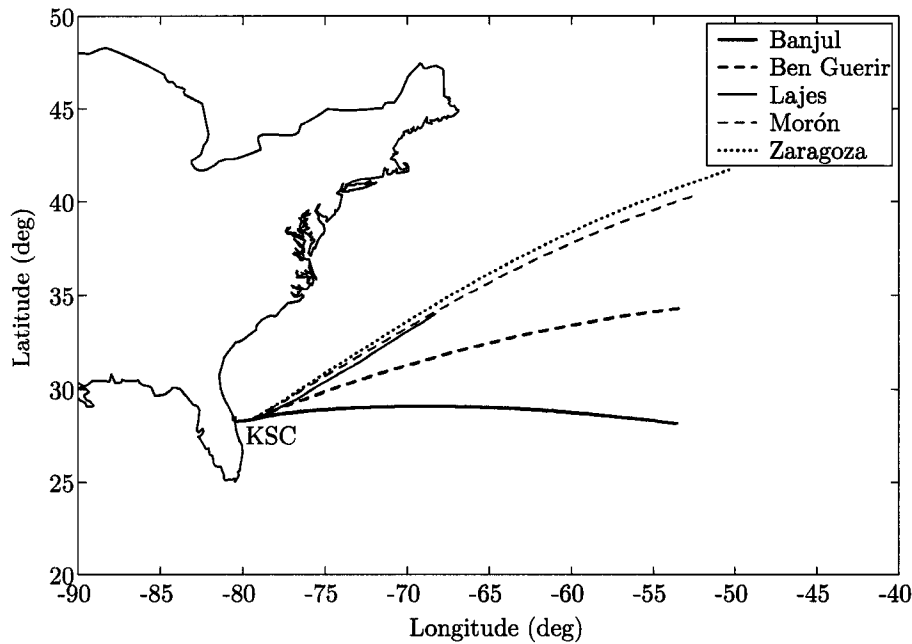
Figure 4.57 BC TAL ground tracks based on conditions in Tables 4.8 and 4.9

Figures 4.58, 4.59 and 4.60 depict similar profiles to those of BCB. All three trajectories intersected NEP at lower values. Again, the intersecting portion of all three guidance parameters is very narrow and can be approximated linearly. Figure 4.58 also shows that except for Lajes, all other four destinations will require flying to a slightly

higher altitude before intersecting NEP. Figure 4.59 delineates Lajes intersected at a lower velocity. This is because Lajes is closer compared to other four designations. One unequivocally noticeable difference is that there are no "boost" at the end just before intersecting NEP in any BC maneuver cases. Figure 4.60 shows all five cases have similar final flight-path-angle.
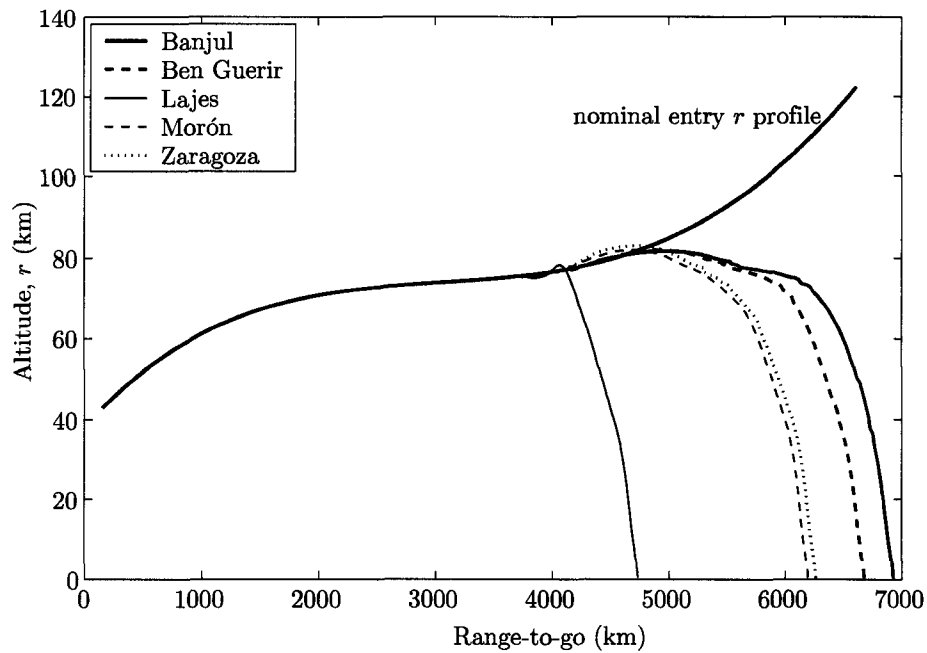
Figure 4.58   BC TAL altitude trajectories intersecting NEP based on conditions in Tables 4.8 and 4.9
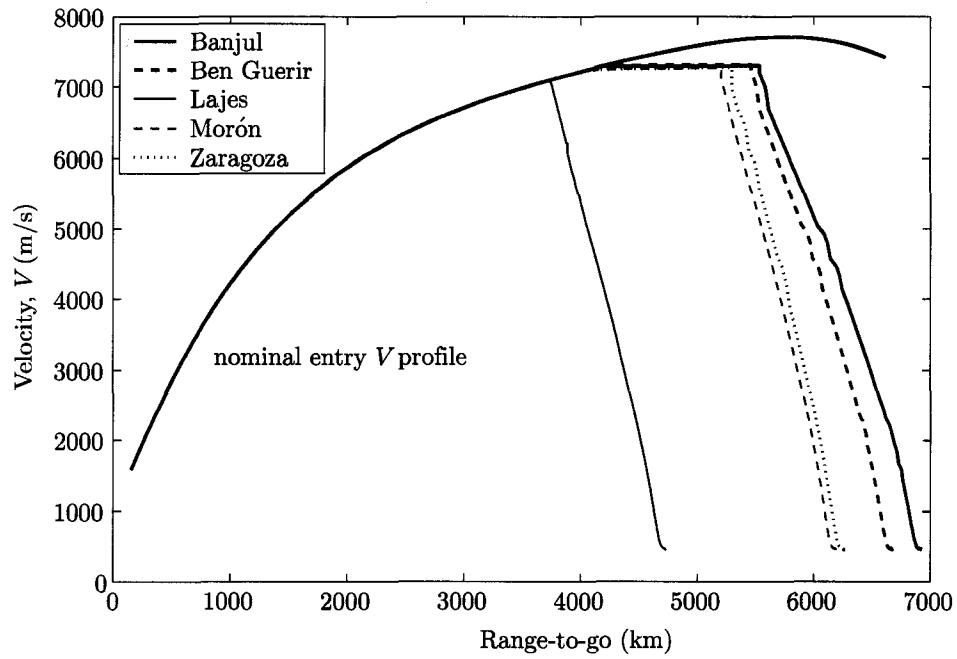
Figure 4.59   BC TAL velocity trajectories intersecting NEP based on conditions in Tables 4.8 and 4.9
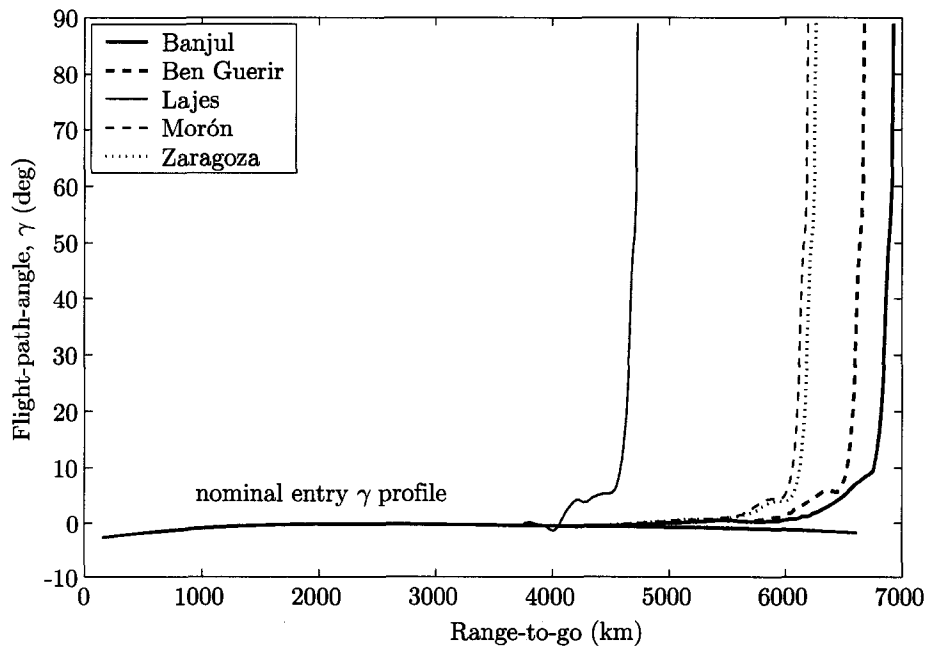
Figure 4.60   BC TAL flight-path-angle trajectories intersecting NEP based on conditions in Tables 4.8 and 4.9

Furthermore, BC will require a larger yaw maneuver (Figure 4.61) in the first phase because it needs to align itself with the target before the coast phase begins (engines are cut-off when coast begins). The pitch angle profile (Figure 4.62) is similar to that of BCB. However, instead of a last correction of either pitching up or down before MECO, BC pitch remains coasting. Once again, roll angle (or roll rate in (Figure 4.61) is purposely set to zero. This is to show that roll angle has very little impact on ascent trajectory.
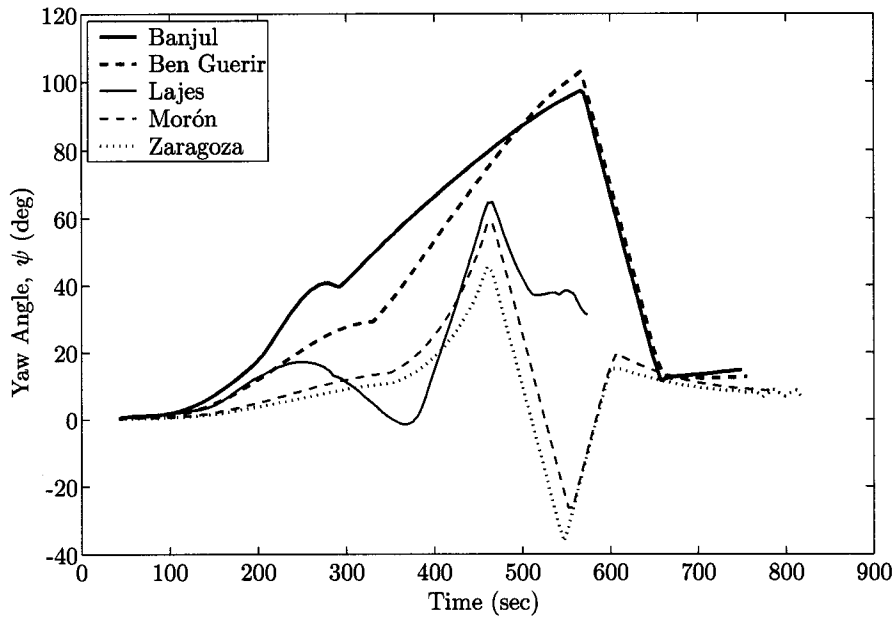
Figure 4.61   BC TAL yaw angle profiles based on conditions
in Tables 4.8 and 4.9
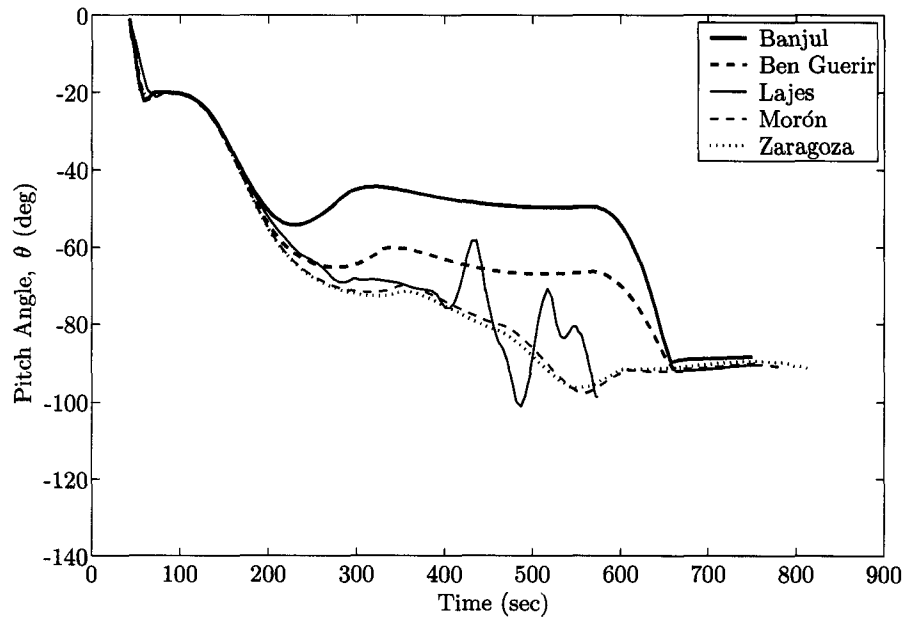
Figure 4.62   BC TAL pitch angle profiles based on conditions in Tables 4.8 and 4.9
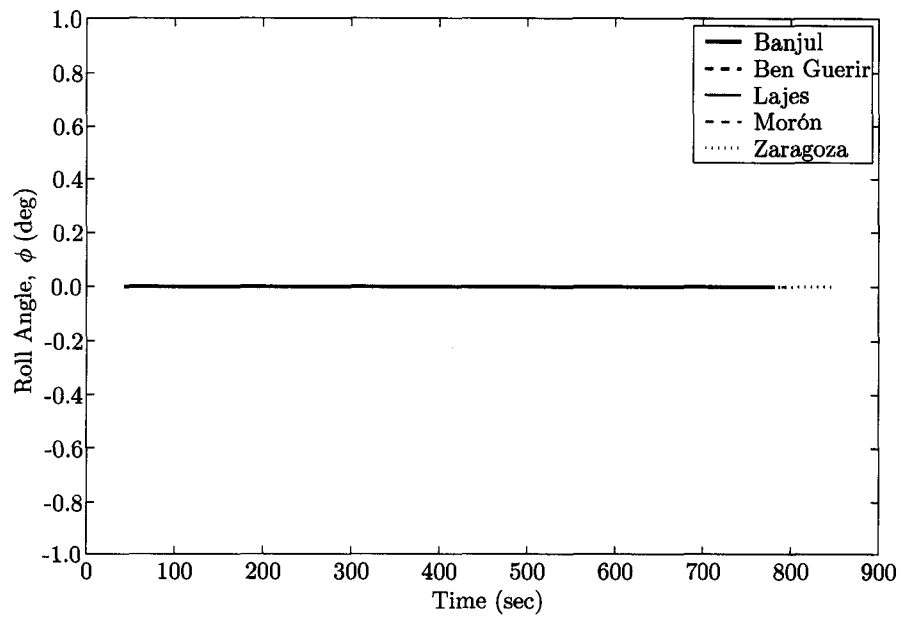
Figure 4.63   BC TAL roll angle profiles based on conditions in Tables 4.8 and 4.9

Figures 4.64 , 4.65 and 4.66 resemble to those of BCB. There are approximately 300 seconds where $q\alpha$ are at its peak. This period corresponds to when the X-33 is trying to gain as much altitude as possible with its remaining engine. Dynamic pressure in Figure 4.66 ended with coasts instead of "boosts" to intersect at higher NEP values. Figure 4.67 is also similar to that of BCB with the exception of no final "boost" at the end. Detailed MECO conditions for each case can be found in Appendix C, Section C.3 starting on page 279.
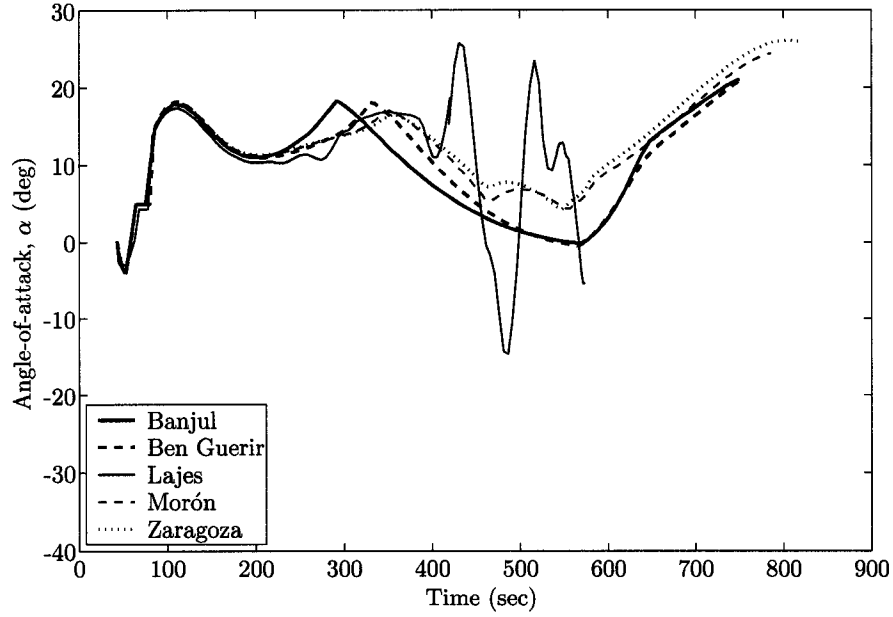
Figure 4.64   BC TAL angle-of-attack inequality constraint profiles based on conditions in Tables 4.8 and 4.9
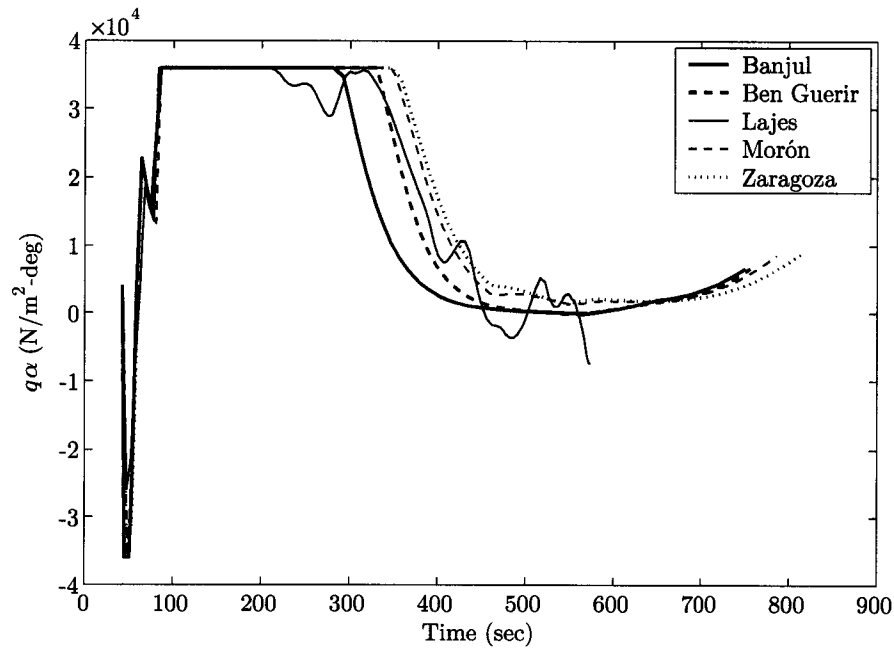
Figure 4.65   BC TAL $q\alpha$ inequality constraint profiles based on
conditions in Tables 4.8 and 4.9
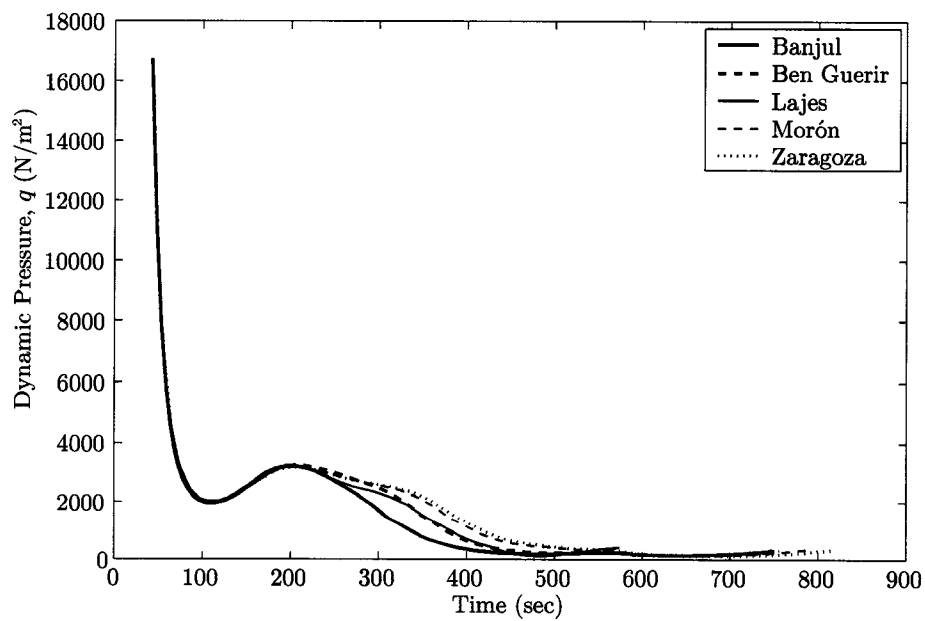
Figure 4.66   BC TAL dynamic pressure inequality constraint
profiles based on conditions in Tables 4.8 and 4.9
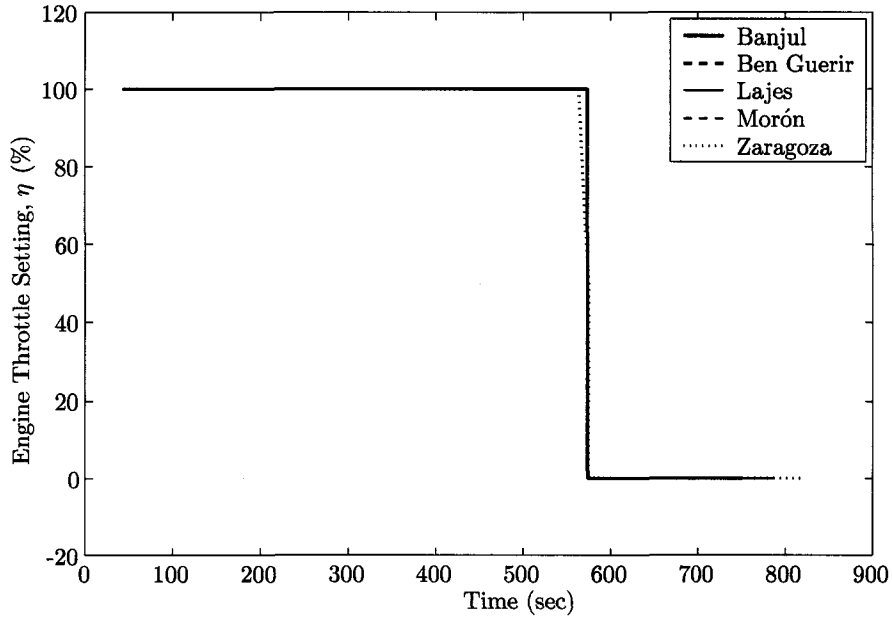
Figure 4.67 BC TAL engine throttle setting inequality constraint profiles based on conditions in Tables 4.8 and 4.9

4.8 Return-to-Launch-Site Results

Return-to-launch-site (RTLS) abort mode consists of two parts: a downrange and a fly-back part. However, these two parts may be further divided into phases in order to facilitate computation. The initial conditions used for all RTLS trajectories are enumerated in Table 4.10.

The 2-phase RTLS trajectory consists of a downrange (phase 1) and a fly-back part (phase 2). In addition to the inequality constraints imposed on all ascent trajectories, the equality constraints imposed for the downrange phase include altitude and range. An arbitrary altitude of 60 km with a range of 4° (440 km or 240 nautical miles) away from KSC are chosen so that the X-33 has enough altitude to perform a powered pitch-around

Table 4.10 Initial conditions for all RTLS trajectories
with $i = 51.6°$

$J = \min t_f$			
abort time =	39.40 sec	# of engines =	1
$x =$	6,378,149.78 m	$i =$	51.60°
$y =$	12,314.29 m	yaw $(\psi) =$	0.23°
$z =$	12,365.78 m	pitch $(\theta) =$	−1.00°
$V_x =$	207.12 m/s	roll $(\phi) =$	N/A
$V_y =$	291.16 m/s	mass $(m) =$	111,396.13 kg
$V_z =$	293.85 m/s	throttle setting $(\eta) =$	100%

(PPA) maneuver as described in Subsection 2.1.3 on page 19. The flight-path-angle at the end of the downrange phase is set to be a positive angle to ensure a PPA rather than a PPD (powered pitch-down) maneuver. The MECO constraints used for phase 2 are similar to those of TAL trajectories — the values of MECO altitude (r_f^*), velocity (V_f^*), and flight-path-angle (γ_f^*) are to be intersected anywhere on NEP using Equations (4.28) to (4.30) on page 45. Specific constraint values used in the 2-phase RTLS trajectory are outlined in Table 4.11.

Table 4.11 Constraints values used for 2-phase RTLS trajectories

Constraints:	Values:
Axial acceleration limit, a_a	$a_a \leq 4g$
Dynamic pressure limit, q	$0 \leq q \leq 18,194.4$ N/m^2 (380 psf)
$q\alpha$ and $q\beta$ limit	±35,910 N/m^2-deg (750 psf-deg)
Angle-of-attack, α	$-4° \leq \alpha \leq 12°$ (up to 11 km)
Phase 1 engine throttle setting, η	$50\% \leq \eta \leq 100\%$
Phase 1 altitude, r_{1ph}	60 km
Phase 1 range, s_{1ph}	4° away from KSC
Phase 1 flight-path-angle, γ_{1ph}	$\gamma_{1ph} > 0°$

The 3-phase RTLS trajectory is a burn-coast-burn (BCB) maneuver. The exact same constraints imposed at the end of phase 1 in a 2-phase trajectory are now imposed at the end of phase 2 in a 3-phase trajectory, with the exception of engine throttle setting is set to 51% of operational usage (coast). The MECO altitude, velocity and flight-path-angle are also to be determined based on Equations (4.28) to (4.30). Specific constraint values used in the 3-phase RTLS trajectory are listed in Table 4.12.

Table 4.12   Constraints values used for 3-phase RTLS trajectories

Constraints:	Values:
Axial acceleration limit, a_a	$a_a \leq 4g$
Dynamic pressure limit, q	$0 \leq q \leq 18,194.4$ N/m^2 (380 psf)
$q\alpha$ and $q\beta$ limit	$\pm 35,910$ N/m^2-deg (750 psf-deg)
Angle-of-attack, α	$-4° \leq \alpha \leq 12°$ (up to 11 km)
Phase 1 engine throttle setting, η	$50\% \leq \eta \leq 100\%$
Phase 1 altitude, r_{1ph}	not constrained
Phase 1 range, s_{1ph}	not constrained
Phase 2 engine throttle setting, η	51%
Phase 2 altitude, r_{2ph}	60 km
Phase 2 range, s_{2ph}	4° away from KSC
Phase 2 flight-path-angle, γ_{2ph}	$\gamma_{2ph} > 0°$

The ground track profiles in Figure 4.68 depicts two different cases — one with roll maneuver (3 phases) and one without roll maneuver (2 phases). The ground track with the 3-phase configuration turned out to resemble closely that which is illustrated in Figure 2.4 on page 19 as described by NASA [60]. The vehicle travelled downrange to dissipate propellant and made a coordinated yaw/pitch/roll maneuver to turn itself around pointing back to landing site. The 2-phase configuration, on the other hand, travelled downrange with a large yaw maneuver (Figure 4.69) before turning itself around. The large yaw maneuver is due to the fact that there is no roll capability to make a smoother coordinate turn.

For the 2-phase configuration case, Figure 4.69 shows the large negative yaw maneuver happening just before commencing PPA (as shown in Figure 4.70) without roll maneuver (as illustrated in Figure 4.71). The large yaw motion inherently has large side-slip-angle motion, exhibited in Figure 4.76, thus making it impossible to control. As for the 3-phase configuration case, Figure 4.69 delineates the smaller negative yaw maneuver happening just before commencing PPA (as portrayed in Figure 4.70) with some roll maneuver aiding in a smoother coordinate turn (Figure 4.71).
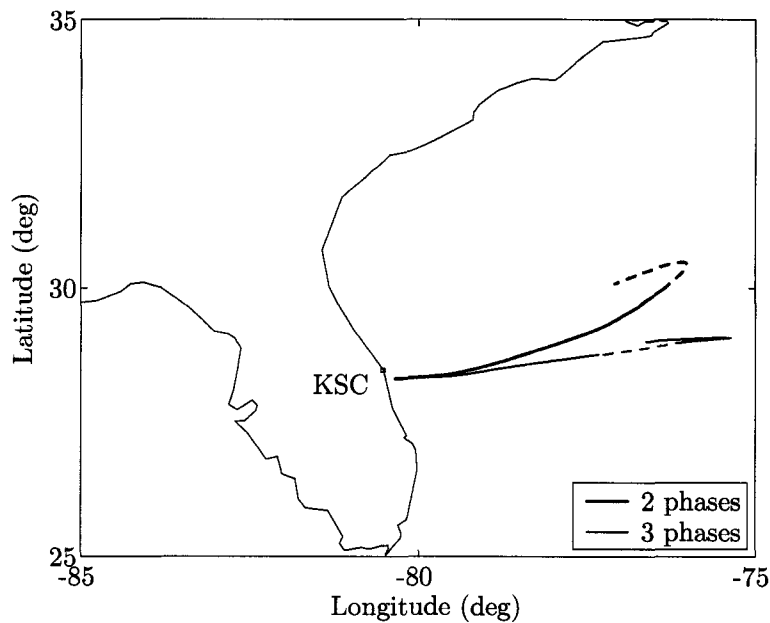
Figure 4.68   RTLS ground track profiles for $i = 51.6°$ based on conditions in Tables 4.10 to 4.12
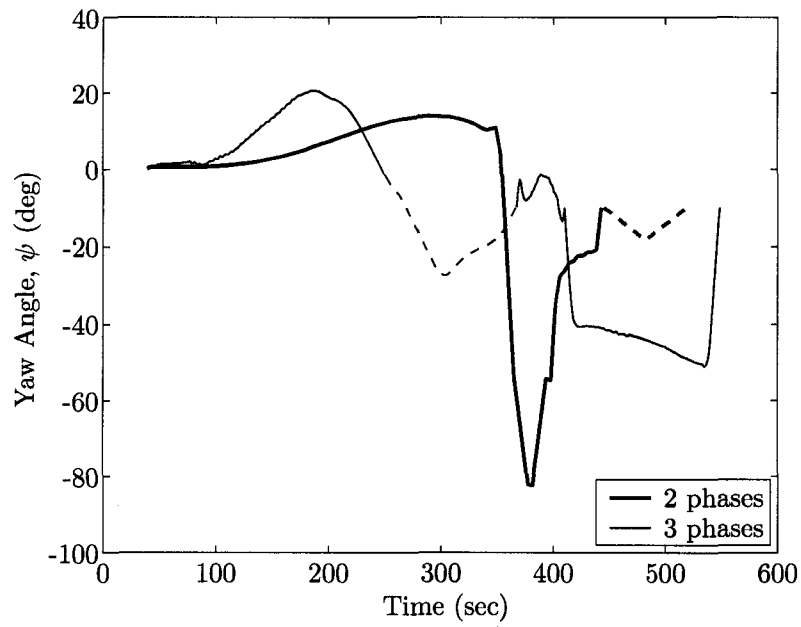
Figure 4.69   RTLS yaw angle profiles for $i = 51.6°$ based on
conditions in Tables 4.10 to 4.12
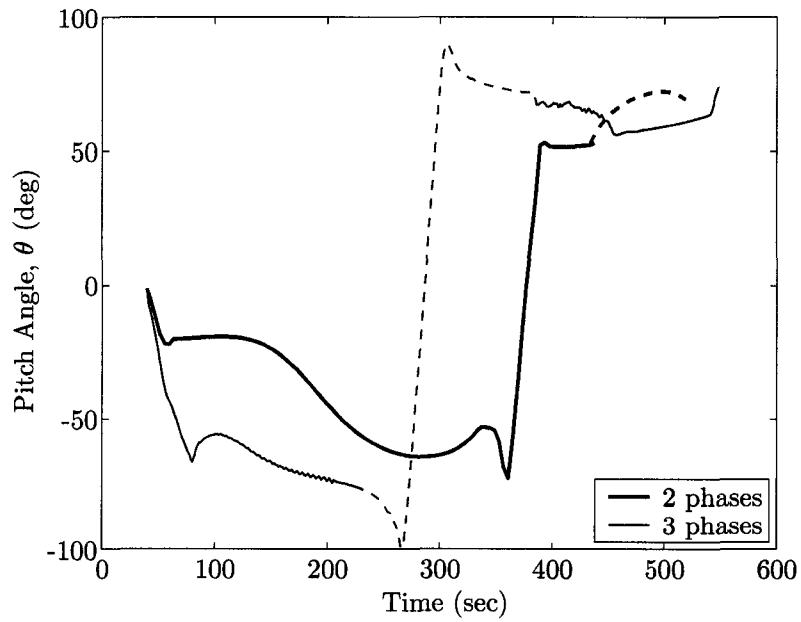
Figure 4.70   RTLS pitch angle profiles for $i = 51.6°$ based
on conditions in Tables 4.10 to 4.12
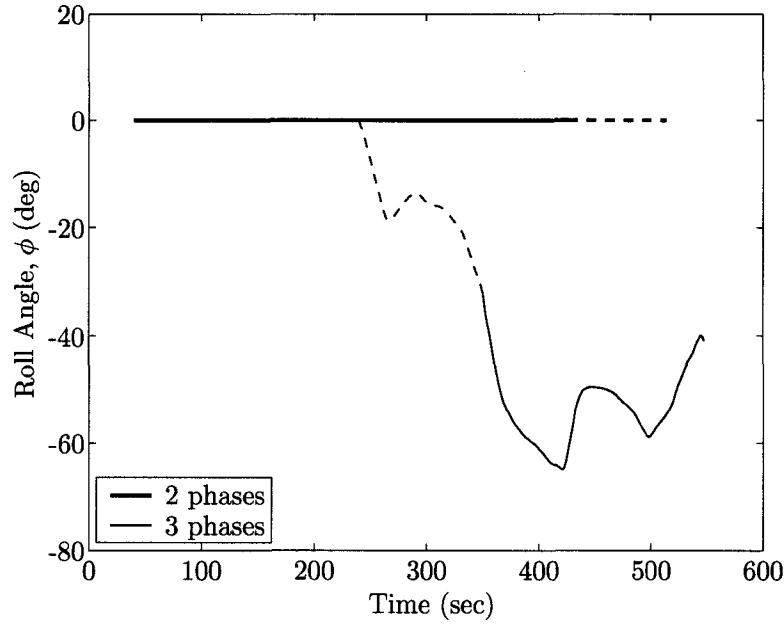
Figure 4.71   RTLS roll angle profiles for $i = 51.6°$ based on
conditions in Tables 4.10 to 4.12

Altitude profiles illustrated in Figure 4.72, velocity profiles in Figure 4.73 and flight-path-angle profiles in Figure 4.74 all depict close resemblance. Due to the fact that coasting is imposed in the 3-phase configuration test case, the peak altitude and velocity attained are slightly lower and the vehicle had to "dive" in order to gain velocity quickly. The decrease in the velocity between the time of 350 and 515 seconds displayed in Figure 4.73 is in preparation for the PPA. Velocity had to be reduced in order to avoid violating structural constraints such as q, $q\alpha$, and a_a.

Figure 4.75 is the angle-of-attack profile and Figure 4.76 is the side-slip-angle (β) profile. As mentioned earlier, large β is difficult or impossible to control. The 2-phase configuration exhibits a β angle as large as $-40°$ and 3-phase configuration is within $\pm 10°$, which is more reasonable. Figure 4.77 shows the vehicle is under most intensive stress between $100 < t < 320$ seconds because the value of $q\alpha$ during this period is at

its peak. The increase in dynamic pressure at the end in Figure 4.78 is because the

X-33 has descended to an altitude of approximately 55 km where density is not paltry.

Figure 4.79 shows the throttle setting needed in the 2-phase configuration is 100% while

the 3-phase configuration had a 100%, 51% followed by 100% setting.
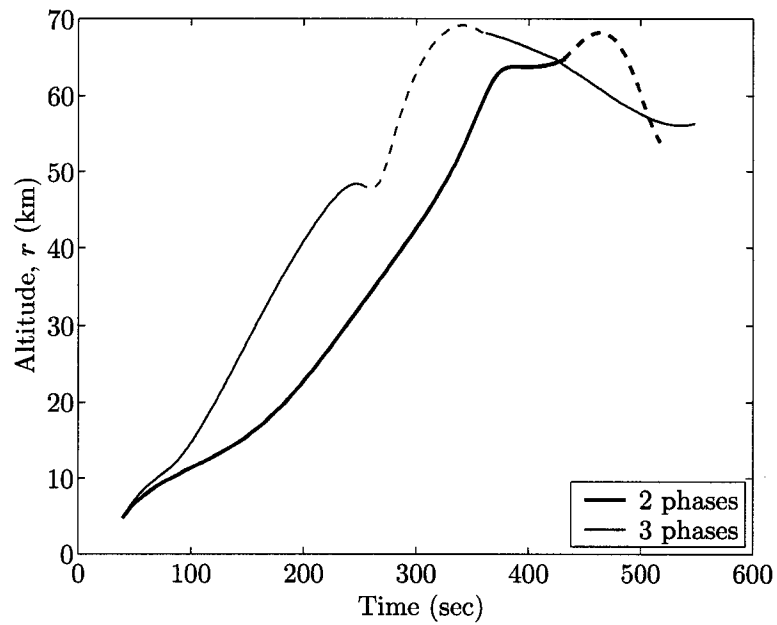
Figure 4.72   RTLS altitude profiles for i = 51.6° based on
conditions in Tables 4.10 to 4.12
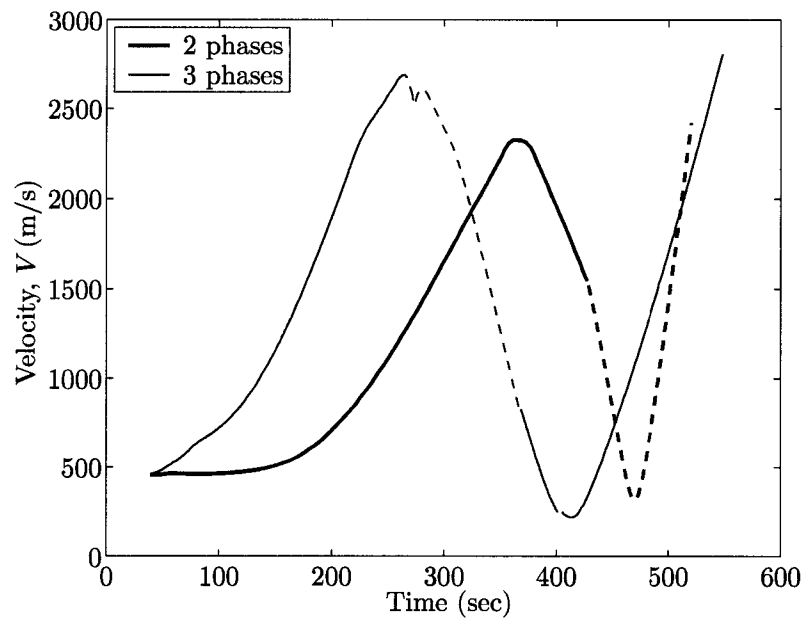
Figure 4.73   RTLS velocity profiles for $i = 51.6°$ based on conditions in Tables 4.10 to 4.12
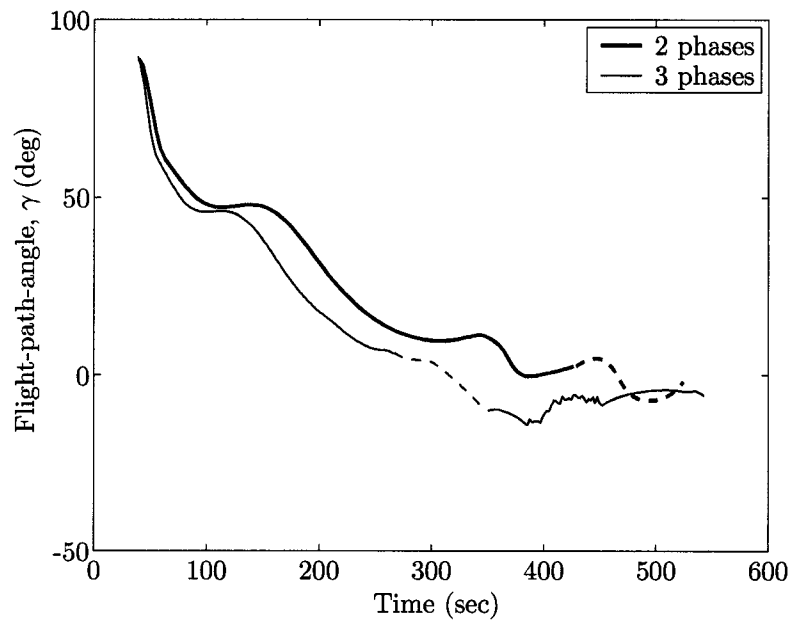
Figure 4.74   RTLS gamma profiles for $i = 51.6°$ based on conditions in Tables 4.10 to 4.12
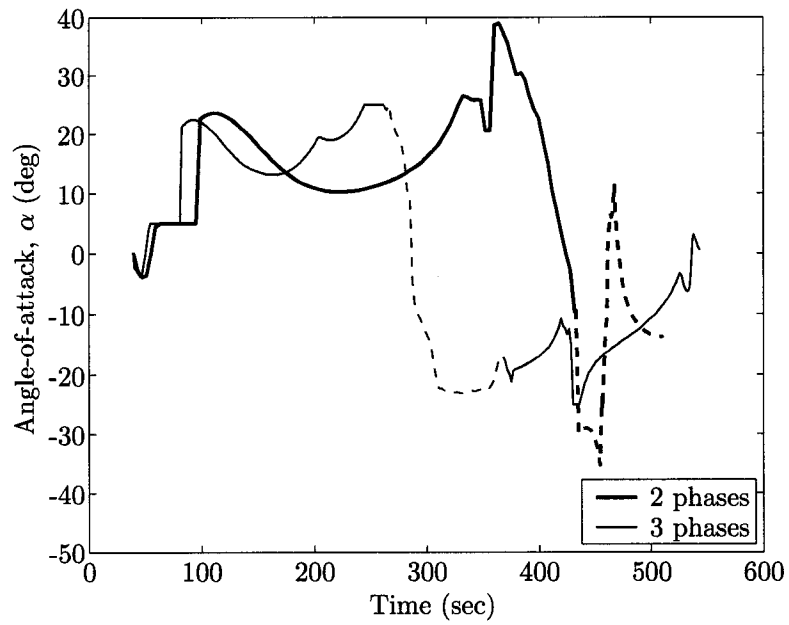
Figure 4.75   RTLS angle-of-attack profiles for $i = 51.6°$
based on conditions in Tables 4.10 to 4.12
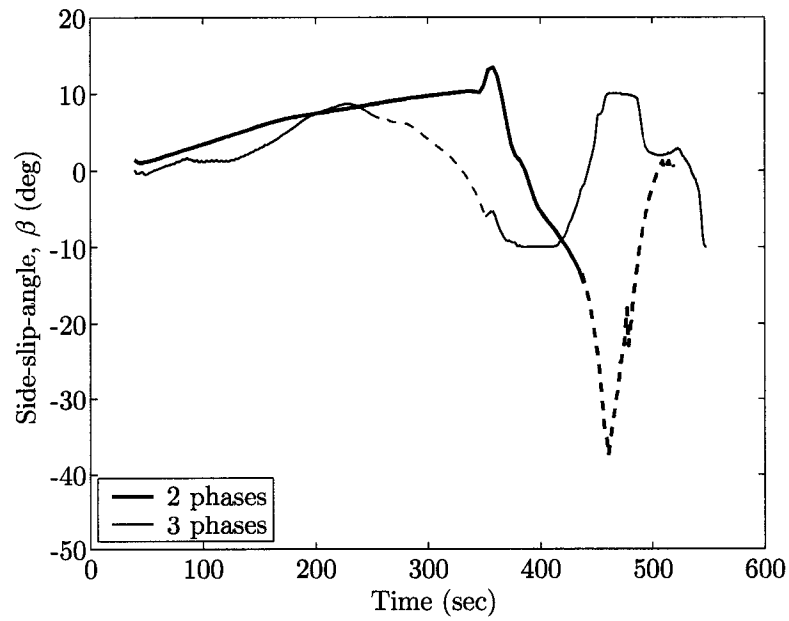
Figure 4.76   RTLS side-slip-angle profiles for $i = 51.6°$ based
on conditions in Tables 4.10 to 4.12
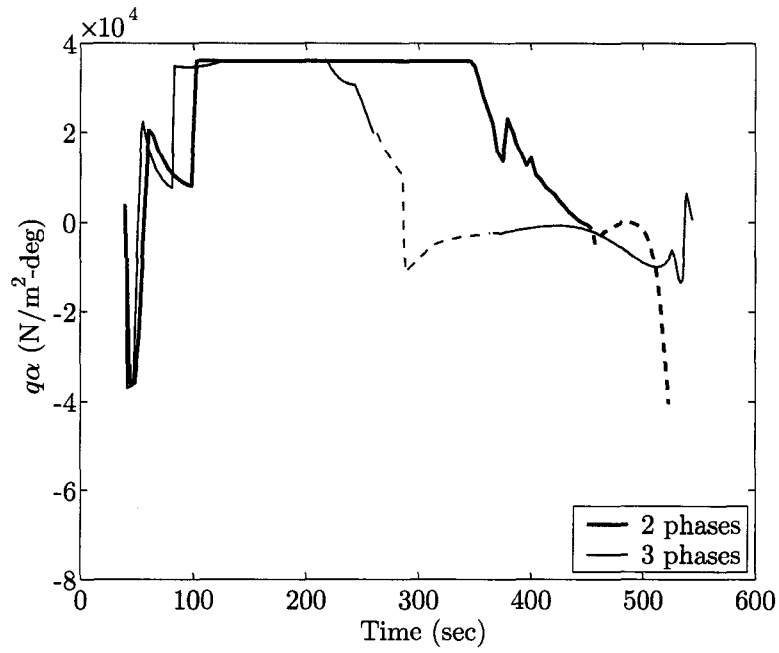
Figure 4.77 RTLS $q\alpha$ profiles for $i = 51.6°$ based on conditions in Tables 4.10 to 4.12
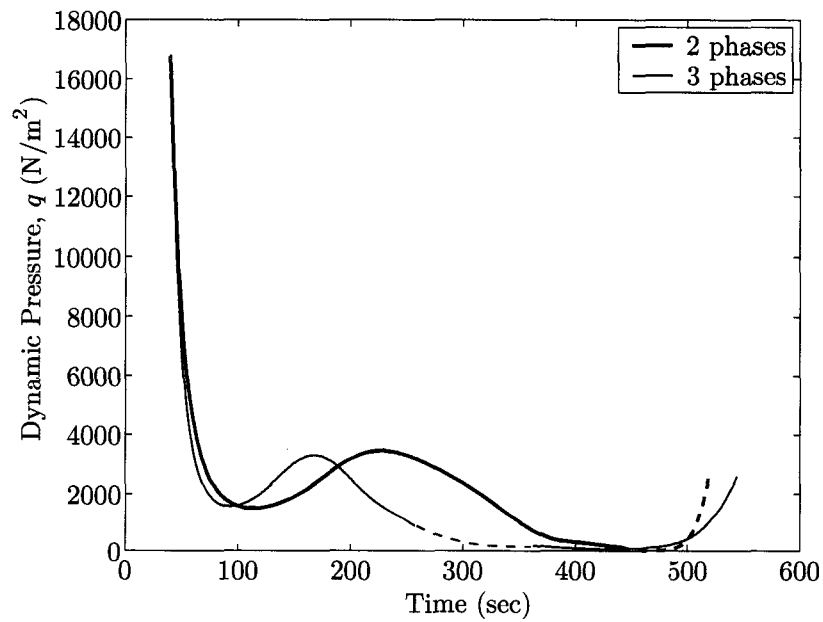
Figure 4.78 RTLS dynamic pressure profiles for $i = 51.6°$ based on conditions in Tables 4.10 to 4.12
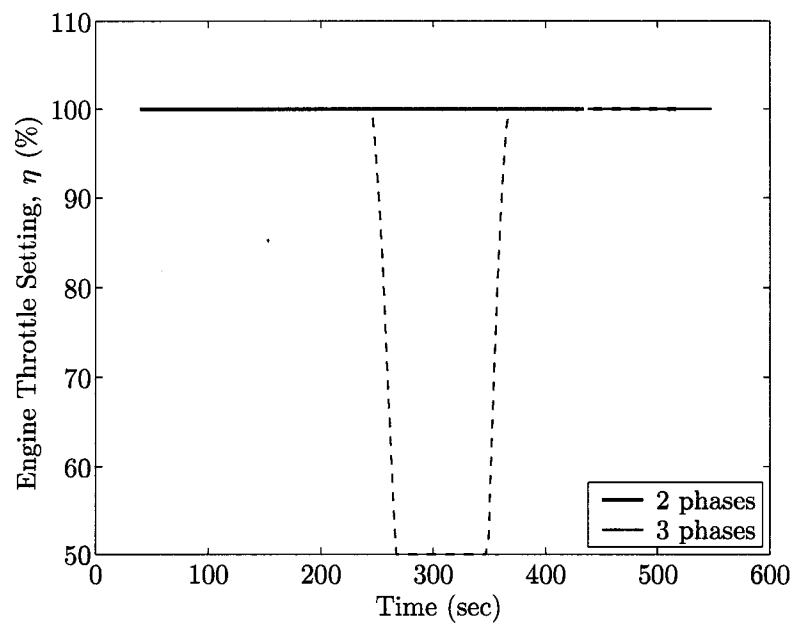
Figure 4.79   RTLS   engine   throttle   setting   profiles   for
$i = 51.6°$ based on conditions in Tables 4.10
to 4.12

CHAPTER 5   OPTIMAL ENTRY TRAJECTORY DESIGNS

The re-entry corridor is in fact so narrow,
that if this basketball were the Earth,
and this softball were the Moon,
and the two are placed fourteen feet apart,
the crew would have to hit a target
no thicker than this piece of paper.

— *Excerpt from Apollo 13* [97]

CONTROLLED unpowered flight is how the shuttle descends after re-entry. The only means of attitude control are the use of control surfaces such as flaps and elevons at lower altitudes and a reaction control system (RCS) at higher altitudes.

The fundamental entry trajectory requirement is to reach the terminal area energy management (TAEM) interface (defined by a nominal velocity and altitude) within specified limits on range from the TAEM heading alignment cone (HAC), a given flight-path-angle value, and a velocity heading angle within a few degrees of tangency with the HAC. The entry trajectory must stay within the confinement of the entry flight corridor defined by the heat rate $\left(\dot{Q}_{max} \right)$, aerodynamic load ($n_a$), dynamic pressure ($q$) and equilibrium glide condition (EGC) constraints.

5.1 Equations of Motion for Entry Flight

The nondimensional point-mass and windless equations of motion (EOMs) for the entry flight including the effects of Earth rotation are described by [98, 99]

$$\dot{r}_c = V_r \sin \gamma \tag{5.1}$$

$$\dot{\Theta} = \frac{V_r \cos \gamma \sin \Psi}{r_c \cos \Phi} \tag{5.2}$$

$$\dot{\Phi} = \frac{V_r \cos \gamma \cos \Psi}{r_c} \tag{5.3}$$

$$\dot{V}_r = -D - \left(\frac{\sin \gamma}{r_c^2} \right) + \omega^2 r_c \cos \Phi \left(\sin \gamma \cos \Phi - \cos \gamma \sin \Phi \cos \Psi \right) \tag{5.4}$$

$$\dot{\gamma} = \frac{1}{V_r} \left[L \cos \sigma + \left(V_r^2 - \frac{1}{r_c} \right) \left(\frac{\cos \gamma}{r_c} \right) + 2 \omega V_r \cos \Phi \sin \Psi \right.$$

$$\left. + \omega^2 r_c \cos \Phi \left(\cos \gamma \cos \Phi - \sin \gamma \cos \Psi \sin \Phi \right) \right] \tag{5.5}$$

$$\dot{\Psi} = \frac{1}{V_r} \left[\frac{L \sin \sigma}{\cos \gamma} + \frac{V_r^2}{r_c} \cos \gamma \sin \Psi \tan \Phi - 2 \omega V_r \left(\tan \gamma \cos \Psi \cos \Phi - \sin \Phi \right) \right.$$

$$\left. + \frac{\omega^2}{\cos \gamma} \sin \Psi \sin \Phi \cos \Phi \right] \tag{5.6}$$

where r_c is the radial distance from the center of the Earth to RLV; γ is flight-path-angle; Θ and Φ are longitude and geodetic latitude; Ψ is velocity azimuth angle; ω is Earth rotation rate (see Equation 4.17); V_r is Earth relative velocity; σ is bank angle defined in such way that lift is in the local vertical plane at zero bank; D and L are the aerodynamic drag and lift accelerations in g's as shown in Equations (5.7) and (5.8) (m is the dry weight of the X-33). Again, all distance related terms have been normalized by R_0, velocity related terms by $\sqrt{R_0 g_0}$, and time related terms by $\sqrt{R_0/g_0}$.

$$D = \frac{1}{2} \frac{\rho V_r^2 S_{ref} C_d}{m g_0} \tag{5.7}$$

$$L = \frac{1}{2} \frac{\rho V_r^2 S_{ref} C_\ell}{m g_0} \tag{5.8}$$

5.2 Equality Constraints for Entry Flight

Equality constraints for entry analyses are the terminal conditions at the terminal area energy management (TAEM) point. These conditions will ensure that the vehicle under TAEM guidance can reach the runway for a safe landing. Four typical terminal conditions associated with entry phase include final altitude (r_f^*), final velocity (V_f^*), range-to-HAC (r_{HAC}^*) and the velocity azimuth (Ψ_f^*) pointing to the tangency of the HAC. The values for these terminal conditions for the X-33 are:

☆ TAEM altitude is $r_f^* = 30.48$ km (100,000 ft);

☆ TAEM velocity is $V_f^* = 908.15$ m/s (2979.5 ft/s);

☆ Range-to-HAC at TAEM interface is $r_{HAC}^* = 55.56$ km (30 nm); and

☆ The difference between the velocity azimuth angle (Ψ) and the line-of-sight (Ψ_{LOS}) must be $\Delta\Psi = \|\Psi - \Psi_{LOS}\| \leq 1°$ as illustrated in Figure 5.1. This conditions guarantees that final velocity must align at the HAC tangency within $\pm 1°$ accuracy.
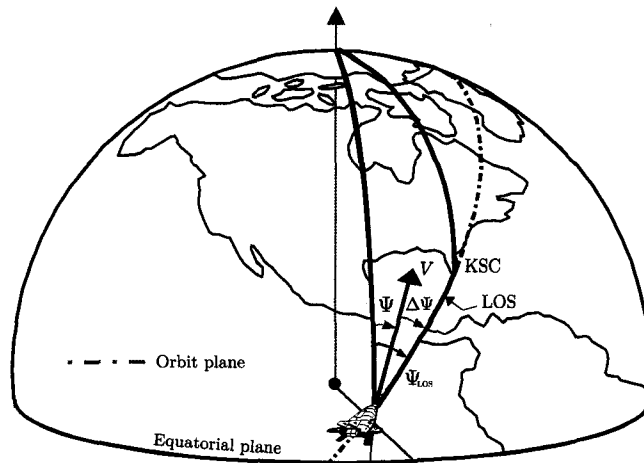
Figure 5.1   Final velocity alignment with HAC tangency

These four terminal constraints must be satisfied in order to allow *TAEM guidance* and *A/L guidance* to steer the vehicle for a safe landing. In addition to these four terminal conditions, flight-path-angle (γ) may or may not be imposed as a constraint. This research imposes $\gamma_f^* = -7.36°$ as an active constraint.

5.3 Inequality Constraints for Entry Flight

Since entry phase is an unpowered flight mode, the only means to satisfy the range requirement is through the modulation of aerodynamics force (direction and magnitude) Flight control considerations (minimize phugoid motion) as well as vehicle load limits also impose additional constraints on the design of entry trajectory. Typical inequality constraints associated with entry trajectory include

$$\dot{Q} \leq \dot{Q}_{max} \tag{5.9}$$

$$\|L\cos\alpha + D\sin\alpha\| \leq n_{a_{max}} \tag{5.10}$$

$$q \leq q_{max} \tag{5.11}$$

$$\left(\frac{1}{r_c} - V_r^2\right)\left(\frac{1}{r_c}\right) - L\cos\sigma_{EQ} \leq 0 \tag{5.12}$$

where Equation (5.9) is the heating rate constraint on a stagnation point on the surface of the RLV; Equation (5.10) is a constraint on the aerodynamic load (g's) in the body-normal direction; Equation (5.11) is the dynamic pressure constraint; and Equation (5.12) is the equilibrium glide condition (EGC) constraint. These constraints will be explained further in the following subsections.

5.3.1 Heat Rate Constraint

The heat flux used for optimal entry trajectory is a one-dimensional adiabatic steady-state heating model [100]. The empirical equation used to calculate heat rate is

$$\dot{Q} = k\sqrt{\rho}\, V_r^{3.15} \tag{5.13}$$

for a constant k value of 9.43692×10^{-5} (dimensional value). The peak heat rate for the X-33 is $\dot{Q}_{max} = 794{,}425$ Watt/m^2 (70 BTU/ft^2·sec) [73]. The purpose of the heat rate constraint is to ensure that the backface temperature stays within design limits. The heat rate constraint is particularly important at high Mach numbers (Mach > 16) because this is when temperature is most severe (enthalpy). Other reasons that make the heat rate constraint crucial include the combined effects of surface catalysis and gas chemistry, aerodynamic induced vibration loads, and low density flows [101–104].

5.3.2 Normal Load Constraint

Normal load (n_a) is defined as the magnitude of the resulting aerodynamic acceleration in the body normal direction. The specified value for normal load is based on the structural limitations. Normal load is particularly important when Mach number is 4.5 < Mach < 16, according to NASA [103, 104]. This constraint is later depicted in the entry flight corridor (Figure 5.2).

5.3.3 Dynamic Pressure Constraint

In order to avoid exceeding the limits of control surface hinge moment, parameters such as the dynamic pressure (q) must be constrained between $0 \leq q \leq 14{,}364$ N/m^2 (300 psf) in the trajectory design to satisfy structural design limits and prevent structural failures. Dynamic pressure is most prominent at lower Mach numbers (Mach < 4.5). The product of dynamic pressure and angle-of-attack $(q\alpha)$ and side-slip-angle $(q\beta)$ are constrained for structural integrity [73, 103, 104].

These entry constraints relative to range, re-entry heating, and vehicle loads have resulted in very confining operationally allowed angle-of-attack profiles as shown in Equation (5.14) [73].

$$\alpha = \begin{cases} 45° & \text{for} \quad \text{Mach} \geq 10 \\ 45° - 0.612 \times (\text{Mach} - 10)^2 & \text{for} \quad 2.5 \leq \text{Mach} < 10 \end{cases} \tag{5.14}$$

The α profile is based on extensive wind tunnel testings that provides the best aerothermal protection and creates suitable drag to slow down the spacecraft flying at an initial speed of Mach 23.

5.3.4 Equilibrium Glide Condition Constraint

Equilibrium glide condition (EGC) is a constraint that reduces the phugoid oscillations in altitudes along the entry profile. Phugoid oscillations are particularly noticeable when bank reversal and/or angle-of-attack modulation occur. Unlike the previous three constraints, EGC is a soft constraint in the sense that it does not need to be enforced strictly. EGC constraint shown in Equation (5.12) is obtained by omitting the Earth rotation term and setting $\dot{\gamma} = 0$ and $\gamma = 0$ in Equation (5.5).

5.4 Entry Flight Corridor

The combination of these four inequality constraints comprises an entry flight corridor (also known as r-V design space) pictured in Figure 5.2. Any trajectory outside of the entry flight corridor is considered an infeasible solution. A too shallow entry will cause the spacecraft to skip out of the atmosphere while a too steep entry will burn the spacecraft. The width of the entry flight corridor depends on $\dot{Q}_{max}$, $n_{a_{max}}$, q_{max} and σ_{EQ} values.
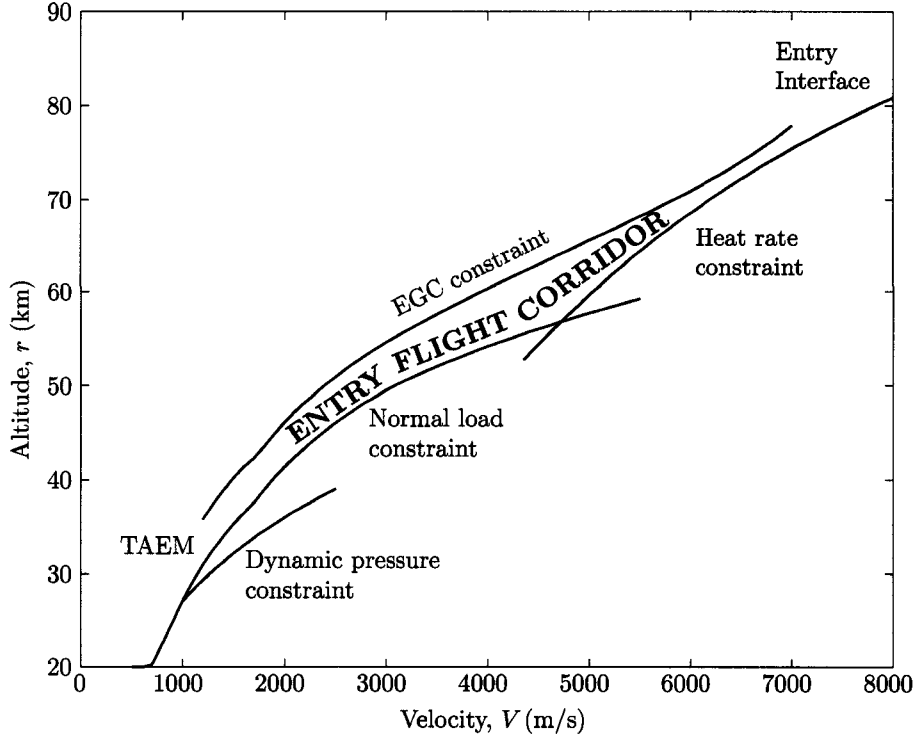
Figure 5.2   Typical entry trajectory design space, also known
as the entry flight corridor

5.5   Objective of Entry Trajectory Design

The objective of entry trajectory design is to find the best drag modulation via bank angle (σ) to satisfy the range, heat rate, normal load, dynamic pressure, EGC requirements and TAEM conditions. Given the restrictions on the angle-of-attack profile and vehicle aerodynamics, the only achievable attitude command available to accomplish drag modulation and range control is σ. The two constraints imposed on the trajectory control profile include a maximum banking rate of $\dot{\sigma}_{max} = \pm 5.0$ deg/sec and a maximum banking acceleration of $\ddot{\sigma}_{max} = \pm 3.5$ deg/sec^2 for the X-33. Therefore, the control for entry trajectory is $u = [\ \ddot{\sigma}\ ]$. Using acceleration instead of angle as the control is to minimize σ fluctuation and thus make the trajectory more realistic [73].

Table 5.1 is a summary of entry test cases set by Marshall Space Flight Center (MSFC) to cover a range of entry conditions [73]. Table 5.1 is further subdivided into three sets of test conditions. The first case from each set is the nominal case where the spacecraft is lined up with TAEM HAC (thus a small crossrange). The second case from each set has a large positive crossrange simulating an "early" entry. The third case from each set has a large negative crossrange simulating a "late" entry. The goal of each set is to test different peak heat rates, crossranges and inclinations. As an example, entry guidance case #13 (EG13) is an entry condition with high heat rate returning from the International Space Station (ISS) orbit of $i = 51.6°$. EG14 is a high heat rate case with "early" entry from ISS orbit (thus a large positive crossrange). EG15 is a high heat rate case with "late" entry from ISS orbit (thus a large negative crossrange). "Early" and "late" refer to when the deorbit maneuver is performed compared to the intended deorbit time.

Table 5.1   Overview of all entry from orbit scenarios for the X-33

Case #	Inclination (deg)	Downrange (km)	Crossrange (km)	Peak heat rate (Watt/m^2)
EG13	51.6	6,519	59	794,425
EG14	51.6	6,554	809	794,425
EG15	51.6	6,589	−848	794,425
EG16	51.6	8,160	148	680,935
EG17	51.6	8,715	883	680,935
EG18	51.6	8,197	−778	680,935
EG19	28.5	7,360	267	680,935
EG20	28.5	7,282	752	680,935
EG21	28.5	7,625	380	680,935

The performance index chosen for all nominal entry trajectories is to minimize the heat load acquired by the spacecraft throughout the entry phase as shown in Equation (5.15).

$$J = \min \int_0^t \dot{Q} \, dt \qquad (5.15)$$

Minimizing the heat load means less stress for the thermal protection system (TPS), thereby, increasing the life-cycle of thermal tiles.

5.6 Nominal Entry Results

The purpose of an optimal nominal entry trajectory is to steer the spacecraft on an optimal path within an entry corridor defined by $\dot{Q}_{max}$, n_a, q and EGC constraints. All ground tracks are planned as a function of energy instead of time in order to track a given drag profile. The only control variable in this research is the bank reversal logic (σ angle).

5.6.1 EG13-15 Trajectories

Tables 5.2 through 5.4 are the initial test conditions for cases EG13-15 set by MSFC for orbital entry ($i = 51.6°$ and $\dot{Q}_{max} = 794{,}425$ W/m^2). These are the high inclination and high heat rate re-entry test cases. Table 5.5 enumerates the path and terminal constraint values used for cases EG13-15.

Table 5.2 Initial conditions for EG13 entry trajectory

$J = \min \int \dot{Q} \, dt$			
Altitude, $r_i =$	121.199 km	Flight-path-angle, $\gamma_i =$	$-1.438°$
Longitude, $\Theta_i =$	$-117.007°$	Velocity azimuth angle, $\Psi_i =$	$-38.329°$
Latitude, $\Phi_i =$	$-18.255°$	Angle-of-attack, $\alpha_i =$	$45.00°$
Velocity, $V_i =$	7,599 m/s	Bank angle, $\sigma_i =$	$-0.002°$
Inclination, $i =$	$51.6°$	—	—

Table 5.3 Initial conditions for EG14 entry trajectory

$J = \min \int \dot{Q} \, dt$			
Altitude, $r_i =$	122,558 km	Flight-path-angle, $\gamma_i =$	$-1.438°$
Longitude, $\Theta_i =$	$-111.007°$	Velocity azimuth angle, $\Psi_i =$	$-39.856°$
Latitude, $\Phi_i =$	$-22.510°$	Angle-of-attack, $\alpha_i =$	$45.00°$
Velocity, $V_i =$	7,621 m/s	Bank angle, $\sigma_i =$	$-0.002°$
Inclination, $i =$	$51.6°$	—	—

Table 5.4 Initial conditions for EG15 entry trajectory

$J = \min \int \dot{Q} \, dt$			
Altitude, $r_i =$	120.374 km	Flight-path-angle, $\gamma_i =$	$-1.438°$
Longitude, $\Theta_i =$	$-125.007°$	Velocity azimuth angle, $\Psi_i =$	$-36.812°$
Latitude, $\Phi_i =$	$-12.223°$	Angle-of-attack, $\alpha_i =$	$45.00°$
Velocity, $V_i =$	7,622 m/s	Bank angle, $\sigma_i =$	$0.002°$
Inclination, $i =$	$51.6°$	—	—

Table 5.5 Constraints imposed on entry trajectories EG13-15

Constraints:	Values:
Final altitude, r_f^*	30.427 km
Final velocity, V_f^*	908.15 m/s
Final range-to-go, r_{togof}^*	55.56 km (30.0 nm)
Normal load limit, n_a	$n_a \leq 2.5g$
Heating rate limit, $\dot{Q}$	**$0 \leq \dot{Q} \leq 749{,}029$ Watt/m^2 (66 BTU/ft^2·sec)**
Dynamic pressure limit, q	$0 \leq q \leq 14{,}364$ N/m^2 (300 psf)
Equilibrium bank angle, σ_{EQ}	$5°$

As mentioned earlier, EG13 is a case where the spacecraft entered the atmosphere with a velocity azimuth angle closely aligned with TAEM HAC. This is clearly depicted in the ground track profile shown in Figure 5.3. The trajectory has mostly a straight line ground track until a last minute energy level adjustment and HAC alignment correction takes place. EG14 and EG15 represent the "early" and "late" trajectories, respectively. Figure 5.4 is a closer inspection at the TAEM interface. Notice all trajectories ended 55.60 km (30 nm) away from HAC and the velocity azimuth is less than 1° off of tangency with the HAC. Figure 5.5 illustrates the entry trajectory design space — all three cases are within the entry corridor (the four dotted lines) with minimum oscillations.
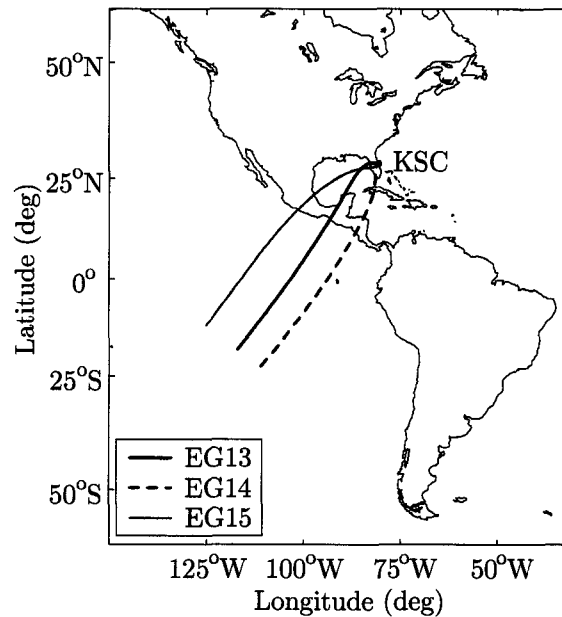
Figure 5.3   EG13-15 ground track profiles based
on conditions in Tables 5.2 to 5.5
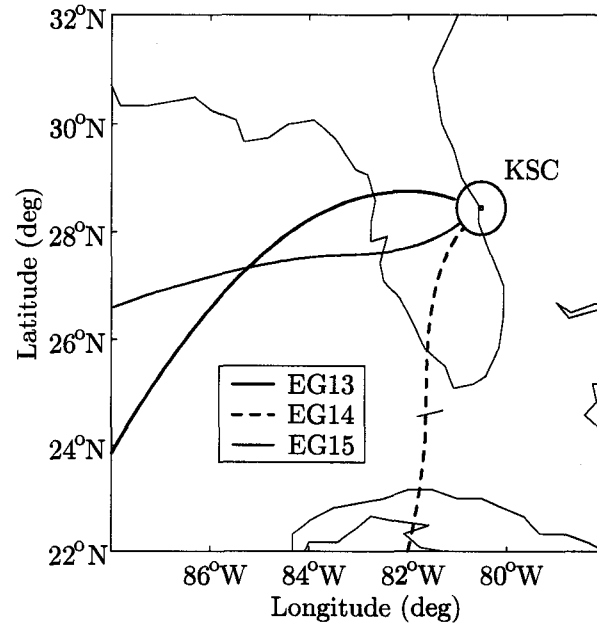
Figure 5.4   EG13-15 ground track profiles in detail
based on conditions in Tables 5.2 to 5.5
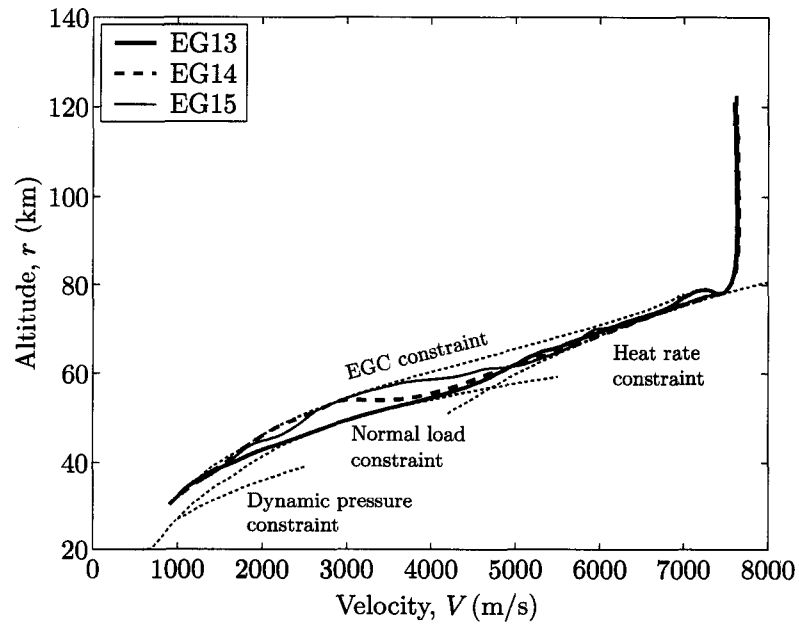
Figure 5.5   EG13-15 altitude vs velocity profiles based
on conditions in Tables 5.2 to 5.5

The altitude and velocity profiles (Figures 5.6 and 5.7, respectively) delineate the spacecraft descending from an initial altitude and speed to a specified final altitude and speed. Figure 5.8 is the scheduled operationally allowed angle-of-attack profiles for each case. Angle-of-attack remains at a constant value of 45° throughout the hypersonic region of the flight to achieve the maximum L/D (lift over drag). Bank profiles depicted in Figure 5.9 have been carefully designed to incorporate one bank reversal per case. This is to take into account the limited RCS fuel onboard to be used for course changes. Depending on the entry interface condition, the spacecraft will bank one direction followed by a bank reversal (change sign) for a final course change to align with HAC. The bank reversal time is unknown and is determined by the optimizer. The final time for EG13 is 1,161.58 seconds, EG14 is 1,203.43 seconds, and EG15 is 1,222.71 seconds.
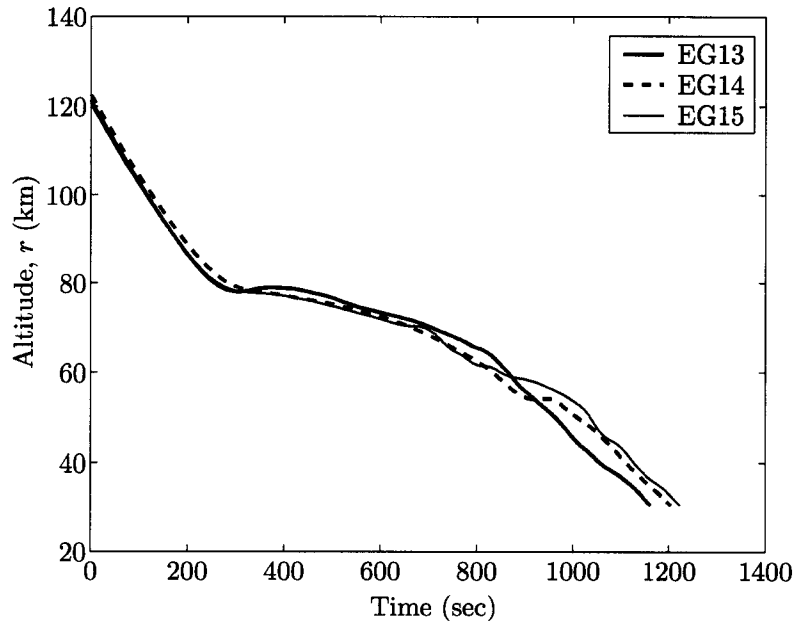
Figure 5.6   EG13-15 altitude profiles based on conditions in Tables 5.2 to 5.5
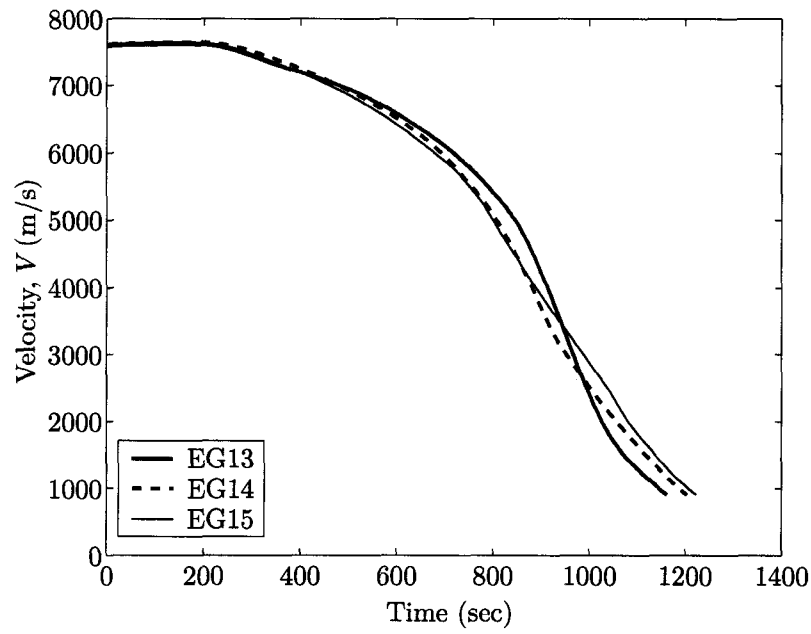
Figure 5.7   EG13-15 velocity profiles based on conditions in Tables 5.2 to 5.5
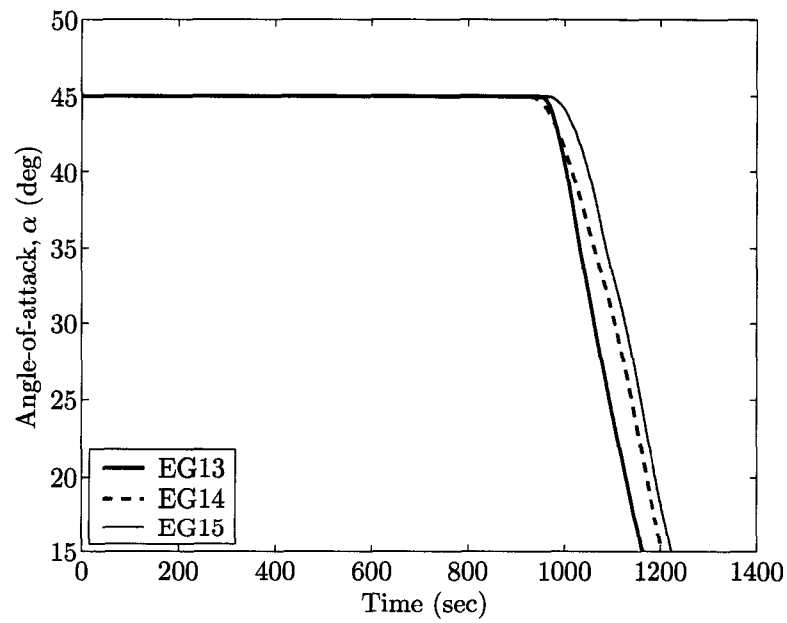
Figure 5.8   EG13-15 angle-of-attack profiles based on conditions in Tables 5.2 to 5.5
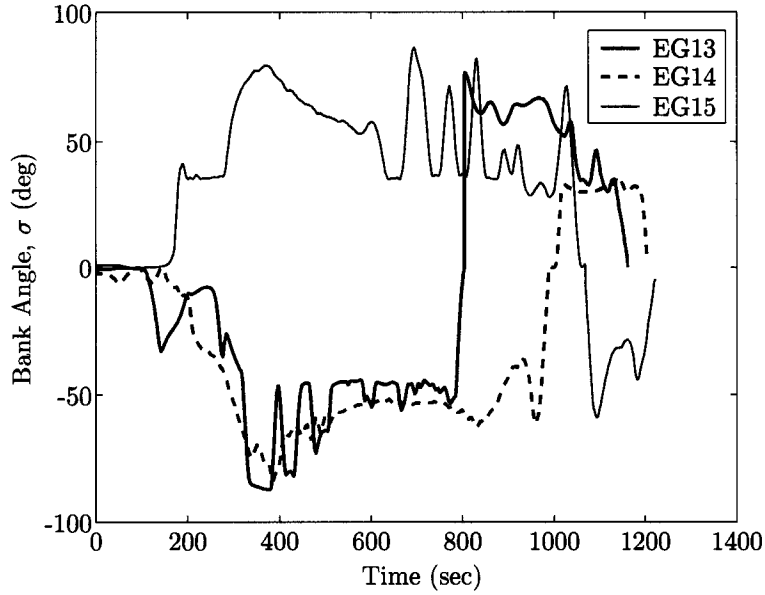
Figure 5.9 EG13-15 bank angle profiles based on conditions in Tables 5.2 to 5.5

The flight-path-angle profiles depicted in Figure 5.10 are nearly constant in the hypersonic region (approximately the first 1,000 seconds of the flight in this case) in order to achieve maximum downrange. Figure 5.11 illustrates the heat rate profiles. EG14-15 reached the upper bounds quite a few times, but did not fly at the upper bound all the time. EG13 is well below the upper bound of 749,029 Watt/m^2. Thus EG13-15 can be flown with a lower $\dot{Q}_{max}$ to increase the life-cycle of TPS tiles (further discussion in Section 5.7 starting on page 140). Figures 5.12 and 5.13 show that the dynamic pressure and normal load are within the constraint limits. Figure 5.14 displays the aerodynamic profiles (L/D characteristics) of an entry vehicle. The fluctuation in the beginning of the flight is due to the inaccuracy of C_ℓ and C_d at high speeds. C_ℓ and C_d are functions of Mach number and speed of sound is not well defined at hypersonic speeds. Notice L/D is constant throughout most of the flight and the maximum achievable L/D value is approximately 1.35 (inside of atmosphere). This value is well in accordance with typical hypersonic vehicle aerodynamics [99, 102, 105, 106].
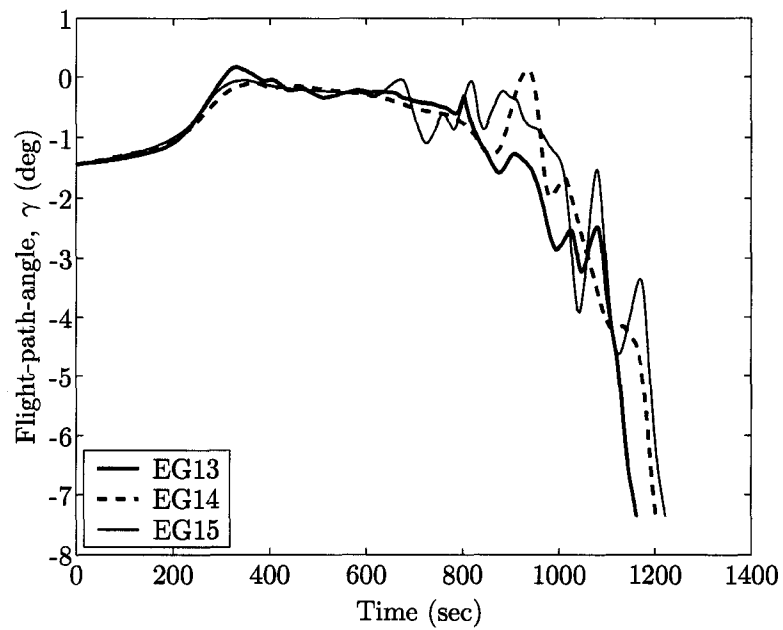
Figure 5.10   EG13-15 flight-path-angle profiles based on
conditions in Tables 5.2 to 5.5
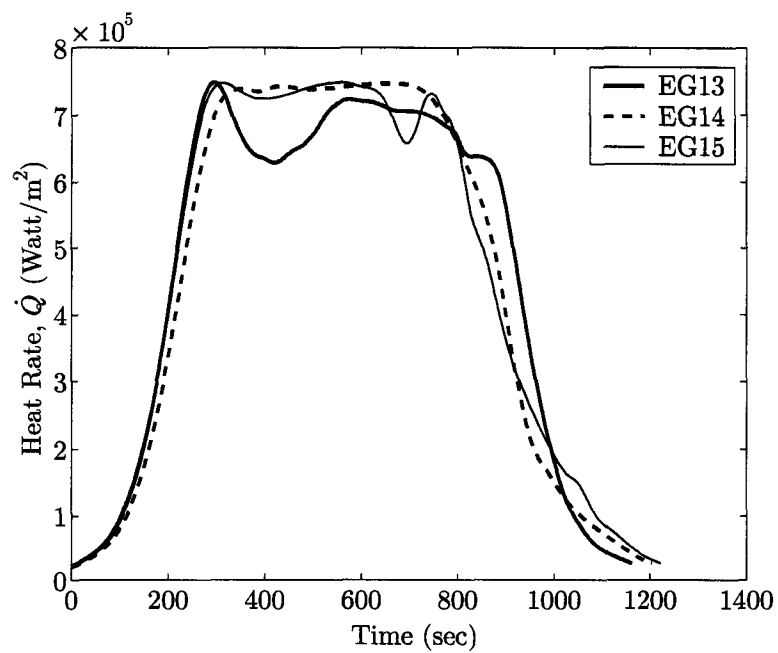
Figure 5.11   EG13-15 heat load profiles based on condi-
tions in Tables 5.2 to 5.5
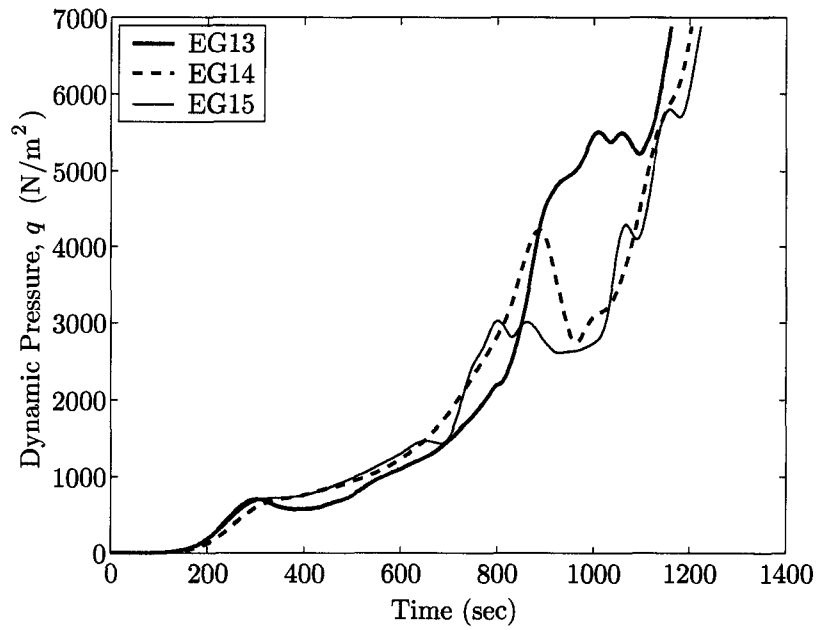
Figure 5.12   EG13-15 dynamic pressure profiles based
on conditions in Tables 5.2 to 5.5
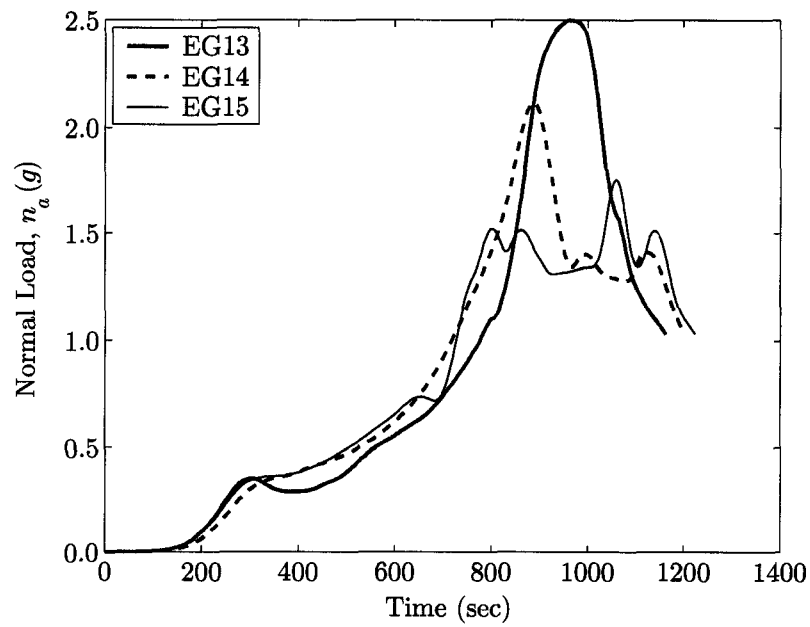
Figure 5.13   EG13-15 normal load profiles based on con-
ditions in Tables 5.2 to 5.5
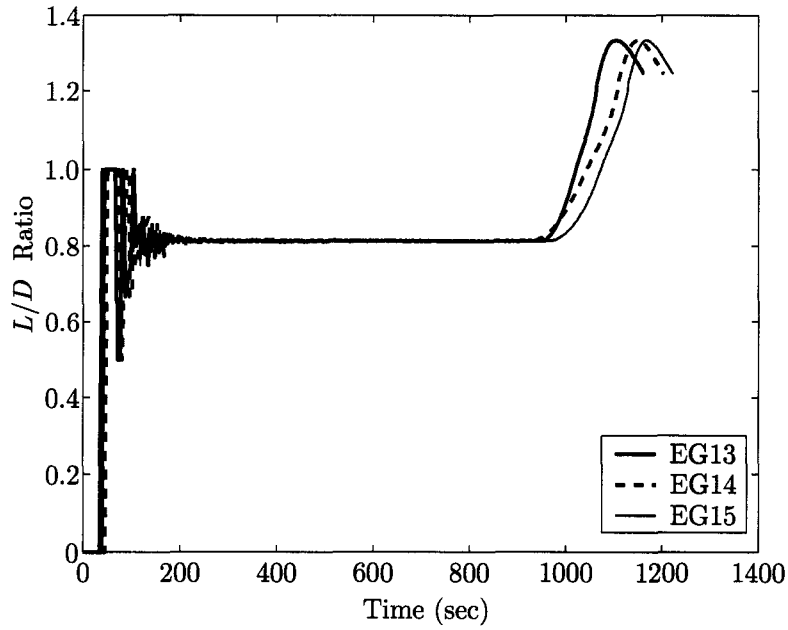
Figure 5.14   EG13-15 L/D profiles based on conditions
in Tables 5.2 to 5.5

5.6.2   EG16-18 Trajectories

Tables 5.6 through 5.8 are the initial entry conditions for test cases EG16-18 ($i =$ 51.6° and $\dot{Q}_{max} = 680{,}935$ W/m^2). These are the high inclination and low heat rate re-entry test cases. Table 5.9 has the path and terminal constraints for EG16-18 as well as EG19-21.

Table 5.6   Initial conditions for EG16 entry trajectory

$J = \min \int \dot{Q}\, dt$			
Altitude, $r_i =$	121.858 km	Flight-path-angle, $\gamma_i =$	$-1.249°$
Longitude, $\Theta_i =$	$-127.498°$	Velocity azimuth angle, $\Psi_i =$	$43.447°$
Latitude, $\Phi_i =$	$-29.516°$	Angle-of-attack, $\alpha_i =$	$45.00°$
Velocity, $V_i =$	7,625 m/s	Bank angle, $\sigma_i =$	$-0.002°$
Inclination, $i =$	$51.6°$	—	—

Table 5.7   Initial conditions for EG17 entry trajectory

$J = \min \int \dot{Q}\, dt$			
Altitude, $r_i =$	123.104 km	Flight-path-angle, $\gamma_i =$	$-1.249°$
Longitude, $\Theta_i =$	$-122.498°$	Velocity azimuth angle, $\Psi_i =$	$46.062°$
Latitude, $\Phi_i =$	$-33.263°$	Angle-of-attack, $\alpha_i =$	$45.00°$
Velocity, $V_i =$	7,625 m/s	Bank angle, $\sigma_i =$	$-0.002°$
Inclination, $i =$	$51.6°$	—	—

Table 5.8   Initial conditions for EG18 entry trajectory

$J = \min \int \dot{Q}\, dt$			
Altitude, $r_i =$	120.132 km	Flight-path-angle, $\gamma_i =$	$-1.249°$
Longitude, $\Theta_i =$	$-134.498°$	Velocity azimuth angle, $\Psi_i =$	$40.410°$
Latitude, $\Phi_i =$	$-23.751°$	Angle-of-attack, $\alpha_i =$	$45.00°$
Velocity, $V_i =$	7,627 m/s	Bank angle, $\sigma_i =$	$0.002°$
Inclination, $i =$	$51.6°$	—	—

Table 5.9   Constraints imposed on entry trajectories EG16-21

Constraints:	Values:
Final altitude, r_f^*	29.431 km
Final velocity, V_f^*	919.86 m/s
Final range-to-go, r_{togof}^*	55.56 km (30.0 nm)
Normal load limit, n_a	$n_a \leq 2.5g$
Heating rate limit, $\dot{Q}$	$\mathbf{0 \leq \dot{Q} \leq 680{,}935\ Watt/m^2\ (60\ BTU/ft^2 \cdot sec)}$
Dynamic pressure limit, q	$0 \leq q \leq 14{,}364\ N/m^2\ (300\ psf)$
Equilibrium bank angle, σ_{EQ}	$5°$

EG16-18 test cases are similar to those of EG13-15 in the sense that they entered the Earth's atmosphere from the same inclination, thus the trajectories were similar as well. This is reflected in Figures 5.15 through 5.26. Two major differences in EG16-18 cases are the longer downrange requirement and the lower $\dot{Q}_{max}$ constraint (refer to Table 5.1). The most noticeable change resulting from these two differences was the longer overall flight time. EG16 had a total flight time of 1,390.78 seconds, EG17 had 1,418.62 seconds, and EG18 had 1,433.94 seconds. Even with the lower $\dot{Q}_{max}$, all three test cases still are not "cruising" on the upper bound of the $\dot{Q}_{max}$ as shown in Figure 5.23. This is compensated by the longer downrange and the spacecraft does not have to descend as fast. Therefore, EG16-18 can also be flown at a lower $\dot{Q}_{max}$ value.
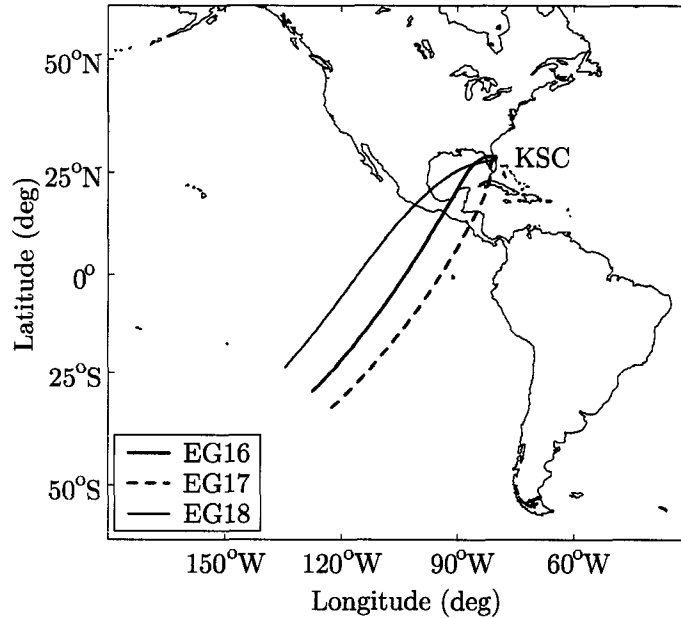
Figure 5.15   EG16-18 ground track profiles based
on conditions in Tables 5.6 to 5.9
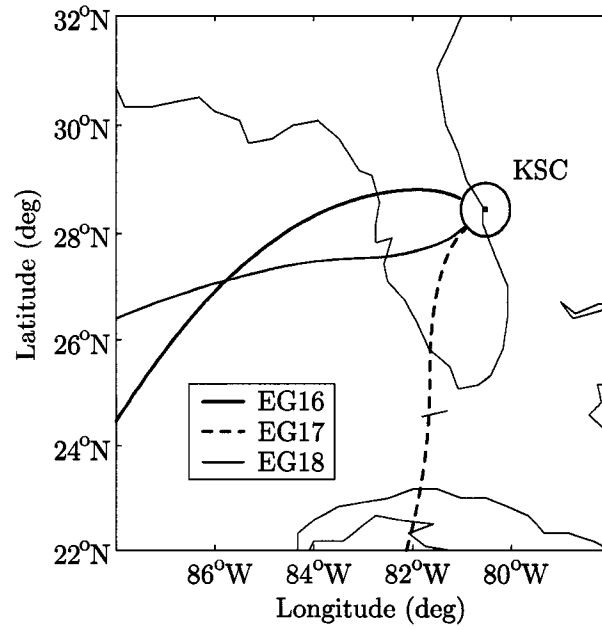
Figure 5.16   EG16-18 ground track profiles in detail
based on conditions in Tables 5.6 to 5.9
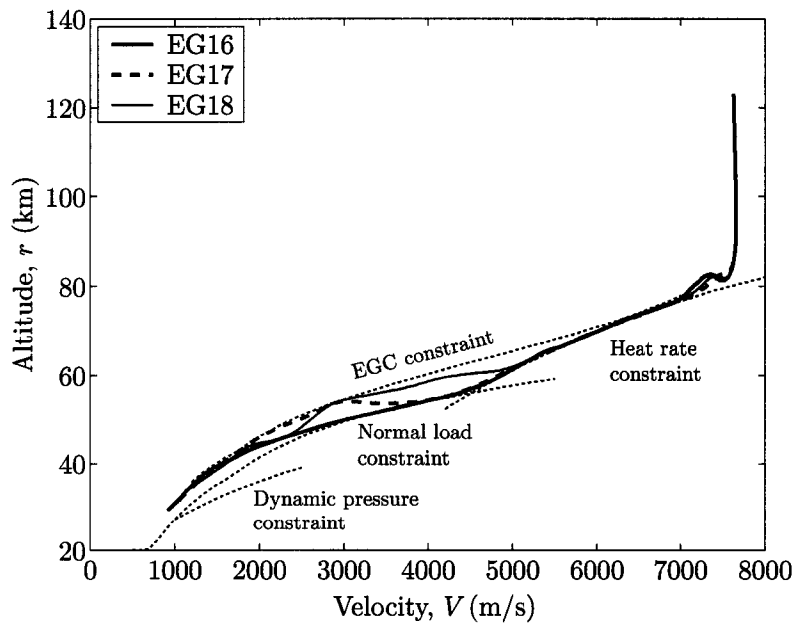
Figure 5.17   EG16-18 altitude vs velocity profiles based
on conditions in Tables 5.6 to 5.9
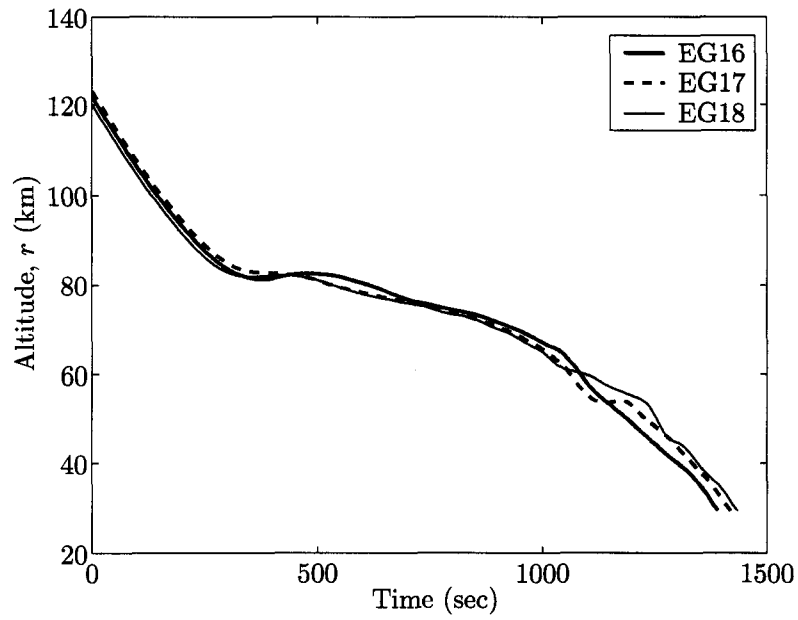
Figure 5.18 EG16-18 altitude profiles based on conditions in Tables 5.6 to 5.9
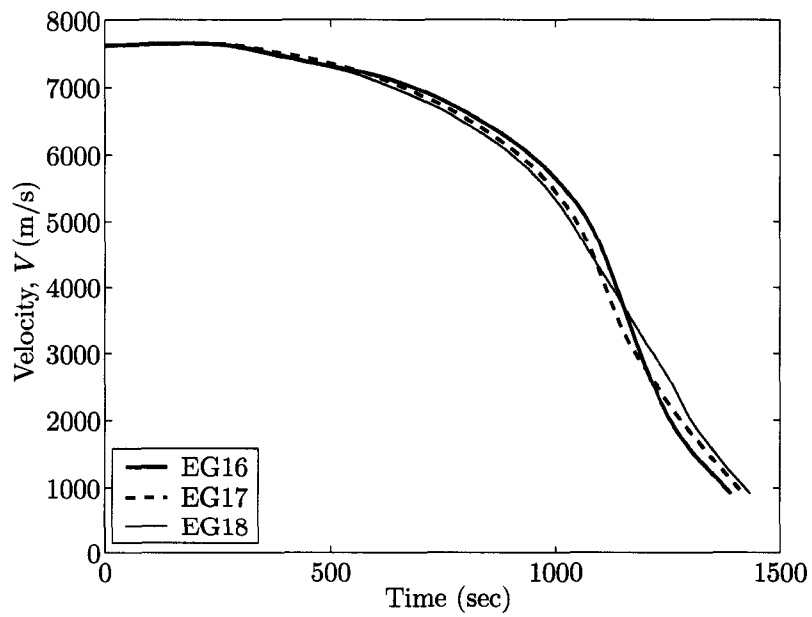
Figure 5.19 EG16-18 velocity profiles based on conditions in Tables 5.6 to 5.9
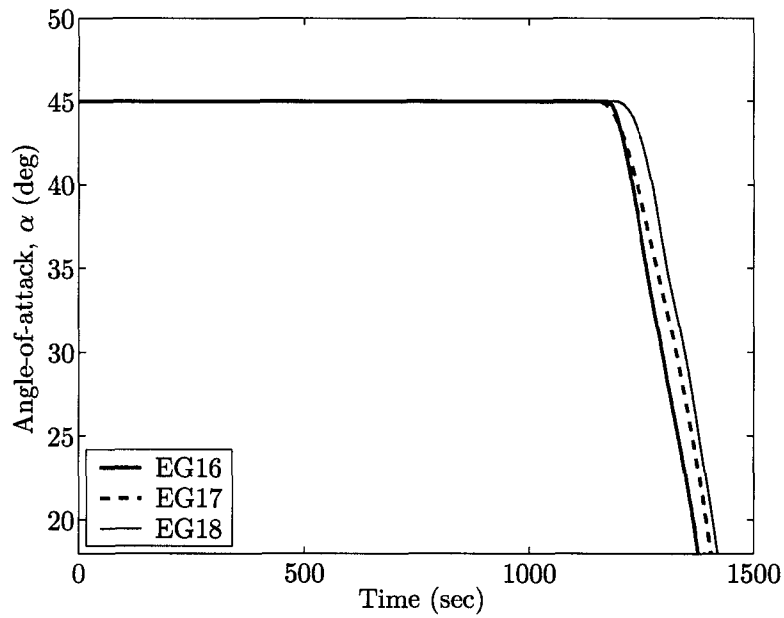
Figure 5.20   EG16-18 angle-of-attack profiles based on conditions in Tables 5.6 to 5.9
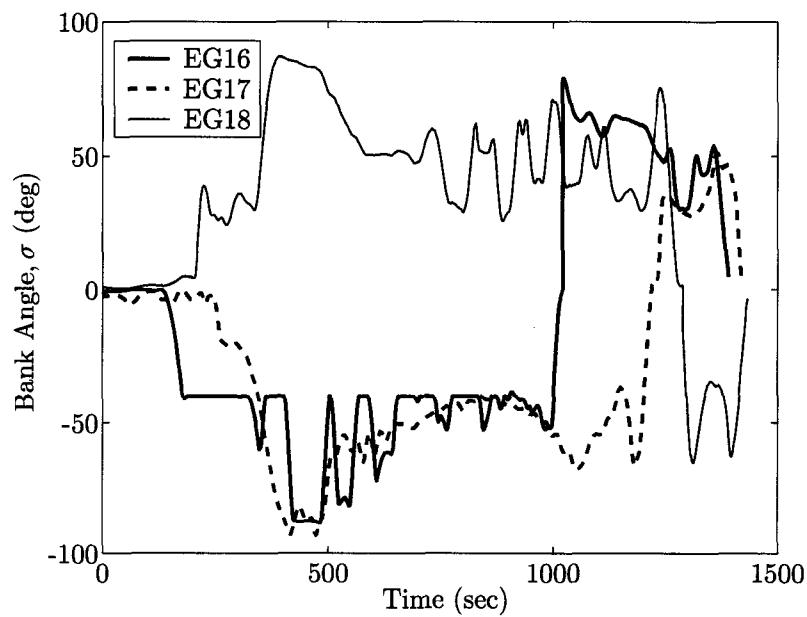
Figure 5.21   EG16-18 bank angle profiles based on conditions in Tables 5.6 to 5.9
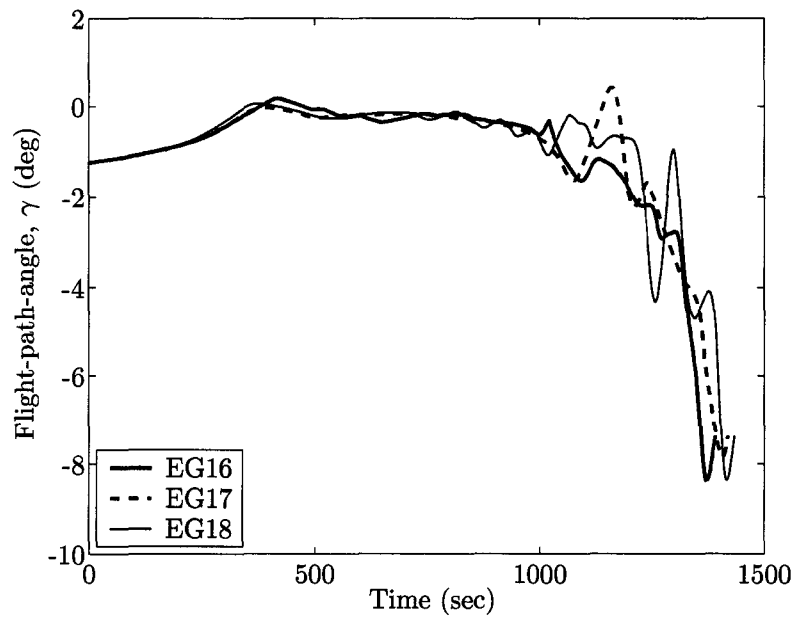
Figure 5.22   EG16-18 flight-path-angle profiles based on conditions in Tables 5.6 to 5.9
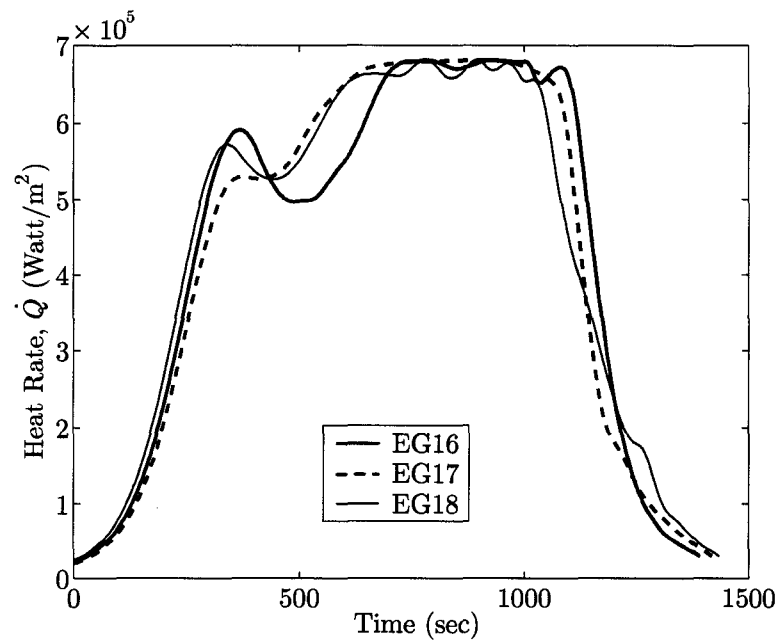
Figure 5.23   EG16-18 heat load profiles based on conditions in Tables 5.6 to 5.9
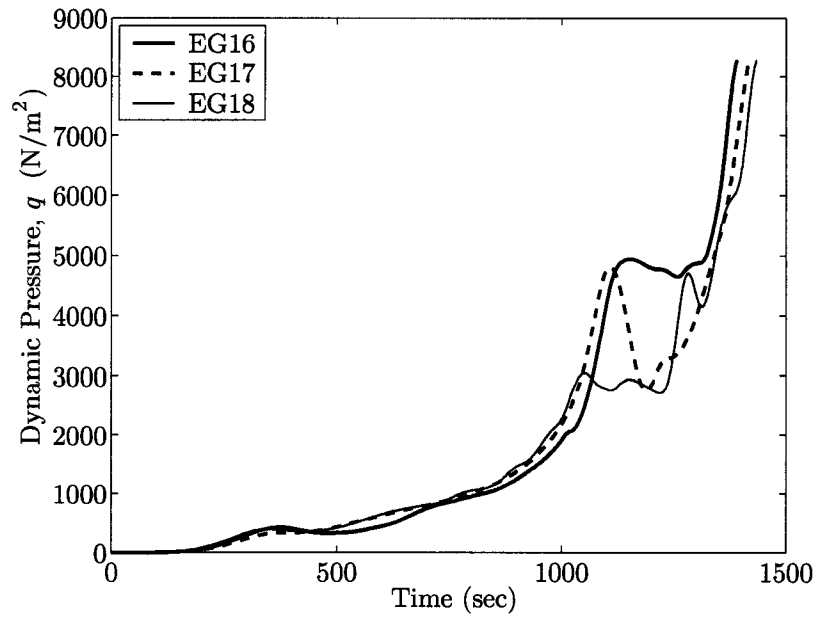
Figure 5.24   EG16-18 dynamic pressure profiles based on conditions in Tables 5.6 to 5.9
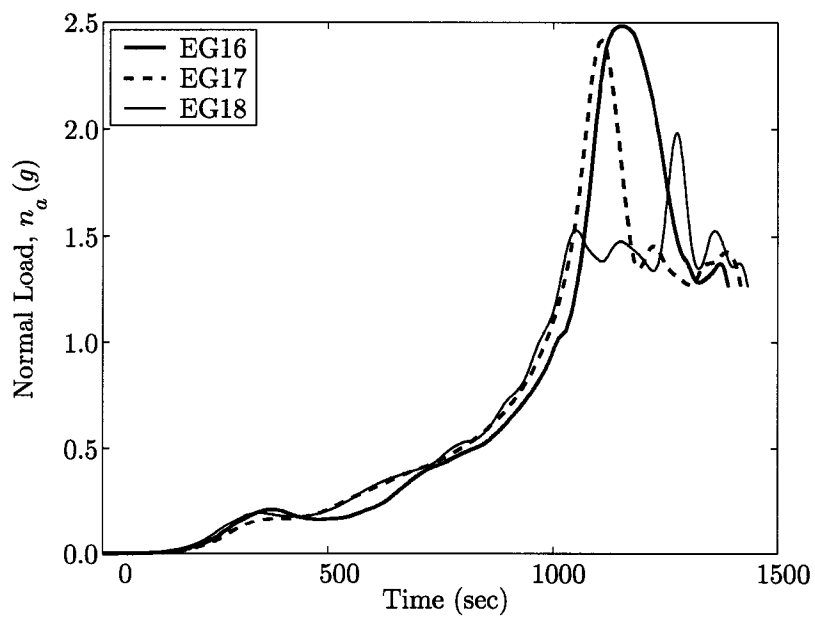
Figure 5.25   EG16-18 normal load profiles based on conditions in Tables 5.6 to 5.9
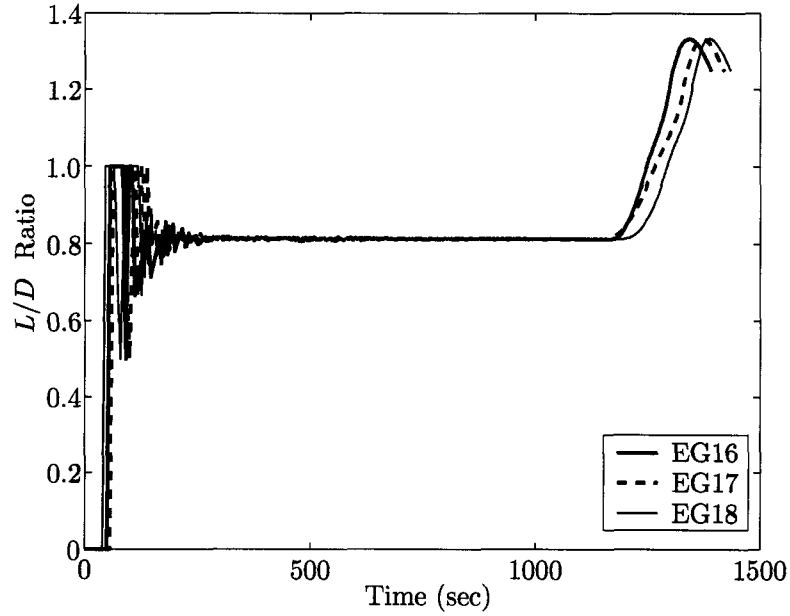
Figure 5.26   EG16-18 L/D profiles based on conditions
in Tables 5.6 to 5.9

5.6.3   EG19-21 Trajectories

Tables 5.10 through 5.12 are the initial entry conditions for test cases EG19-21 ($i =$ 28.5° and $\dot{Q}_{max}$ = 680,935 W/m^2). These are the low inclination and low heat rate re-entry test cases. Table 5.9 has the path and terminal constraints for EG19-21 (same as the ones imposed on EG16-18).

Table 5.10 Initial conditions for EG19 entry trajectory

$J = \min \int Q \, dt$			
Altitude, $r_i =$	121.649 km	Flight-path-angle, $\gamma_i =$	$-1.027°$
Longitude, $\Theta_i =$	$-141.724°$	Velocity azimuth angle, $\Psi_i =$	$59.854°$
Latitude, $\Phi_i =$	$-2.305°$	Angle-of-attack, $\alpha_i =$	$45.00°$
Velocity, $V_i =$	7,442 m/s	Bank angle, $\sigma_i =$	$-0.002°$
Inclination, $i =$	$28.5°$	—	—

Table 5.11 Initial conditions for EG20 entry trajectory

$J = \min \int Q \, dt$			
Altitude, $r_i =$	122,079 km	Flight-path-angle, $\gamma_i =$	$-1.028°$
Longitude, $\Theta_i =$	$-137.724°$	Velocity azimuth angle, $\Psi_i =$	$61.026°$
Latitude, $\Phi_i =$	$-8.446°$	Angle-of-attack, $\alpha_i =$	$45.00°$
Velocity, $V_i =$	7,442 m/s	Bank angle, $\sigma_i =$	$-0.002°$
Inclination, $i =$	$28.5°$	—	—

Table 5.12 Initial conditions for EG21 entry trajectory

$J = \min \int \dot{Q} \, dt$			
Altitude, $r_i =$	124.848 km	Flight-path-angle, $\gamma_i =$	$-1.028°$
Longitude, $\Theta_i =$	$-157.724°$	Velocity azimuth angle, $\Psi_i =$	$71.454°$
Latitude, $\Phi_i =$	$-1.028°$	Angle-of-attack, $\alpha_i =$	$45.00°$
Velocity, $V_i =$	7,440 m/s	Bank angle, $\sigma_i =$	$-0.002°$
Inclination, $i =$	$28.5°$	—	—

Low inclination and low heat rate test cases EG19-21 have similar flying character-istics of those EG13-15 and EG16-18 as exhibited in Figures 5.27 through 5.38. Notice the bank profiles depicted in Figure 5.33 all started with "negative" banking followed by a bank reversal to "positive" banking for final HAC alignment. This is because all initial bank angles at the entry interface point have small negative value of $\sigma_i = -0.002°$. The heat rate profiles illustrated in Figure 5.35 show that none of the three test cases are "cruising" on the upper bound of the heat rate constraint.
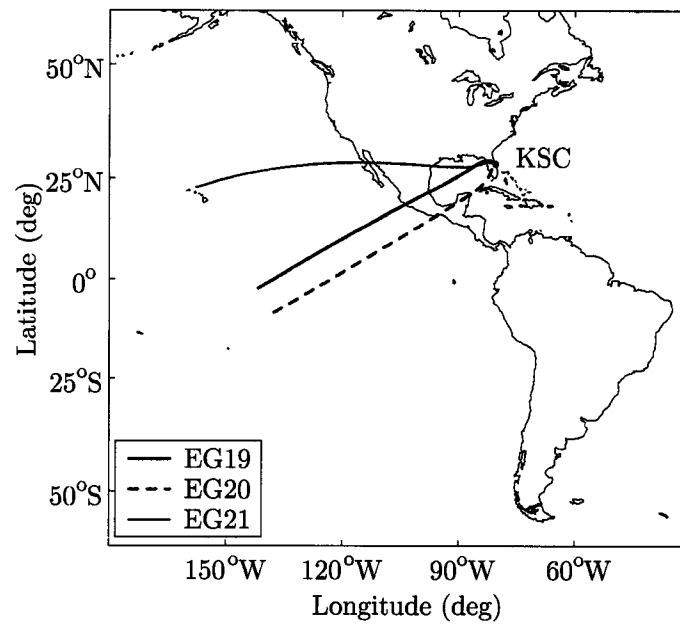
Figure 5.27   EG19-21 ground track profiles based on
conditions in Tables 5.10 to 5.12 and 5.9
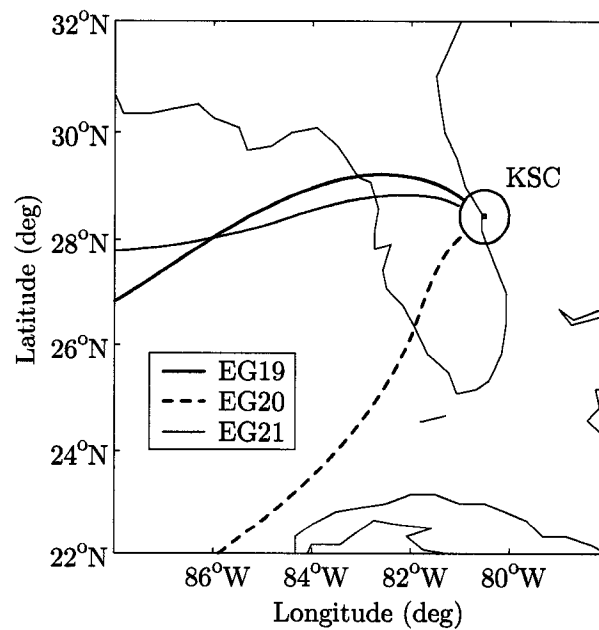
Figure 5.28   EG19-21 ground track profiles in detail based
on conditions in Tables 5.10 to 5.12 and 5.9
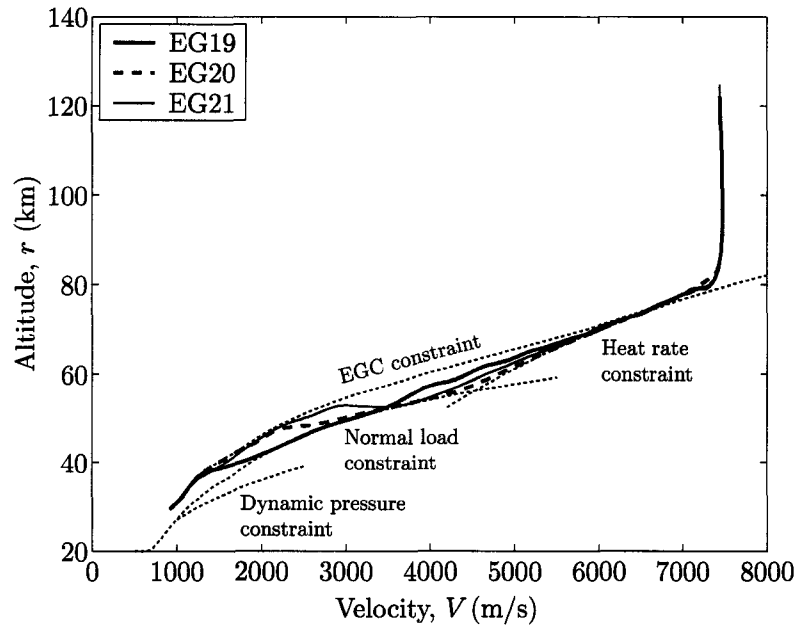
Figure 5.29   EG19-21 altitude vs velocity profiles based
on conditions in Tables 5.10 to 5.12 and 5.9
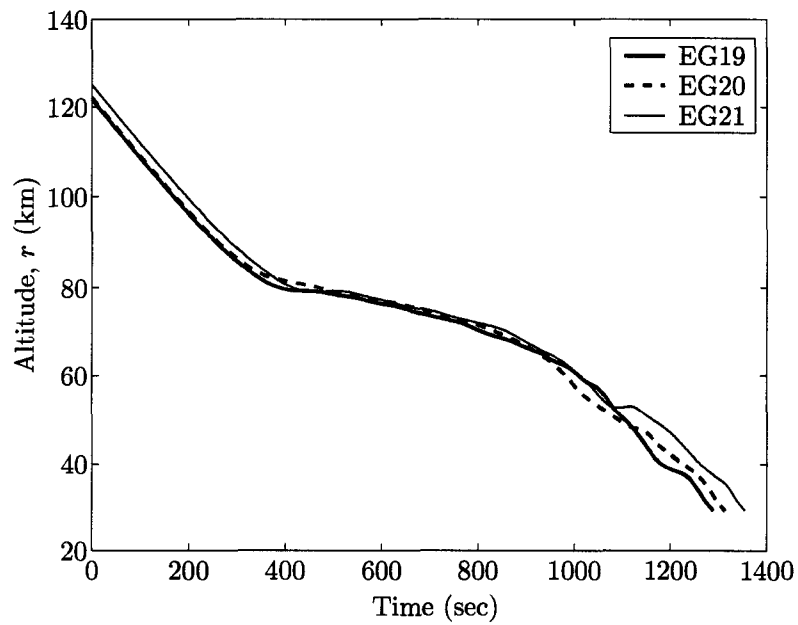
Figure 5.30   EG19-21 altitude profiles based on condi-
tions in Tables 5.10 to 5.12 and 5.9
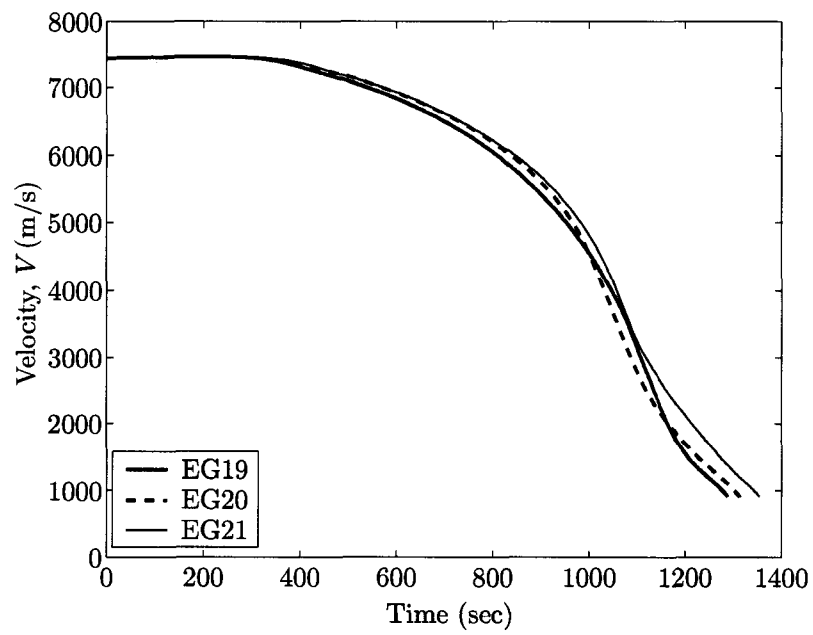
Figure 5.31 EG19-21 velocity profiles based on conditions in Tables 5.10 to 5.12 and 5.9
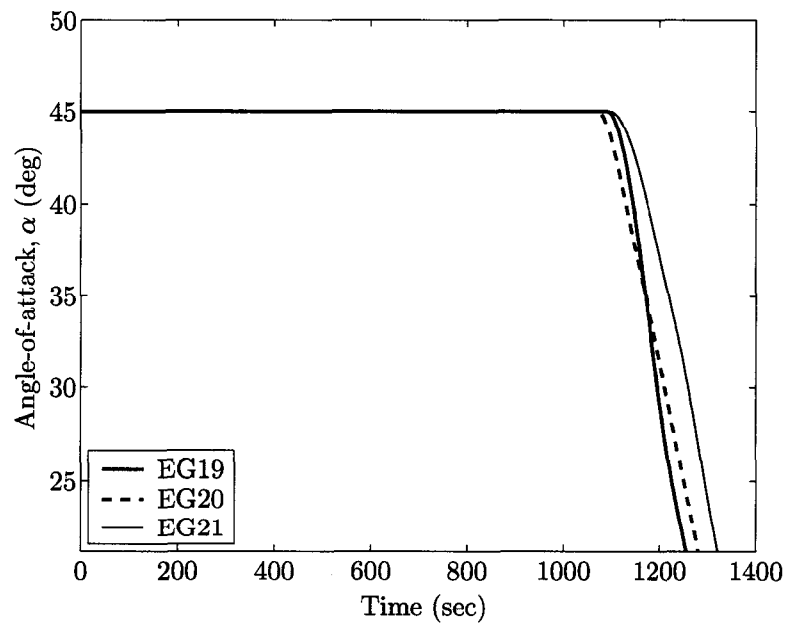
Figure 5.32 EG19-21 angle-of-attack profiles based on conditions in Tables 5.10 to 5.12 and 5.9
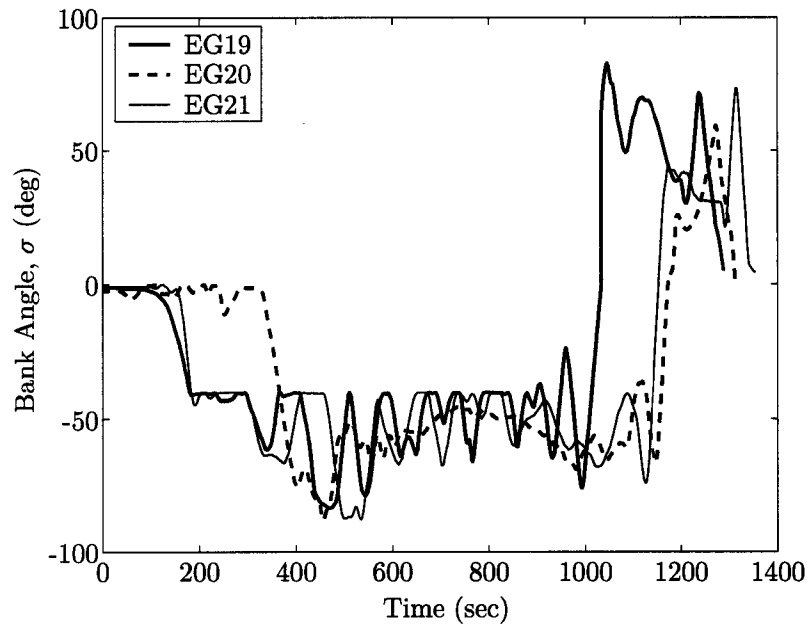
Figure 5.33   EG19-21 bank angle profiles based on conditions in Tables 5.10 to 5.12 and 5.9
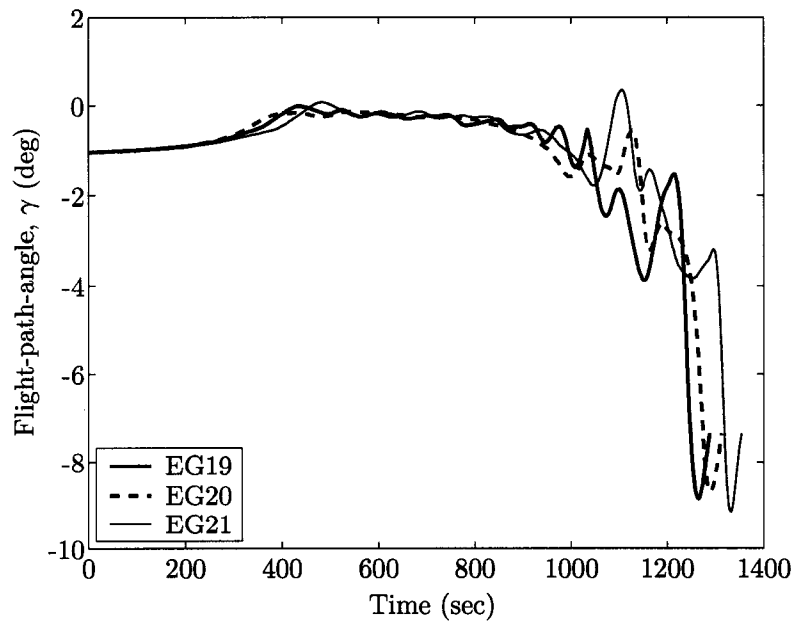
Figure 5.34   EG19-21 flight-path-angle profiles based on conditions in Tables 5.10 to 5.12 and 5.9
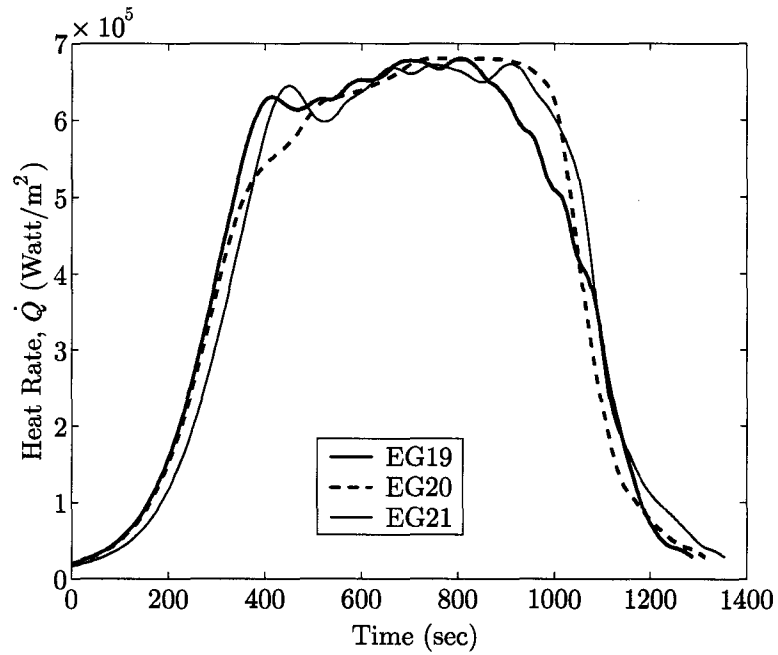
Figure 5.35   EG19-21 heat load profiles based on conditions in Tables 5.10 to 5.12 and 5.9
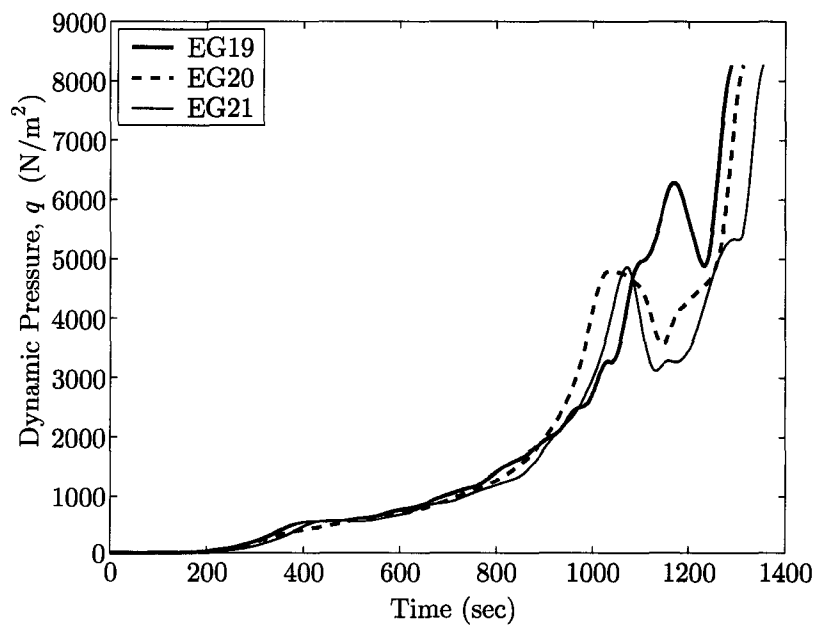
Figure 5.36   EG19-21 dynamic pressure profiles based on conditions in Tables 5.10 to 5.12 and 5.9
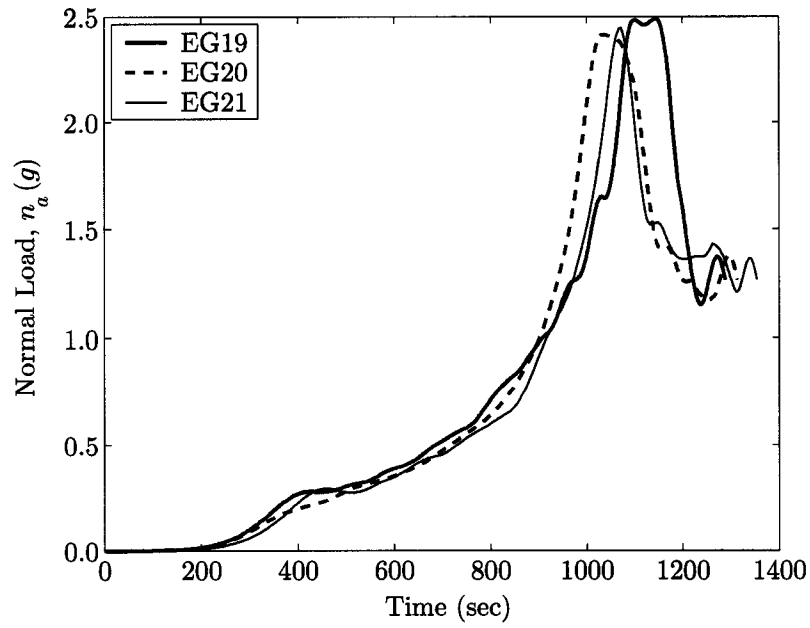
Figure 5.37   EG19-21 normal load profiles based on conditions in Tables 5.10 to 5.12 and 5.9
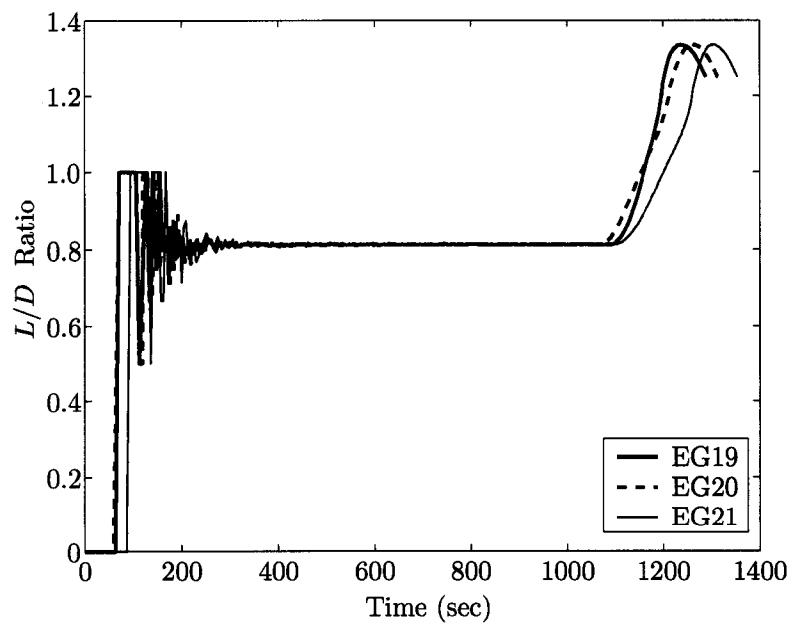
Figure 5.38   EG19-21 L/D profiles based on conditions in Tables 5.10 to 5.12 and 5.9

5.7 Minimize Peak Heat Rate

Finding the lowest heat rate value is also of interest to the trajectory designer because to be able to fly at a lower $\dot{Q}_{max}$ means lower maintenance and increase tile life-cycle expectancy as discussed in Section 2.3 on page 22. Furthermore, Figures 5.11, 5.23 and 5.35 all show that there is room to fly at a lower $\dot{Q}_{max}$ value. While flying at a lower $\dot{Q}_{max}$ may lower maintenance and increase tile life-cycle expectancy, this also implies that the entry corridor will be narrower, thus making the problem more challenging. The performance index used to investigate the minimum $\dot{Q}_{max}$ value is:

$$J = \min \dot{Q}_{max} \qquad (5.16)$$

Using Equation (5.16) as the performance index, optimal trajectories are generated using the same equality and inequality constraints as nominal entry trajectories with the exception that $\dot{Q}_{max}$ is not imposed. This is because $\dot{Q}_{max}$ is now a parameter instead of an inequality constraint. Depending on the initial conditions, trajectories with or without EGC constraint may make a difference in finding the lowest $\dot{Q}_{max}$ value. Since EGC is a soft constraint, it does not need to be enforced strictly. Table 5.13 summarizes the lowest heat rate value determined for each of the three groups as initially described in Table 5.1. The baseline values in the third column refer to those values used for nominal entry trajectories. Table 5.14 illustrates the relationship between heat load and heat rate. Notice that by flying at lower $\dot{Q}_{max}$ values (8 to 10% lower than the specified values) resulted in an approximately 0.5 to 1% increase in overall head load measured in mega Joules per squared meter (MJ/m^2). This subtle difference is expected because the entry corridor is indeed so tightly constrained by the range requirement along with $\dot{Q}_{max}$, n_a, q and EGC constraints that it does not allow too much variation. The values of heat load obtained for the X-33 are comparable to that of the Space Shuttle (5,675 MJ/m^2 or 50×10^3 BTU/ft^2) and the X-38 (11,450 MJ/m^2 or 100×10^3 BTU/ft^2) [107].

Table 5.13 Summary of minimizing $\dot{Q}_{max}$ for EG15, EG18 and EG21

	without EGC	with EGC	baseline
EG15	691,603 Watt/m^2 (60.94 BTU/ft$^2\cdot$ sec)	691,036 Watt/m^2 (60.89 BTU/ft$^2\cdot$ sec)	749,029 Watt/m^2 (66 BTU/ft$^2\cdot$ sec)
EG18	613,863 Watt/m^2 (54.09 BTU/ft$^2\cdot$ sec)	656,876 Watt/m^2 (57.88 BTU/ft$^2\cdot$ sec)	680,935 Watt/m^2 (60 BTU/ft^2 sec)
EG21	626,347 Watt/m^2 (55.19 BTU/ft$^2\cdot$ sec)	658,238 Watt/m^2 (58 BTU/ft$^2\cdot$ sec)	680,935 Watt/m^2 (60 BTU/ft$^2\cdot$ sec)

Table 5.14 Comparison of minimizing heat load vs heat rate

	$J = \min \int \dot{Q}\, dt$			$J = \min \dot{Q}_{max}$		
	Time (sec)	$\dot{Q}_{max}$ (Watt/m^2)	Heat Load (MJ/m^2)	Time (sec)	$\dot{Q}_{max}$ (Watt/m^2)	Heat Load (MJ/m^2)
EG13	1,162		5,442			
EG14	1,203		5,400			
EG15	1,223	749,029	5,491	1,205	691,603	5,566
EG16	1,391		6,079			
EG17	1,419		6,033			
EG18	1,434	680,935	6,162	1,449	613,863	6,188
EG19	1,288		5,383			
EG20	1,313		5,342			
EG21	1,354	680,935	5,383	1,352	626,347	5,450

Every investigated $J = \min \dot{Q}_{max}$ case has similar flight features, thus only one case will be presented here (detailed final conditions can be found in Tables D.10 through D.12 starting on page 288). EG21 is the "late" entry from $i = 28.5°$ starting its entry interface above Hawaii as pictured in Figure 5.39. The three ground tracks shown are: ① $J = \min \dot{Q}_{max}$ with all but EGC constraint; ② $J = \min \dot{Q}_{max}$ with every constraint; and ③ $J = \min \int \dot{Q}\, dt$ (baseline).

Figure 5.40 is the EG21 entry trajectory in the r-V design space showing cases #1 (without EGC) and #2 (with EGC) have very close similarity. The baseline (#3) also did not show any significant deviation. This confirms that EGC is indeed a soft constraint. A further look at Figure 5.41 supports that the EGC constraint is only violated slightly at the two small regions indicated by the arrows.

The test cases #1 (without EGC), #2 (with EGC), and #3 (the baseline) did not show any significant deviation in any aspect of the flight as shown in Figures 5.42 through 5.50.
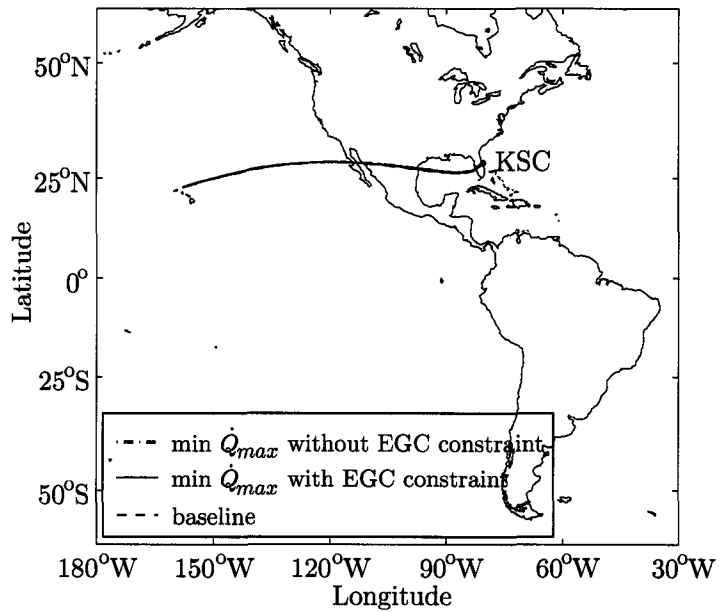
Figure 5.39   EG21 ground tracks with $J = \min \dot{Q}_{max}$
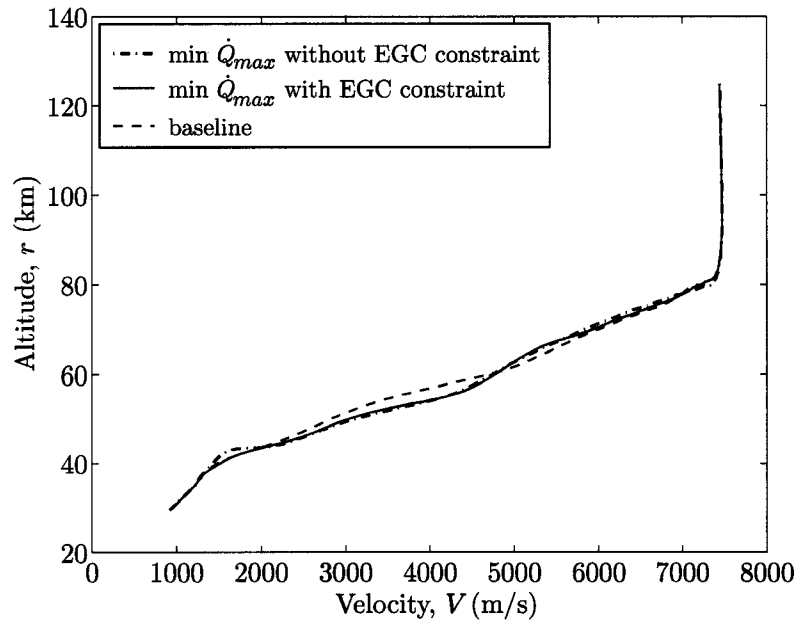
Figure 5.40   EG21 altitude vs velocity profiles with
$J = \min \dot{Q}_{max}$
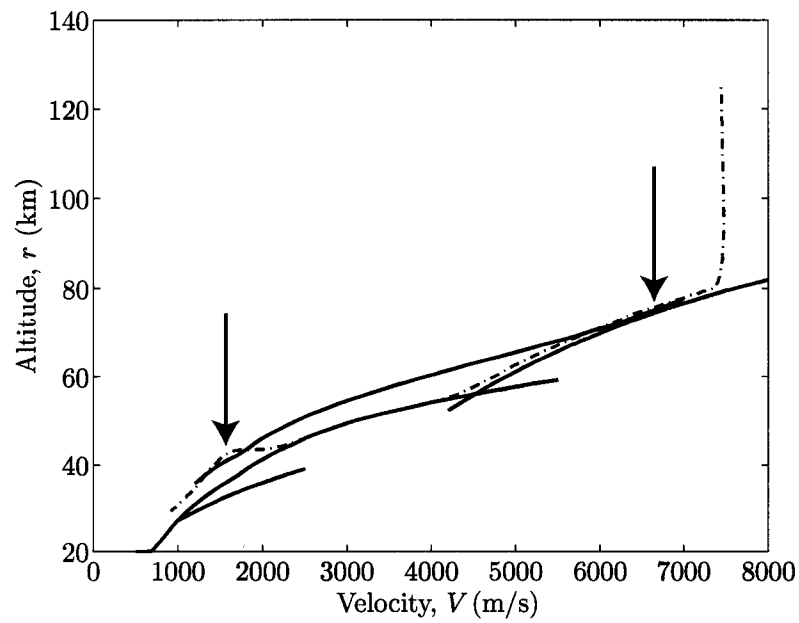
Figure 5.41   EG21 altitude vs velocity without EGC constraint
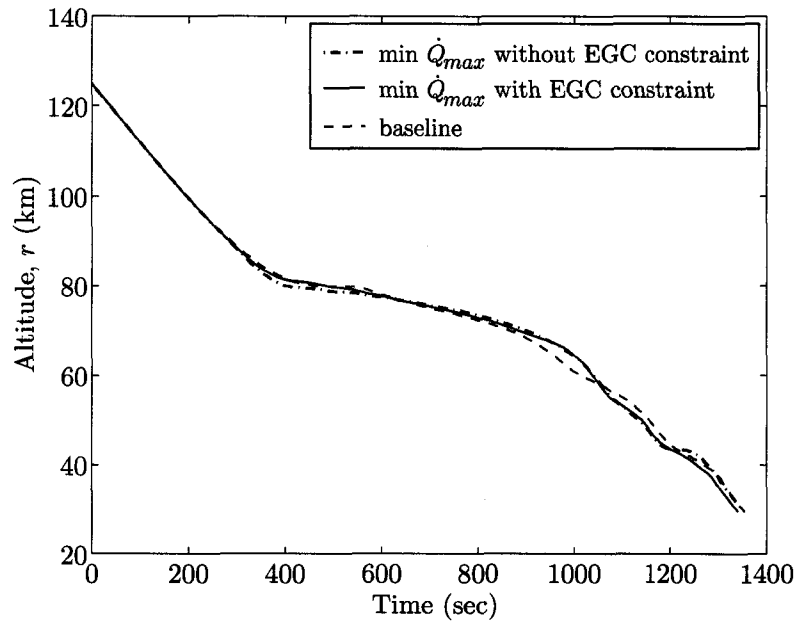
Figure 5.42   EG21 altitude profiles with $J = \min \dot{Q}_{max}$
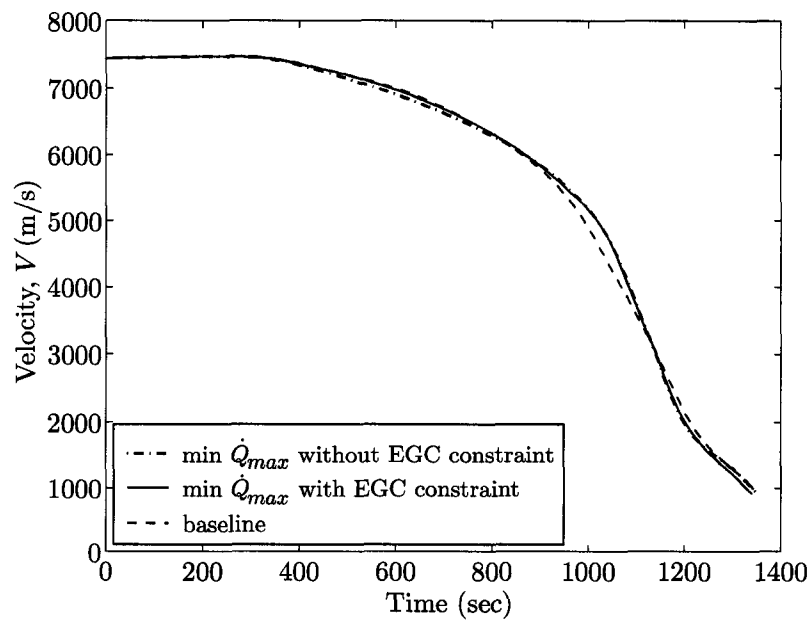
Figure 5.43   EG21 velocity profiles with $J = \min \dot{Q}_{max}$
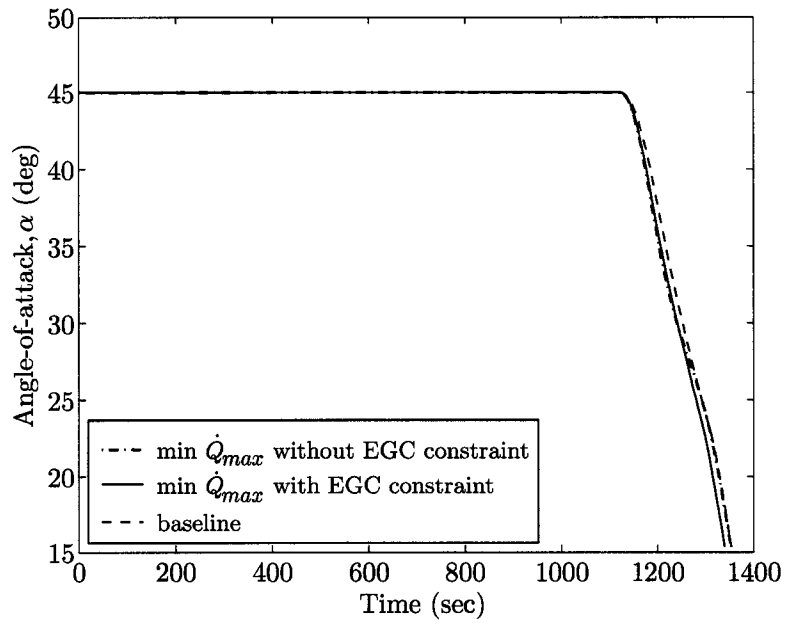
Figure 5.44   EG21 angle-of-attack profiles with
$$J = \min \dot{Q}_{max}$$
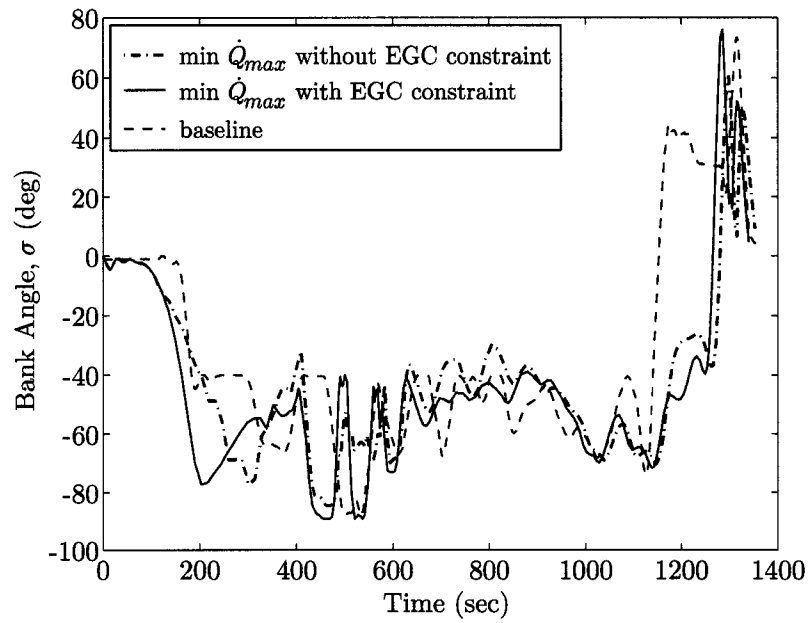
Figure 5.45   EG21 bank angle profiles with
$$J = \min \dot{Q}_{max}$$
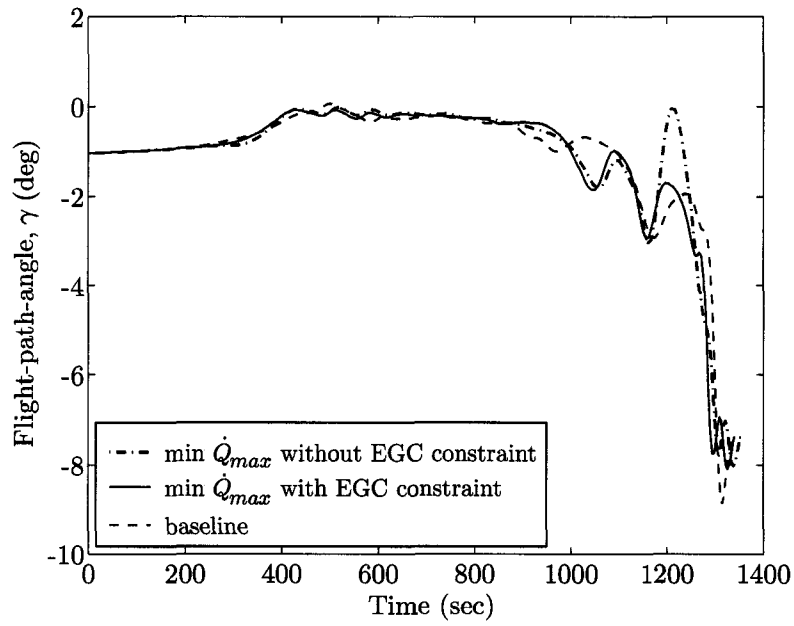
Figure 5.46   EG21   flight-path-angle   profiles
with $J = \min \dot{Q}_{max}$
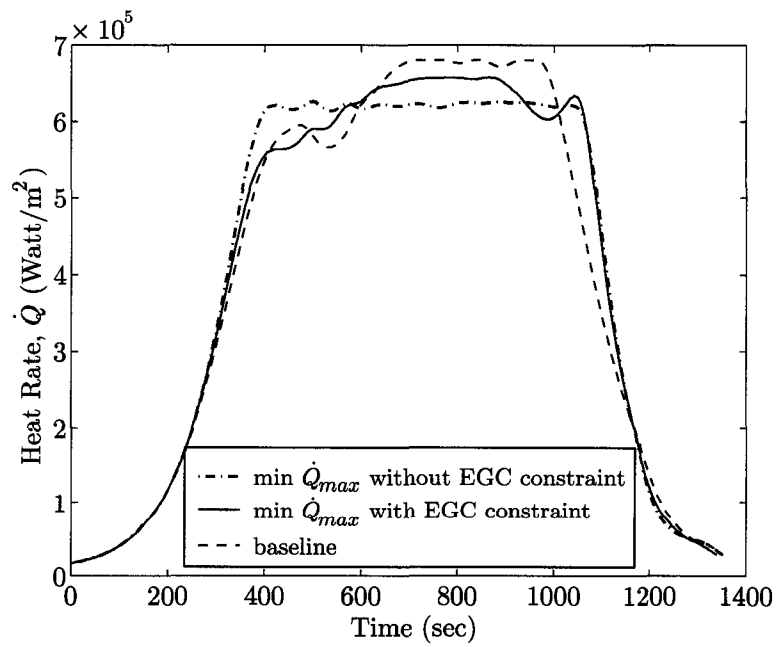
Figure 5.47   EG21 heat rate profiles with $J = \min \dot{Q}_{max}$
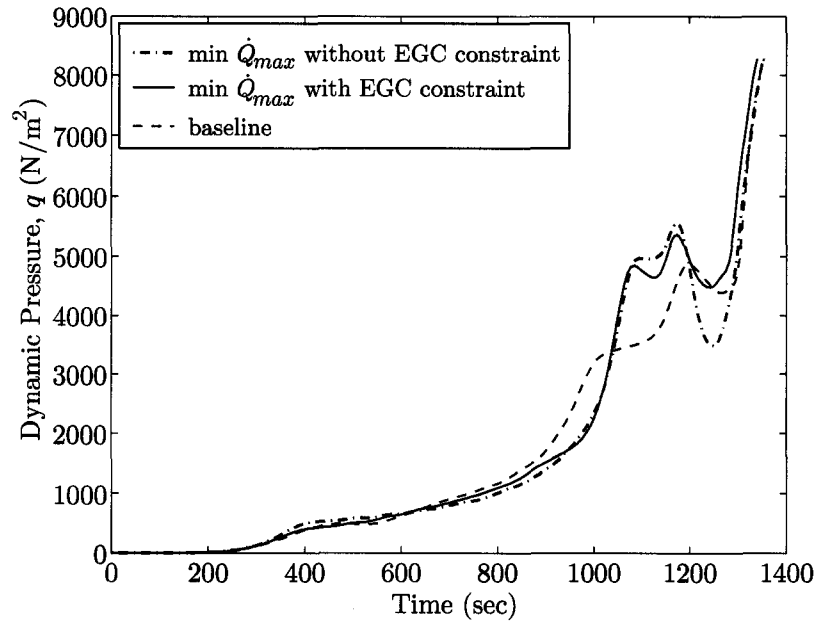
Figure 5.48 EG21 dynamic pressure profiles with $J = \min \dot{Q}_{max}$
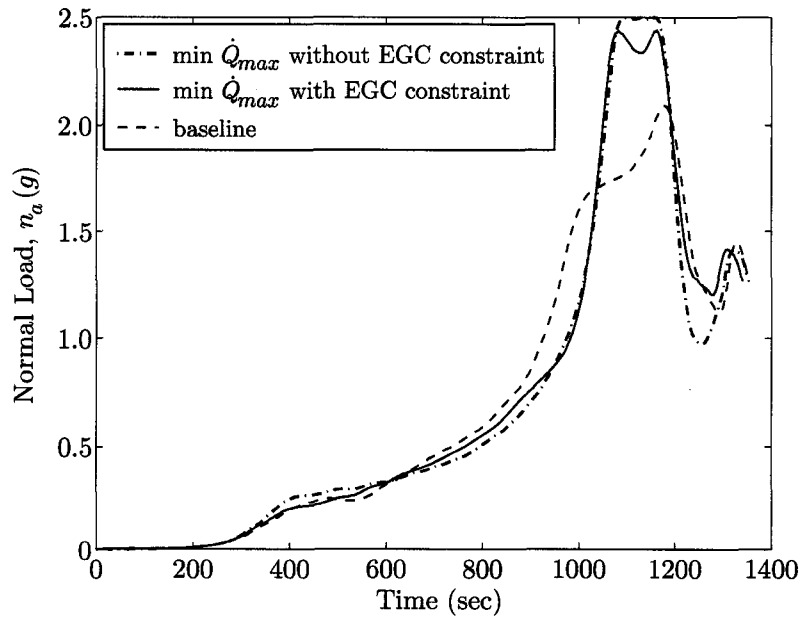
Figure 5.49 EG21 normal load profiles with $J = \min \dot{Q}_{max}$
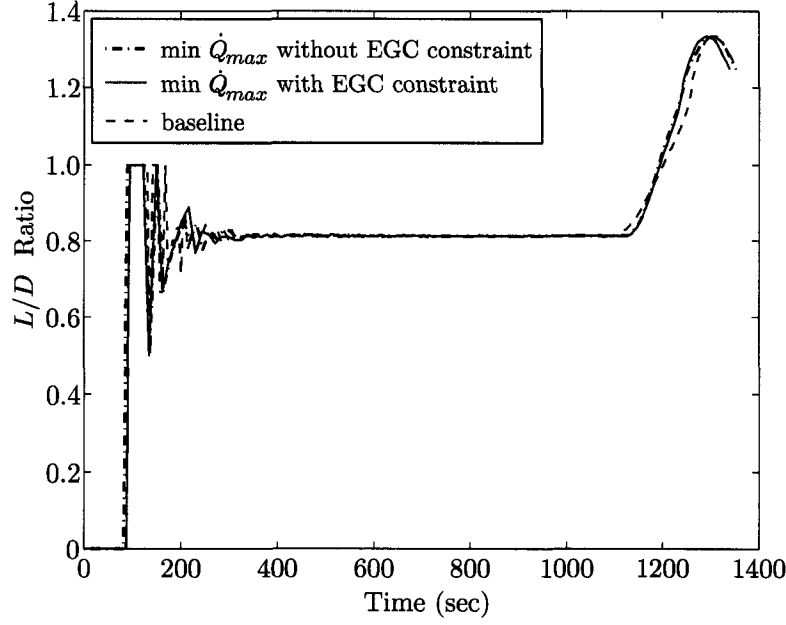
Figure 5.50   EG21 L/D profiles with $J = \min \dot{Q}_{max}$

5.8   Footprint of Re-entry Vehicle

The maximum area reachable by a vehicle on the surface of the Earth during re-entry is extremely important for mission planners. The footprint information allows the mission planner to select an alternate landing site when necessary.

The governing EOMs for footprint calculation are the same as the nominal entry calculations, $x = \begin{bmatrix} \dot{r}_c & \dot{\Theta} & \dot{\Phi} & \dot{V}_r & \dot{\gamma} & \dot{\Psi} \end{bmatrix}^T$. However, angle-of-attack is now an active control instead of a pre-scheduled control as shown in Equation (5.14). Therefore, $u = \begin{bmatrix} \alpha & \sigma \end{bmatrix}^T$ with $15° < \alpha < 40°$ and $-90° < \sigma < 90°$. Furthermore, both α and σ are subjected to a maximum rate of $\dot{\alpha}_{max} = \dot{\sigma}_{max} = \pm 5.0$ deg/sec and a maximum acceleration of $\ddot{\alpha}_{max} = \ddot{\sigma}_{max} = \pm 3.5$ deg/sec² for the X-33. More precisely, the controls are $u = \begin{bmatrix} \ddot{\alpha} & \ddot{\sigma} \end{bmatrix}^T$ for the reason that controlling the accelerations will in turn minimize angles fluctuation.

Lastly, footprint determination is based on computing the maximum crossrange for a given final downrange [78, 99, 108–110]. Crossrange (CR) is defined as the angle between the landing site radius vector and its projection onto the plane defined by the vehicle's initial radius and velocity vector as portrayed in Figure 5.51. Downrange (DR) is defined as the angle between the vehicle's radius vector and the projection of the landing site radius vector.
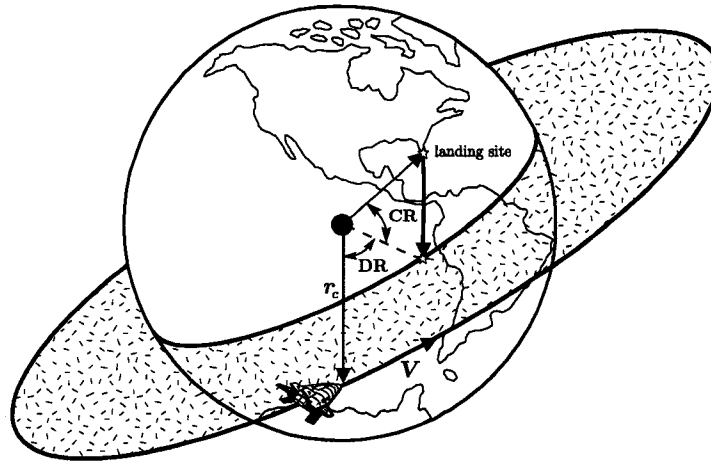
Figure 5.51   Definition of crossrange and downrange

For simplicity, the footprint is determined on the equatorial plane as displayed in Figure 5.52. Therefore, a maximum crossrange (latitude) can be computed for a given final downrange (longitude, Θ_f). Finally, a coordinate transformation outlined by Lu *et al.* [111] will be performed to correlate with an actual ground track.
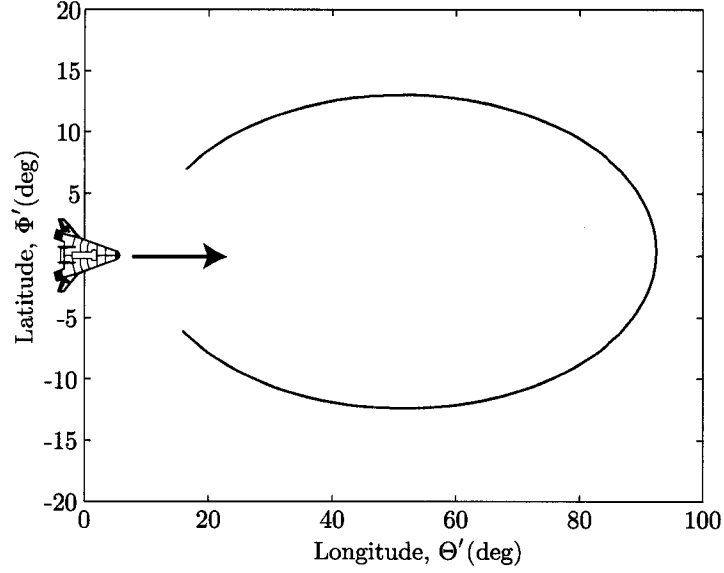
Figure 5.52   Example of a footprint in equatorial plane

The idea behind coordinate transformation is to be able to address the need to efficiently generate different trajectories for each orbital inclination, but otherwise same entry conditions. Lu *et al.* [111] presented a canonical coordinate system to perform the coordinate transformation to treat this type of problem.

The new equatorial plane is defined by the great-circle plane containing the nominal entry point E and the target point T as illustrated in Figure 5.53. The new longitude Θ' is measured in this plane from point E; the new latitude Φ' is calculated from the great-circle plane (Figure 5.54); and the new velocity azimuth angle Ψ' is measured clockwise from the new North. The EOMs in this new coordinate frame are the same as those presented in Equations (5.1) through (5.6). The reference entry trajectory is now defined in terms of the new coordinates $(r, \ \Theta', \ \Phi', \ V, \ \gamma, \ \Psi')$. The corresponding values of Θ', Φ' and Ψ' can be computed for any current values of Θ, Φ and Ψ in the original Earth-centered Earth-fixed (ECEF) system.
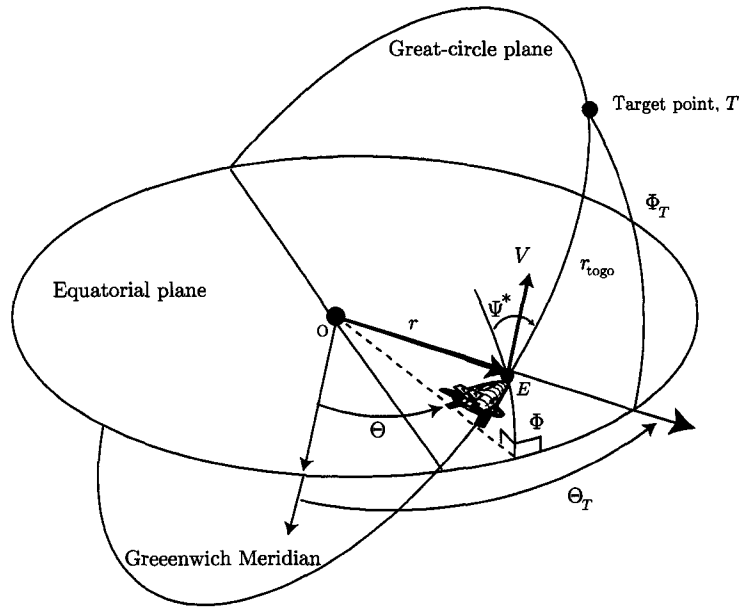
Figure 5.53   Coordinate transformation between different inclinations, courtesy of Ref. [111]
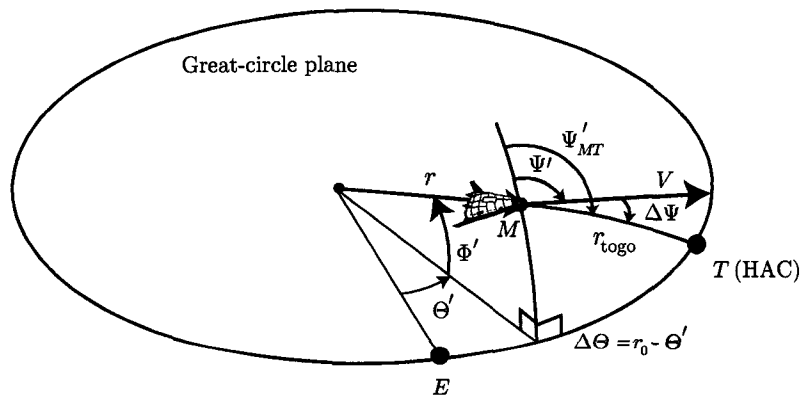
Figure 5.54   Detailed   range-to-go   geometry   in   the great-circle plane, courtesy of Ref. [111]

Suppose that point E has coordinates (Θ_E, Φ_E) in the original ECEF frame and point T has (Θ_T, Φ_T), the law of cosines in spherical trigonometry defines the range angle in radian between E and T as

$$r_0 = \cos^{-1}\left[\sin\Phi_T \sin\Phi_E + \cos\Phi_T \cos\Phi_E \cos(\Theta_T - \Theta_E)\right] \qquad (5.17)$$

The azimuth angle of the great-circle passing through E and T from E is

$$\Psi_{ET} = \tan^{-1}\left[\frac{\sin(\Theta_T - \Theta_E)\cos\Phi_T \cos\Phi_E}{\sin\Phi_T - \sin\Phi_E \cos(r_0)}\right] \qquad (5.18)$$

For any given spacecraft location M with coordinates (Θ, Φ) in the ECEF system, the range angle between E and M is computed by

$$r_{EM} = \cos^{-1}\left[\sin\Phi \sin\Phi_E + \cos\Phi \cos\Phi_E \cos(\Theta - \Theta_E)\right] \qquad (5.19)$$

and the azimuth angle at E of the great-circle joining E and M is defined as

$$\Psi_{EM} = \tan^{-1}\left[\frac{\sin(\Theta - \Theta_E)\cos\Phi \cos\Phi_E}{\sin\Phi - \sin\Phi_E \cos(r_{EM})}\right] \qquad (5.20)$$

Therefore, the coordinates of the point M in the new great-circle frame are

$$\Theta' = \tan^{-1}[\cos(\Psi_{ET} - \Psi_{EM})\tan(r_{EM})] \qquad (5.21)$$

$$\Phi' = \sin^{-1}[\sin(\Psi_{ET} - \Psi_{EM})\sin(r_{EM})] \qquad (5.22)$$

Suppose that the vehicle has velocity azimuth angle Ψ in the ECEF frame at point M. The range angle between M and T is

$$r_{MT} = \cos^{-1}[\sin \Phi_T \sin \Phi + \cos \Phi_T \cos \Phi \cos(\Theta_T - \Theta)] \qquad (5.23)$$

and the azimuth angle at M of the great-circle joining M and T is

$$\Psi_{MT} = \tan^{-1}\left[\frac{\sin(\Theta_T - \Theta) \cos \Phi_T \cos \Phi}{\sin \Phi_T - \sin \Phi \cos(r_{MT})}\right] \qquad (5.24)$$

Point T in the great-circle frame is defined as $(r_0, 0)$; therefore, the same arc MT at M has azimuth angle in the great-circle frame

$$\Psi'_{MT} = -\tan^{-1}\left[\frac{\tan(r_0 - \Theta')}{\sin \Phi'}\right] \qquad (5.25)$$

where Θ' and Φ' are obtained in Equations (5.21) and (5.22), and r_0 from Equation (5.17). Then the velocity azimuth angle of the vehicle in the great-circle frame with respect to the new North is

$$\Psi' = \Psi'_{MT} - \Psi_{MT} + \Psi \qquad (5.26)$$

Now, working in reverse will generate the values of Θ, Φ and Ψ for given Θ', Φ' and Ψ', thus transforming from equatorial plane to the actual ground track of footprint.

As discussed in Section 5.8, footprint determination is based on computing the maximum crossrange for a given final downrange, Θ_f. Therefore, the performance index used for entry footprint determination is

$$J = \max \Phi_f \qquad (5.27)$$

Table 5.15 lists the initial conditions used in footprint determination for $i = 51.6°$ on the equatorial plane. Notice that the initial longitude and latitude are both 0° and the velocity azimuth angle is at 90°, pointing eastward.

Table 5.15   Initial conditions for footprint determination on equatorial plane

$J = \max \Phi_f$			
Altitude, $r_i =$	121.199 km	Flight-path-angle, $\gamma_i =$	$-1.438°$
Longitude, $\Theta_i =$	0°	Velocity azimuth angle, $\Psi_i =$	90.00°
Latitude, $\Phi_i =$	0°	Angle-of-attack, $\alpha_i =$	45.00°
Velocity, $V_i =$	7,599 m/s	Bank angle, $\sigma_i =$	$-0.002°$
Inclination, $i =$	51.6°	—	—

Table 5.16 delineates the maximum crossrange (Φ) for a given downrange (Θ) in the equatorial plane. Calculations are performed with all initial bank angles of $-0.002°$. Thus, a maximum crossrange in the "negative" portion of the latitude is determined for each given downrange distance. A symmetrical "positive" maximum crossrange is assumed to be true for the same downrange distance.

Table 5.16   Maximum crossrange for a given down-
range in equatorial plane

Θ (deg)	Φ (deg)	Θ (deg)	Φ (deg)
25	8.81	85	-6.58
28	10.12	83	-8.04
30	10.72	76	-10.85
33	11.80	72	-12.02
44	13.61	66	-13.03
55	13.90	55	-13.90
66	13.03	44	-13.61
72	12.02	33	-11.80
76	10.85	30	-10.72
83	8.04	28	-10.12
85	6.58	25	-8.81
88	0.00		

A coordinate transformation is performed to correlate the data from Table 5.16 into what is pictured in Figure 5.55. The textured area is the footprint for the high inclination entry (EG13-18).
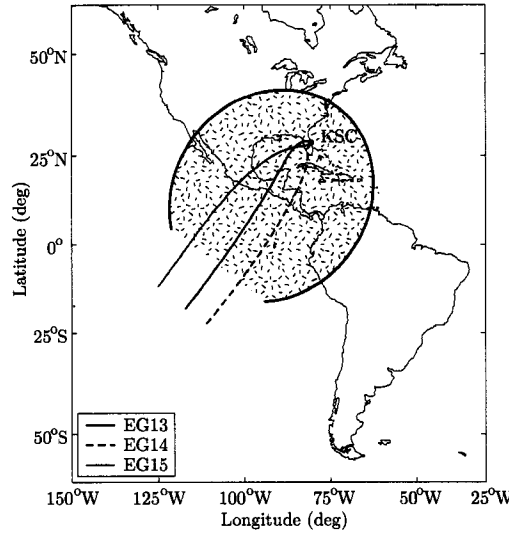
Figure 5.55   High inclination footprint

Other parameters of interest include the r-V, α, σ and $\dot{Q}$ history profiles. Figure 5.56 portrays the trajectory in the r-V design space. The results resembled those of nominal entry except for the drastic altitude drop in the beginning. This is because X-33 is gliding at lower angles of attack compared to those of nominal glide. Figure 5.57 show that $\alpha \approx 25°$ for the most of the trajectory is because that gives the maximum L/D as illustrated in Figure 5.58. The few spikes in the α profiles refer to those trajectories that will require quick altitude drop (i.e., those with smaller downrange). The drop in altitude can be seen in Figure 5.56. The few spikes in the L/D profiles are for last minute energy adjustments. Figure 5.59 depicts no bank reversal in the footprint determination. Figure 5.59 also shows every bank profile stayed on the "negative" side because $\sigma_i = -0.002°$. Lastly, Figure 5.60 illustrates $\dot{Q}$ profiles for footprint determination. The value of $\dot{Q}_{max}$ is highest at the shortest downrange distance.
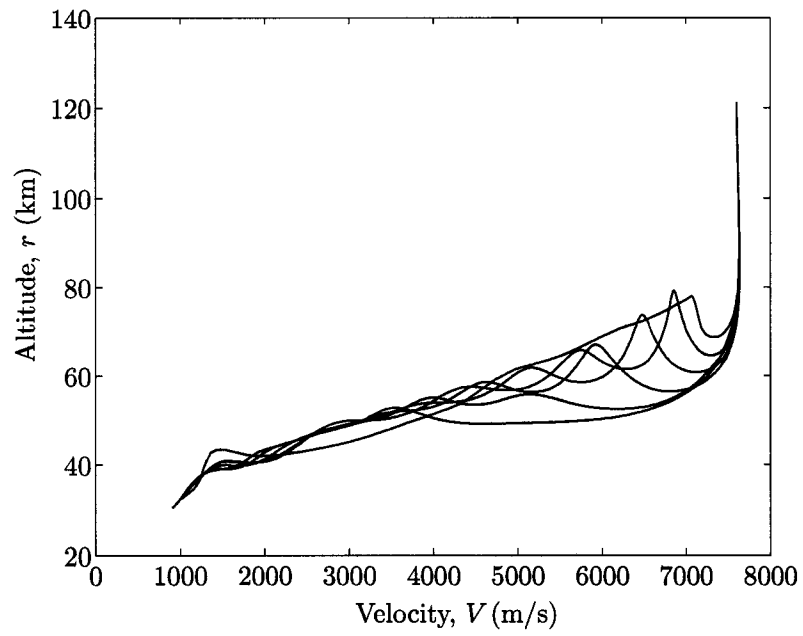
Figure 5.56   High inclination altitude vs velocity profiles
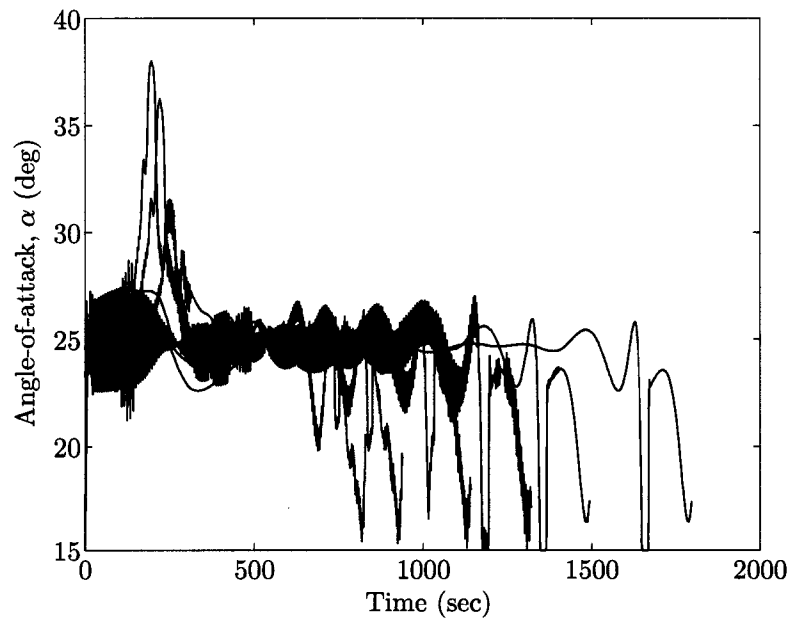
Figure 5.57   High inclination angle-of-attack profiles
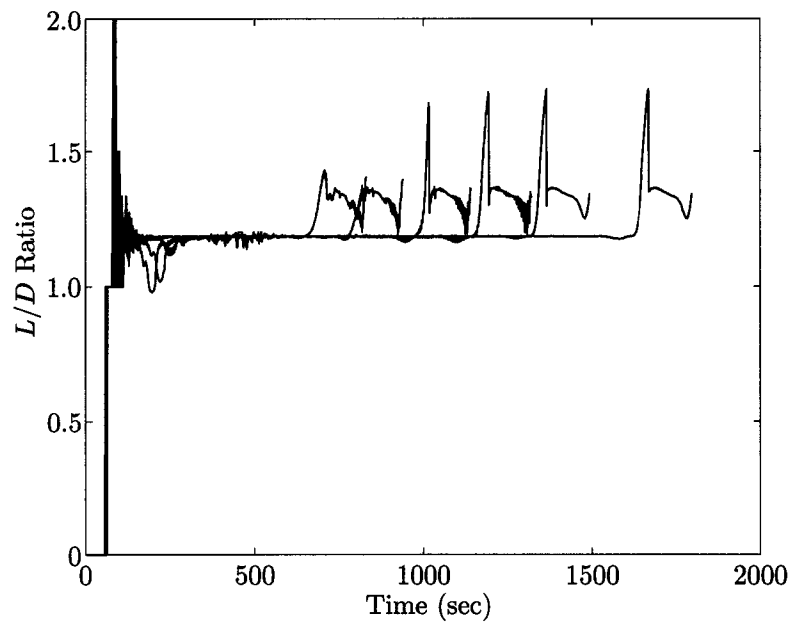
Figure 5.58   High inclination L/D profiles
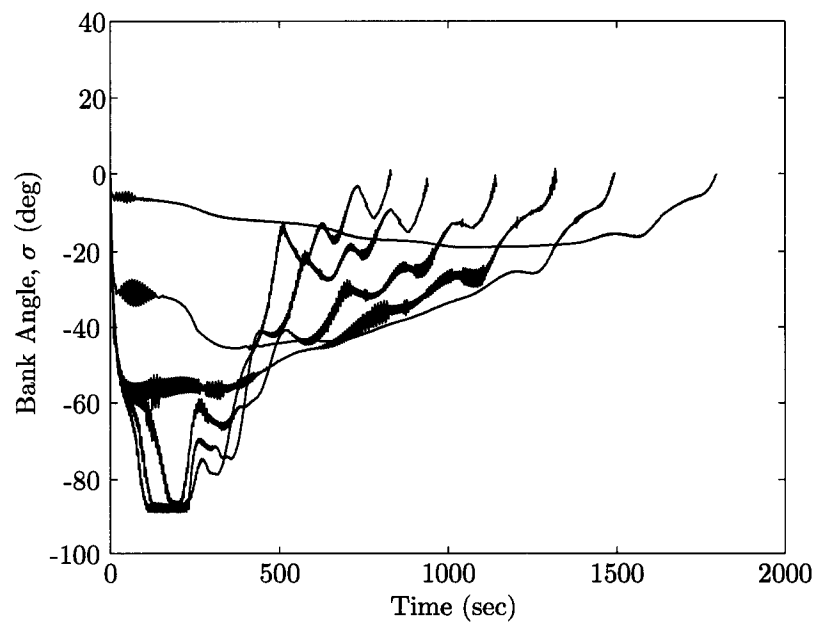
Figure 5.59   High inclination bank angle profiles
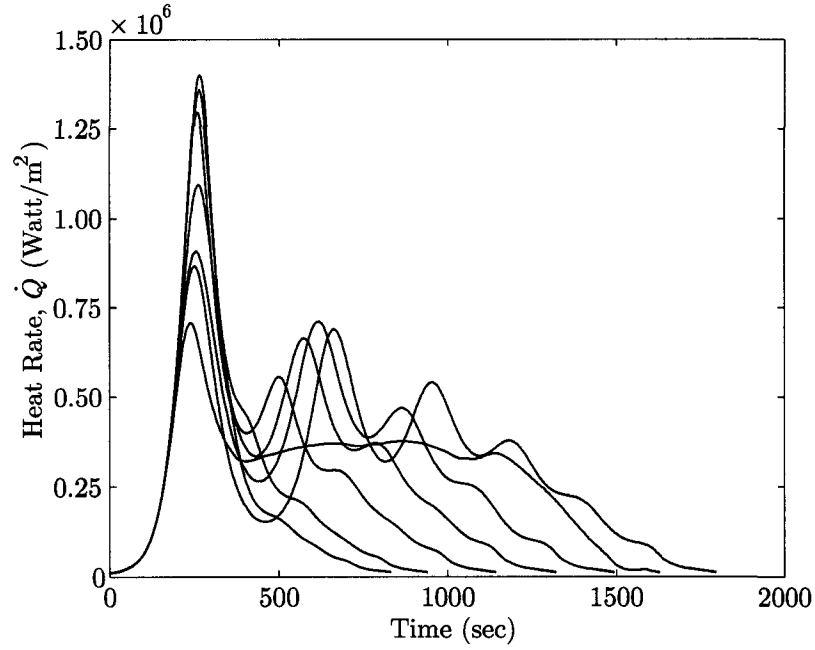
Figure 5.60   High inclination heat rate profiles

Table 5.17 outlines the initial conditions used in footprint determination for $i = 28.5°$ on the equatorial plane. Notice that initial longitude and latitude are both 0° and the velocity azimuth angle is at 90°, pointing eastward.

Table 5.17   Initial conditions for footprint determination for $i = 28.5°$ on equatorial plane

$J = \max \Phi_f$			
Altitude, $r_i =$	121.649 km	Flight-path-angle, $\gamma_i =$	$-1.027°$
Longitude, $\Theta_i =$	0°	Velocity azimuth angle, $\Psi_i =$	90.00°
Latitude, $\Phi_i =$	0°	Angle-of-attack, $\alpha_i =$	45.00°
Velocity, $V_i =$	7,442 m/s	Bank angle, $\sigma_i =$	$-0.002°$
Inclination, $i =$	28.5°	—	—

Table 5.18 shows the maximum crossrange (Φ) for each given downrange (Θ) in the equatorial plane. Calculations are performed with all initial bank angles of $-0.002°$. Thus, a maximum crossrange in the "negative" portion of the latitude is determined for each given downrange distance. A symmetrical "positive" maximum crossrange is assumed to be true for the same downrange distance.

Table 5.18   Maximum crossrange for a given down-range in equatorial plane

Θ (deg)	Φ (deg)		Θ (deg)	Φ (deg)
30	13.72		77	−4.41
40	11.95		75	−6.58
50	11.68		70	−8.47
60	9.98		60	−9.98
70	8.47		50	−11.68
75	6.58		40	−11.95
77	4.41		30	−13.72
78	0.00			

A coordinate transformation is performed to correlate the data from Table 5.18 into what is depicted in Figure 5.61. The textured area is the footprint for the low inclination entry (EG19-21).

Additional parameters of interest include the r-V, α, σ and $\dot{Q}$ history profiles. Figure 5.62 displays the trajectory in the r-V design space. The results resembled those of nominal entry except for the drastic altitude drop in the beginning. Again, Figure 5.63 show that $\alpha \approx 25°$ for the most of the flight is because that results the maximum L/D as pictured in Figure 5.64. Figure 5.65 exhibits no bank reversal in the footprint determination. Figure 5.65 also delineates every bank profile stayed on the "negative" side because $\sigma_i = -0.002°$. Last, Figure 5.66 illustrates $\dot{Q}$ profiles for footprint determination. The value of $\dot{Q}_{max}$ is highest at the shortest downrange distance.
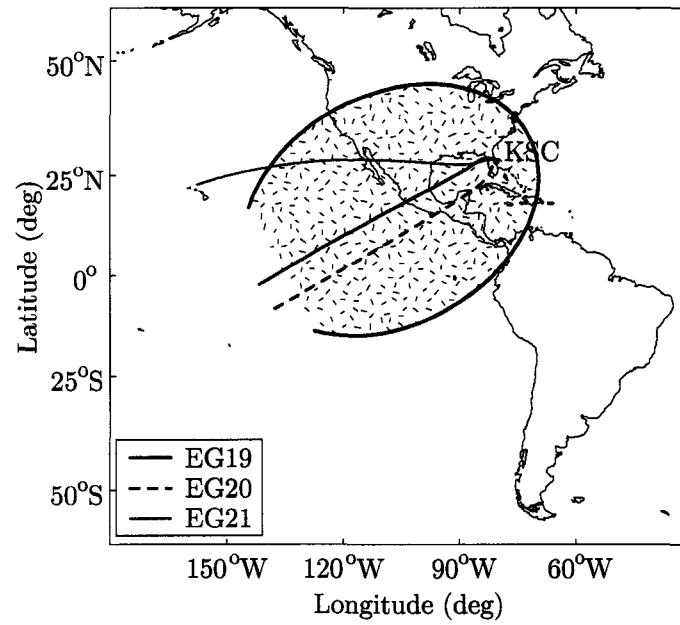
Figure 5.61   Low inclination footprint
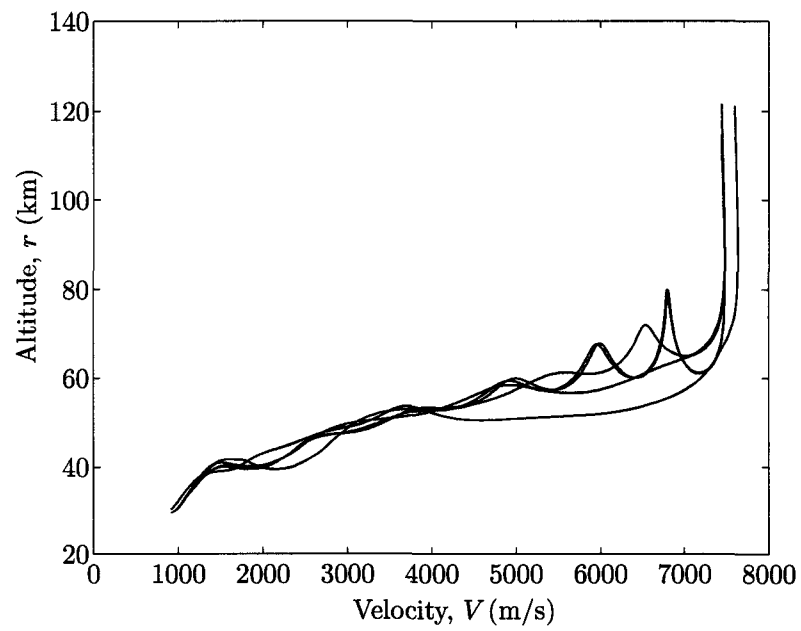
Figure 5.62   Low inclination altitude vs velocity profiles
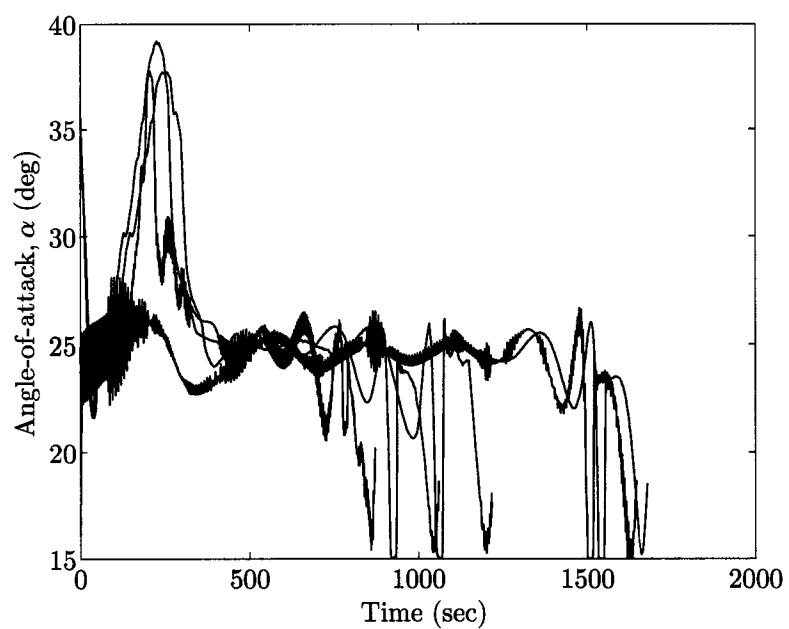
Figure 5.63   Low inclination angle-of-attack profiles
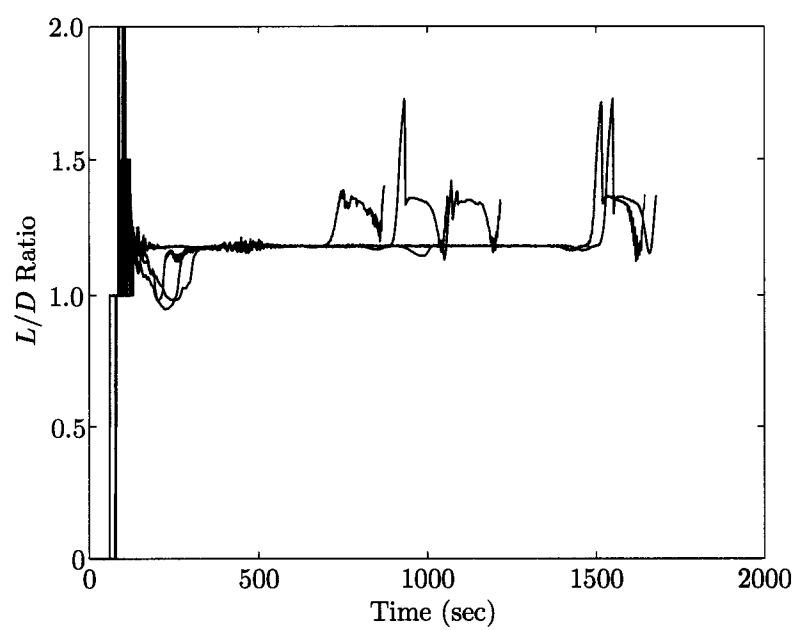
Figure 5.64   Low inclination L/D profiles
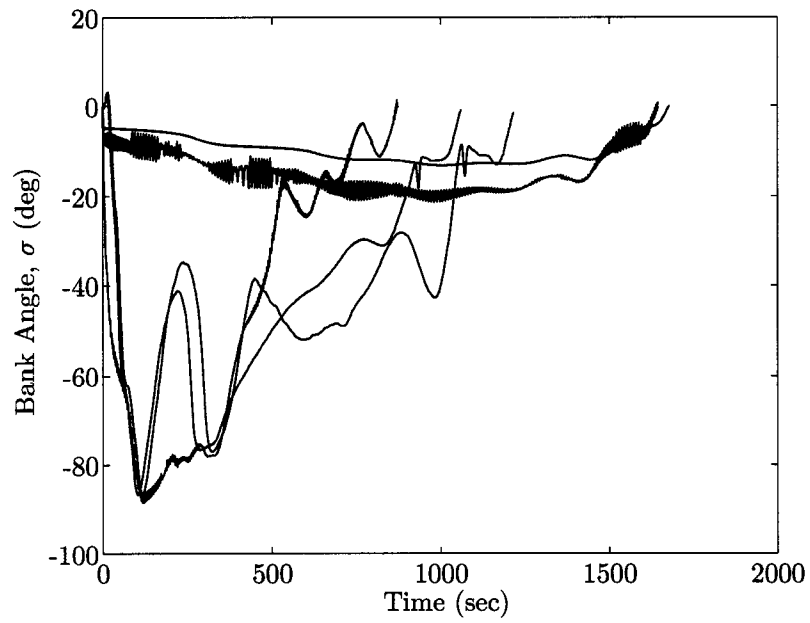
Figure 5.65   Low inclination bank angle profiles
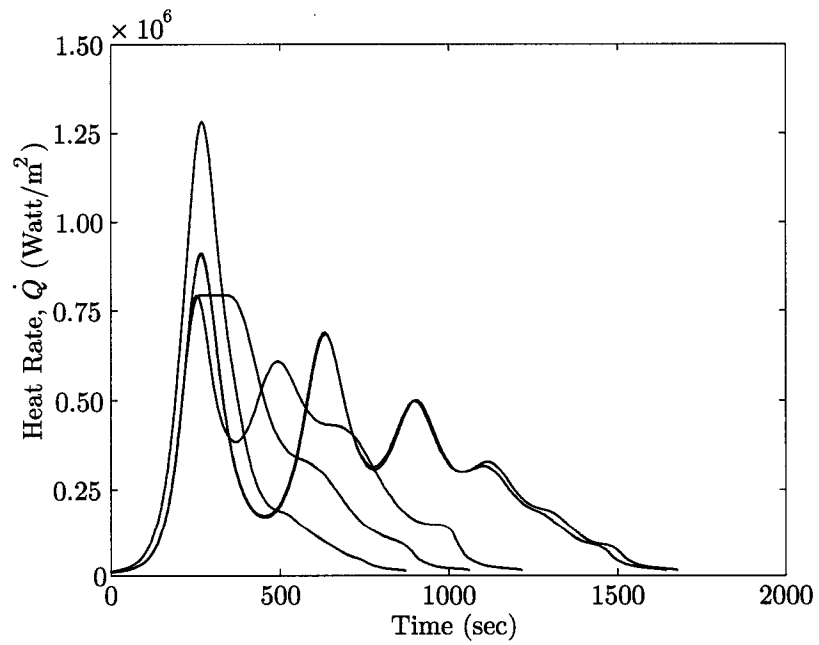
Figure 5.66   Low inclination heat rate profiles

CHAPTER 6   LOH'S THEORY FOR ENTRY TRAJECTORIES

As far as the laws of mathematics refer to reality,
they are not certain;
and as far as they are certain,
they do not refer to reality.

— Dr. Albert Einstein [1]

EQUATIONS of motion for entry cannot be solved analytically [99]. However, approximate analytical solutions can be obtained upon confining the solution to a limited region. Loh's theory for entry trajectories is one such example. The assumptions used in Loh's approximate analytical solutions include vertical plane motion only, constant gravitational force, strictly exponential atmosphere, non-rotating Earth, constant C_ℓ, constant C_d, zero bank angle, and also based on extensive numerical integration observations. Loh's theory is empirical [99, 101, 112].

6.1   Loh's First-Order Entry Solutions

The entry Equations (5.1), (5.4) and (5.5) presented in Chapter 5 are reproduced here again for the convenience of discussion. These equations are further simplified to neglect the effect of Earth rotation.

$$\frac{d}{dt} r_c = V_r \sin \gamma \tag{6.1}$$

$$\frac{d}{dt} V_r = -D - \left(\frac{\sin \gamma}{r_c^2} \right) \tag{6.2}$$

$$\frac{d}{dt} \gamma = \frac{1}{V_r} \left[L \cos \sigma + \left(V_r^2 - \frac{1}{r_c} \right) \left(\frac{\cos \gamma}{r_c} \right) \right] \tag{6.3}$$

In Loh's theory, variable $U \equiv \frac{1}{2} \left(\frac{V_r^2}{g_0 R_0} \right)$; V_r is the relative velocity; g_0 is the gravitational constant; R_0 is the initial radial distance; γ is the flight-path-angle, b is a scale height with a constant value of $\frac{900}{R_0}$ for Earth; $\frac{C_\ell}{C_d}$ is the coefficients of lift-over-drag ratio; $\varphi \equiv \cos \gamma$; and n is proportional to the atmospheric density defined as

$$n \equiv \frac{\rho_{SL} S_{ref} C_d}{2mb} e^{-br} \tag{6.4}$$

where S_{ref} is the vehicle reference area; C_d is the coefficient of drag; ρ_{SL} is the density at sea level; m is the mass of vehicle; and r is the altitude.

After taking derivatives of variables U, n and φ and substituted Equations (6.1)-(6.3) into the differentiated U, n and φ equations, these three equations can be reduced down to two differential equations by eliminating $\frac{dn}{dt}$. Thus,

$$\frac{dU}{dn} = \frac{2U}{\sin \gamma} + \frac{1}{nbR_0} \tag{6.5}$$

$$\frac{d\varphi}{dn} = \frac{C_\ell}{C_d} \cos \sigma - \frac{1}{nbR_0} \left(\frac{1}{2U} - 1 \right) \varphi \tag{6.6}$$

Loh's theory only considered the vertical plane motion with zero bank angle. Thus, Equations (6.5) and (6.6) are reduced to

$$\frac{dU}{dn} = \frac{2U}{\sin\gamma} + \frac{1}{nbR_0} \tag{6.7}$$

$$\frac{d\varphi}{dn} = \frac{C_\ell}{C_d} - \frac{1}{nbR_0}\left(\frac{1}{2U} - 1\right)\varphi \tag{6.8}$$

For a gliding entry at small flight path angles, i.e., $\sin\gamma \approx \gamma$, $\cos\gamma \approx 1$, Equation (6.8) becomes

$$\frac{C_\ell}{C_d} - \frac{1}{nbR_0}\left(\frac{1}{2U} - 1\right) = 0 \tag{6.9}$$

Solving for U, Equation (6.9) is now

$$U = \frac{1}{2\left[1 + bR_0\left(\frac{C_\ell}{C_d}\right)n\right]} \tag{6.10}$$

Finally, the flight-path-angle can be obtained by taking the derivative of Equation (6.10) with respect to U

$$\gamma = \sin^{-1}\left[-\frac{1}{\left(\frac{C_\ell}{C_d}\right)UbR_0}\right] \tag{6.11}$$

Notice that the only difference between Equations (6.6) and (6.8) is the "$\cos\sigma$" term that allows for the inclusion of a constant bank angle. Thus, "$\cos\sigma$" will be added to the lift component so that one can compare Loh's analytical solutions to those obtained previously with numerical integration. Therefore, Equations (6.9) through (6.11) become

$$\frac{C_\ell}{C_d}\cos\sigma - \frac{1}{nbR_0}\left(\frac{1}{2U} - 1\right) = 0 \tag{6.12}$$

$$U = \frac{1}{2\left[1 + bR_0\left(\frac{C_\ell}{C_d}\cos\sigma\right)n\right]} \tag{6.13}$$

$$\gamma = \sin^{-1}\left[-\frac{1}{\left(\frac{C_\ell}{C_d}\cos\sigma\right)UbR_0}\right] \tag{6.14}$$

Equations (6.12) through (6.14) will now be referred to as the modified Loh's first-order entry solutions. The σ value used is the average σ value obtained from numerical integration.

6.2 Loh's Unified Solution for Entry

The first-order solution presented in Section 6.1 is only good for one type of entry. Loh has empirically derived a more general solution that covers the entire spectrum of lift-to-drag ratios and initial γ's. This general solution is commonly referred to as the Loh's second-order solution. For the same reason as before, the term "$\cos\sigma$" will be added onto the lift term. Therefore, the modified fundamental Loh's equations are

$$\frac{dU}{dn} = \frac{2U}{\sin\gamma} + \frac{z^2}{nbR_0} \tag{6.15}$$

$$\frac{d\varphi}{dn} = \frac{C_\ell}{C_d}\cos\sigma - \frac{z^2}{nbR_0}\left(\frac{1}{2U} - \frac{1}{z}\right)\varphi \tag{6.16}$$

where n is proportional to the atmospheric density defined as

$$n = \frac{SC_d}{2mb}\rho \tag{6.17}$$

The first assumption made by Loh is to set $z = 1$. Furthermore, Loh noticed empirically that

$$G \equiv \frac{1}{nbR_0}\left(\frac{1}{2U} - 1\right)\varphi \tag{6.18}$$

remained nearly constant regardless of the type of entry trajectory even though G is a function of n, U and φ.

With $z = 1$ and G treated as a constant, Equation (6.16) can be rewritten as

$$\frac{d\varphi}{dn} = \frac{C_\ell}{C_d} \cos\sigma - G \tag{6.19}$$

Equation (6.19) can be integrated and solved for flight-path-angle since lift-to-drag ratio is constant.

$$\cos\gamma = \frac{\cos\gamma_0 + \left(\frac{C_\ell}{C_d}\cos\sigma\right) n \left(1 - \frac{n_0}{n}\right)}{1 + \left(\frac{1}{bR_0}\right)\left(1 - \frac{n_0}{n}\right)\left(\frac{1}{2U} - 1\right)} \tag{6.20}$$

Equation (6.15) with γ as the independent integration variable becomes

$$\frac{dU}{d\gamma} + \frac{2U}{\frac{C_\ell}{C_d}\cos\sigma - G} = -\frac{\sin\gamma}{nbR_0\left(\frac{C_\ell}{C_d}\cos\sigma - G\right)} \tag{6.21}$$

After many algebraic manipulations, Equation (6.21) can now be expressed as

$$U = U_0 e^{(K_0\gamma_0)} + \left[F(\gamma) - e^{(K_0\gamma_0 - K\gamma)}F(\gamma_0)\right] \tag{6.22}$$

where

$$K_0 \equiv \frac{2}{\frac{C_\ell}{C_d}\cos\sigma - \frac{1}{bR_0 n_0}\left(\frac{1}{2U_0} - 1\right)\cos\gamma_0} \tag{6.23}$$

$$F(\gamma) \equiv e^{-K\gamma}\int e^{K\gamma}f(\gamma)d\gamma \tag{6.24}$$

$$K \equiv \frac{2}{\frac{C_\ell}{C_d}\cos\sigma - G} \tag{6.25}$$

$$f(\gamma) \equiv \frac{\sin \gamma}{bR_0 \left(\cos \gamma_0 - \cos \gamma\right)} \tag{6.26}$$

6.3 Loh's Second-Order Solution for Entry

According to Vinh [99], Loh's unified solution can be further simplified by omitting the $\frac{1}{bR_0}$ factor in the second term of Equation (6.22) since it is generally very small. Furthermore, assuming that $\frac{n_0}{n} \ll 1$ will simplify Equations (6.20) and (6.22) into

$$\cos \gamma = \frac{\cos \gamma_0 + \left(\frac{C_\ell}{C_d} \cos \sigma\right) n}{1 + \frac{1}{bR_0} \left(\frac{1}{2U} - 1\right)} \tag{6.27}$$

$$\log \left(\frac{U}{U_0}\right) = \frac{2 \left(\gamma_0 - \gamma\right)}{\frac{C_\ell}{C_d} \cos \sigma - \left(\frac{1}{bR_0}\right) n \left(\frac{1}{2U} - 1\right) \cos \gamma} \tag{6.28}$$

Finally, eliminating n will give

$$\gamma = \gamma_0 - \frac{1}{2} \left(\frac{C_\ell}{C_d} \cos \sigma\right) \log \left(\frac{U}{U_0}\right) \left[1 + \frac{1}{bR_0} \frac{\left(\frac{1}{2U} - 1\right)}{\left(1 - \frac{\cos \gamma_0}{\cos \gamma}\right)}\right]^{-1} \tag{6.29}$$

After determining γ, a variable n that is proportional to the atmospheric density can be obtained by

$$n = n_0 + \left(\frac{C_\ell}{C_d} \cos \sigma\right)^{-1} \left[\left(\cos \gamma - \cos \gamma_0\right) + \frac{1}{bR_0} \left(\frac{1}{2U}\right) \cos \gamma\right] \tag{6.30}$$

Altitude (r) can now be computed by

$$r = -\log \left(\frac{2mnb}{\rho_{SL} S_{ref} C_d}\right) b^{-1} \tag{6.31}$$

Finally, γ-V and r-V can be compared against those obtained from numerical integration.

6.4 Reduction of Second-Order Solution to First-Order Solution

The 1st order approximation is based on specific application (i.e., small γ), physical reasoning, and limited region from the 2nd order unified solution presented in the previous section [99].

For a gliding entry with small flight-path-angle, the empirical theory to approximate the 1st order analytical solution for this type of entry is as follows. Assuming that γ is small (i.e., $\cos\gamma \approx \cos\gamma_0 \approx 1$), then Equation (6.20) becomes

$$\frac{1}{bR_0}\left(\frac{1}{2U} - 1\right) = \left(\frac{C_\ell}{C_d}\cos\sigma\right)n \tag{6.32}$$

Equation (6.18) is now

$$\frac{1}{bR_0}\left(\frac{1}{2U} - 1\right) = Gn \tag{6.33}$$

A closer examination of Equations (6.32) and (6.33) shows that G is equal to the constant lift-to-drag ratio. Thus,

$$\frac{C_\ell}{C_d}\cos\sigma - \frac{1}{nbR_0}\left(\frac{1}{2U} - 1\right)\cos\gamma \tag{6.34}$$

Now, solving for γ,

$$\gamma = \sin^{-1}\left[-\frac{1}{\left(\frac{C_\ell}{C_d}\cos\sigma\right)UbR_0}\right] \tag{6.35}$$

After determining γ, a variable n that is proportional to the atmospheric density can be obtained by

$$n = \left(\frac{C_\ell}{C_d}\cos\sigma\right)^{-1}\frac{\left(\frac{1}{2U}-1\right)\cos\gamma}{bR_0} \tag{6.36}$$

Altitude (r) can now be computed by using Equation (6.31). In addition to r and γ, the constant σ shown in Equation (6.35) can be backed out provided that distance traveled (s_f) is specified. Since this is a longitudinal analysis, distance traveled is an equivalent of downrange in the numerical 3D case.

$$\sigma = \cos^{-1}\left[\frac{2s_f}{R_0\log\left(\frac{1-2U}{1-2U_0}\right)}\left(\frac{C_\ell}{C_d}\cos\sigma\right)^{-1}\right] \tag{6.37}$$

Rewriting Equation (6.37) in terms of distant traveled, s_f,

$$s_f = \frac{R_0}{2}\left(\frac{C_\ell}{C_d}\cos\sigma\right)\log\left(\frac{1-2u}{1-2u_0}\right) \tag{6.38}$$

where σ is the average σ obtained from numerical integration.

6.5 Comparison of Loh's Analytical Results vs Numerical Integration Results

Equation (6.37) yields an analytically calculated σ (column #3 in Table 6.1) for each s_f obtained from numerical solution (column #1). Notice that the calculated constant σ in column #3 may or may not be close to the averaged numerically obtained σ listed in column #2. Thus, various values of σ's have been used to evaluate the impact of σ on s_f. The results are listed in columns #4 through #7 in Table 6.1. Furthermore, a parametric study of σ on γ and r-V profiles have also been conducted.

Table 6.1   Numerical vs first-order downrange and bank angle comparisons

	Numerical solution		First-order approximate solution				
	Actual s_f (km)	Avg σ (deg)	Calc σ (deg)	Calculated s_f based on			
				$\sigma = 0°$	$\sigma = -20°$	$\sigma = -40°$	$\sigma = -60°$
EG13	6495.89	−21.80	−3.35	6507.00	6114.58	4984.65	3253.50
EG14	6529.70	−13.61	−12.62	6691.35	6287.81	5125.87	3345.67
EG15	6569.99	−12.68	−11.31	6700.06	6296.00	5132.55	3350.03
EG16	8135.88	−22.43	−36.26	10089.61	9481.13	7729.09	5044.80
EG17	8146.79	−11.36	−36.15	10089.61	9481.13	7729.09	5044.80
EG18	8175.02	−10.99	−36.09	10116.18	9506.10	7749.45	5058.09
EG19	7343.95	−24.93	−26.83	8230.26	7733.91	6304.74	4115.13
EG20	7364.32	−12.58	−26.52	8230.26	7733.91	6304.74	4115.13
EG21	7617.48	−25.97	−37.35	8214.39	7668.79	6292.59	4107.20
	#1	#2	#3	#4	#5	#6	#7

The purpose of Figures 6.1 through 6.18 is to compare the first-order solutions to those obtained from numerical integrations using the computed σ values (column #3). Every entry case (EG13-21) showed that first-order analytical solution has captured the gist of entry trajectory in spite of every case ending with a higher final altitude than desired. Another interesting observation is that none of the cases violated the $\dot{Q}_{max}$ constraint even though $\dot{Q}_{max}$ cannot be enforced analytically. On the other hand, most cases have violated the EGC constraint. As discussed in Subsection 5.3.4 on page 112, EGC is a "soft" constraint and it is not as important as the $\dot{Q}_{max}$ constraint. Overall, 1st order solutions are good enough in the conceptual phase.
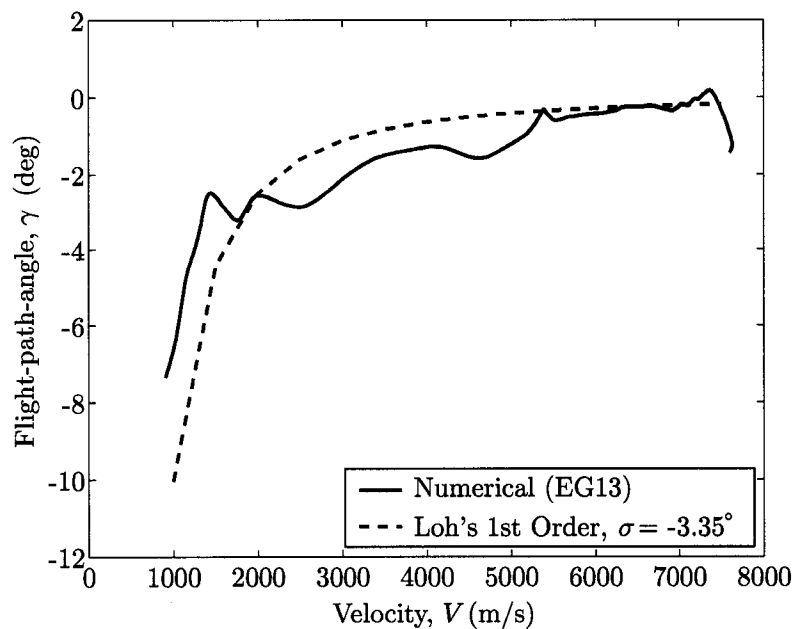
Figure 6.1   Loh's 1$^{\text{st}}$ order flight-path-angle vs velocity compared with EG13
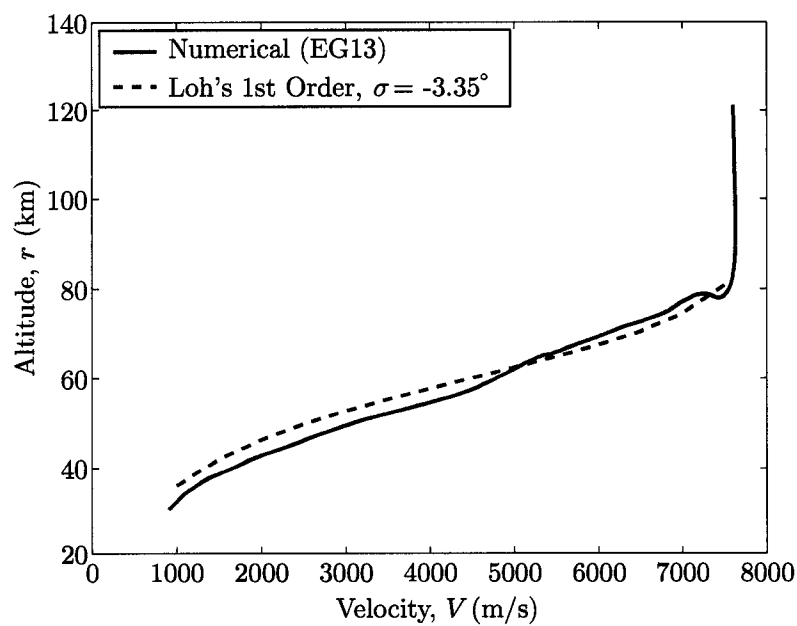
Figure 6.2   Loh's 1$^{\text{st}}$ order altitude vs velocity compared with EG13
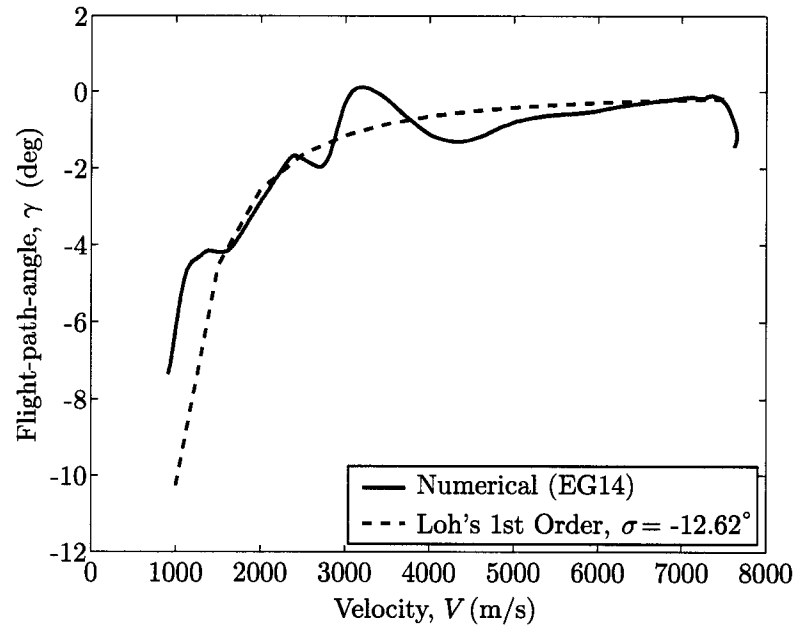
Figure 6.3   Loh's 1st order flight-path-angle vs velocity compared with EG14
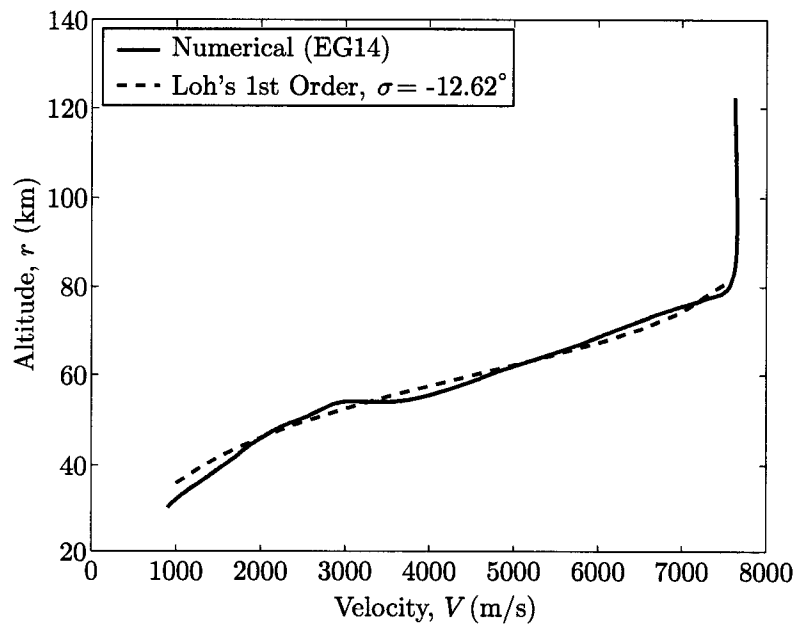
Figure 6.4   Loh's 1st order altitude vs velocity compared with EG14
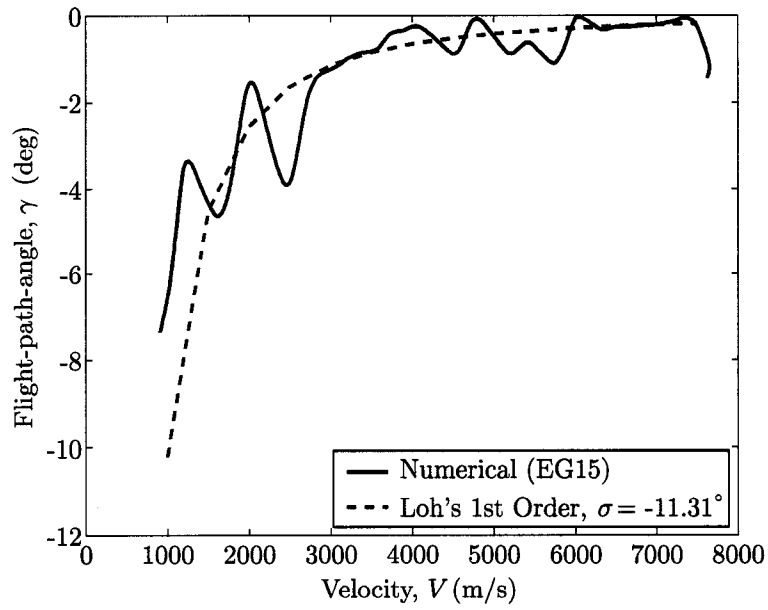
Figure 6.5   Loh's 1st order flight-path-angle vs velocity compared with EG15
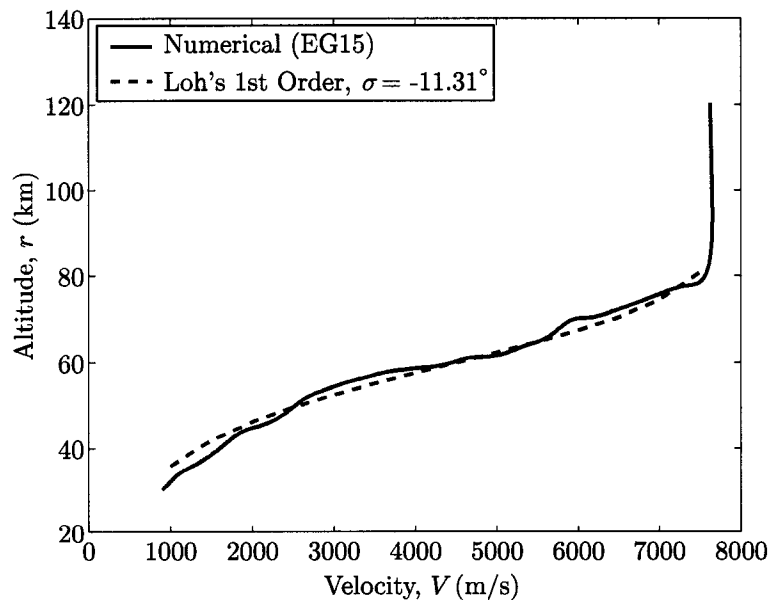
Figure 6.6   Loh's 1st order altitude vs velocity compared with EG15
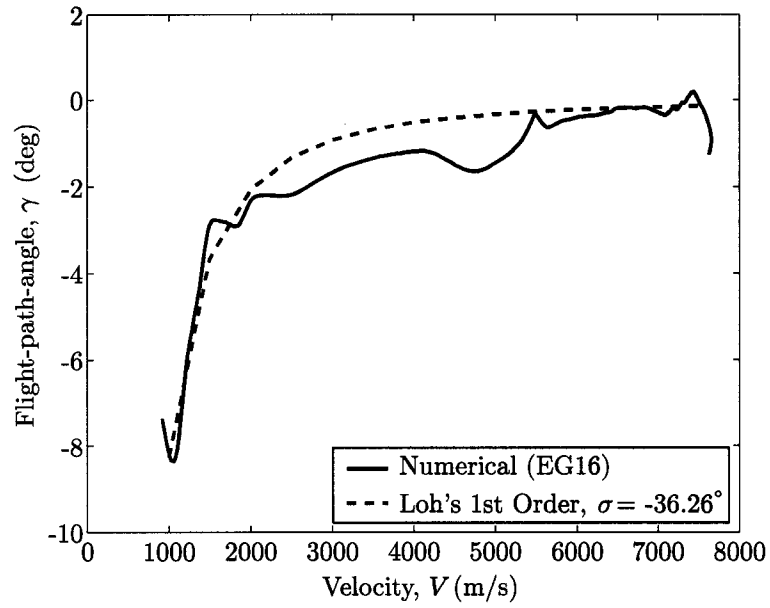
Figure 6.7   Loh's 1st order flight-path-angle vs velocity compared with EG16
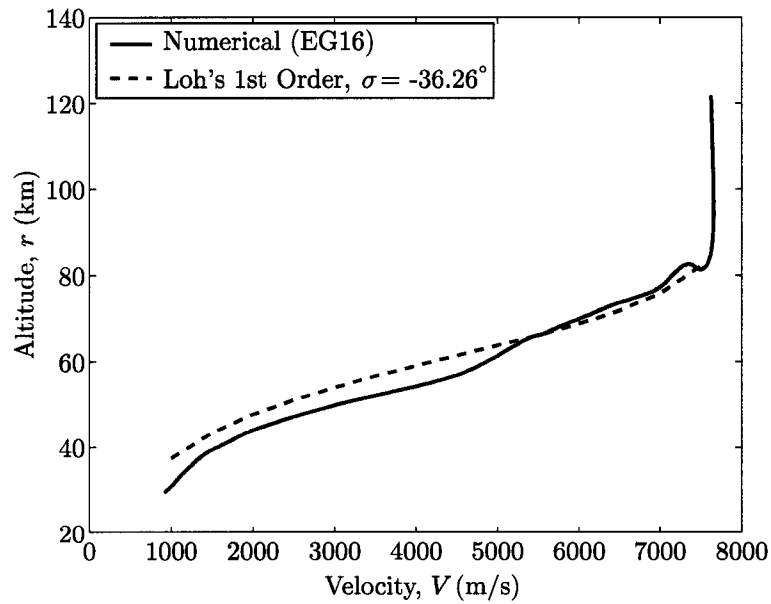
Figure 6.8   Loh's 1st order altitude vs velocity compared with EG16
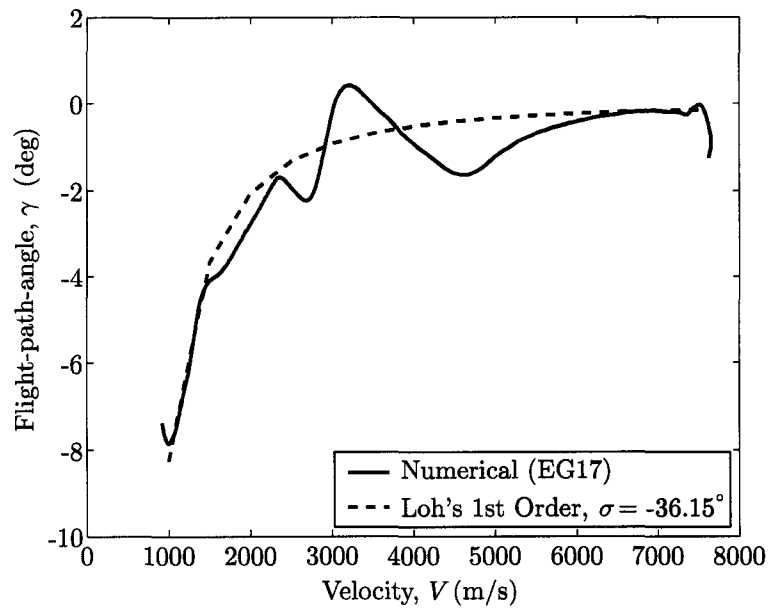
Figure 6.9   Loh's 1st order flight-path-angle vs velocity compared with EG17
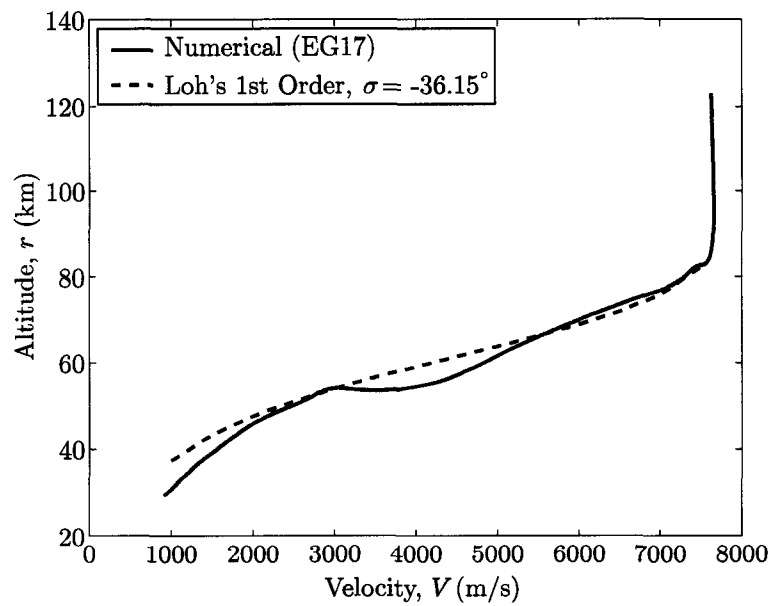
Figure 6.10   Loh's 1st order altitude vs velocity compared with EG17
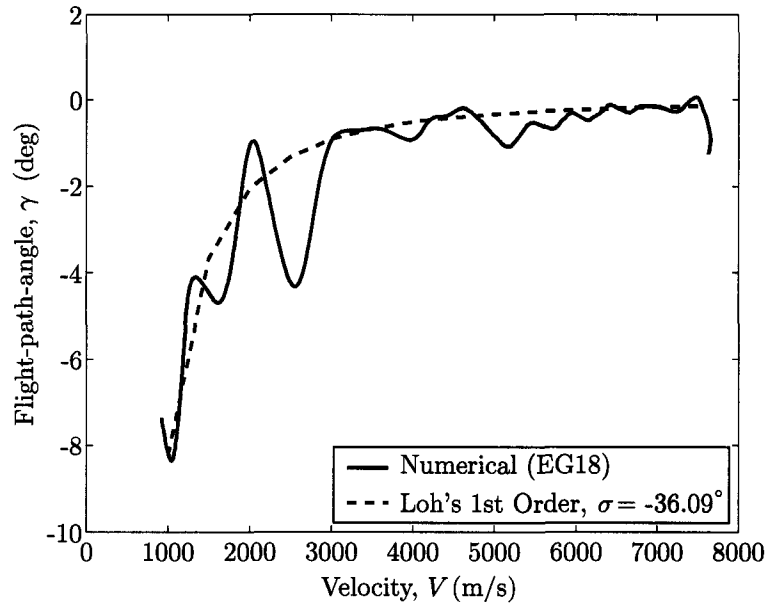
Figure 6.11   Loh's 1st order flight-path-angle vs velocity compared with EG18
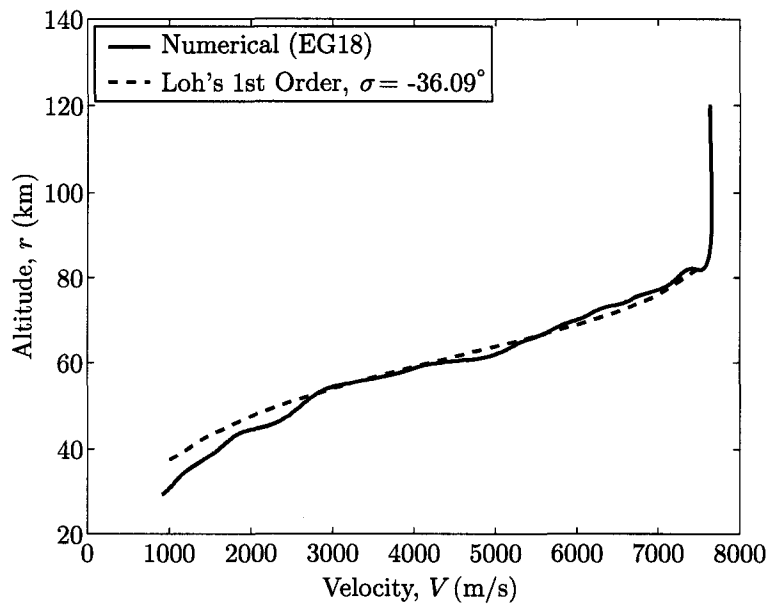
Figure 6.12   Loh's 1st order altitude vs velocity compared with EG18
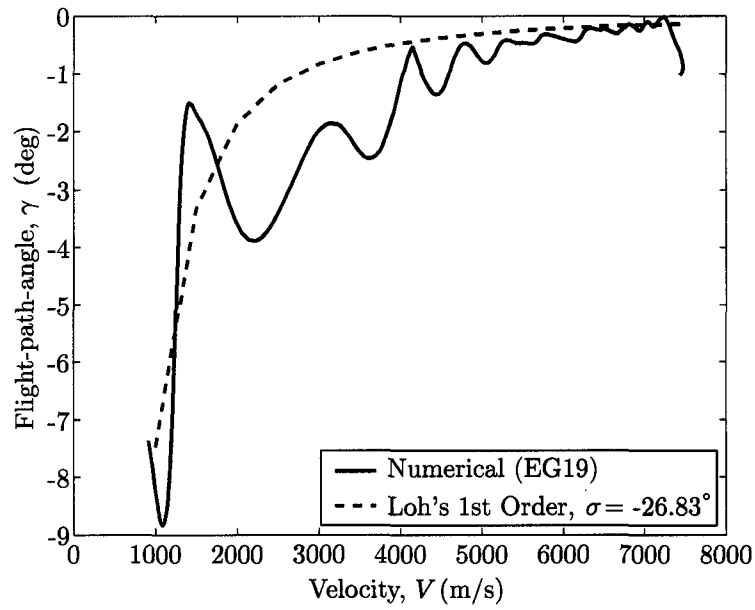
Figure 6.13   Loh's 1st order flight-path-angle vs velocity compared with EG19
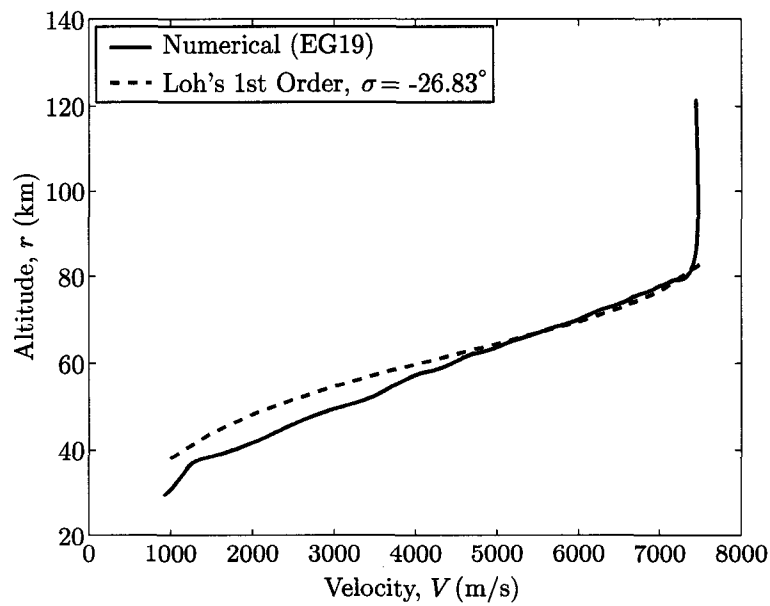
Figure 6.14   Loh's 1st order altitude vs velocity compared with EG19
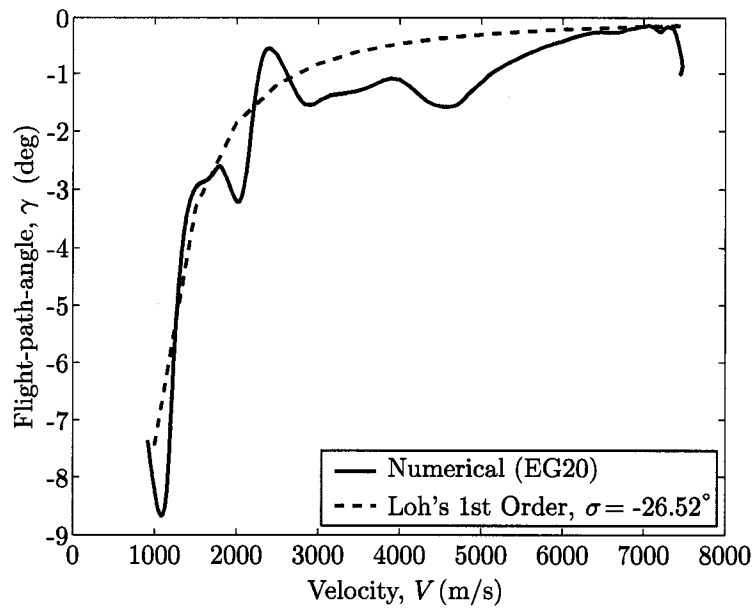
Figure 6.15   Loh's 1st order flight-path-angle vs velocity compared with EG20
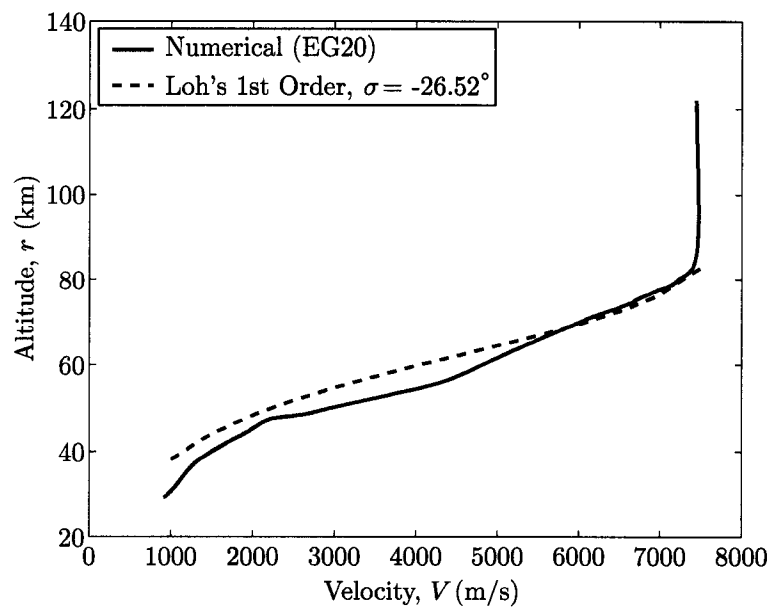
Figure 6.16   Loh's 1st order altitude vs velocity compared with EG20
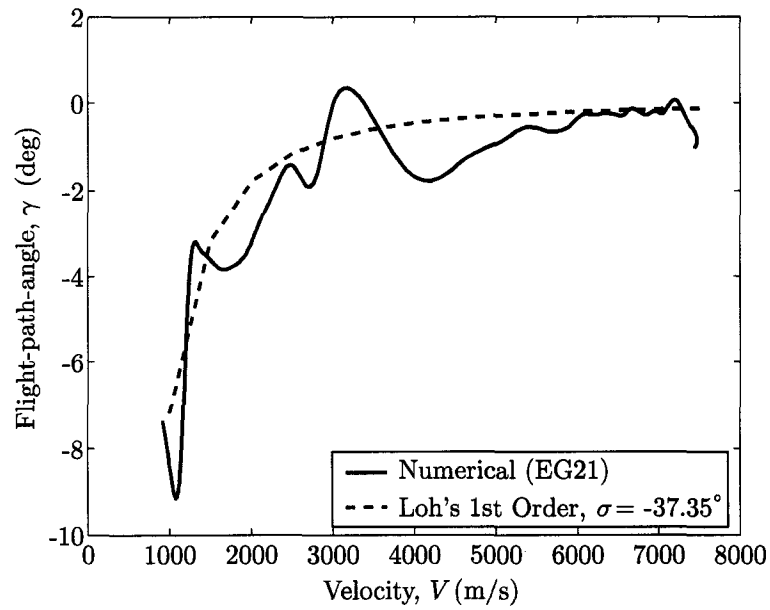
Figure 6.17   Loh's 1st order flight-path-angle vs velocity compared with EG21
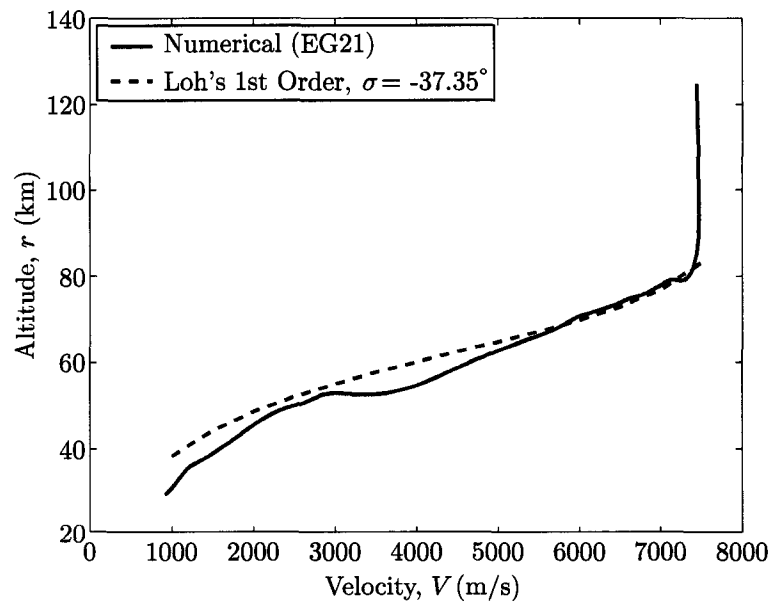
Figure 6.18   Loh's 1st order altitude vs velocity compared with EG21

Loh's second-order unified solutions exhibited remarkably close resemblance to those of first-order solutions in the r-V design space. This is because the first-order solutions were simplified from 2nd order solutions based on the assumption that γ is small, i.e., $\cos\gamma = 1$. Since $0° \geq \gamma \geq -20°$ still yield $\cos\gamma \approx 0.94$, this did not affect the overall results. Furthermore, γ is not a major contributing factor in the shaping of entry trajectory.

Figures 6.19, 6.21, 6.23, 6.25, 6.27, 6.29, 6.31, 6.33, and 6.35 illustrate how nominal, 1st and 2nd order γ profiles compared to each other for each entry case (EG13-21, respectively). One interesting observation about 2nd order γ profiles is that γ remained constant until a velocity of approximately 1,500 m/s. This re-confirms that γ does not significantly affect the entry dynamics.

Figures 6.20, 6.22, 6.24, 6.26, 6.28, 6.30, 6.32, 6.34, and 6.36 delineate the resemblance of 2nd order compared to 1st solutions for each σ value chosen to test each entry case (EG13-21, respectively). Every entry case (regardless of high/low inclination or high/low peak heat rate constraint) showed 2nd order solutions in close resemblance to those of 1st order solutions in the r-V design space.

In conclusion, 1st order approximation is adequate for glide entries with small γ's. First-order is easier and faster to compute, yet yields the accuracy of 2nd order approximation.
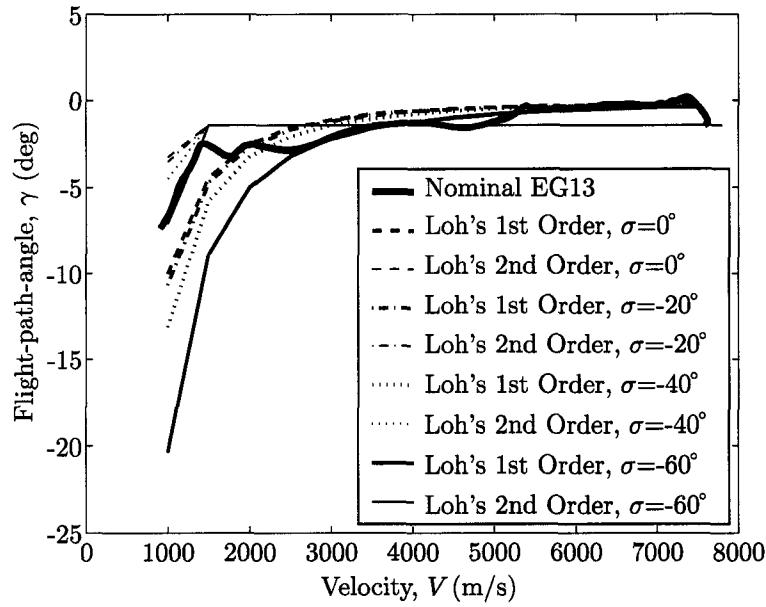
Figure 6.19   Loh's 1st order vs 2nd order flight-path-angle vs velocity compared with EG13
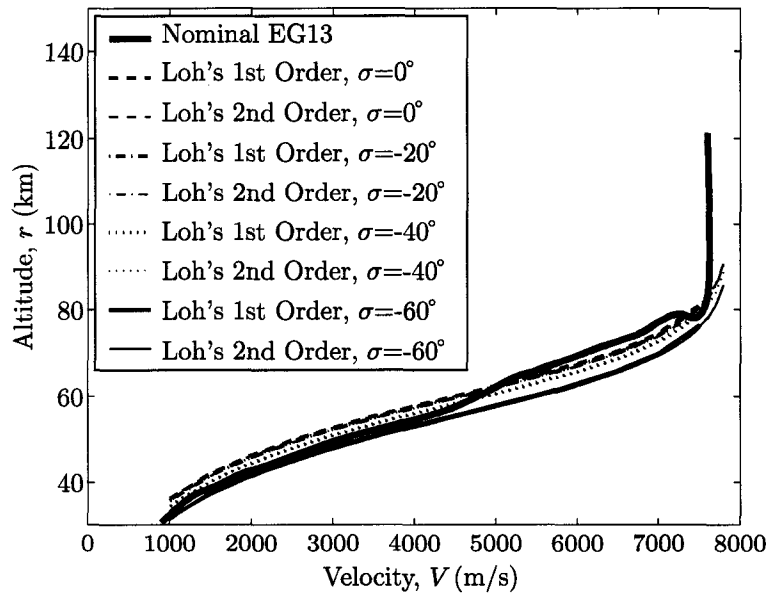
Figure 6.20   Loh's 1st order vs 2nd order altitude vs velocity compared with EG13
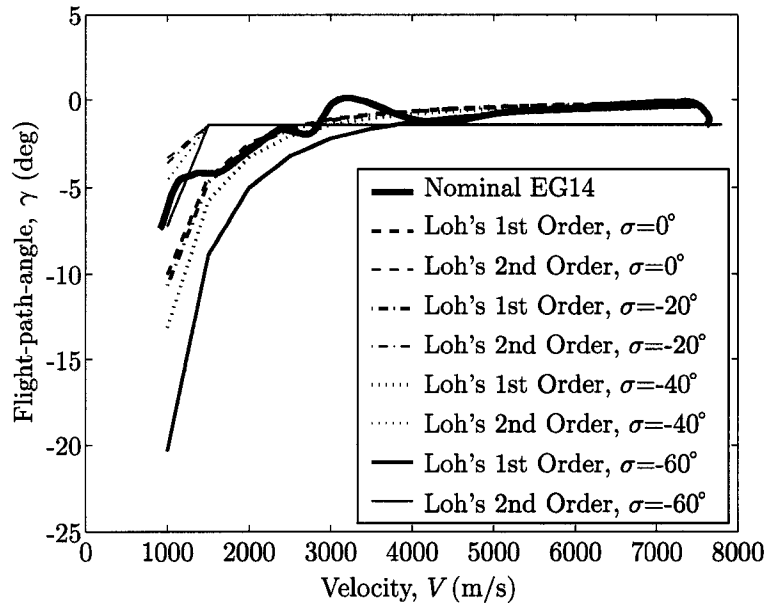
Figure 6.21   Loh's 1st order vs 2nd order flight-path-angle vs velocity compared with EG14
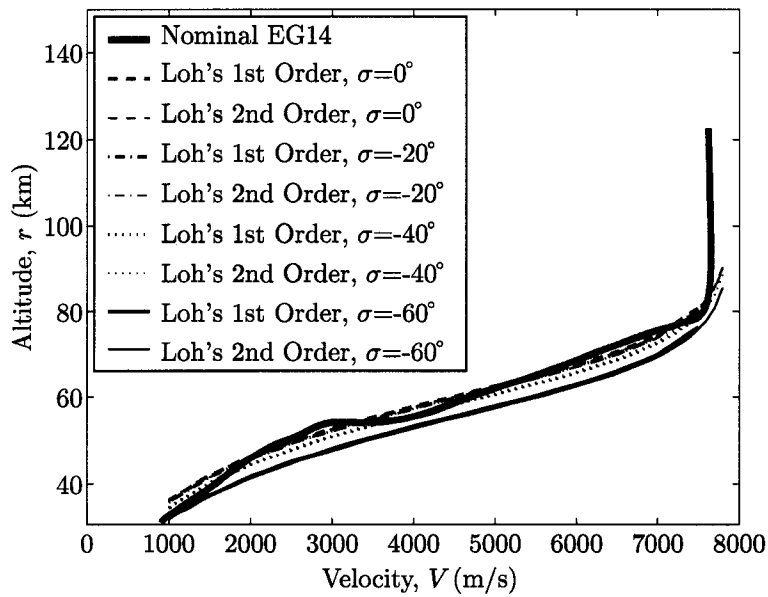
Figure 6.22   Loh's 1st order vs 2nd order altitude vs velocity compared with EG14
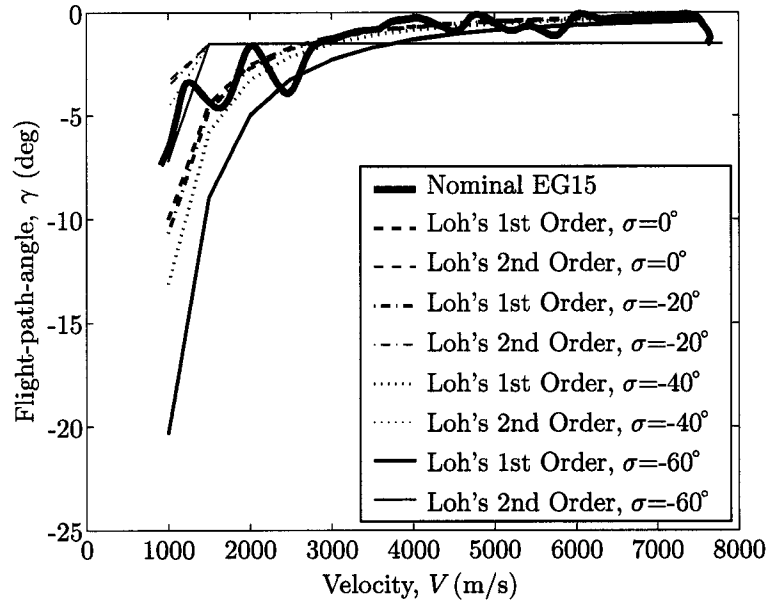
Figure 6.23 Loh's 1st order vs 2nd order flight-path-angle vs velocity compared with EG15
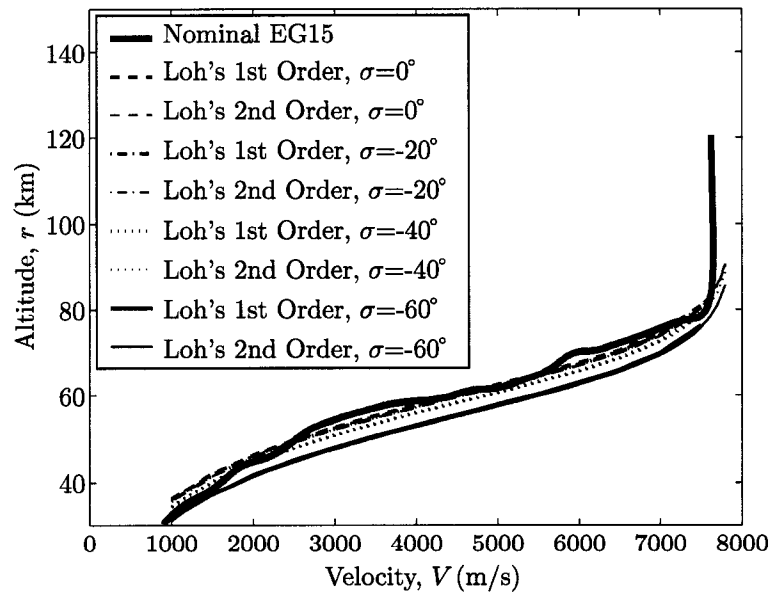
Figure 6.24 Loh's 1st order vs 2nd order altitude vs velocity compared with EG15
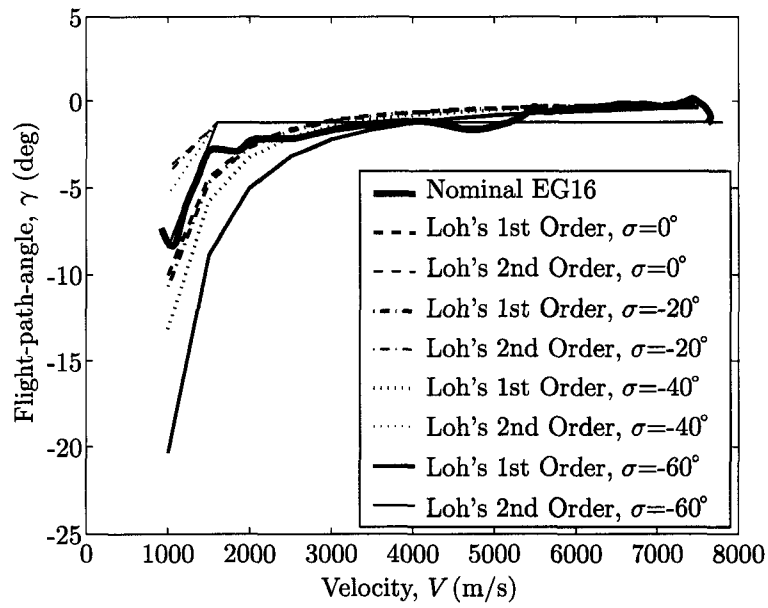
Figure 6.25   Loh's 1st order vs 2nd order flight-path-angle vs velocity compared with EG16
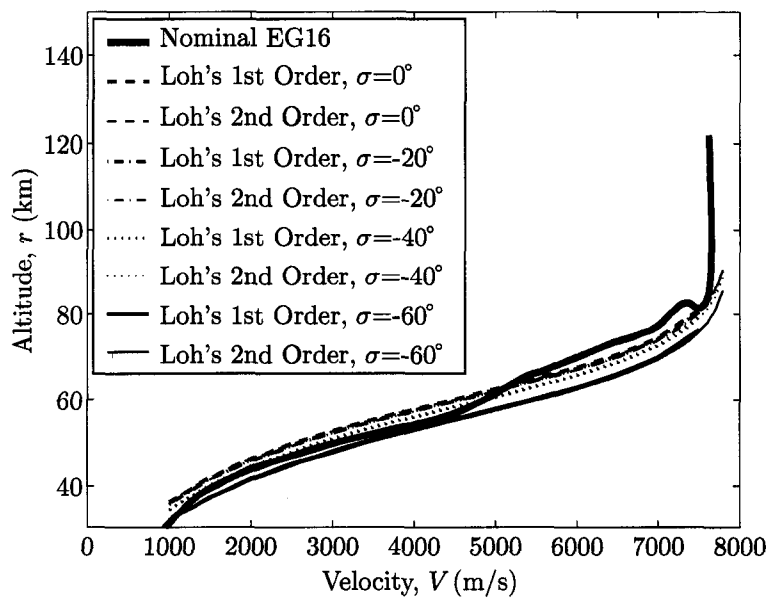
Figure 6.26   Loh's 1st order vs 2nd order altitude vs velocity compared with EG16
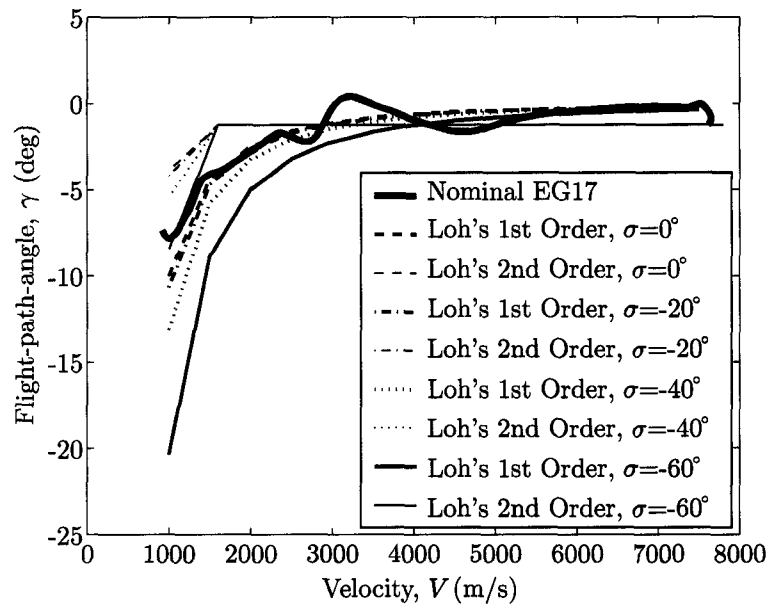
Figure 6.27 Loh's 1st order vs 2nd order flight-path-angle vs
velocity compared with EG17
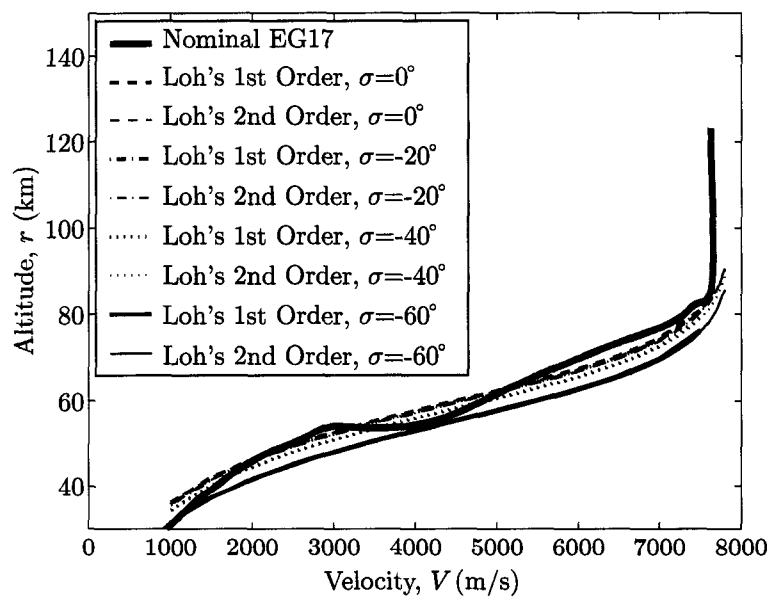
Figure 6.28 Loh's 1st order vs 2nd order altitude vs velocity
compared with EG17
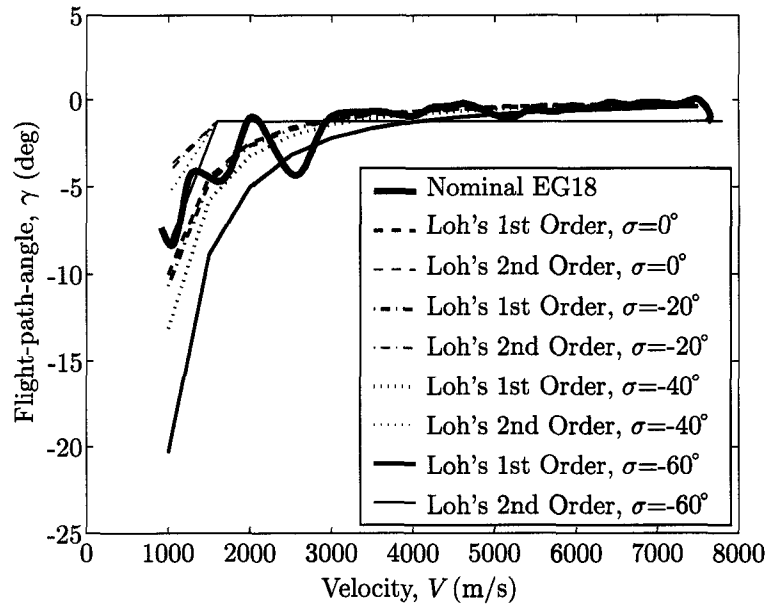
Figure 6.29   Loh's 1ˢᵗ order vs 2ⁿᵈ order flight-path-angle vs
velocity compared with EG18
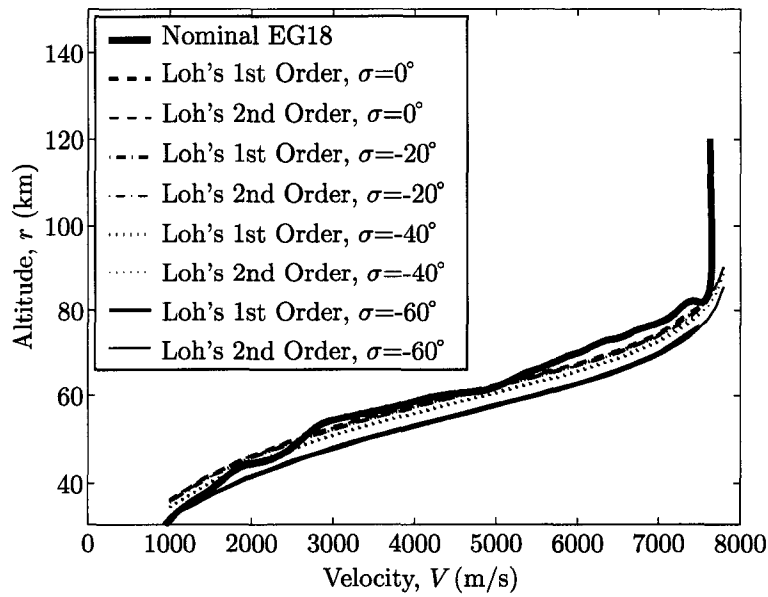
Figure 6.30   Loh's 1ˢᵗ order vs 2ⁿᵈ order altitude vs velocity
compared with EG18
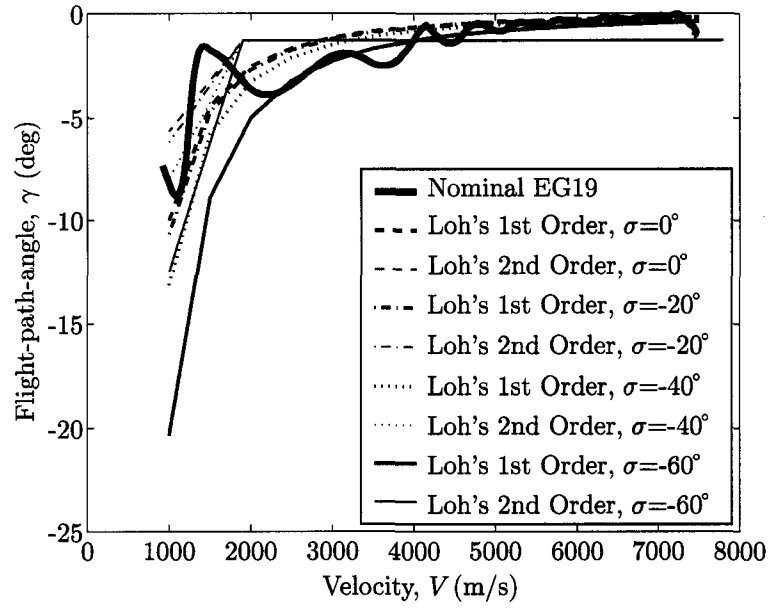
Figure 6.31   Loh's 1st order vs 2nd order flight-path-angle vs velocity compared with EG19
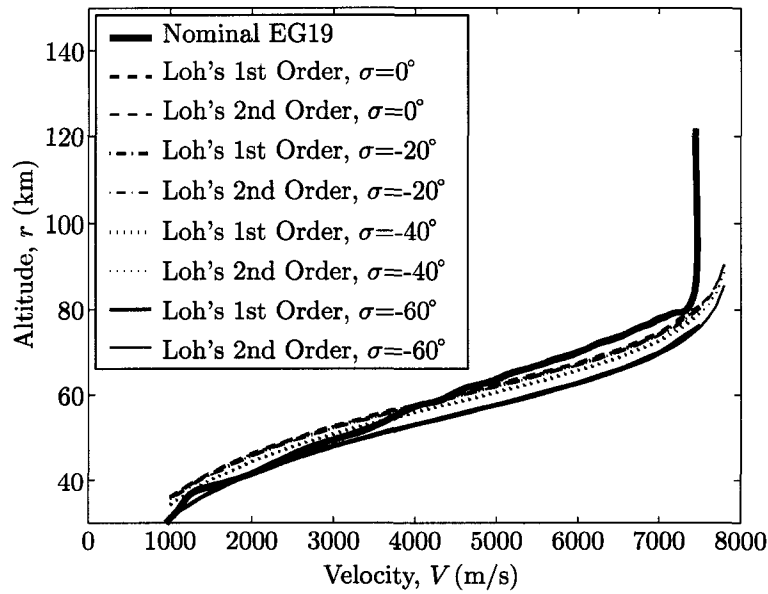
Figure 6.32   Loh's 1st order vs 2nd order altitude vs velocity compared with EG19
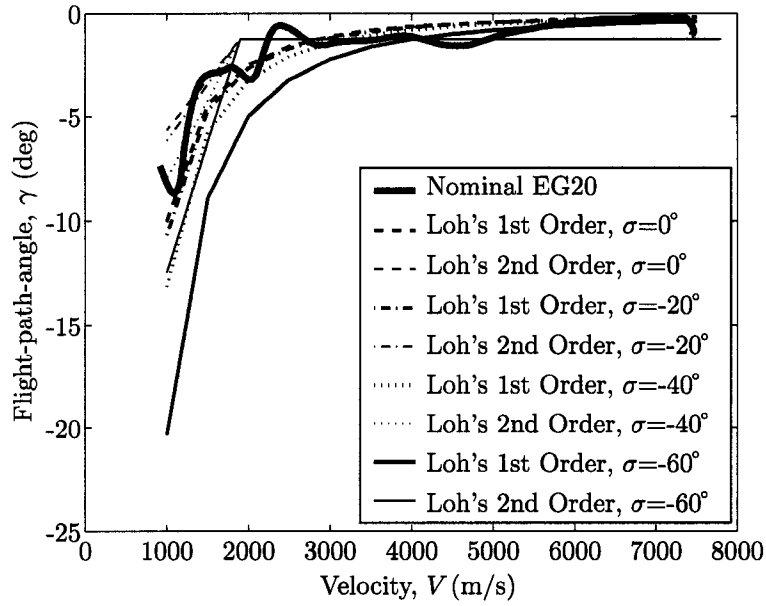
Figure 6.33　Loh's 1st order vs 2nd order flight-path-angle vs velocity compared with EG20
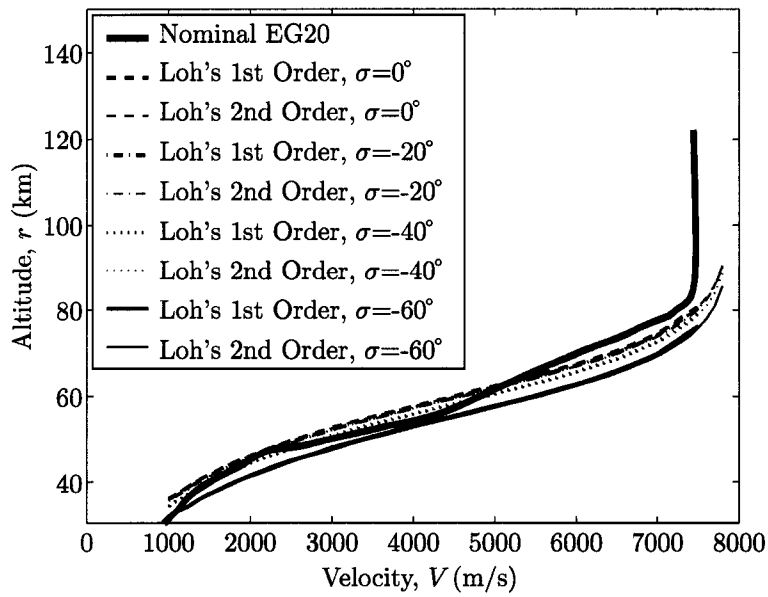
Figure 6.34　Loh's 1st order vs 2nd order altitude vs velocity compared with EG20
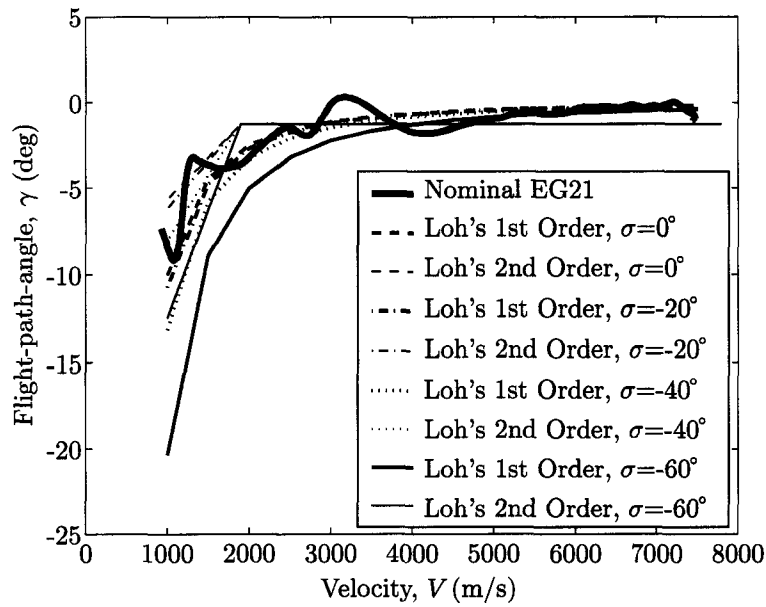
Figure 6.35   Loh's 1st order vs 2nd order flight-path-angle vs velocity compared with EG21
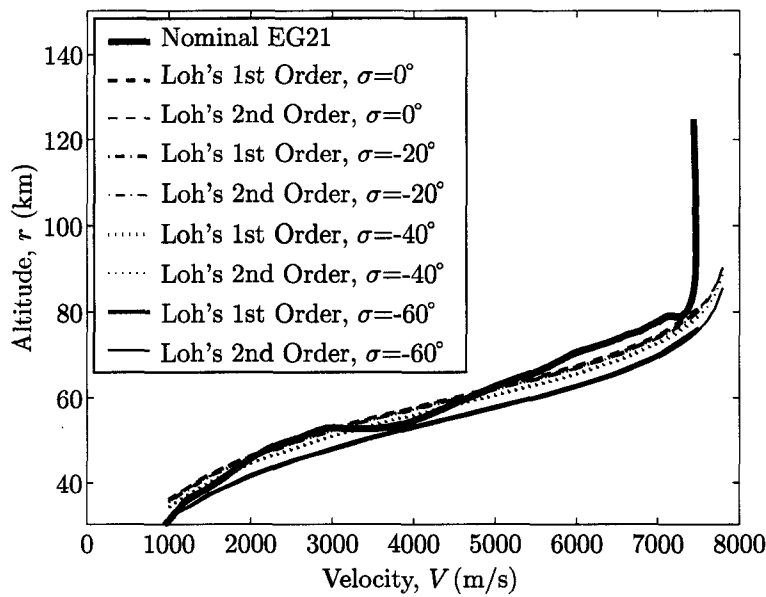
Figure 6.36   Loh's 1st order vs 2nd order altitude vs velocity compared with EG21

Finally, several σ's ranging from $-60° \leq \sigma \leq 0°$ have been analyzed and are illustrated in Figures 6.37 through 6.54 to better understand the effect of σ in the r-V design space. Furthermore, analytical solutions have no capability of enforcing constraints such as heat rate, normal acceleration, dynamic pressure and EGC. All above inadequacies contributed in the inaccuracies of the first-order approximations.

Figures 6.37 through 6.54 all exhibited a common trend regardless of initial entry conditions: $-20° \geq \sigma$ will violate the heat rate constraint in every case while $-20° < \sigma$ will violate the EGC constraints. Since EGC is a "soft" constraint, it is not as critical compared to observing the heat rate constraint (please refer to Figure 5.2 on page 113 for the detailed entry flight corridor descriptions).
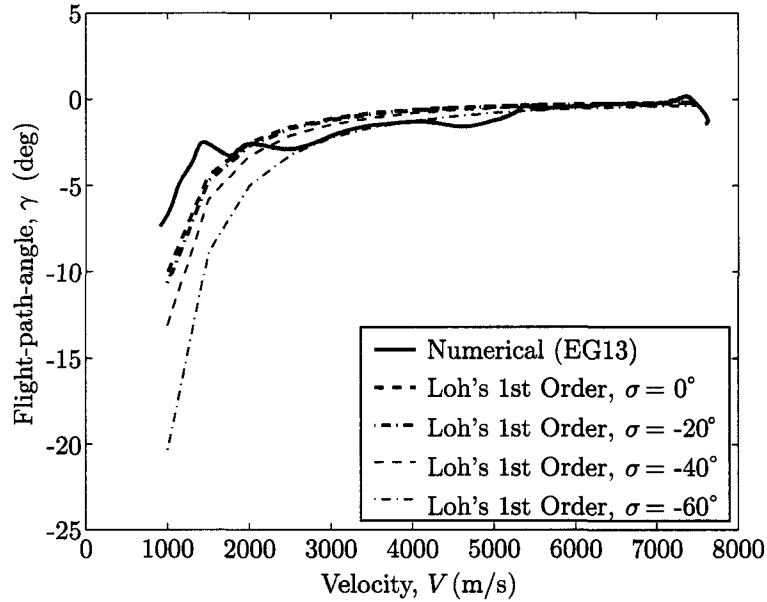
Figure 6.37   Loh's 1st order flight-path-angle vs velocity with different σ's compared with EG13
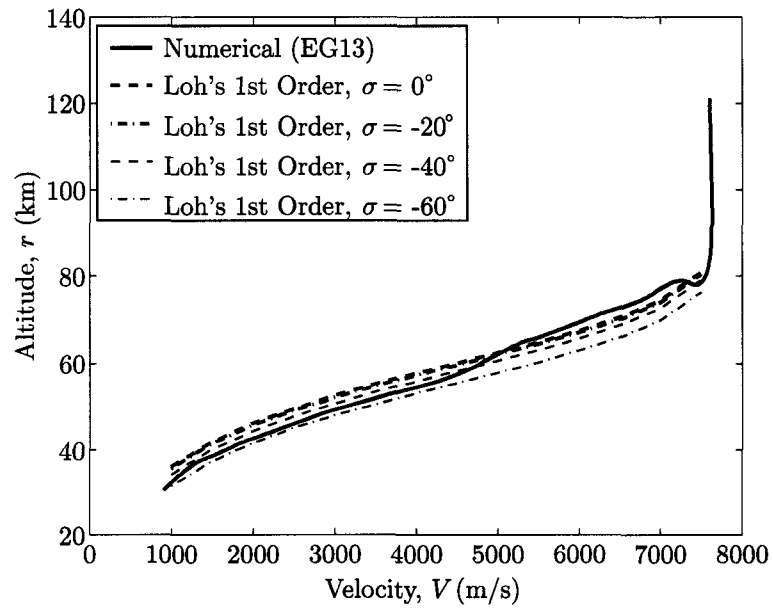
Figure 6.38   Loh's 1st order altitude vs velocity with different σ's compared with EG13
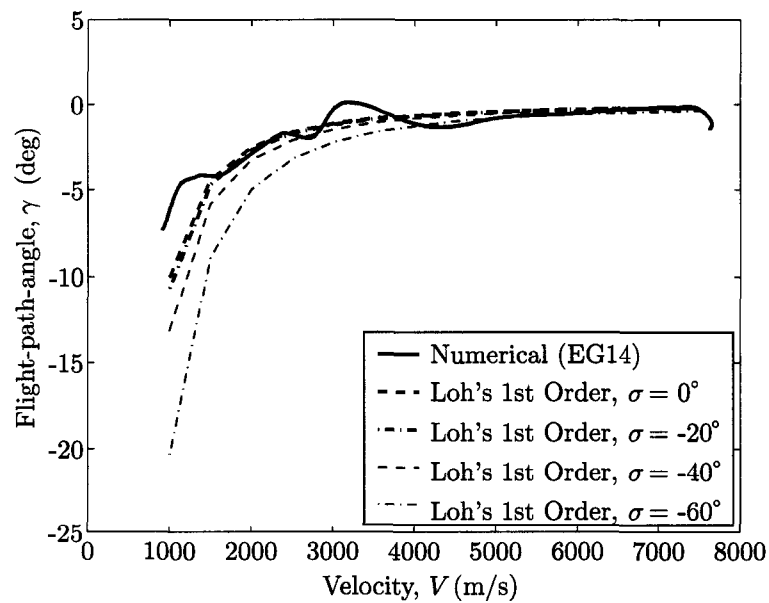
Figure 6.39   Loh's 1st order flight-path-angle vs velocity with different σ's compared with EG14
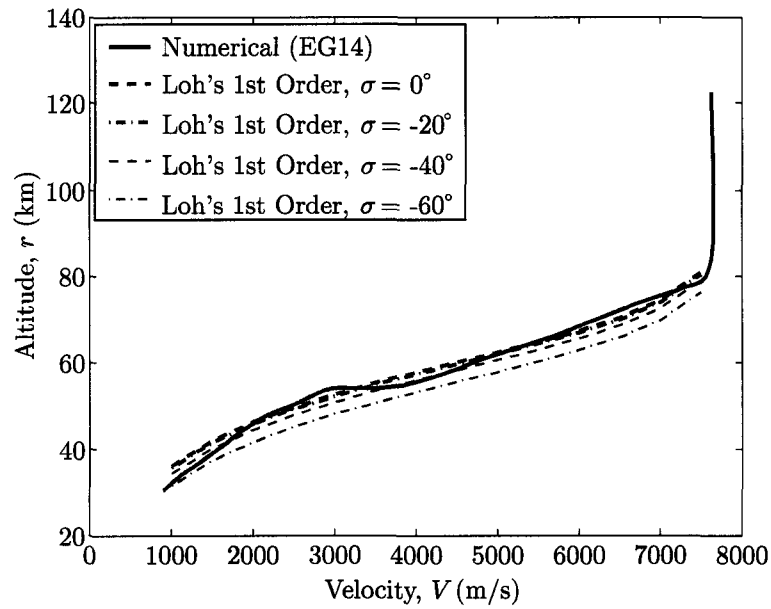
Figure 6.40 Loh's 1st order altitude vs velocity with different σ's compared with EG14
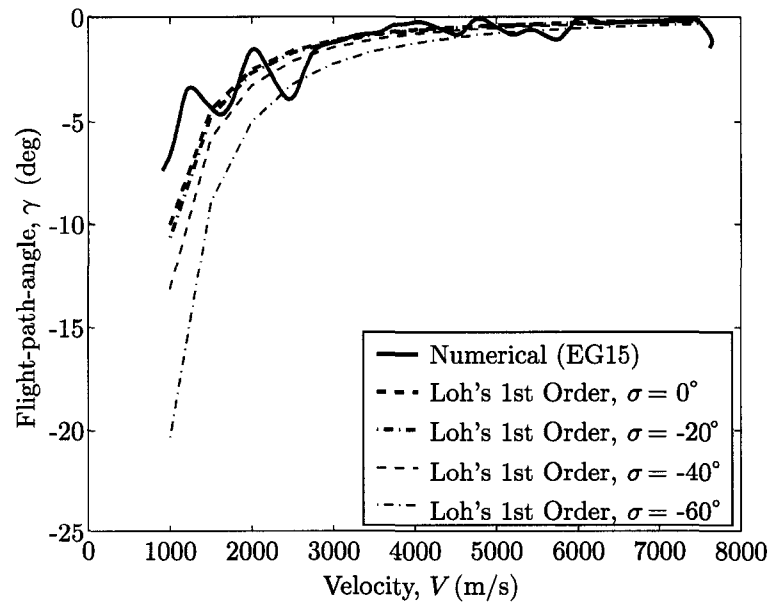
Figure 6.41 Loh's 1st order flight-path-angle vs velocity with different σ's compared with EG15
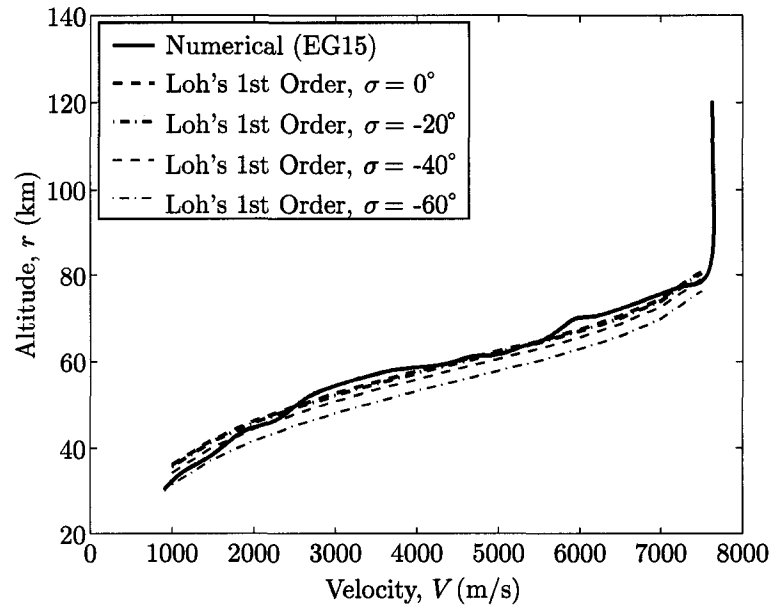
Figure 6.42 Loh's 1ˢᵗ order altitude vs velocity with different σ's compared with EG15
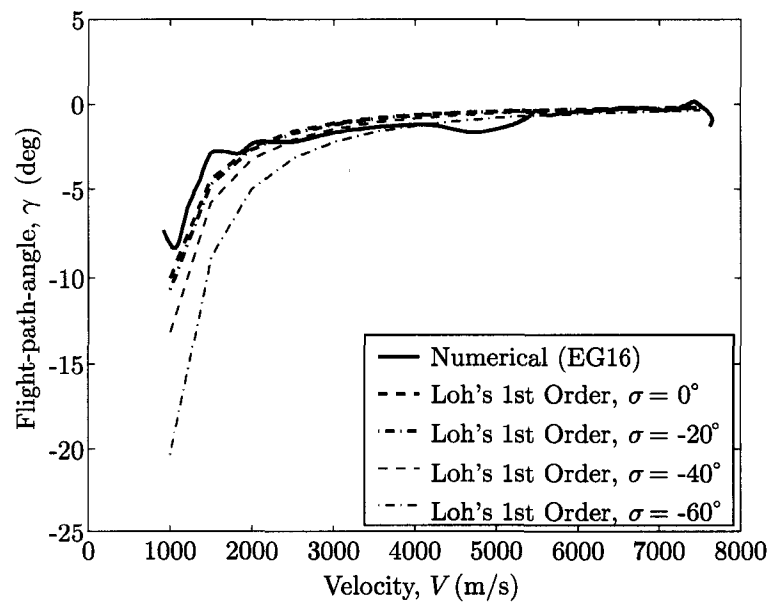
Figure 6.43 Loh's 1ˢᵗ order flight-path-angle vs velocity with different σ's compared with EG16
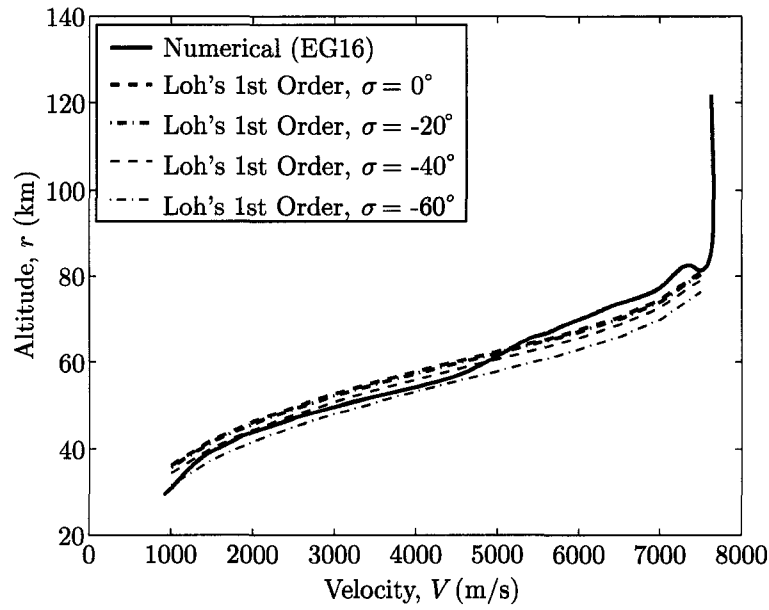
Figure 6.44   Loh's 1st order altitude vs velocity with different σ's compared with EG16
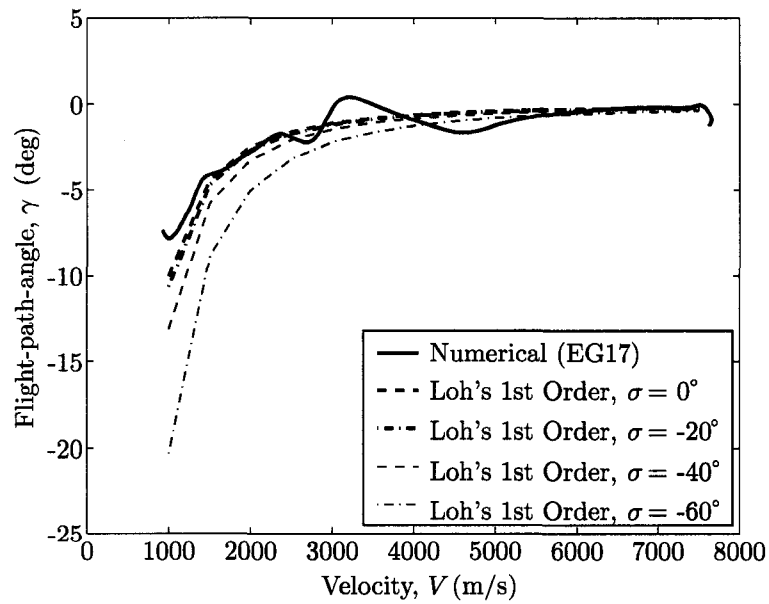
Figure 6.45   Loh's 1st order flight-path-angle vs velocity with different σ's compared with EG17
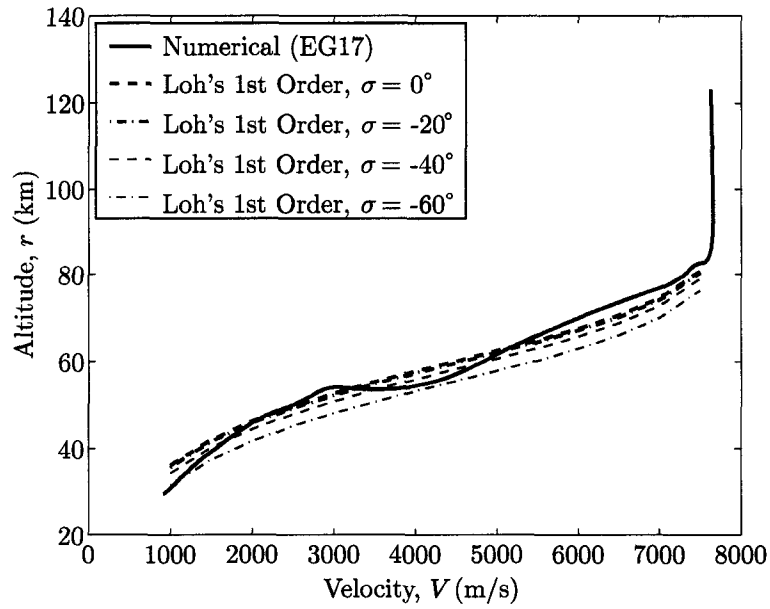
Figure 6.46   Loh's 1st order altitude vs velocity with different σ's compared with EG17
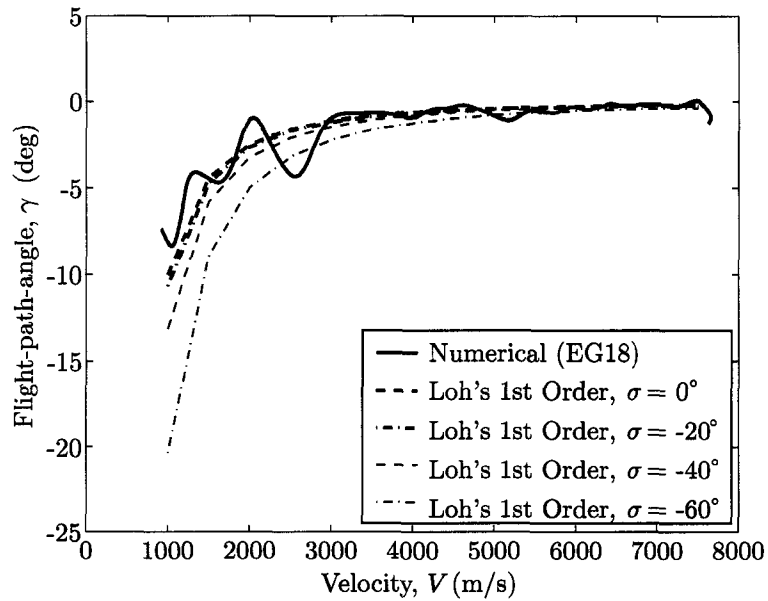
Figure 6.47   Loh's 1st order flight-path-angle vs velocity with different σ's compared with EG18
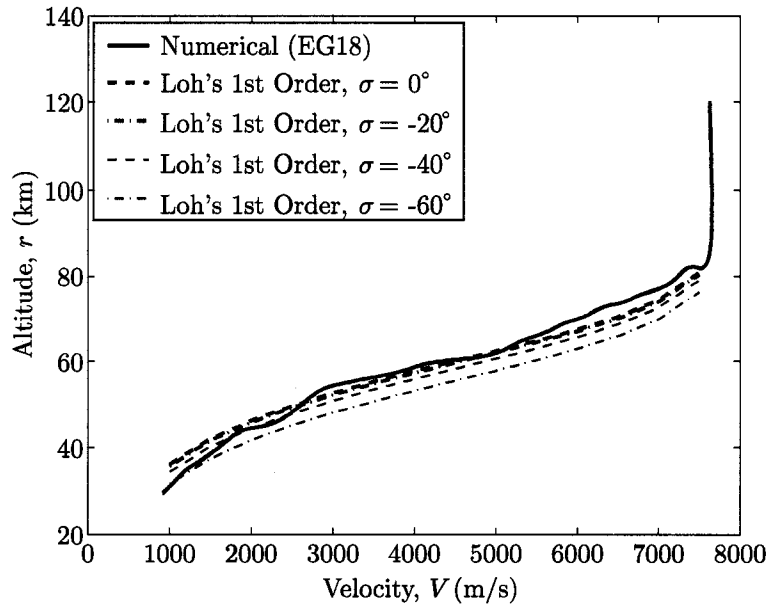
Figure 6.48 Loh's 1st order altitude vs velocity with different σ's compared with EG18
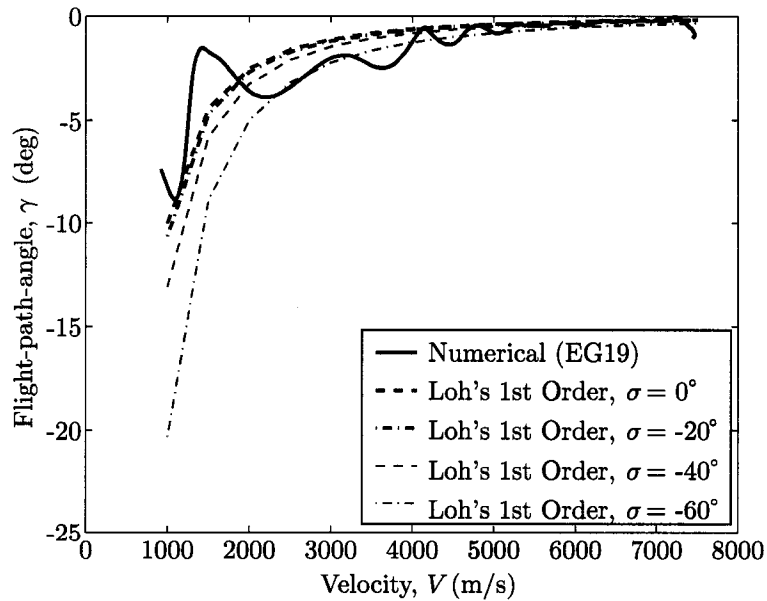
Figure 6.49 Loh's 1st order flight-path-angle vs velocity with different σ's compared with EG19
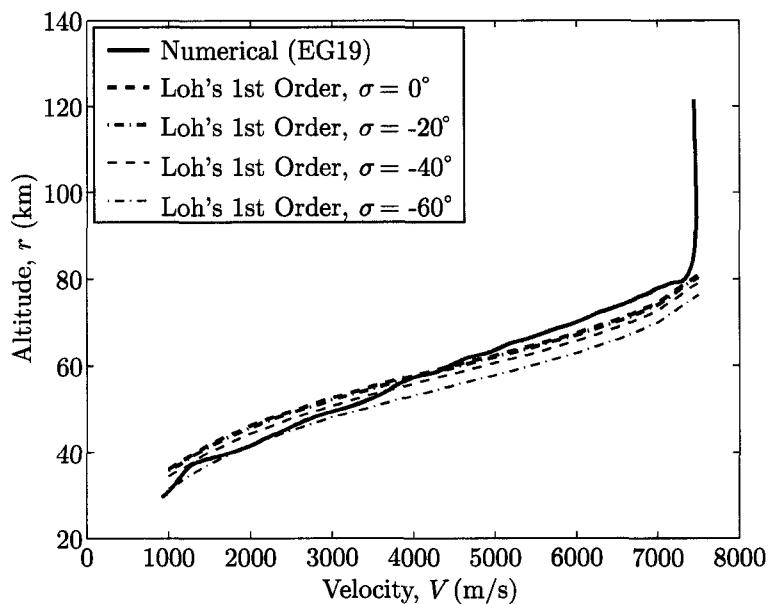
Figure 6.50   Loh's 1st order altitude vs velocity compared
with different σ's with EG19
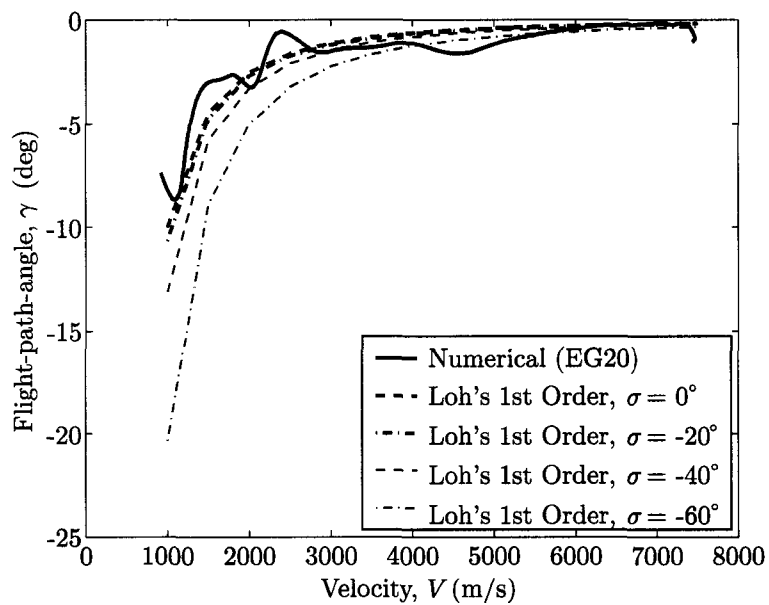
Figure 6.51   Loh's 1st order flight-path-angle vs velocity with
different σ's compared with EG20
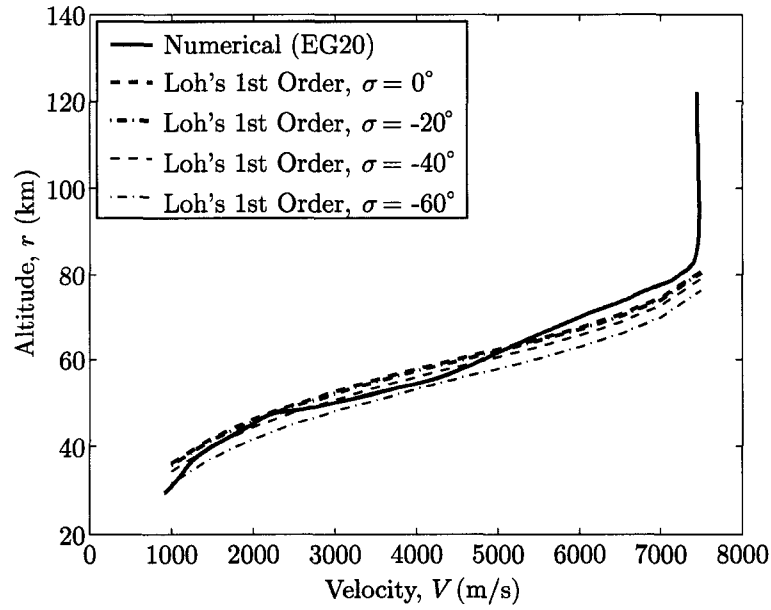
Figure 6.52   Loh's 1st order altitude vs velocity with different σ's compared with EG20
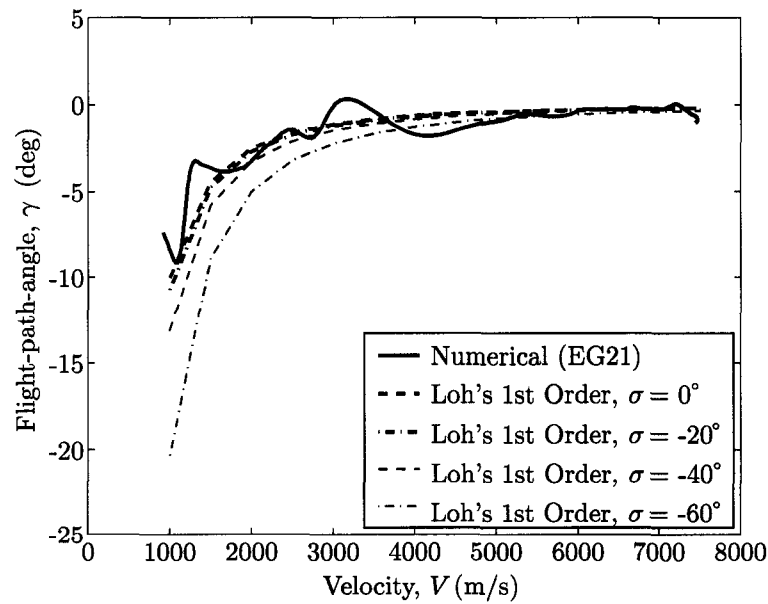
Figure 6.53   Loh's 1st order flight-path-angle vs velocity with different σ's compared with EG21
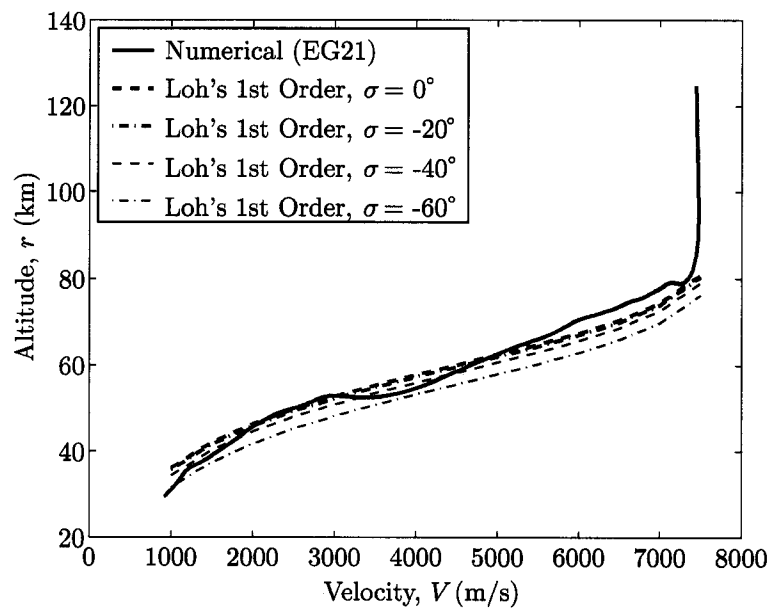
Figure 6.54 Loh's 1st order altitude vs velocity with different σ's compared with EG21

CHAPTER 7 SYSTEM ENGINEERING MANAGEMENT PLAN

*It's a very sobering feeling to be up in space and realize that
one's safety factor was determined by
the lowest bidder on a government contract.*

— *Alan Bartlett Shepard Jr.* [52]

ENGINEERING a complex system poses an interesting as well as demanding information management problem for system integration. Systems engineering became standard practice in the 1960's and 1970's with the awareness of complex development requirements needed for large-scale programs [113–115]. The key elements to a successful design during the initial phase of a complex project is how to overcome many uncertainties that will infiltrate different aspects of the final product, meet the needs of the customer, and complete the project in a timely and cost-effective manner. This chapter focuses on the project management and system engineering development process required to identify the areas of concentration for the flight mechanics team in a network centric environment.

> The Space Launch Initiative is the work of a nation, with industry, academia and government partners from around the country. Working to build the launch capability of the entire nation, the Space Launch Initiative is putting tools in the hands of those who will build the next generation rockets and create science and business environments unlike any in existence today.
>
> NASA's Space Launch Initiative [116]
> April 2002

The Space Shuttle has been a very successful program and is also the only reusable launch vehicle today. Even though the shuttle is a successful program, it has its share of problems and is costly to operate. The first generation reusable launch vehicle (RLV, referring to the Space Shuttle) is old in spite of constant upgrades on the three-decade old technology and with an extensive maintenance program. Space Launch Initiative (SLI) is a \$4.5 billion investment over a six-year period started by NASA in 2001 to expand access to space [117]. The goal of the initiative is to bring the US space transportation system into the 21st century, thus making the US space program more competitive, safe and reliable in the world-wide space market [118, 119].

In order to accomplish this, NASA has set the focus of SLI to reduce the technical and business risks associated with the development of a 2nd Generation RLV system. The four fundamental principles of SLI are [119, 120]:

① Commercial convergence: NASA seeks to maximize the convergence between commercial, NASA, and where possible Department of Defense (DoD) mission needs, technology requirements and operations considerations. NASA seeks to fly its unique missions on privately owned and operated launch systems within an integrated architecture.

② Competition: NASA seeks to create an environment of competition to assure the best and most innovative ideas are developed and supported by the SLI. SLI seeks to enable at least two viable commercial competitors in the 2005 timeframe.

③ Assured access: NASA seeks to provide access to the International Space Station (ISS) on more than one U.S. launch vehicle. Assured access will be facilitated by developing systems flexibility and standardization as keys to enabling access on more than one launch vehicle.

④ Evolvability: NASA seeks to develop systems that can affordably evolve to meet future mission requirements.

NASA hopes that SLI will enable working, traveling and living in space to be routine, 10 times cheaper and 100 times safer by 2010.

7.1 Major Technologies for RLV Program

The Space Transportation System (STS, also known as the Space Shuttle) has been the proud brainchild of the United States. Albeit the shuttle is an engineering marvel, the development of such a complex system required more than just an exceptional engineering design. It also required rigorously controlled system engineering plans throughout the life-cycle of the program in order to keep the shuttles safe and operational. Learning from more than twenty years of shuttle operations, NASA has identified ten major technology areas (displayed in Figure 7.1) as the cornerstone to design the next generation fully reusable launch vehicle that can achieve the "routine, 10 times cheaper and 100 times safer" goal set by NASA [23, 121].
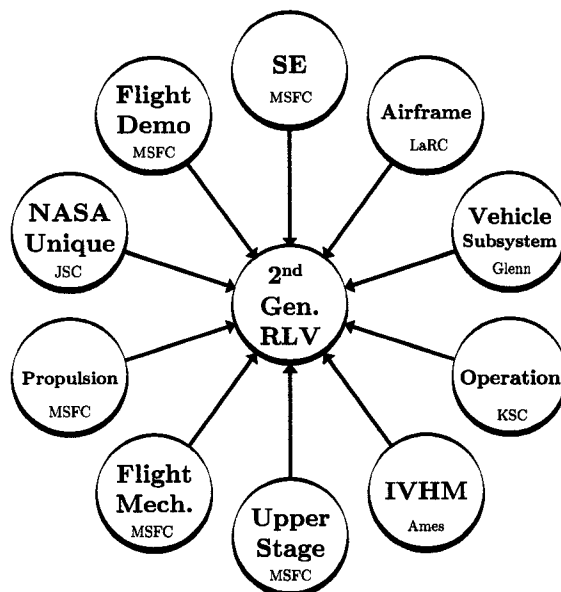
Figure 7.1   Major technologies required to design the
2nd generation reusable launch vehicle

NASA's Marshall Space Flight Center (MSFC) in Huntsville, Alabama is the lead center for space transportation development. MSFC was appointed to manage the 2nd Generation RLV Program which integrates the different areas of expertise of NASA centers across the country in order to accomplish a common goal — "bring us closer to our home in space" cheaper and safer. Subsections 7.1.1 to 7.1.10 briefly summarize the mission of each major technology area (TA).

7.1.1   TA-1: Systems Engineering Team

Systems engineering (SE) approach has always been associated with the development of requirements (definition and convergence of goals and objectives), risk reduction activities (reliability and maintainability) and trade analysis from the expertise and knowledge of difference sources. NASA has a long history of following a set of outlined documents such as *NASA Systems Engineering Handbook* [122] when conducting program development in order to maintain consistency. NASA has been paying particular

attention to the systems engineering and architecture of the 2nd Generation RLV development in order to properly evaluate technical feasibility, streamline project schedule, mitigate development risks, and culminate safety and reliability plans.

MSFC leads the systems engineering development with support from all other NASA centers and the Air Force Research Laboratory (AFRL).

7.1.2 TA-2: Airframe Team

The Airframe Team is responsible for the development and optimization of spacecraft structures such as the fuselage, wings, tails, and fuel tanks with maximum strength and minimum weight. The design of the structure must also satisfy the need in accordance with vehicle aerodynamics and thermodynamics.

NASA's Langley Research Center (LaRC) in Hampton, Virginia is in charge of the airframe technology development with support from all other NASA centers and AFRL.

7.1.3 TA-3: Vehicle Subsystems Team

Powerful actuators, advanced power systems and robust avionics are the major technologies that the Vehicle Subsystems Team is developing and testing.

NASA's Glenn Research Center (GRC) in Cleveland, Ohio heads the vehicle subsystems technology development with support from all other NASA centers and AFRL.

7.1.4 TA-4: Integrated Vehicle Health Management Team

Integrated Vehicle Health Management (IVHM) is a collection of sensors, diagnostic and prognostic software, and information logistic software used to collect, process and integrate data in real time to determine the vehicle's health. Precise sensor data, accurate diagnosis/prognosis of the problem and prompt delivery of the information are vital for critical decision making. The collected data will also be used for preventive maintenance purposes to increase safety.

NASA's Ames Research Center (ARC) in Moffett Field, California oversees the IVHM development with support from all other NASA centers and AFRL.

7.1.5 TA-5: Operations Team

Ground operations are expensive and dangerous. As an example, improper draining and venting of cryogenic propellants could lead to horrific results. The Ground Operations Team at Kennedy Space Center (KSC) is responsible for fluid transfer technologies, data analysis and retrieval technologies and ground-to-flight interfaces (fuel, power, data).

NASA's KSC in Cape Canaveral, Florida leads the operations development with support from all other NASA centers and AFRL.

7.1.6 TA-6: Upper Stage Team

Upper stage refers to the part of the spacecraft that will travel into space. The major technological development for the Upper Stage Team include reusable propulsion, expendable propulsion, upper stage unique material and structure, as well as auxiliary systems.

MSFC is in charge of the upper stage development with support from all other NASA centers and AFRL.

7.1.7 TA-7: Flight Mechanics & Navigation Team

NASA is looking into the possibility of using "adaptive systems" as part of the flight mechanics technology. In simple terms, an "adaptive system" is basically a computer commander aboard the spacecraft with memory and decision making capabilities. The new GN&C algorithm can make corrections to a spacecraft during flight (generating trajectories onboard) and records to its memory in case the situation arises in the future.

Abort decisions can also be made with this adaptive system so that there is no need to pre-program each emergency scenario into the flight software.

MSFC leads the flight mechanics & navigation technology development with support from all other NASA centers and AFRL.

7.1.8 TA-8: Propulsion Team

Escaping Earth's gravitational pull has been a design challenge for the propulsion engineers as that typically requires approximately half of the total energy. A higher thrust-to-weight ratio, cost-effective and reliable propulsion system is highly desired in order to achieve the $1,000 per pound goal.

MSFC heads the propulsion technology development with support from all other NASA centers and AFRL.

7.1.9 TA-9: NASA Unique Team

Human space flight (HSF) is unique to NASA, thus making the safe return of the crew a top priority. NASA Unique Team is currently designing and evaluating crew escape systems to be used on-ground, in-flight and on-orbit.

NASA's Johnson Space Center (JSC) in Houston, Texas oversees the NASA unique development with support from all other NASA centers and AFRL.

7.1.10 TA-10: Flight Demonstration Team

Before the 2nd generation reusable launch vehicle can be built for operational usage, it must go through extensive technology verifications and validations. The responsibility of the flight demonstration team is to flight test all key enabling technologies (Subsections 7.1.2 to 7.1.9) in the ascent, in orbit and entry environments.

MSFC is in charge of the flight demonstration development with support from all other NASA centers and AFRL.

7.2 Top Level Aerospace System

Engineering integration is a balancing act. The master plan at the top level of designing the next generation reusable launch vehicle (may it be a single-stage or a two-stage design) must address all goals and requirements as stated in Section 1.1 on page 3. The project master plan (limned in Figure 7.2) must also integrate different areas of launch vehicle design (aerodynamics, structures, propulsion, performance, thermal, and avionics) with systems engineering (reliability, safety and operability) in order to perform technology readiness level (TRL) assessment, selection and implementation of the best design to verify that the design is properly built and integrated. Furthermore, trade-off between requirements and vehicle attributes are also done in order to fine tune the system (modify design, requirements and/or operational plan) and achieve the best final design [105, 115, 123, 124].
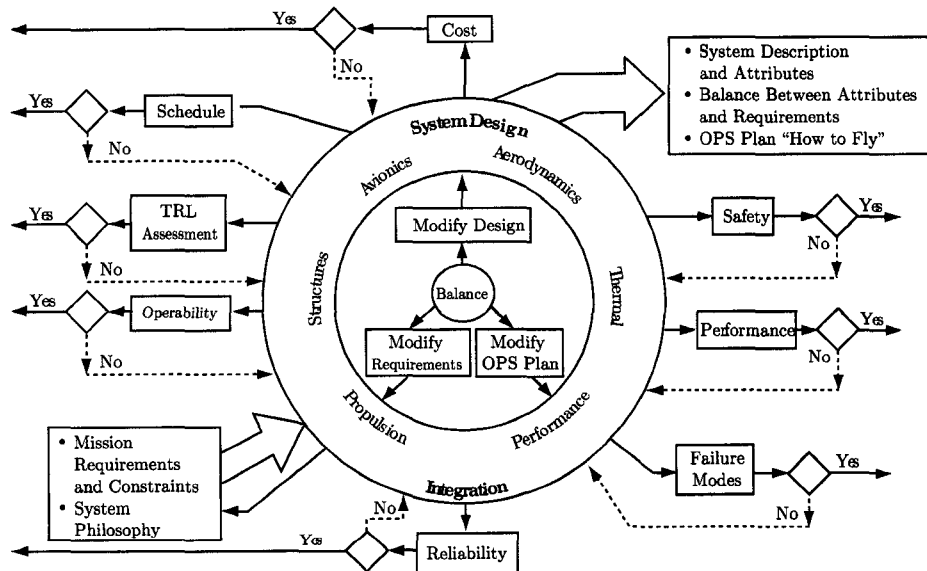
Figure 7.2 Top level systems design analysis functions, courtesy of Ref. [125]

While it is important to incorporate and integrate different areas of launch vehicle design, it is just as important to develop a system requirement master plan (Figure 7.3) that will ensure that all design criteria have been considered, analyzed and implemented throughout the design phase. Figure 7.3 is a standard system engineering (SE) "Vee" diagram adapted for the development of flight software.
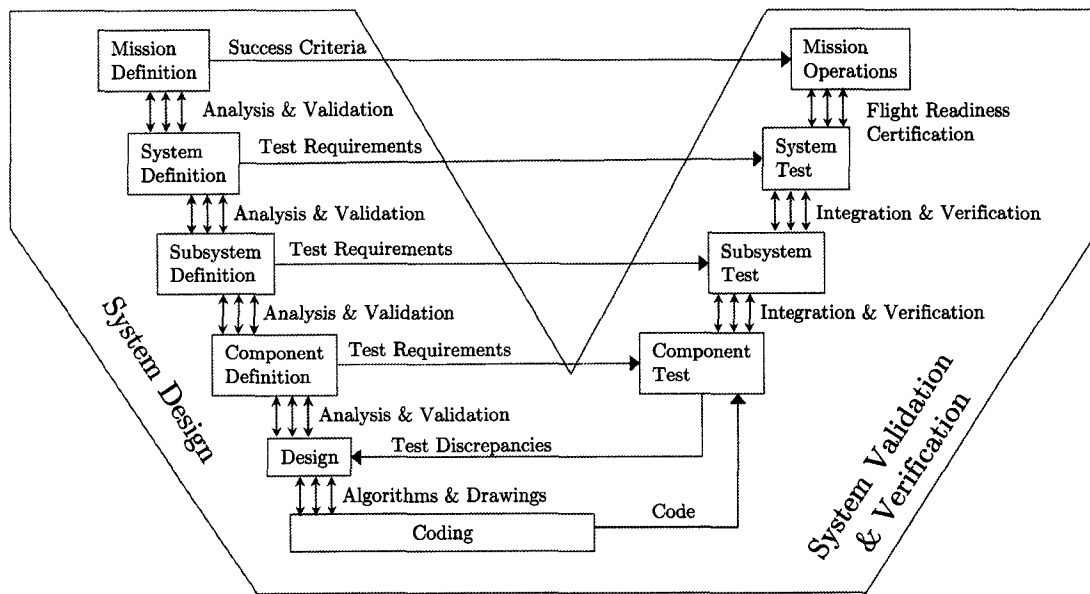
Figure 7.3   G&C system requirement development
(SE "Vee"), adapted from Ref. [123]

7.3   Guidance & Control Project

The Guidance & Control (G&C) Team is part of the TA-7 Flight Mechanics & Navigation Team in Figure 7.1 and part of the "performance" in the top level systems design analysis functions as illustrated in Figure 7.2. The G&C Team holds an integral role in the success of the 2nd Generation RLV development, thus careful planning is an indispensable task.

NASA has only developed the general "Level 1 Requirements" [126] for request for proposal (RFP) purposes. It is the responsibility of the contractors to produce lower level requirements. The project development process in acquiring the requirements for the G&C Team is depicted in Figure 7.4. The development is based on evaluations of project formulation and baseline requirements to derive a project implementation plan.
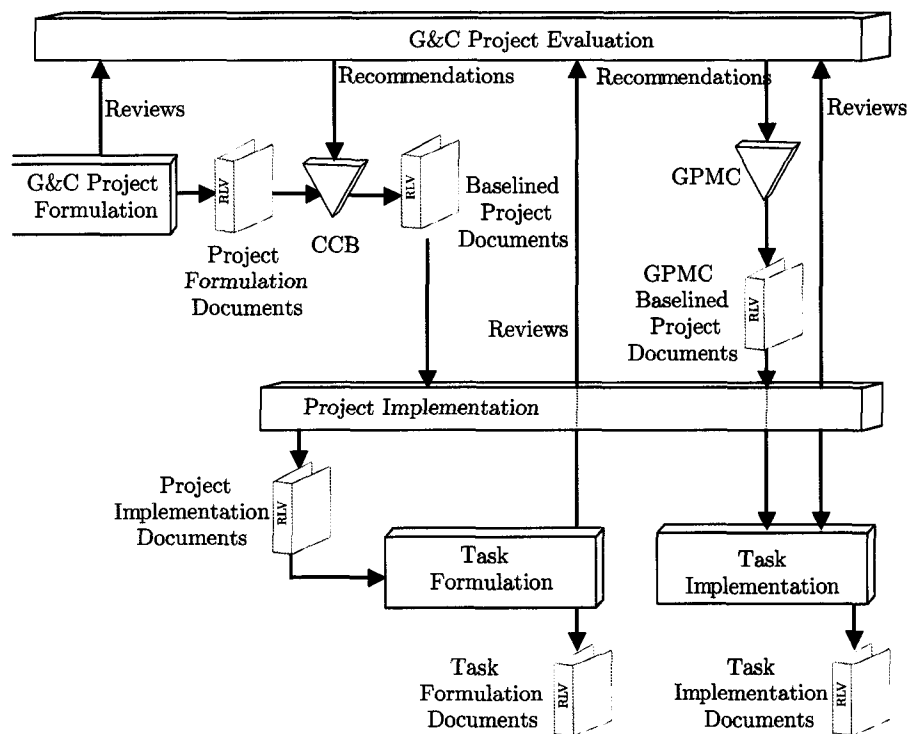
Figure 7.4 Top level G&C project development process, adapted from Ref. [127]

Once a project implementation plan has been established, the plan will be further scrutinized as shown in Figure 7.5 to verify the validity of the plan to meet the top level project requirements. Part of the investigation includes availability of technology, risk assessment, budget & schedule estimation, trade-off studies, and implementation options. After several iterations of the formulation process, the results of such activities include concept definition, concept of operations, configuration layout, configuration management plan, data management plan, resource planning, work breakdown structure, project plan, project schedule, system specifications, evaluation criteria, cost estimates, request for proposal, and risk management plan [128, 129].

Figure 7.5   Top level project formulation process overview, adapted from Ref. [127]

Before the project advances into implementation phase, it is important to develop system engineering (SE) function task breakdowns for the whole design as well as for each individual system. The SE function task breakdown as applied to the G&C Team is displayed in Figure 7.6. The SE process starts with a set of requirements and specifications and proceeds to a system analysis of the requirements to determine what needs to be done and how to do it in order to satisfy the requirements and specifications. The selected solution must be integrated and verified to comply with the original requirements (or the latest version of the requirements because this is an iterative process) [127, 130, 131].
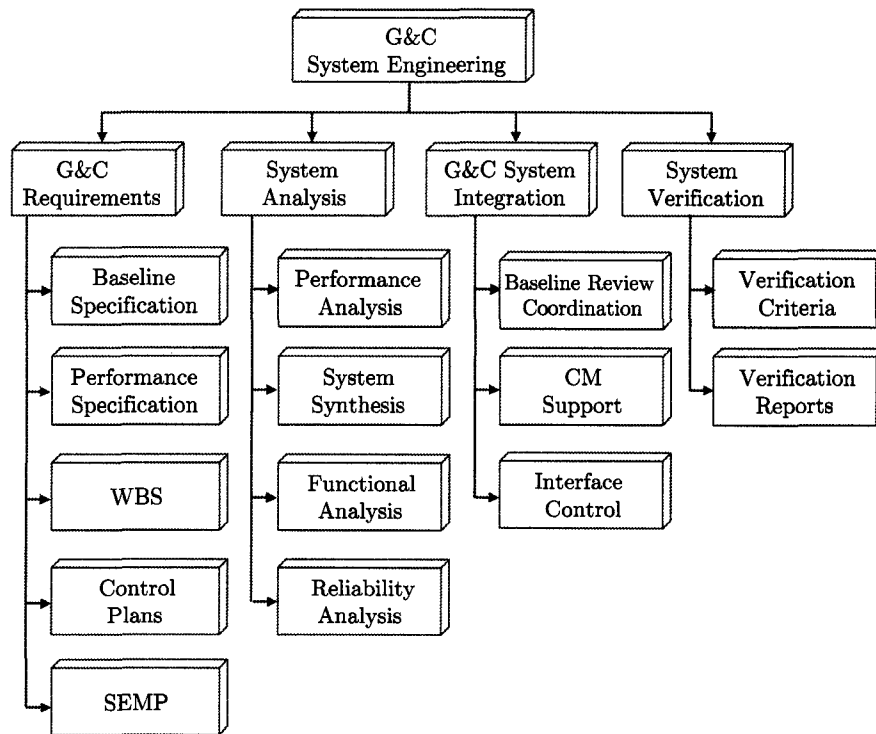
Figure 7.6 G&C project system engineering function task breakdown, adapted from Ref. [127]

7.3.1 System Requirements

The 2nd Generation RLV initial architecture requirements are derived from an understanding of NASA, DoD, and commercial mission needs, and from deficiencies in the existing fleet of launch vehicles, including inadequate space transportation system safety and reliability, and excessive space transportation user costs.

The G&C Team system requirements encompasses activities required to transform a need as established in a top level project document (Subsection 7.1.7) into a comprehensive set of performance requirements. System requirements activities pertain to the G&C Team include baseline specifications, performance specifications, project work breakdown structure (WBS), control plans (establish configuration management), and system engineering management plan (also known as SEMP to document all activities and milestones required to meet the objective of design).

In order to properly define the system operational requirements for this research, it is necessary to ask the following questions [123]:

① What function(s) will the system perform?

② When will the system be required to perform its intended functions?

③ Where will the system be utilized?

④ How will the system accomplish its objective?

According to SLI report NRA8-30 Flight Mechanics Risk Reduction [132], NASA expects the GN&C offeror to:

❶ Solicits technologies that provide an innovative and efficient approach for modeling natural and induced environments and simulation tools for developing trajectory simulations and computer based test-beds for GN&C algorithms.

❷ Solicits analytical processes and computer tools that provide an efficient method for formulating and performing comprehensive Monte Carlo flight dispersion analyses.

❸ Solicits technology that would provide fast and accurate post-flight trajectory reconstruction.

❹ Solicits advanced GN&C technologies such as adaptive GN&C systems, on-board performance monitoring, autonomous abort guidance, reconfigurable control systems, propellant utilization algorithms and efficient processes for the development, verification and validation of flight software.

❺ Solicits technologies or processes that would reduce or eliminate operations associated with the generation, verification and loading day-of-launch software updates (I-loads) for GN&C systems.

❻ Solicits technologies, algorithms, simulations and test beds for the development of automatic rendezvous and docking, and automated landing.

In response to request ❹, the specific functionalities for Iowa State's Guidance Team include:

☆ Ascent trajectory optimization (on-board and off-line)

☆ Entry trajectory optimization (on-board and off-line)

☆ 3 and 6-DOF ascent / entry simulation

☆ Interface to MSFC MAVERIC analysis tool

☆ A specific environment model (gravity and atmosphere)

☆ A specific single-stage-to-orbit vehicle model

The process used to analyze G&C system requirements is delineated in Figure 7.7.
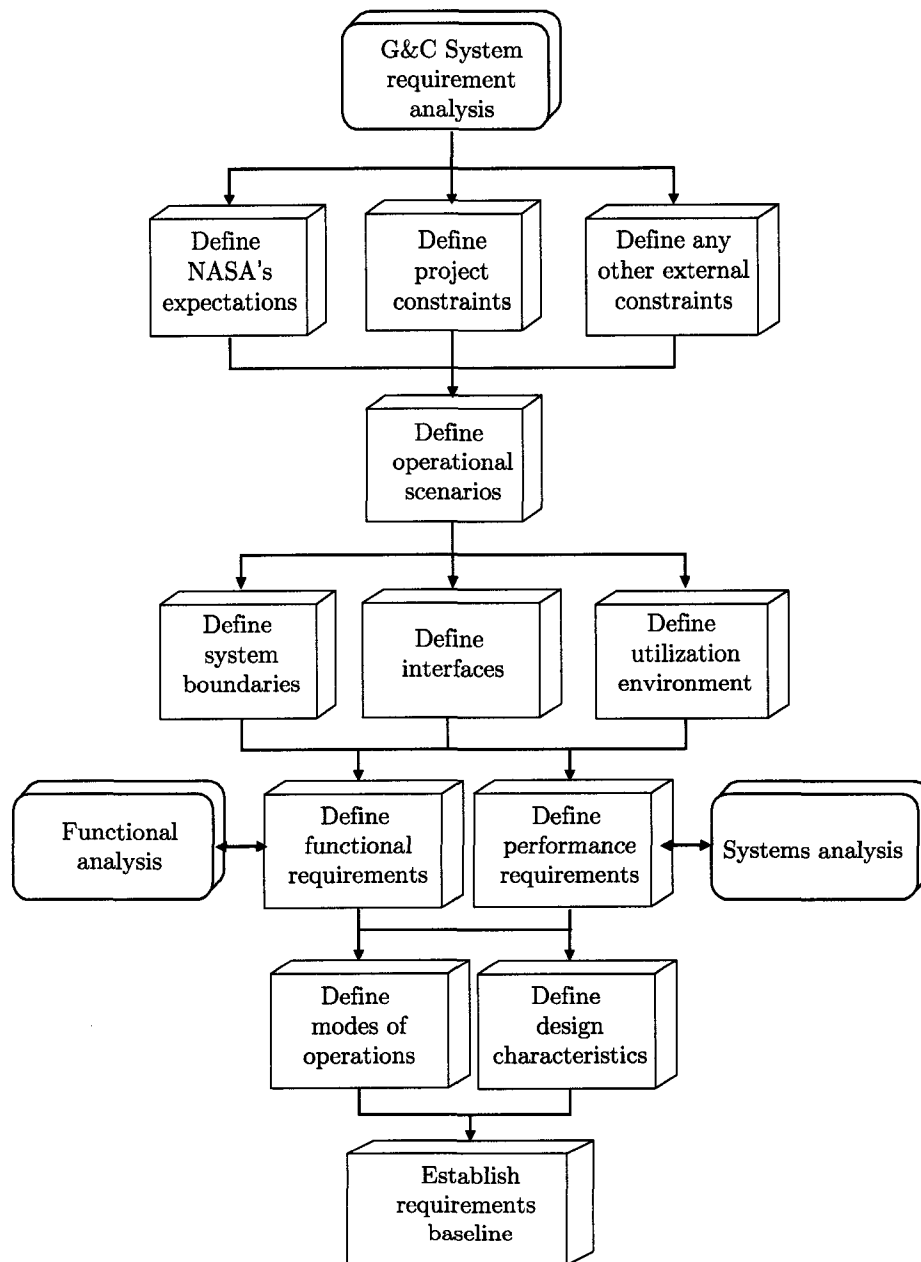
Figure 7.7   G&C system requirements analysis, adapted from Ref. [133]

The criteria used to evaluate the G&C system requirements are derived from DoD's *Systems Engineering Fundamentals* and [134] and IEEE Standard 1220 [133]. These ten criteria include:

① **Customer expectations:** clear understanding of customer's expectations in terms of functions, operational requirements documents, mission needs, and/or technology-based opportunity.

② **Project constraints:** identify and define constraints that might affect design solution, i.e., costs, required metrics for measuring progress, team assignments and structure, and project control mechanisms.

③ **External constraints:** identify and define external constraints that might affect design solution, i.e., regulations (industry, international, others), technology base, and interface capabilities.

④ **Operational scenarios:** identify and define operational scenarios that cover the anticipated uses.

⑤ **Measure of effectiveness and suitability:** identify and define how the G&C system effectiveness measures to that of customer's expectations as well as satisfaction. These include mission performance, safety and reliability.

⑥ **Utilization environments:** define the operational environments and how they may impact the system performance.

⑦ **Life-cycle:** analyze the above criteria and focus on the cost that are anticipated to impact supportability (upgrades, maintenance) and affordability over the entire life-cycle of the system.

⑧ **Functional requirements:** define what the system must be able to accomplish.

⑨ **Performance requirements:** define the performance requirements for each G&C software component.

⑩ **Technical performance measures:** identify the critical indicators of system performance that will be tracked during the design process. These critical indicators may have disastrous effect on cost, schedule, and/or performance.

7.3.2 System Analysis

Performance analyses for the G&C Team include orbital and flight mechanics analyses, attitude control analyses, onboard computer & memory utilization analysis, dynamics analysis, guidance & navigation analysis, and autocommander analysis. The system analysis model shown in Figure 7.8 includes assessment on requirement conflicts, functional alternatives, design alternatives and risk factors for these different tasks. The ultimate goal of system analysis is to establish a preferred system configuration, to measure the performance characteristics of the system (and subsystems), and a recommendation to future course of action.

After the system and performance analyses, system synthesis is performed to determine a preferred G&C system configuration and establish feasible performance qualities. Functional analysis is then performed to assess whether the system capabilities meet the G&C Team project requirements. Interface analysis is performed to guarantee that G&C software subsystems will work cohesively. This analysis will identify the common functional features that all interfaces must have.
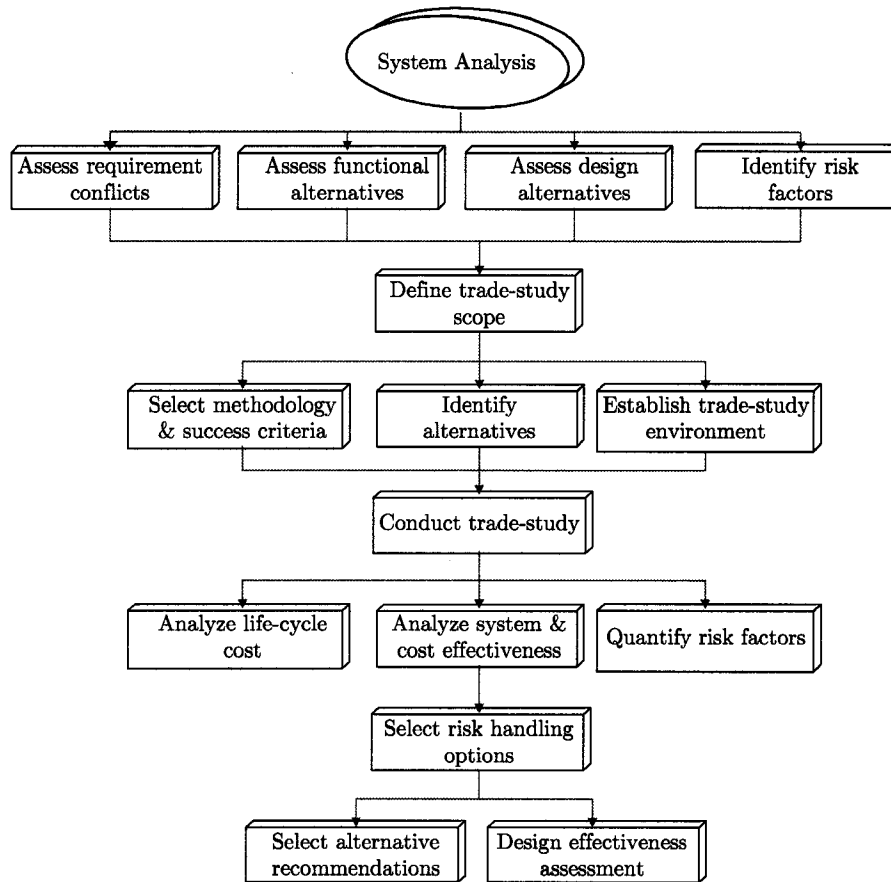
Figure 7.8 G&C system analysis process, adapted from Ref. [133]

7.3.3 System Integration

A critical function of the system integration is to review the overall G&C system, by itself and as part of the "big picture." Project requirements review (PRR) of the baseline requirements will ensure that the project requirements have been thoroughly defined, properly documented, and will be verifiable upon the completion of system implementation. During the integration phase, additional reviews such as preliminary design review (PDR) and critical design review (CDR) will be conducted to confirm that the system requirements have been met and there is enough progress to allow further software integration.

While performing G&C system integration, system engineers will support and manage any changes to the baseline requirements. More detail about system support is discussed later in Subsection 7.4.1. Last, interface control is to enforce the identified common functional features in all interfaces while implementing. System integration ultimately is to combine the lower-level G&C element results in a functioning and unified higher-level element.

7.3.4 System Verification

The ultimate goals of system verification is to build the product right and to establish a level of confidence that the system will perform. The basis for the verification process is that the product must meet its original baseline design requirements. Some questions that need to be answered during the system verification process include [123]:

① What is the *true* effectiveness of the system?

② What is the *true* performance of the system?

③ What is the *true* effectiveness of the system support capability?

④ Does the system meet all of the requirements as covered through the specified Technical Performance Measures (TPMs)?

⑤ Does the system meet all consumer requirements?

A summary of G&C software design verification process is delineated in Figure 7.9.
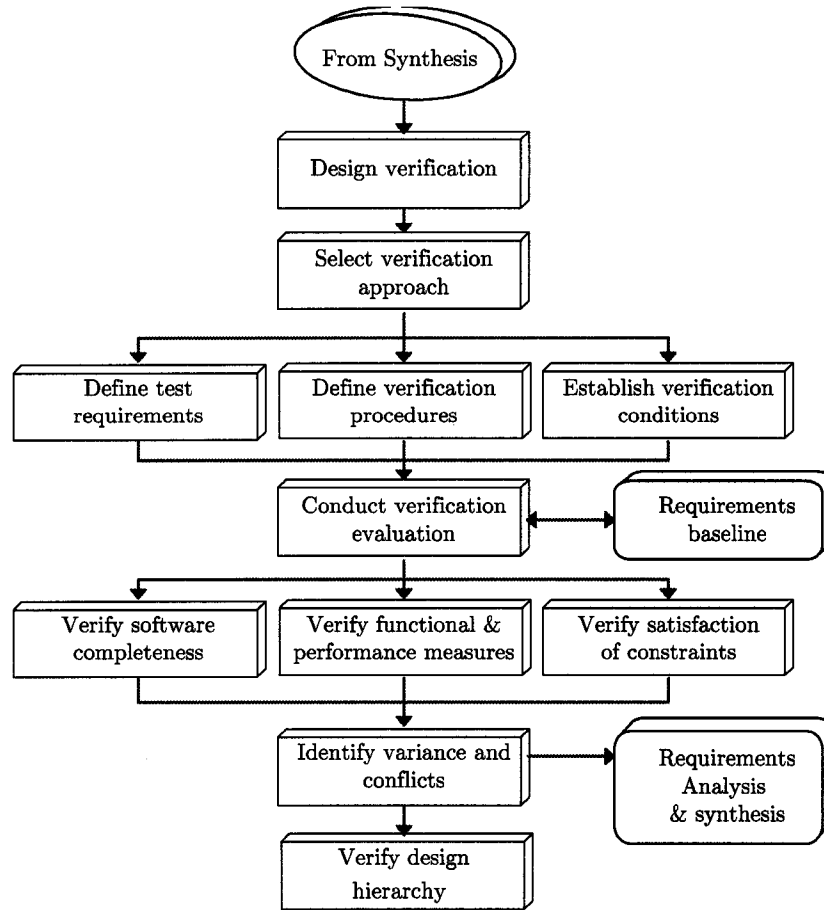
Figure 7.9 G&C software design verification process, adapted from Ref. [133]

7.4 Configuration Management Plan

Configuration management plays an important role in the success of any project. In order to avoid any confusion or chaos during the development of a project, it is necessary to have systematic planning and management [105, 115, 129, 135–137]. The following is a definition from MIL-HDBK-61 [135] entitled *Configuration Management Guidance*:

> Configuration management is defined as a process for establishing and maintaining consistency of a product's performance, func-

tional and physical attributes with its requirements, design and operational information through its life.

A good configuration management program allows proper product identification [138], product traceability [139], engineering change is controlled and documented [131, 135, 140, 141], and the final product and its supporting documentation is consistent [134].

7.4.1 Configuration Control

The main purpose of configuration control is to allow proper systematic change management process. This process entails the coordination, preparation, evaluation, justification, and implementation of engineering change proposals (ECPs, more details in Subsection 7.4.2) that may effect the configuration items (CIs, more details in Subsection 7.4.3) and baselined configuration documentation (describes the performance, functional and physical characteristics of a product) [136, 137]. Moreover, configuration control also regulates the following according to DoD [135]:

☆ Allow optimum design and development latitude with the appropriate degree, and depth of configuration change control procedures during the life-cycle of a system/CI

☆ Provides efficient processing and implementation of configuration changes that maintain or enhance operational readiness, supportability, interchangeability and interoperability

☆ Ensures complete, accurate and timely changes to configuration documentation maintained under appropriate configuration control authority

☆ Eliminates unnecessary change proliferation

In order to properly execute the systematic change management process, it is necessary to define the organizational chart as rendered in Figure 7.10 in the very beginning of the project so that all involved parties know the organizational structure of the project. According to Aerospace America [142] and Hanson [143], TA-7 Flight Mechanics Risk Reduction was awarded partially to Ohio University as the lead contractor for the Guidance and Control Project.

```
                    ┌────────────────────┐
                    │  Flight Mechanics  │
                    │   & Navigation     │
                    └────────────────────┘
          ┌──────────────────┼──────────────────┐
          ▼                  ▼                  ▼
   ┌─────────────┐    ┌─────────────┐    ┌─────────────┐
   │ Universities │    │     USL      │    │    NASA      │
   │              │    │              │    │   Marshall   │
   └─────────────┘    └─────────────┘    └─────────────┘
          │                  │                  │
          ▼                  ▼                  ▼
   ┌─────────────┐    ┌─────────────┐    ┌─────────────┐
   │ Guidance and │    │  Simulation  │    │  Navigation  │
   │   Control    │    │ Environment  │    │              │
   └─────────────┘    └─────────────┘    └─────────────┘
          │
          ├───▶ ┌──────────────────────┐
          │     │   Auburn University   │
          │     └──────────────────────┘
          ├───▶ ┌──────────────────────┐
          │     │  Iowa State University │
          │     └──────────────────────┘
          ├───▶ ┌──────────────────────┐
          │     │    Ohio University    │
          │     └──────────────────────┘
          └───▶ ┌──────────────────────┐
                │  University of Alabama │
                │     at Huntsville      │
                └──────────────────────┘
```
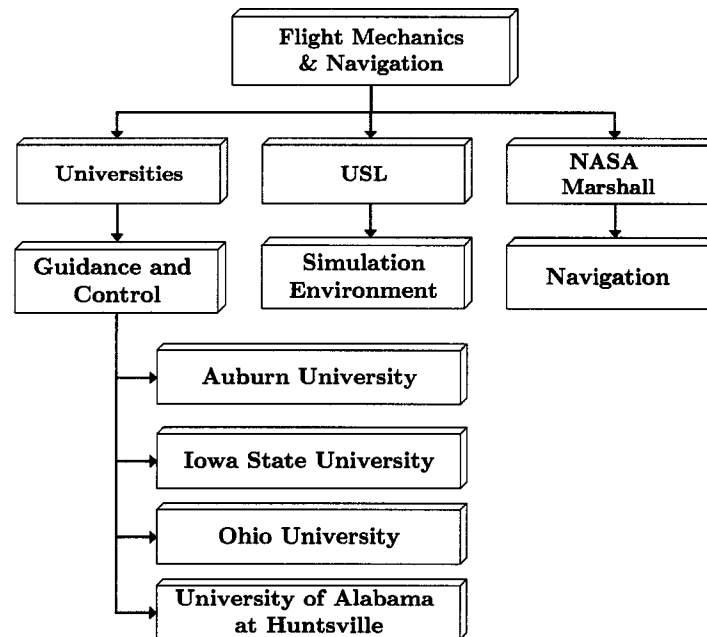
Figure 7.10   Configuration management for flight mechanics
and navigation group

Ohio University sought further collaboration of three universities to integrate the strength and expertise of different universities in order to accomplish a common goal — bring the development of 2nd Generation RLV a step closer to reality. The strength, expertise and responsibility of each university is outlined in Figure 7.11.
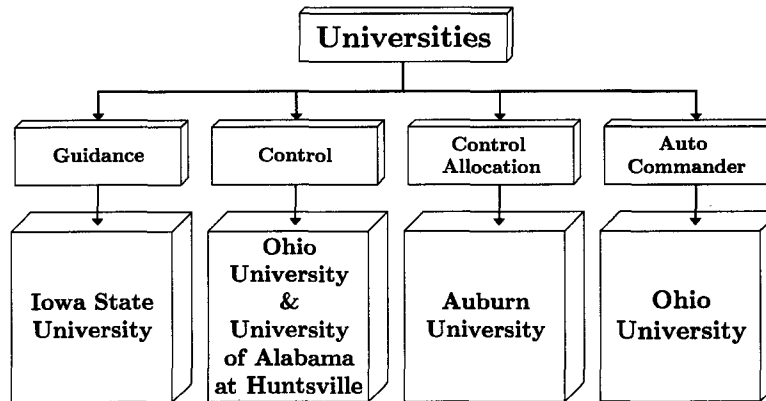
Figure 7.11   Configuration management for guidance and control
group, a division of flight mechanics and navigation
group

Ohio University in Athens, Ohio oversees the overall progress of the project at the
G&C system level. Ohio University also integrates the subsystem developed by each uni-
versity into a final product. Another important function at the system level is the con-
figuration control board (CCB) that consists of an executive management team (EMT)
that will evaluate engineering change proposals (more detail in Subsection 7.4.2). The
EMT is composed of the collaborate principal investigators (co-PIs) from each univer-
sity, a NASA contact and a configuration management librarian (CML). This group of
people makes decisions regarding any changes to the project baselines and the CML
keeps a record of these changes. A top level configuration management is depicted in
Figure 7.12.

At the subsystem level, Professor Ping Lu is the co-PI at Iowa State who oversees and
ensures the progress of the entire guidance aspect of the project. Each graduate student
is assigned a task within the guidance code development as delineated in Figure 7.13.
The configuration control board (CCB) at this lower level consists of Professor Lu who
will evaluate engineering change proposals with each flight engineer.
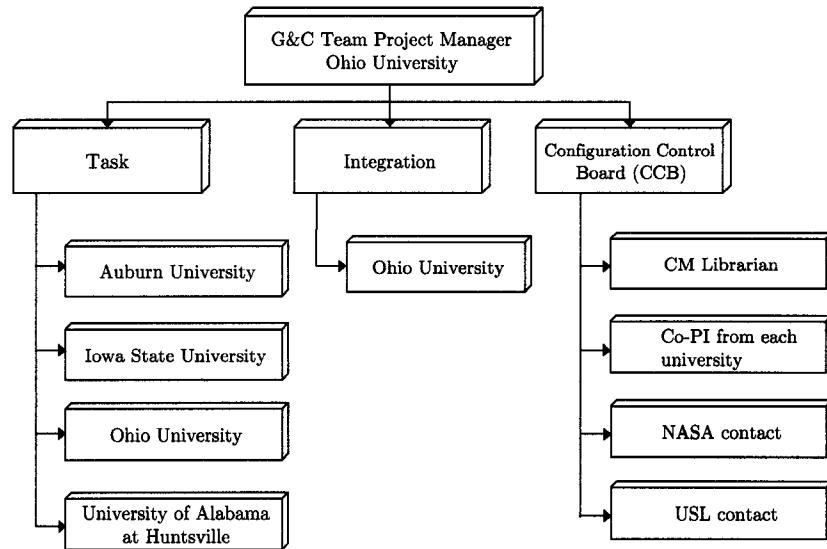
Figure 7.12   Configuration management organization for G&C Team
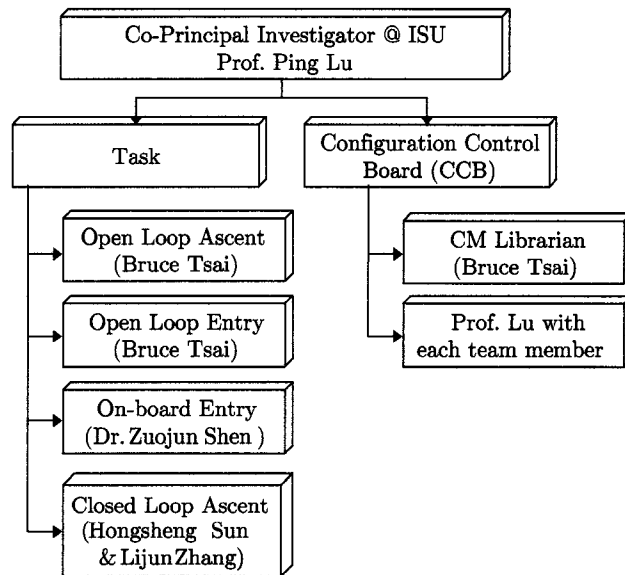
Figure 7.13   Configuration management organization at Iowa State University

Another important task of the CCB is to evaluate the project progress (milestones). If the project is behind and the milestones are not being met, it will be the responsibility of the CCB to apply the 5 steps of "Theory of Constraint (TOC)" to improve the current situation [144]. The 5 steps are as follows:

STEP 1.   IDENTIFY the system's* constraint(s).

STEP 2.   Decide how to EXPLOIT the system's* constraint(s).

STEP 3.   SUBORDINATE everything else to the above decision.

STEP 4.   ELEVATE the system's* constraint(s).

STEP 5.   If in a previous step a constraint has been broken, go back to step 1, but do not allow INERTIA to cause a system's constraint.

* The word "system" can be substituted with software or design.

A configuration management librarian (CML) is the person who keeps records of all documents related to G&C project. This may include up-to-date information from data management, configuration management, and interface management as pictured in Figure 7.14. The CML is in charge of keeping all records updated and archived periodically. The CML also releases updated information and helps prepare reports as required by higher echelons [145].
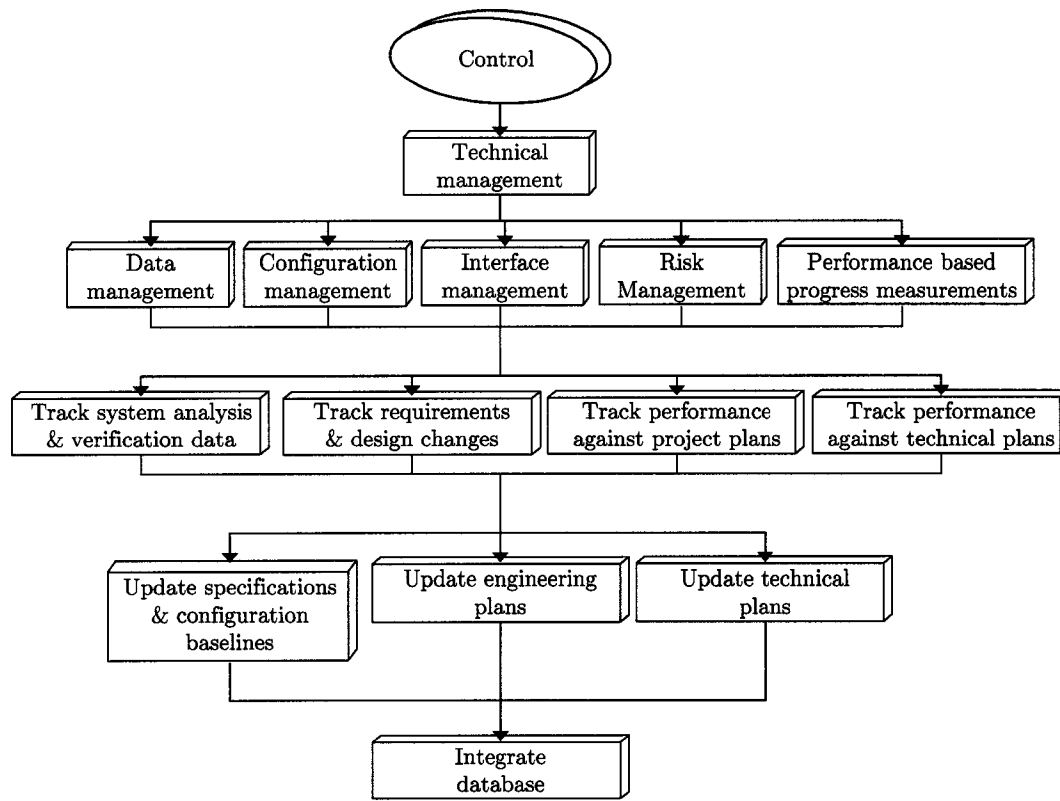
Figure 7.14 Configuration control board control process, adapted from Ref. [133]

7.4.2 Engineering Change Proposal

According to the Department of Defense (DoD), "An engineering change proposal (ECP) is the management tool used to propose a configuration change to a configuration item (CI) and its baselined performance requirements and configuration documentation" [135]. If there is a deficiency in the engineering design in hardware or software, the engineer in charge of that CI will examine the baseline to the experimental results. If the engineer feels that the baseline has to be changed, he/she will submit an ECP as exhibited in Figure E.1 in Appendix E.1 on page 290 to the configuration control board (CCB) for review. The ECP originator engineer must first obtain a ECP number from

the CML. The format for the ECP number is as follows: ISU-N830-ECP-001. ISU is for Iowa State University, N830 is the project designation, ECP is engineering change proposal, and 001 is the ECP number in sequential order. The ECP originator will then have to fill out a short description of the problem, severity of the problem, impact of the problem and proposed solution(s). After the approval or disapproval of the change, the ECP will be signed by a co-PI. This document will then be archived and recorded by the CML. Spreadsheets similar to Table 7.1 are used to record all requested ECPs, Table 7.2 is used to record all outgoing files and a similar one is used to record all incoming files [146].

Table 7.1   Internal record of requested engineering change proposals

	ECP Number	Date	To	From	Subject	Approved	Implemented
1	ISU-N830-ECP-001	Jan. 23, 2003				Yes	No
2	ISU-N830-ECP-002						
3	ISU-N830-ECP-003						
4	ISU-N830-ECP-004						
5	ISU-N830-ECP-005						

Table 7.2   Exchange of information log for outgoing files

	File Name	Date	To	From	Purpose
1	ISU-N830-OL-05-13-2003D.zip	May 13, 2003			Deliverable for QR
2	ISU-N830-ECP-005.doc	Jun. 5, 2003			Requesting ECP
3					
4					
5					

The ECPs are approved by the CCB based on knowledge of change overall impact and the change offers significant benefit. Other reasons may include: to provide new capabilities desired by the customer; enhance product support; upgrade with new technology (product improvement); and preventive maintenance. Figure 7.15 delineates the ECP approval process.
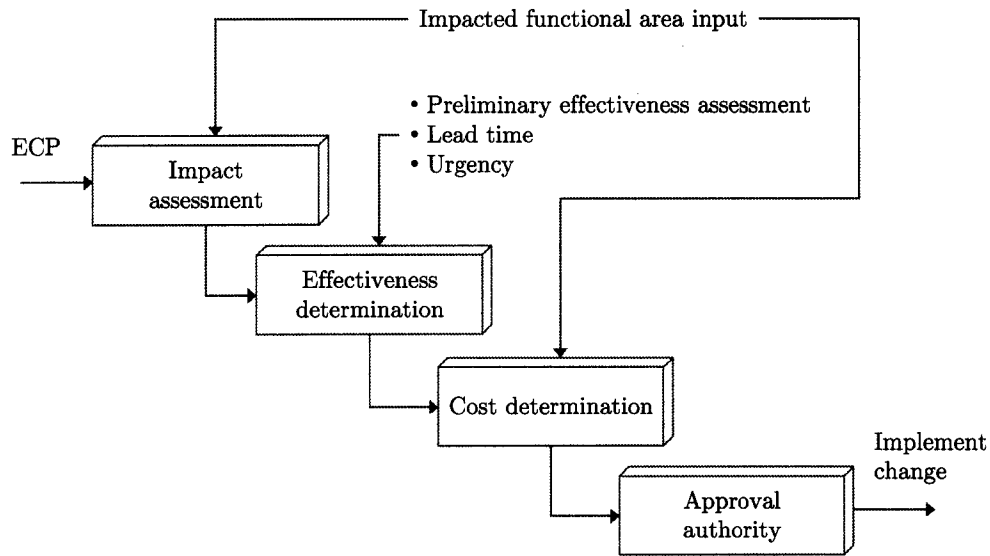
Figure 7.15 Engineering change proposal change process

7.4.3 Configuration Item

The concept of configuration item (CI) is to provide means to identify critical items (software, hardware or documentation) that are associated with the project. In other words in laymen terms, CIs are the basic units of configuration management. The designation of a system CI increases management control throughout the life cycle of the product. There are no rules of thumb to determine the optimum number of CIs for a given system, however, too many CIs are a waste of resources and too few CIs may decrease the ability to assess progress. The G&C Project uses the major component level of the work breakdown structure (please refer to Section 7.6) as the CIs.

7.4.4 Configuration Identification

Effective configuration identification is the key to successful configuration management. Configuration identification allows the establishment and maintenance of logical coherence between the product, its information and its attributes. This logical coherence is maintained throughout the life-cycle of the product and its configuration information

becomes more elaborated and unequivocal as it matures. This configuration information will eventually become part of a configuration baseline.

Configuration identification is used to select configuration items (CIs) to be managed. This process also includes item reference for identification, i.e., there is a unique identification number for each managed CI. According to MIL-HDBK-61, the configuration identification process includes [135]:

① Selecting configuration items at appropriate levels of the product structure to facilitate the documentation, control and support of the items and their documentation

② Determining the types of configuration documentation required for each CI to define its performance, functional and physical attributes, including internal and external interfaces. Configuration documentation provides the basis to develop and procure software/parts/material, fabricate and assemble parts, inspect and test items and maintain systems

③ Issuing identifiers for the CIs and the configuration documentation

④ Maintaining the configuration identification of CIs to facilitate effective logistics support of items in service

⑤ Releasing configuration documentation; and

⑥ Establishing configuration baselines for the configuration control of CIs.

All ISU software components are labeled as follows: organization identifier (ISU), its function identifier (CL for closed-loop) and a brief description (Guess285 for $i = 28.5°$ initial guess). The naming was adapted for easy identification in the integrated environment. Table 7.3 has all the current CIs developed by Iowa State. Every identified CI is a critical component in the integrated environment because a malfunctioning of any CI will halt the overall simulation [138, 146].

Table 7.3   Current ISU software components in the integrated environment

	ID #	Last Modified	Description:
1	ISU_CL_ascent.dll	May 13, 2003	CL ascent FORTRAN in Simulink file
2	ISU_CL_Guess285.dat	May 02, 2003	CL ascent guess for $i = 28.5°$
3	ISU_CL_Guess300.dat	May 02, 2003	CL ascent guess for $i = 30.0°$
4	ISU_CL_Guess516.dat	May 02, 2003	CL ascent guess for $i = 51.6°$
5	ISU_CL_INP.dat	May 02, 2003	CL ascent input parameters
6	ISU_CL_out.dat	May 15, 2003	CL ascent output file
7	ISU_Entry_AlphaTable.dat	Dec. 19, 2002	Entry Alpha reference table
8	ISU_Entry_E_KLQgain.dat	Jan. 29, 2003	Entry LQR gain table #1
9	ISU_Entry_E_KLQRgainVR.dat	Jan. 29, 2003	Entry LQR gain table #2
10	ISU_Entry_Guidance.dll	May 14, 2003	Entry FORTRAN in Simulink file
11	ISU_Entry_TmlRevE_KLQRgain.dat	Jan. 19, 2003	Entry LQR gain table #3
12	ISU_OL_ascent.dll	Feb. 06, 2003	OL ascent FORTRAN in Simulink file
13	ISU_OL_ascent_commands.dat	Jan. 07, 2003	OL ascent commands file

Configuration identifiers typically change to reflect updates (i.e., ISU-N830-ECP-001a, ISU-N830-ECP-001b, ISU-N830-ECP-001c). The conventional practice of reflecting changes is ignored in the integrated environment to avoid the need to recompile source codes. A log of when the file was last modified is used instead.

7.4.5   Configuration Status Accounting

The configuration status accounting (CSA) process is used to develop a systematic knowledge base to evaluate the implementation of the CSA. This knowledge base is also used to support all activities such as management, system engineering, and manufacturing throughout the life-cycle of the product [135].

The CSA system should include at least the following items from MIL-STD-973 entitled *Configuration Management* [131]:

① Identify the current approved configuration documentation and identification number associated with each CI.

② Record and report the status of proposed engineering changes from initiation to final approval/contractual implementation.

③ Record and report the results of configuration audits to include the status and final disposition of identified discrepancies.

④ Record and report the status of all critical and major requests for deviations and waivers which affect the configuration of a CI.

⑤ Record and report implementation status of authorized changes.

⑥ Provide the traceability of all changes from the original base-lined configuration documentation of each CI.

⑦ Report the effectivity and installation status of configuration changes of all CIs at all locations.

The current practice of CSA at Iowa State is done at the time of quarterly reviews and informal weekly meetings.

7.4.6 Configuration Verification and Audit

There are three main reasons to perform a configuration verification and audit (CVA). The first reason is to ensure that the CI meets its required configuration performance and requirements. The second reason is to ensure that a development program has achieved its performance requirements and to verify against its technical documentation with a CI product baseline. Last, to establish confidence that the CM process is performing as intended [131, 135, 147].

Contractual Provisions

Configuration Status Accounting
Tasks

1. Record the current approved configuration documentation and configuration identifiers associated with each System/CI(s).
2. Record and report the status of proposed engineering changes from initiation to final approval to contractual implementation
3. Record and report the status of all critical and major requests for deviation which affect the configuration of a system/CI(s).
4. Record and report the results of configuration audits to include the status and final disposition of identified discrepancies and action items
5. Record and report implementation status of authorized changes
6. Provide the traceability of all changes from the original released configuration documentation of each System/CI(s)
7. Report the effectivity and installation status of configuration changes to all system/CI(s) at all locations, including design, production, modification, retrofit and maintenance changes
8. Record the digital data file(s)identifiers and document representations of all revisions/versions of each document and software which has been delivered, or made accessible electronically, in support of the contract.

Approved Configuration Documentation

Change Identification, Document, Disposition

Configuration Verification

Change Verification & Validation

Action Items

Status

Configuration Information

Performance Measurement

CM Planning

Documented CM process

Communication

Automated CM System based on CM Data Model & Data Element Dictionary

Figure 7.16   Configuration status accounting activity model, courtesy Ref. [135]

Design Process

Requirements

Design requirements

Assumptions

Experience Based Knowledge

Customer & certification requirements and industry standards

Validation Plan

Matrix (initial)

Completeness & correctness checks

Matrix (final)

Validation summary report

Validation Level Determination

Validation of Assumptions
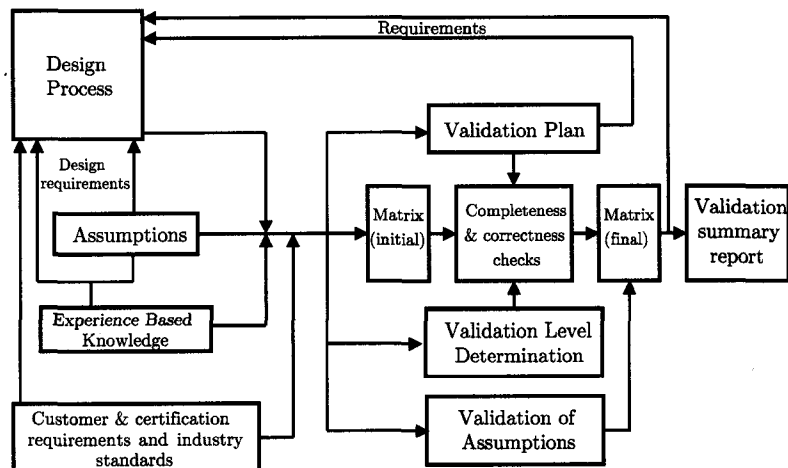
Figure 7.17   Configuration verification model

7.5 Flight Guidance System

The guidance system determines how best to get from point A to B, the navigation system tells where the vehicle currently is, and the flight control system is to assimilate guidance inputs into course changes, thus GN&C. The trajectory design analysis function at top level as shown in Figure 7.18 was determined as a part of the earliest conceptual feasibility studies. Figure 7.19 is the function used to consider different aspects of design within trajectory function. The function progressively improved through the design process. The primary responsibility of the trajectory design function is to determine the trajectory time histories in order to optimize a given performance index subject to all applicable constraints. In addition, its functions also include identifying payload performance and limitations, flight performance (nominal and abort cases) and propellant uncertainties. Since the flight guidance algorithm may be on-board or off-line, the adequacy of avionic

sensors (accuracy) and flight computer (computation time) is imperative. Parameter studies on a typical launch vehicle make trajectory design a highly interactive and iterative process [148].
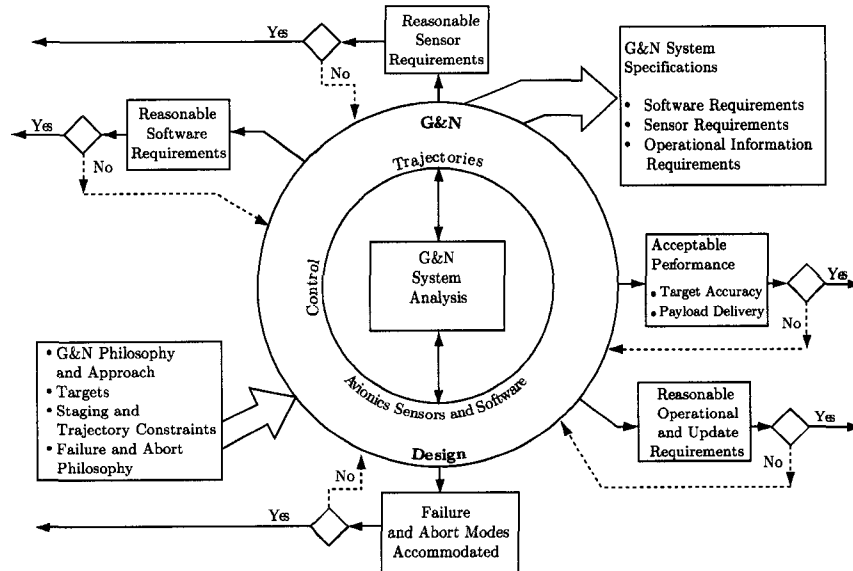
Figure 7.18   System level G&N design analysis functions, courtesy of Ref. [125]
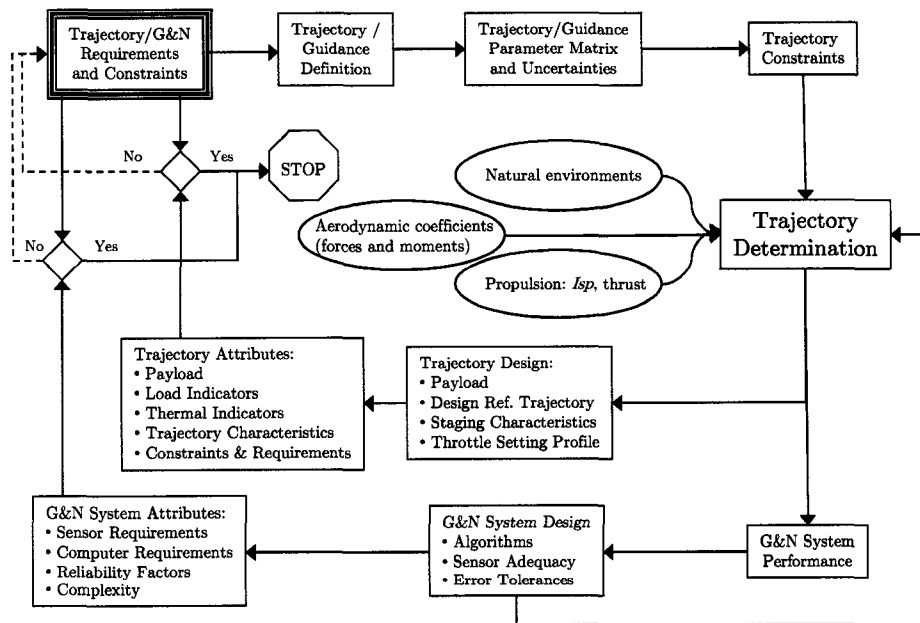
Figure 7.19   Trajectory design functions, courtesy of Ref. [125]

7.6 Work Breakdown Structure

The development of a work breakdown structure (WBS) is often thought of as the skeleton of the project. The WBS includes identification of activities, functions (subfunctions) and tasks (subtasks) necessary for the successful completion of any given project. The WBS acts as the link throughout the acquisition process. It provides the linkage between planning, budgeting, configuration management and performance measurement report. However, it is important to mention that subdividing the major tasks into smaller and smaller subtasks until the WBS is a daily "to do" list is not the intent of such exercise. Furthermore, development of WBS beyond third level of indenture may constrain the contractor's ability to manage the program resource [123, 149, 150].

The Department of Defense has its own unique definitions for WBS. According to MIL-HDBK-881 entitled *Work Breakdown Structure* [149], WBS' definitions are:

① A **product-oriented family tree** composed of hardware, software, services, data, and facilities. The family tree results from systems engineering efforts during the acquisition of a defense materiel item.

② A WBS displays and defines the product, or products, to be developed and/or produced. It **relates the elements** of work to be accomplished to each other and to the end product.

③ A WBS can be expressed down to any level of interest. However the top **three levels** are as far as any program or contract need go unless the items identified are high cost or high risk. Then, and only then, is it important to take the work breakdown structure to a lower level of definition.

Using the top down approach, the WBS usually has three levels of activities. At level one, one would identify the scope of work for the overall program. This includes how the system will be developed, implemented and delivered. At level two, one would identify the different types of activities that must be completed to meet the requirements. Level three is where one would list all the necessary activities, functions, and tasks in order to subordinate the different types of activities from level two. Within these three levels, some common elements include integration, systems engineering, training, system test and evaluation, industrial facilities, peculiar support equipment, assembly, data acquisition, and common support equipment [123, 149].

7.6.1 Program Work Breakdown Structure

A program work breakdown structure (PWBS) is often developed to be included in a RFP or an invitation for bid (IFB) for government contracts. The PWBS is developed for the purpose of budgetary, resource management, scheduling and reporting because the PWBS covers all system activities and functions [123, 146]. Table 7.4 is the PWBS for the G&C overall project and Table 7.5 is for the trajectory guidance design team. These tables show the technical objectives of the project in terms of hierarchy based and work processes involved for the completion of final product. Each element of the WBS presents a summary for evaluating technical accomplishments.

The PWBS was developed to clearly define the technical goals of a program or the work to be performed to achieve the desired end product(s). Therefore, it was developed early in the conceptual phase of the program. Due to its purpose, the PWBS must be product oriented. An iterative process was used to develop the program scope and objective, functional design criteria, proposed method, and other technical documentation throughout the development of the PWBS. Last, it is essential to develop a WBS dictionary while formulating a PWBS. The purpose of a WBS dictionary is to list and define the WBS elements in general terms.

Table 7.4   Overall program work breakdown structure for G&C Team

Level 1	Level 2	Level 3
G&C System	Autocommander	Discrete-even system model G&C reconfiguration Abort mode decision
	Control Allocation	Reconfigurable linear affine control allocation law Bang-bang control
	Control	Bang-bang control
	Guidance	Open loop ascent Open loop entry Closed-loop ascent Adaptive entry

Table 7.5   Work breakdown structure for trajectory guidance design [150]

Level 2 Activities	Level 3 Tasks
Requirement determination	1. Obtain fundamental concept 2. Top-level payload requirements and constraints 3. Obtain initial vehicle flight specifications
Preliminary performance estimates	1. Use initial inputs to obtain performance 2. Obtain acceptable solution to all parties
Detailed performance evaluations	1. Perform detail trajectory simulation 2. Sensitivity, trade-off, margin info for possible adjustments to requirements, constraints and allocations
Design reference trajectories	1. Obtain trajectories within the trajectory/system/ environment parameter space 2. Update as program matures
Verification	1. Test in high-fidelity simulation 2. Verify trajectory design over range of expected parameters and conditions
Validation	1. Obtain final validation from flight test

7.6.2 Functional Analysis

According to Blanchard and Fabrycky, "Functional analysis is the process of translating system requirements into detailed design criteria, along with the identification of specific resource requirements at the subsystem level and below [151]." Furthermore, the functional analysis ensures the following [123]:

① That all facets of system design and development, production, operation, and support are covered, that is, all significant activities within the system life cycle.

② That all elements of the system are fully recognized and defined, that is prime equipment, spare/repair parts, test and support equipment facilities, personnel, data, and software.

③ That a means is provided for relating system packaging concepts and support requirements to specific system functions, that is, satisfying requirements of good functional design.

④ That the proper sequences of activities and design relationship are established, along with critical design interfaces.

A function is referred to as a specific action required in order to accomplish an objective [150]. As an example, a series of activities that a system must execute in order to attain its desired objective. The functional analysis is accomplished using a functional flow block diagram (FBD) as depicted in Figure 7.21 to organize system requirements into "functional terms." This technique can also be applied in operations and maintenance. Figures 7.20 through 7.24 show the initial identification of all the functions that are necessary in order to accomplish the proposed system software requirement in a FBD. It includes all the necessary steps in order to accomplish the goal — find an optimal open loop trajectory with a set of given initial conditions.

1. Given initial conditions	→	2. Compute guidance commands	→	3. Check for equality & inequality constraints	→	4. Check for optimality conditions
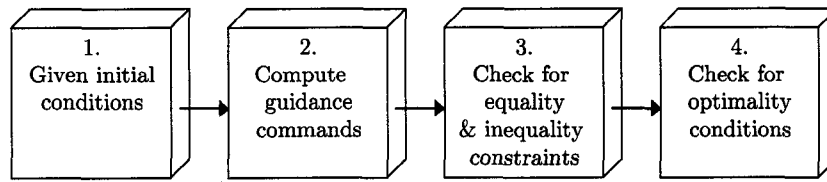
Figure 7.20 Functional block diagram for top level for open loop trajectory optimization

1. Given initial conditions	→	1.1 Set-up initial & final state values	→	1.2 Set-up initial & final control values	→	1.3 Set bounds for states & controls	→	1.4 Set bounds or values for equality & inequality constraints
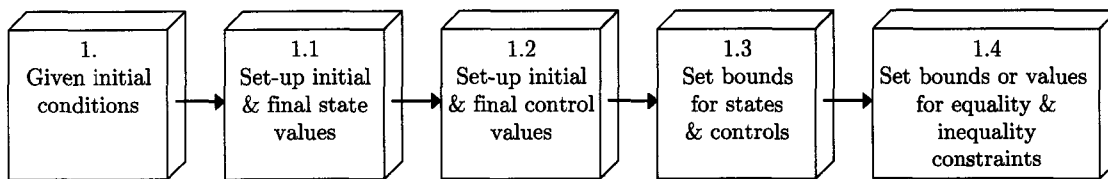
Figure 7.21 Functional block diagram for first level input task

2. Compute guidance commands	→	2.1 Compute position vector in guidance frame	→	2.2 Compute heading alignment direction	→	2.3 Compute altitude, velocity, and thrust	→	2.4 Compute flight characteristic angles
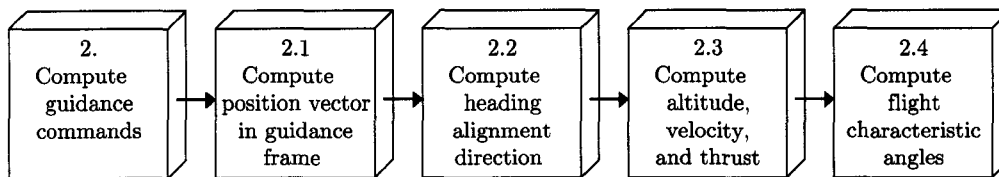
Figure 7.22 Functional block diagram for first level computing guidance commands task

3. Check for equality & inequality constraints	→	3.1 Check for all terminal conditions	→	3.2 Check for path constraints: $q\alpha, \eta, q,$ etc
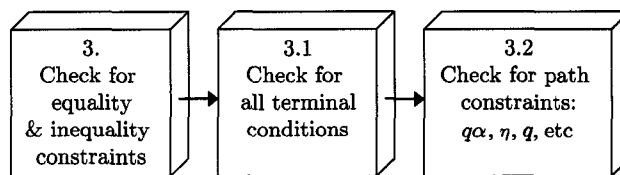
Figure 7.23 Functional block diagram for first level equality and inequality check task

```
┌─────────────┐   ┌─────────────┐   ┌─────────────┐   ┌─────────────┐   ┌─────────────┐
│     4.      │   │    4.1      │   │    4.2      │   │    4.3      │   │    4.4      │
│  Check for  │──▶│  Define     │──▶│  Define     │──▶│  Apply      │──▶│  Solve for  │
│  optimality │   │  Hamiltonian│   │  costate    │   │  stationary │   │  2PBVP      │
│  conditions │   │  equation   │   │  equations  │   │  conditions │   │  problem    │
└─────────────┘   └─────────────┘   └─────────────┘   └─────────────┘   └─────────────┘
```
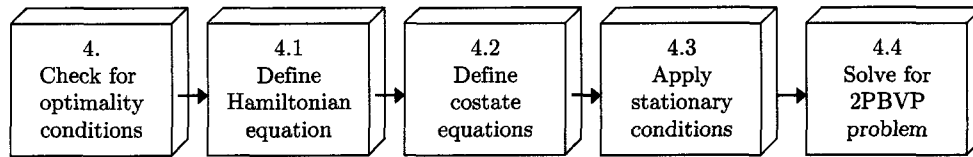
Figure 7.24   Functional block diagram for first level optimization task

7.7   Reliability Analysis

Reliability is a critical criteria to be considered in the overall design of a system. A system without adequate reliability is considered useless. According to Blanchard and Fabrycky, reliability is defined simply as the probability that a system/component will perform its mission satisfactorily when used under specified operating conditions [151]. According to MIL-STD-781D entitled *Reliability Test* [152], the purpose of reliability test is:

> The reliability test program shall be integrated with other development and production tests in accordance with the general requirements of this standard and the task(s) specified by the procuring activity. The reliability tests shall be selected and tailored according to the type of item and for each appropriate acquisition phase.

Reliability analysis typically include three parts: measurements, analysis methods, and system life-cycle. Reliability measurements include the failure rate, mean time between failure (MTBF), mean time between maintenance (MTBM), and component relationships (series and parallel network). Reliability analysis methods include "failure mode, effects, and criticality analysis" (FMECA), fault-tree analysis (FTA), critical useful life analysis, reliability growth analysis, and logic flow diagram (LFD). Reliability in the system life-cycle includes component selection, component part derating,

redundancy in design, and reliability allocation. Since the G&C Project is a software development project, only reliability analysis methods will be explored.

7.7.1 Failure Mode, Effects, and Criticality Analysis

Failure mode, effects, and criticality analysis (FMECA) is an iterative design methodology developed to identify potential failure modes for a product or process, to assess the risk associated with those failure modes, to rank the potential problems in terms of importance and to carry out corrective actions to address the most serious concerns [123, 151, 153]. According to Johnson [154], the seven steps to develop a FMECA are:

① **Construct a functional block diagram:** similar to those in Subsection 7.6.2 to show interrelationship.

② **Use diagram to identify any associated failure modes:** categorize the failure as: complete failure, partial failure, intermittent failure, etc.

③ **Identify effects of failure and assess criticality:** categorize the criticality as: catastrophic, critical, marginal or no effect.

④ **Repeat 2 and 3 for potential consequences:** may find additional failure modes.

⑤ **Identify causes and occurrence rates:** questions such as what causes the failure mode, how likely is that cause and what is the risk shall be answered.

⑥ **Calculate Risk Priority Numbers.**

⑦ **Finalize hazard assessment.**

A sample FMECA worksheet adapted for the G&C Project is illustrated in Figure E.13 in Appendix E on page 297.

7.7.2 Fault Tree Analysis

A fault-tree is defined as, "a graphic depiction or model of the rationally conceivable sequences of events within a complex system that could lead ultimately to the observed failure or potential failure." It is a systematic approach to fault prevention accomplished by postulating potential high level faults, and identifying the primary and secondary causes, down to the lowest possible causes, that could induce the high level fault.

An integral part of successful fault-tree analysis (FTA) is the selection of an orderly structure on which to base the fault-tree and the team participation. The work breakdown structure (WBS) is an ideal starting point for the team as well as for the design. Each event or activity in the WBS is subdivided into its main contributing events or activities, then the tree is subdivided again until the smallest activity that cannot be further subdivided is reached. These final events or activities are the "leaves" of the tree. Figure 7.25 is an example of FTA for the trajectory optimization code.
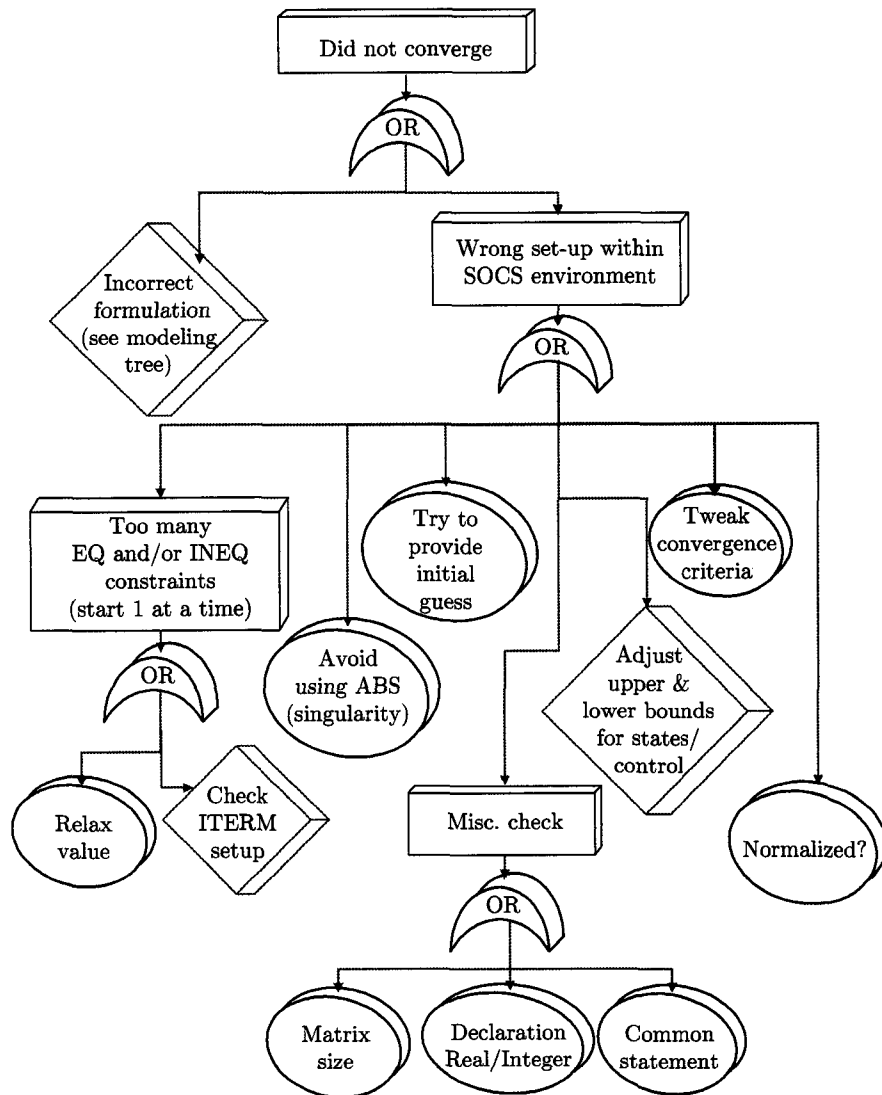
Figure 7.25   Fault-tree analysis for trajectory optimization code

7.7.3 Reliability Growth Management

As with any new product in its infancy, there exist high reliability and performance deficiencies that could not be foreseen in the design phase. Testing plans such as the "Test and Evaluation Program Plan" (please refer to Section 7.8) are developed to analyze the deficiencies and address the fixes. The reliability growth management is a subject area that focuses on program schedules, resources available, amount of testing, and the realism of the test programs to ensure the system reliability and performance characteristics. The G&C Project is not at the stage of development for reliability growth management. However, it is clear that keeping a record of component failure history is extremely important for future improvement of the system [146, 155].

7.8 Test and Evaluation Program Plan

The *Test and Evaluation Program Plan* (TEPP) [156] describes the plan for conducting a complete integration of various tests and analyzing the test results to show how the overall system will satisfy the requirements of the applicable design specification. Figure 7.26 outlines the system evaluation and corrective-action loop relationships.

7.8.1 Objectives of Test and Evaluation

According to DoD's document DI-NTDI-81284 [156], TEPP's objectives include:

① **Verification:** that the design yields the specified performance. It is vital to obtain preliminary trajectory data to verify the mathematical model used to simulate the RLV and the assumptions made in the numerical analysis.

② **Confidence:** that fabrication defects, marginal design, marginal parts, and marginal components (if any exist) are detected early in the test sequence. Because most of the technologies used in the G&C Project are new and have never been flown, it
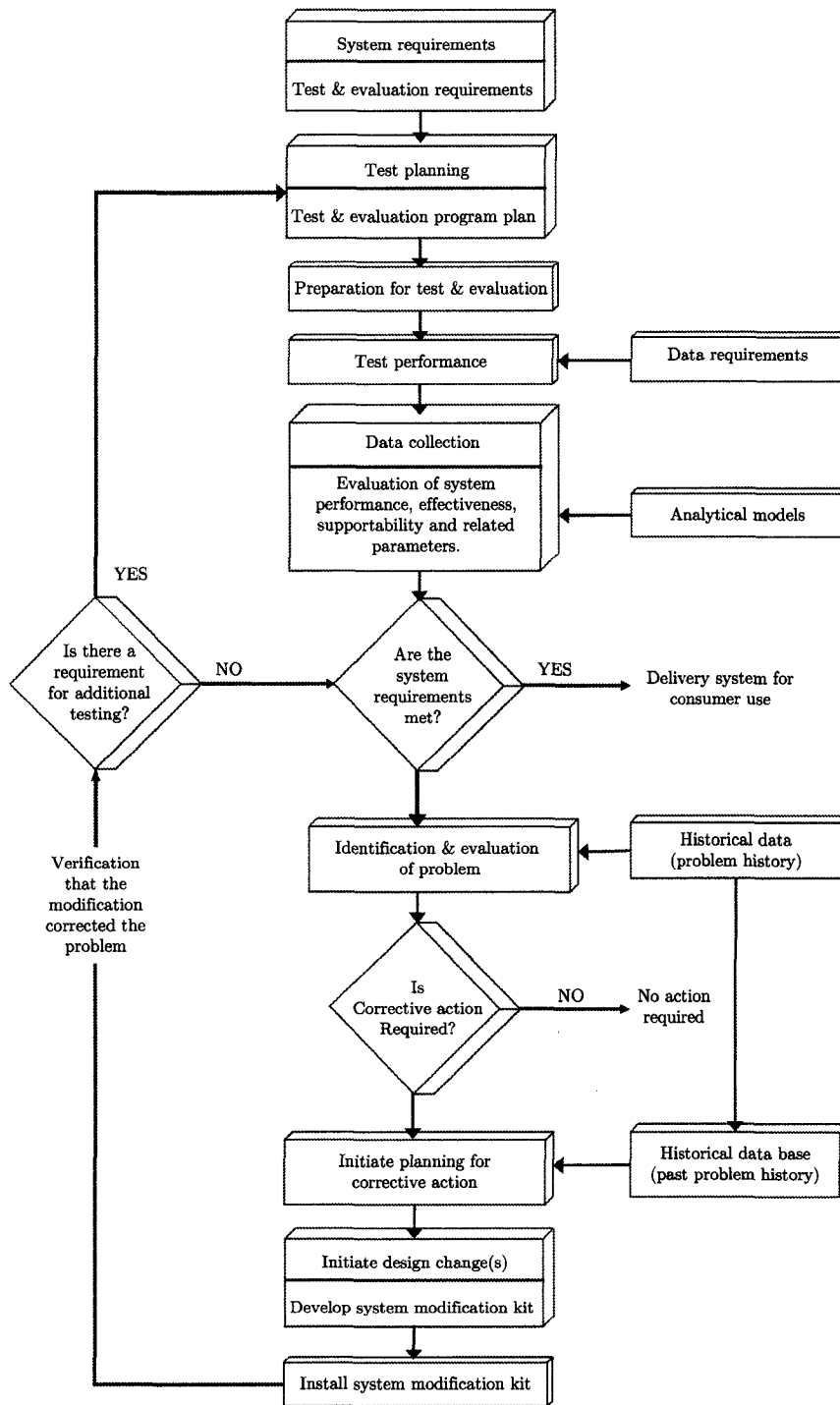
Figure 7.26   System evaluation and corrective-action loop, courtesy of Ref. [123]

is extremely important to go through rigorous testing to achieve high confidence for flight certification.

③ **Minimum risk:** that proceeding with the program's next major effort (field deployment) will not uncover significant design inadequacies.

④ **Compatibility and operational readiness verification:** that the system and all of its subsystems, as built and assembled, are compatible with each other and are capable of performing the required mission functions. All G&C developed software are constantly tested in a common interface environment developed by a NASA contractor. All software will eventually be tested at NASA testing environment.

⑤ **System characterization:** by establishing the operating signature of the performance through calibration and combination of segment, subsystem, and unit level performance data. This will be done at a later time after sufficient software test evaluations have been performed.

⑥ **Buy-off basis:** for the acceptance and delivery of the system. This can only be done at the end of the 4-year study.

7.8.2 Preparation for Test and Evaluation

It is essential to set up the test to the specifications in order to determine whether or not the system will satisfy the requirements of the applicable design expectations. According to Blanchard and Fabrycky [151], items that need to be considered include: selection of test item(s), test and evaluation procedures, test conditions, test personnel and training, and test resources. NASA has rigid procedures, test cases and scoring method to follow for evaluating the adequacy of software.

7.8.3 Failure Reporting, Analysis, and Corrective Action System

Failure reporting is essential to guarantee the reliability and the maintainability of the product are satisfied. The "failure reporting, analysis, and corrective action system" (FRACAS) was developed to collect failure data during the test and evaluation phase, and throughout the life-cycle of the product. It is then that the failure cause can be determined, and a corrective action plan can be developed. Therefore, FRACAS must answer:

① What failed?

② How it failed?

③ Why it failed?

④ How future failures can be eliminated?

In order to develop and implement the corrective action plan, it is important to consider the following [157]:

① The discipline of the report writing itself must be maintained so that an accurate description of failure occurrence and proper identification of the failed item are ensured.

② The proper assignment of priority and the decision for failure analysis must be made with the aid of cognizant design engineers and systems engineers.

③ The status of all failure analyses must be known. It is of prime importance that failure analyses be expedited as priority demands and that corrective action be implemented as soon as possible.

④ The root cause of every failure must be understood. Without this understanding, no logically derived corrective action can follow.

⑤ There must be a means of tabulating failure information for determining failure trends and the mean times between failures of system elements. There should also be a means for management visibility into the status of failure report dispositions and corrective actions.

⑥ The system must provide for high level technical management concurrence in the results of failure analysis, the soundness of corrective action, and the completion of formal actions in the correction and recurrence prevention loop.

⑦ An extremely valuable assurance mechanism is to have active Government involvement in surveillance of the adequacy of the failure reporting, analysis, and corrective action effort.

Figure 7.27 is a graphical representation of a closed-loop failure reporting and corrective actions system. A closed-loop system is an interactive process system with inputs and outputs.
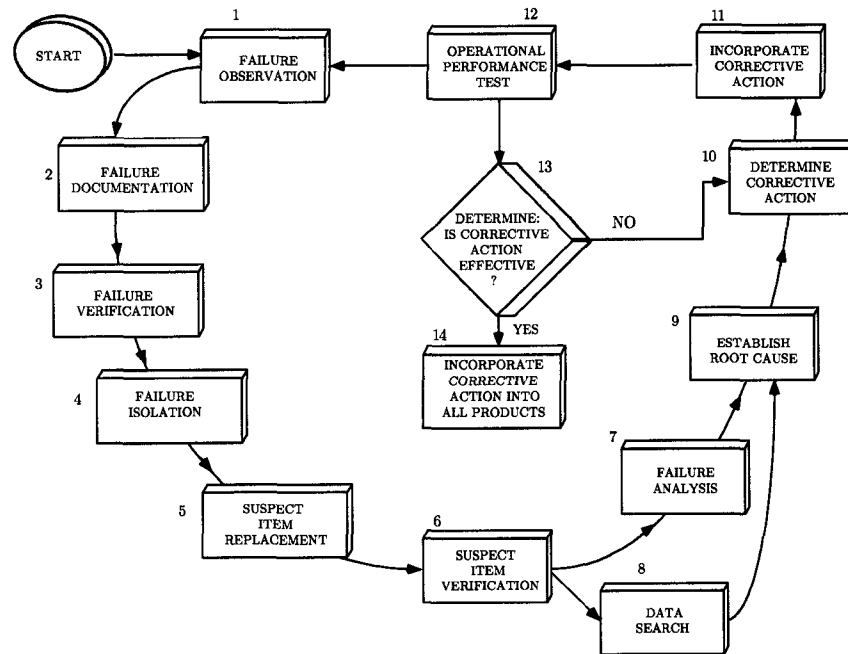
Figure 7.27   Closed-loop   failure   report   and   correction
schematic, courtesy of Ref. [157]

7.9   Continuous Acquisition and Life-Cycle Support

Continuous acquisition and life-cycle support (CALS) was originally developed by the Department of Defense (DoD) to allow better generation, management and exchange of digital data supporting the defense system. The goal of the CALS is to adapt the new technology and modernize from paper-intensive manuals to integrated mode of operation to store, exchange, distribute and manage digital documents as portrayed in Figure 7.28. A full implementation of CALS allows companies or organizations to extend the business/research endeavor to their partners working in full collaboration (concurrent engineering). Even though it was developed for the defense system, many industries have benefited from fully or partially adapting this strategy [140, 141, 158–160].
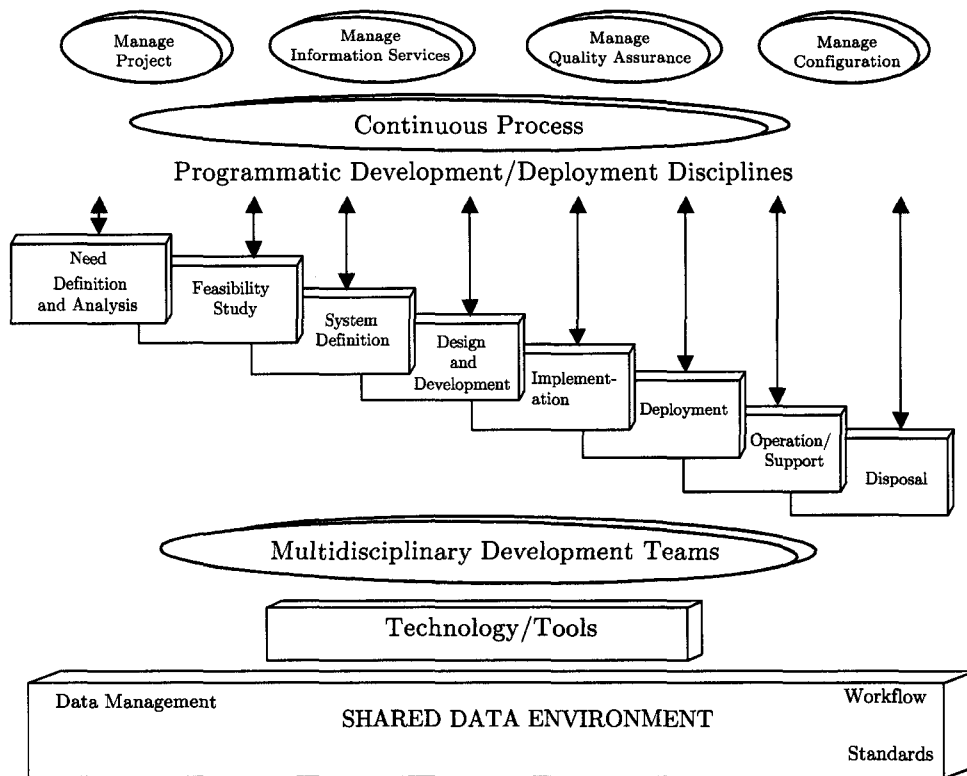
Figure 7.28 G&C project CALS environment, adapted from Ref. [159]

The key to a successful implementation of CALS is the logical structured relationship between the iterative processes of modernizing infrastructure, improving the process, and acquiring/sharing digital data within or between organizations/partners. Figure 7.29 delineates the foundation for the creation, management and use of digital data.
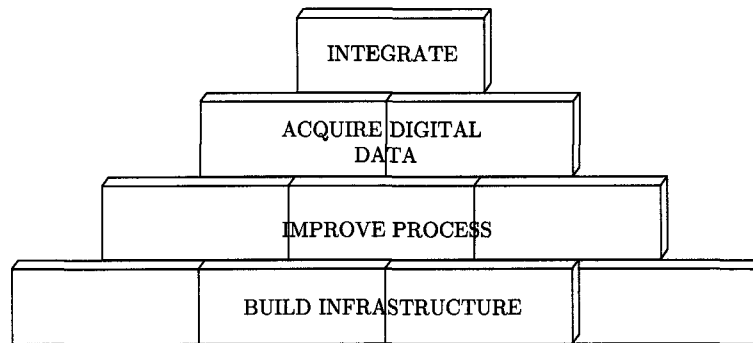
Figure 7.29 Foundation for the CALS strategy, courtesy of Ref. [158]

7.9.1 Infrastructure Modernization

The new infrastructure for digital-based development (also known as electronic data interchange, EDI) includes the use of computer software, computer hardware, and network capability (internet and/or intranet). First of all, there must be a centralized location for all digital media deposit, i.e., secured file transfer protocol (FTP) site. The responsible webmaster (i.e., CML) will file received information so that it is accessible to those who need it at any time they need it. All documentations are published in portable document file (PDF) format because it is accessible from all major operating systems (Windows^{TM}, MacOS^{TM}, UNIX^{TM}, and Linux^{TM}) and platforms (PC, Macintosh^{TM}, Cray^{TM} supercomputer, DEC Alpha^{TM}, SGI^{TM}, Sun^{TM}, and HP^{TM} workstation/server). All forms are published in Microsoft Word^{TM} format, spreadsheets in Microsoft Excel^{TM} format, and presentations are done in Microsoft PowerPoint^{TM} format. All graphics are collected in JPEG, TIFF or postscript formats while all movies are collected in MPEG format Figure 7.30 depicts a general infrastructure of such digital-based development [140, 161, 162].

Windows, Microsoft, Word, Excel, and PowerPoint are trademarks of Microsoft Corporation, MacOS and Macintosh are trademarks of Apple Computer Inc., UNIX is a trademark of American Telephone and Telegraph Bell Laboratories, Linux is a trademark of Linus Torvalds, Cray is a trademark of Tera Computer Company, DEC Alpha and HP are trademarks of Hewlett-Packard Company, SGI is a trademark of Silicon Graphic Inc., and Sun is a trademark of Sun Microsystems, Inc.
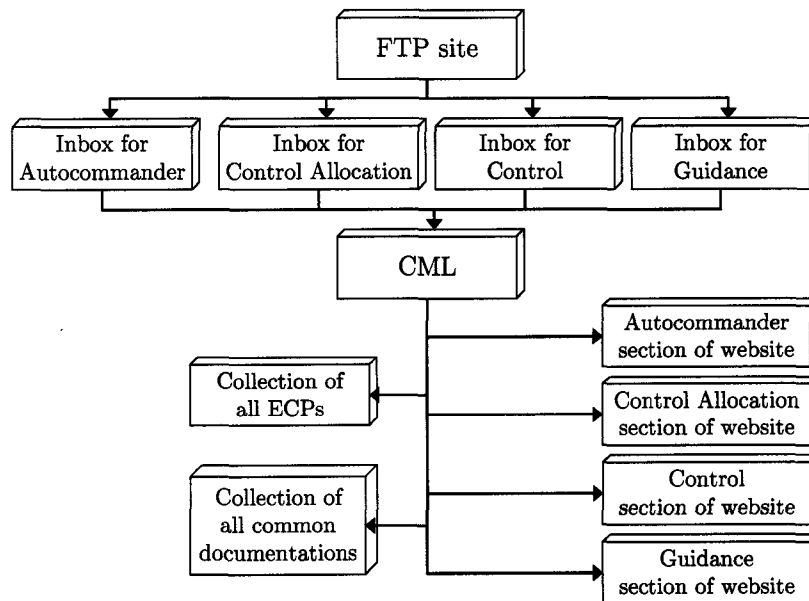
Figure 7.30   General G&C website infrastructure

7.9.2   Process Improvement

According to MIL-HDBK-59B entitled *Continuous Acquisition and Life-Cycle (CALS) Support Implementation Guide* [158], benefits of implementing the process of improvement strategies include:

① Improved information quality for acquisition, management, support planning, re-procurement and maintenance, reliability and maintainability, and equipment designs through direct coupling of design processes and integrated databases;

② Reduced acquisition and support costs through elimination of duplicative, manual, error-prone processes;

③ Reduced space, weight, and storage requirements for digital data media in comparison with paper media and microfiche;

④ Increased opportunities for automated processes such as electronic ordering, electronic contracting, and electronic payments; and

⑤ Increased responsiveness to industrial base through development of integrated design and manufacturing capabilities and industry teaming arrangements to build and support hardware based on digital product descriptions.

Process improvement will be implemented at a later time and throughout the life-cycle of the software.

7.9.3 Acquisition for Digital Data

As mentioned before, the acquisition of digital data facilitates information sharing and exchanging across all operating systems, computer platforms, and around the world. All digital pictures on the web are published in JPG/JPEG or GIF format. All digital documentation are published in PDF format. All digital movies are published in MPG/MPEG format. Web pages are written in HTML format. All of the formats mentioned above are compatible with all operating systems and computer platforms. Note: Even though all documentation is done digitally, paper copies of the documentations are still printed and archived [140, 162, 163].

7.9.4 Integration

The last item on the agenda is to integrate and combine the new infrastructure with the improvement progress and acquisition for digital data.

7.9.5 Documentation

The G&C Project is an ongoing and multi-phase design development effort. Therefore, supportability is essential to maintain and support the system throughout the development. One means of supportability is to have proper documentation. It is especially important for the project in order to pass along the valuable experiences learned to the next group since the majority of the work force are graduate students. Therefore, it is very important to write the documentations as unambiguously as possible. The Department of Defense (DoD) has many suggestions on how to write good documentation in MIL-STD-986A entitled *Data Item Descriptions* [164], MIL-HDBK-1221 entitled *Evaluation of Commercial Off-the-Shelf Manual* [165], MIL-HDBK-38754 entitled *Standard Practice for Manuals, Technical: General Style and Format Requirements* [166] and MWI 7120.4 entitled *Documentation, Preparation Programs/Projects* [167].

① **Language style:** the content of the report are written with an engineering audience in mind. The content and format shall be written in simple, direct and unambiguous structure. The use of symbols and acronyms should be standard to the discipline and explained or spelled out in the first use. Avoid using the same symbol or acronym more than once.

② **Arrangement:** the overall arrangement of the report should be consistent (especially if compiled by many people) and easy to follow. If a specific format is required by NASA or contractor, make sure it is followed carefully. The use of

"story tree" technique is recommended especially for a collaborative report. Please refer to Section E.4 starting on page 298 for examples. Unless otherwise specified, each report should include but not limited to a title page, notice of change (if applicable), table of contents, list of figures/tables (if applicable), nomenclature page, executive summary, introduction, body (may include results), conclusions,

recommendations, appendices and references in this order. Regardless if this was an individual report or a group report, the final product shall read as if it was prepared by one person.

③ **Format:** Unless otherwise specified, the base font for the report shall be Times New Roman and 12 point in size (14 point for headers). No smaller than 8 point font size shall be used. A standard letter size paper (8.5" × 11") with 1.5" margin around shall be used. Figures and tables shall be referenced by applicable paragraphs and shall be placed as close to the reference as possible.

④ **Figures & tables:** "a picture is worth a thousand words." G&C reports contain illustrations along with support text to clarify the intended use information.

⑤ **References:** all referenced documents shall be limited to those pertaining to the project. Avoid using privileged, proprietary and/or classified information. Make effort to use "traceable" references only.

CHAPTER 8 SUMMARIES AND CONCLUSIONS

My salad days,
When I was green in judgment.

— William Shakespeare [3]

NUMERICALLY establishing a benchmark of X-33's operational limitations and flight characteristics was the goal of this research. An in-depth understanding of RLV's limitations and performance features are required in order to make better strategic decision during mission planning. The formulation and optimization tools used to evaluate X-33 will also serve as the cornerstone for future RLV performance and limitations evaluations.

Optimal ascent and entry trajectories have been generated using a direct transcription method. The state and control variables are discretized to cast the optimal control problem as a nonlinear programming problem. The solution to the sparse nonlinear programming problem is then solved using sequential quadratic programming. Optimal trajectories performed included nominal ascent, ATO, TAL, RTLS, nominal entry, and entry footprint. Numerically obtained entry solutions were then compared against Loh's first and second-order analytical entry dynamic solutions.

Moreover, system analyses of the G&C project included a system management plan, configuration management plan, work breakdown structure, reliability, test & evaluation plan, and life-cycle support plan.

8.1 Ascent Analyses

An ascent trajectory performance database has been established. First, an in-depth investigation of the nominal ascent trajectories using different performance indices ($\min t_f$, $\max m_f$, $\max \mathcal{E}_f$, and $\max V_f$) have been carried out. Engine failure abort scenarios have been created at different times to gain a better understanding of vehicle's capabilities.

Different formulations (burn-coast, burn-coast-burn) have been applied to TAL and RTLS to yield physically possible optimized trajectories. The idea of intersecting a nominal entry profile instead of targeting a specific MECO point for TAL and RTLS simulations has proven to be successful. This also eliminated the need to impose those equality and inequality constraints typically associated with entry flight (to ensure that MECO condition is within the confinement of entry flight corridor).

Finally, a timeline of earliest abort time for each abort scenario (ATO, TAL and RTLS) has been determined.

8.2 Entry Analyses

An entry trajectory performance database has also been established. The nine test cases detailing different inclinations, crossrange/downrange requirements and peak heat rate constraints have been performed. A single bank reversal logic is now an inherent trademark of the entry trajectory formulation. An examination of the peak heat rate constraint has revealed that the vehicle can fly at a lower peak heat rate value than what has been specified to increase the life-cycle of TPS without significantly increasing the overall heat load.

A footprint determination for the X-33 has also been analyzed because the maximum area reachable by the vehicle is an important piece of information for mission planners. Footprint analysis showed that there is no bank reversal when trying to achieve maximum

crossrange. It also showed that the spacecraft will not be able to maintain a constant α at high speeds.

Finally, first-order and second-order analytical solutions were carried out and compared with the numerical integrated entry trajectories. While analytical solutions showed inaccuracies due to the many assumptions made, they captured the essence of entry flight trajectories. Furthermore, first and second-order solutions showed remarkably similar $r\text{-}V$ profiles for each tested σ in spite of some differences in the γ profiles. This leads to a conclusion that γ is not a dominant factor in the entry dynamics. Even though analytical solutions are not appropriate in detail design, it is adequate and useful for conceptual design when a quick solution is needed.

8.3 System Engineering Analyses

A thorough system engineering management plan has been developed and documented. Customer's needs are identified and system requirements have been clearly established. Internal and external constraints have also been identified and defined.

Configuration management that defines the management hierarchy, configuration control, engineering change proposal, status accounting, and verification has been developed. Detailed work breakdown structures at the team (G&C Team) level and component (guidance group) level have been developed to clearly define the work and responsibilities of each group.

Reliability analyses such as fault-tree analysis and failure mode, effects, and criticality analysis have been documented to help the next group of engineers get familiarized with the guidance software. These tools also help future engineers to "debug" the code. A method of failure reporting and corrective action planning have also been establish to prevent the same failure in the future.

Lastly, a life-cycle support plan has been proposed to modernize the infrastructure and acquire digital data. The implementation of such a system will certainly streamline the flow of information within the organization. System engineering is an iterative process and will undoubtedly go through many changes and fine tunings to improve the process.

8.4 Overall Conclusions

The development of optimal ascent and entry trajectories benchmark has been completed. A thorough investigation of the optimal endo-atmospheric ascent guidance parameters such as earliest abort time, engine throttle setting, flight performance characteristics and structural design limitations have established a set of benchmarks for making better trade-off decisions. Parametric analyses of the entry trajectories have been investigated and relevant parameters have been pinpointed. Finally, a system engineering management plan has also been developed to ensure that the guidance system meets the definition of vehicle design requirements and constraints.

CHAPTER 9 RECOMMENDATIONS FOR FUTURE WORK

It is difficult to say what is impossible,
for the dream of yesterday is the hope of today
and reality of tomorrow.

— *Dr. Robert Hutchings Goddard* [52]

GROUNDWORKS of X-33 flight performance characteristics and limitations have been established, it is time to perform more detailed analyses. The following are some of the further analyses that are important to the overall success of the project.

9.1 Ascent Trajectory

One of the things that can be improved in the ascent trajectory generation is the throttle profile. Notice the throttle profiles in Figure 4.14 (page 58), Figure 4.18 (page 61), and Figure 4.26 (page 68) all showed little oscillations when reaching the peak dynamic pressure constraint. Throttling up and down this frequently is not highly desired, instead, a throttle "bucket" approach is coveted as shown in Figure 9.1. The idea is to gradually reduce the throttle setting, keep it constant for a while, and then bring it back to full throttle until normal acceleration of $4g$'s is attained.
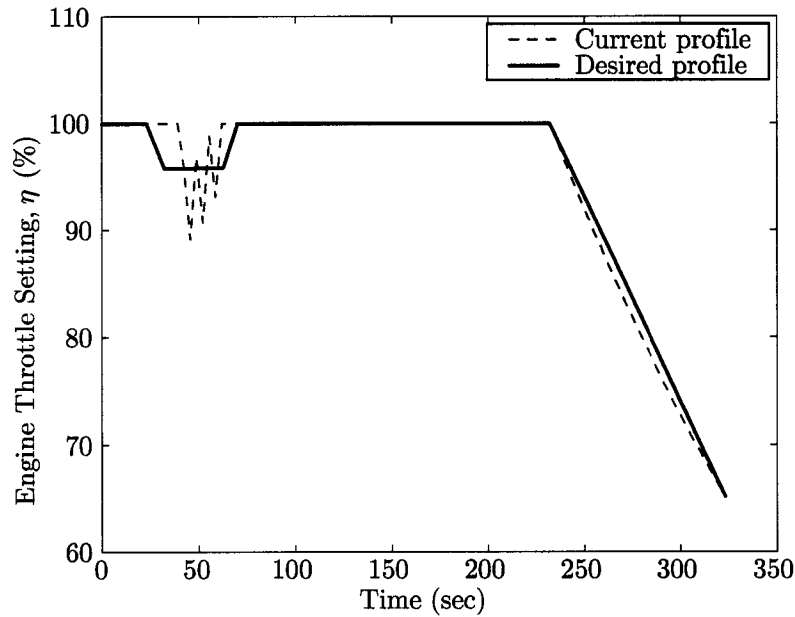
Figure 9.1   Desired vs current throttle setting profile

Another analysis of interest is to re-formulate the RTLS abort cases using only pitch and roll commands. Eliminating the yaw command will in turn obviate the undesired side-slip-angle, thus make the vehicle easier to control. The author has tried to generate an optimal RTLS trajectory using only pitch and roll commands, but it was proving to be difficult for the optimizer. While limiting a degree-of-freedom (DOF) may be easier for the optimizer, this may make it harder to satisfy all the inequality constraints. More parametric analyses must be done in order to better understand the delicate balance between DOF and convergence.

Now that the earliest abort time for each type of ascent abort case has been established as illustrated in Figure 9.2, it is important to determine the latest abort time for RTLS and TAL. The "point-of-no-return" information is also preponderant to the trajectory designer in pre-mission planning.
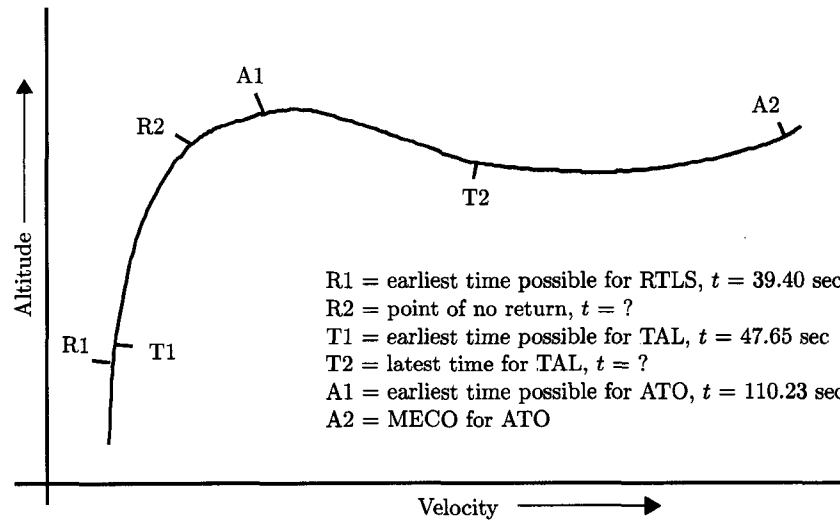
Figure 9.2   Earliest and latest abort timeline during ascent

Finally, further trade-off analyses including "worse case scenario" must be performed in order to clearly define ascent flight limitations of the vehicle. The engine failure scenario considered in this research is a "symmetrical" failure. Future analyses should also include "asymmetrical" failures. This research has also performed reduced control responsiveness (i.e., reduce from maximum pitch rate of ± 10 deg/s to ± 5 deg/s). Again, this is assuming the failure is symmetrical. Future analyses should also include asymmetrical failures (i.e., from ± 10 deg/s to $+5$ deg/s or -5 deg/s).

9.2   Entry Analysis

A single control variable in all entry analyses has proven to be a challenge. In spite of tightly imposing bank acceleration ($\ddot{\sigma}$) and bank rate ($\dot{\sigma}$), bank angle (σ) still fluctuated. Granted that the fluctuations are small and do not cause more than one bank reversal (this is inherently built into the formulation), any unnecessary fuel burned to change

σ may result in a propellant shortage when it is absolutely necessary to make course corrections later in the flight. As a result, a further investigation on how to design a bank history as delineated in Figure 9.3 will be beneficial.
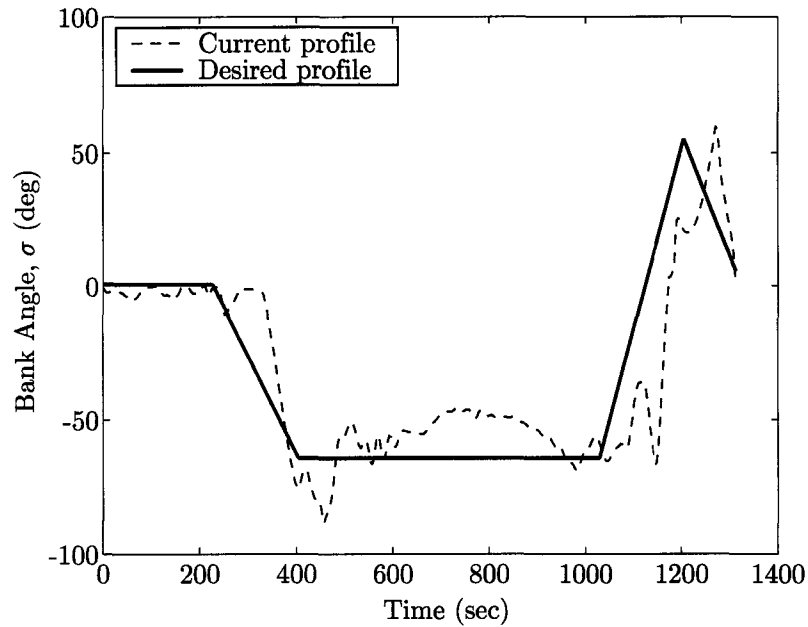
Figure 9.3   Desired vs current bank angle profile

As mentioned in the ascent analysis, further trade-off analyses including "worse case scenario" must be performed in order to clearly define the entry flight limitations of the vehicle. Abort scenarios including failure of a RCS on either side of the vehicle (i.e., vehicle can only bank in one direction) must be analyzed because this may impact the control history significantly.

9.3 System Engineering Analysis

System engineering is a perpetual process. All the analyses performed in this dissertation shall be reviewed and updated regularly. As an example, FTA should be developed for each type of G&C software. As the program progresses, analyses such as reliability growth management (Subsection 7.7.3 on page 244), FRACAS (Subsection 7.8.3 on page 247), and CALS (Section 7.9 on page 249) must be updated.

As for new analyses, trade-off study scoring process should be developed to establish guidance parameter sensitivity. Risk assessments should also be conducted to identify the risks to the project due to the new technology, margin allocation, schedule optimism and requirement stringency. In addition to the interface analysis between the four universities, interface analysis with NASA should also be performed. This analysis ensures the interfaces (internal and external) are compatible and will establish a set of overall interface requirements [127].

Another "system inspection and test" technique is the logic flow diagram (LFD). The LFD starts by identifying a symptom of failure. A step-by-step *yes/no* or *go/no-go* can then be developed to mark the steps needed to diagnose and repair the failure. The LFD technique is particularly useful when used to train new engineers to familiarize themselves with the system. The LFD technique has also been proven useful in the maintenance program [151].

The human interaction with systems is often software driven. Even though the 2nd Generation RLV will be fully autonomous, NASA personnel in the Mission Control Center will still have to interact with software. This interaction still has an important role in system operation, maintenance and support. If the human-computer interface is awkward, this promotes human errors and will slow down operations. Some analyses of interest for the Guidance Team include: use of effective displays, effective wording of error messages, use of color, appropriate graphics, and avoidance data entry [168, 169].

Last but not least, the decline in space procurement budgets instigated a new acqui-
sition essential: affordability! Therefore, lean principles and practices such as the Lean
Aerospace Initiative (LAI) launched at Massachusetts Institute of Technology (MIT) in
1993 should be incorporated into SLI. According to MIT [170],

> LAI has accelerated lean deployment through identified best prac-
> tices, shared communication, common goals, and strategic and im-
> plementation tools. LAI has also promoted collaboration, not com-
> petition, bringing down traditional barriers to improve industry
> and government teamwork.

Lean practices have been traditionally associated with manufacturing (i.e., Toyota's
Kanban manufacturing technique [171]). LAI, on the other hand, is expanding these
principles and practices from conceptual design to manufacturing. The ultimate goal
of LAI is to "strive for lean performance" and design "to deliver value" instead of just
design to deliver a product [170, 172, 173].

Toyota is a trademark of Toyota Motor Company.

APPENDIX A   DESIRABLE ATTRIBUTES FOR THE

NEXT GENERATION LAUNCH VEHICLE

Aeronautics confers beauty and grandeur,
combining art and science for those who devote themselves to it.

— *Georges Besançon* [52]

INTEGRATING a set of transportation system attributes into a conceptual design based on the importance to NASA, to its customers, how much improvement is necessary, and current space transportation characteristics is a daunting task for any system decision. The final prioritized list of highly desirable attributes for the next generation reusable launch vehicle is shown in Figure A.1. It is important to point out that lower ranked attributes do not mean less important; on the contrary, this means there is not a need for immediate improvement because they have worked very well on the current shuttles [174].

In terms of measurable criteria, system decision makers had ranked 64 design features as pictured in Figures A.2 through A.4. The (+) symbol means to increase the percentage or number of that feature while the (−) symbol means to decrease the percentage or number of that feature.

Easily Supportable
Operation and Support
Simple
Launch on Time
Resiliency
Maintainable
Benefit Growth National Product
Ease of Vehicle / System Integration
Robustness
Vehicle / System Replacement
Initial Acquisition
Personnel and Public Safety
Minimum Environmental Impact all Sites
Minimum Effect on Atmosphere
Vehicle Health Management
Flexible
Vehicle Safety
Capacity
Intact Vehicle Recovery
Social Perception
Launch on Demand
Low Cost Sensitivity to Flight Growth
Mission Success
Equipment and Facility Safety

| 0.00 | 2.00 | 4.00 | 6.00 | 8.00 | 10.00 | 12.00 | 14.00 |

Desirable level of each attribute

Figure A.1   Desired attributes of a reusable space transportation system, courtesy of Ref. [174]

# of toxic fluids (–)

System margin (+)

# of systems with BIT BITE (+)

# of confined spaces on vehicles (–)

Hours for turnaround (between launches) (–)

# of different propulsion systems (–)

# of unique stages (flight and ground) (–)

# of active ground systems required for servicing (–)

# of purges required (flight and ground) (–)

# of components with demonstrated high reliability (+)

# of potential leakage / connection sources (–)

# of active systems required to maintain a safe vehicle (–)

% of propulsion system automated (+)

# of hands on activities req'd (–)

# of active components req'd to function including flight ops (–)

Technology readiness levels (+)

# of different fluids in system (–)

Mass Fraction (+)

# of systems requiring monitoring due to hazards (–)

# of parts (different, backup, complex) (–)

0   100   200   300   400   500   600

SCORE

Figure A.2   Top 20 design features of a RLV, courtesy of Ref. [174]

# of expendables (fluid, parts, software) (−)

# of checkouts req'd (−)

pollutive or toxic materials (−)

of inspection points (−)

# of propulsion sub-systems with fault tolerance (+)

# of engines (−)

Ave. Isp on refer. trajectory (+)

# of manhours on sys between on/off cycles (LCF) or use (HCF) (−)

# of criticality 1 failure modes (−)

# of element to element interfaces requiring engineering control (−)

Hours to refurbish propulsion system (−)

# of physically difficult to access areas (−)

% of propulsion subsystems monitored to change from hazard to safe (+)

# of hours to refurbish launch site between each launch (−)

Mean time between major overhaul (−)

Amount of energy release from unplanned reaction of propellant (−)

# of manufacturing, test and operations facilites (recurring) (−)

# of ground power systems (−)

# of active engine systems req'd to function (−)

Margin, mass fraction (+)

Mean time between overhaul as % of $ cost of system (+)

Amount of real time inspection or repair (−)

0   100   200   300   400   500   600

SCORE

Figure A.3   Middle 22 design features of a RLV, courtesy of Ref. [174]

# of hazardous processes (−)
Margin, thrust level / engine chamber press (+)
Hardware cost (−)
# of major systems req'd to ferry or return to launch site (plus logistics support) (−)
# of modes or cycles (−)
# of alternate dedicated emergency abort sites req'd (−)
# of engine restarts req'd (−)
Margin, ave. specific impulse (+)
# of keepout zones (−)
# of aero-control surfaces (−)
# of cleanliness requirements (−)
Facility capitalization cost (−)
Cost of transportation / requirements (−)
% of trajectory time available for abort (+)
Amount of response time to initiate safe abort (−)
# of tools req'd (−)
Margin, % of payload (+)
# of processing steps to manufacture (−)
# of attainable destinations (+)
Ideal delta-V on ref. trajectory (−)
acres permanently affected (−)
new unique approaches (+)

0   100   200   300   400   500   600

SCORE

Figure A.4   Bottom 22 design features of a RLV, courtesy of Ref. [174]

Notice the top two most desirable attributes shown in Figure A.1 were "easily supportable" and "operation and support" and this can be easily explained by the Space Shuttle flight hardware flow diagram illustrated in Figure A.5. Note that the lower level does not necessarily mean less important. On the contrary, it indicates that the need for the current transportation system improvement is not as urgent. The concept of a single-stage-to-orbit (SSTO) or a fly-back booster design (TSTO) will improve the two most desirable attributes by almost 50% as shown in Figure A.6. The following are the acronyms used in Figures A.5 and A.6.

AF	hanger "letter" designation
ARF	Assembly and Refurbishment Facility
EOM	end of mission
ET	external tank
H/W	hardware
HMF	Hypergolic Maintenance Facility
LOV	loss of vehicle
MLP	mobile launch platform (also known as the Crawler)
OMDP*	orbiter maintenance down period
OMM	orbiter major modifications
OPF	Orbiter Processing Facility
PRA	probabilistic risk assessment
QRAS	quantitative risk assessment system
RPSF	Rotation, Processing, and Surge Facility
RSRM	reusable solid rocket motor
SCA	shuttle carrier aircraft
SRB	solid rocket booster
SRM	solid rocket motor
SSME	Space Shuttle main engine
SSV	Space Shuttle vehicle
VAB	Vehicle Assembly Building

* OMDP refers to the maintenance that was done at Boeing/Palmdale. However, that plant has been dismantled and all the work has been moved to KSC in 2002 to be more cost effective. The maintenance performed at KSC is now referred to as orbiter major modifications (OMM).
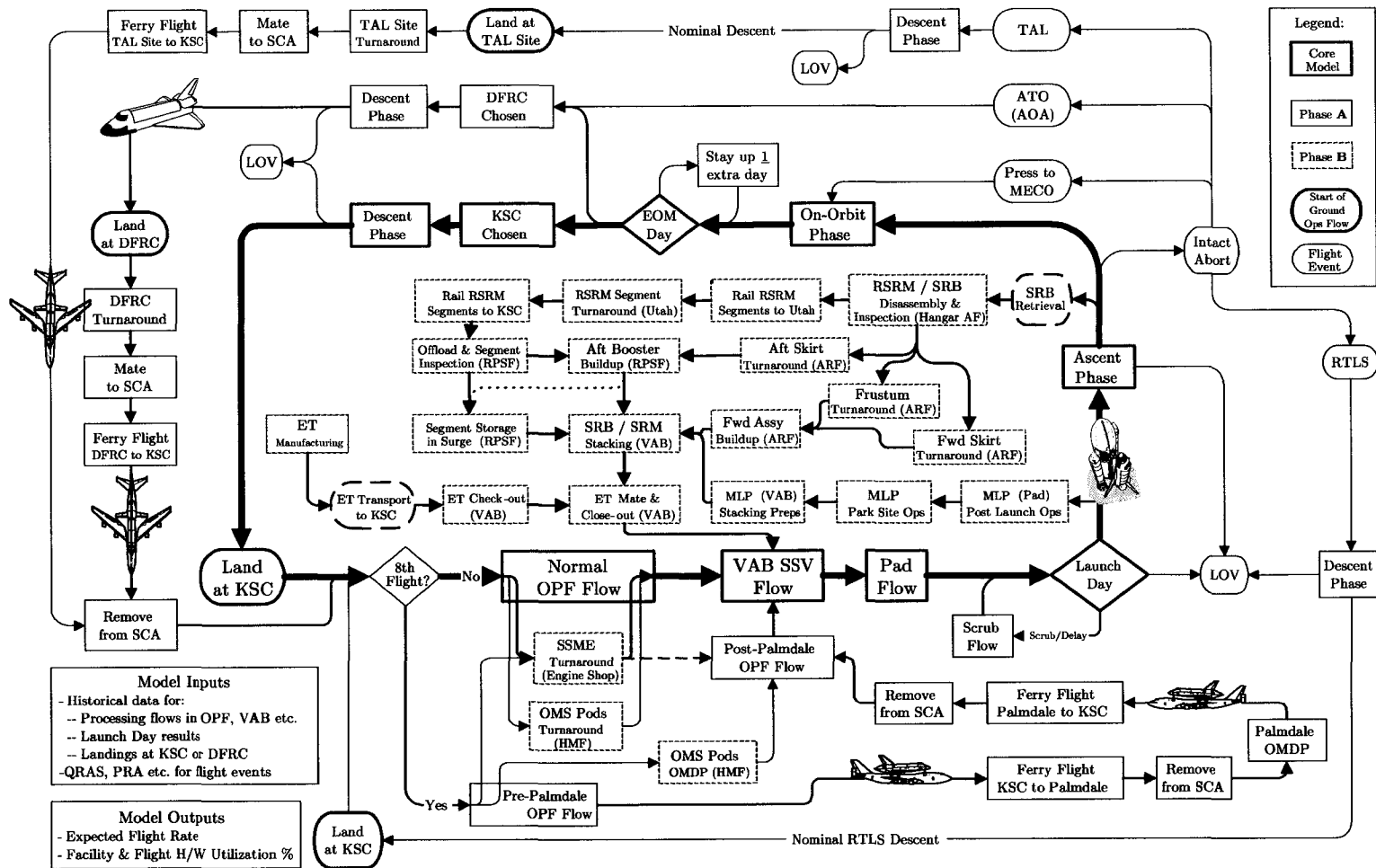
Figure A.5   Space Shuttle flight hardware flow diagram, courtesy of Ref. [175]

Figure A.6   X-33 flight hardware flow diagram, adapted from Ref. [175]

APPENDIX B   X-33 ENGINE SPECIFICATIONS

The simple expression
"Suck, Squeeze, Bang and Blow"
is the best way to remember the working cycle of the gas turbine.

— *Rolls Royce 2002 training manual* [52]

NASA awarded Rocketdyne Propulsion & Power unit of The Boeing Company[*] to bring a 30-year old idea, the linear aerospike rocket engine (LARE), and update it with 21st century technology to power the X-33 and VentureStar [176]. A major advantage of LARE is the effective nozzle area ratio of the engine increases as the air density decreases during the ascent phase; hence, there is no performance loss at higher altitudes. Furthermore, a series of combustion chambers along the unwrapped inverted bell can be controlled individually to achieve differential thrust vectoring effect, thus eliminates the need for the heavy gimbals and actuators used in traditional nozzles to control direction of flight. As a result, LARE performance is very desirable and efficient throughout the entire ascent trajectory compare to a bell-shaped nozzle engine (used in the current Space Shuttles) as rendered in Figure B.1. A detailed comparison of the two engines is outlines in Table B.1 [177, 178].

---

[*] Rocketdyne Division of Rockwell International won the bid to develop, design and build the Space Shuttle Main Engines (SSMEs) in July 1971. The Space and Defense divisions (including Rocketdyne) of Rockwell International was acquired by Boeing on December 5, 1996 [30].

Normal Bell-Nozzle
Rocket Engine

Linear Aerospike
Rocket Engine
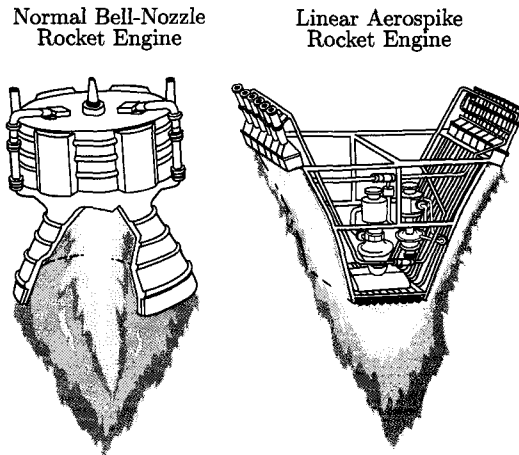
Figure B.1   Illustration of bell-shaped and linear
aerospike engine, courtesy NASA [179]

Table B.1   Space Shuttle and X-33 engines specification[‡] [177, 180]

	Space Shuttle	X-33
Propellant Combination:		
Oxidizer:	Liquid Oxygen (LOX)	Liquid Oxygen (LOX)
Fuel:	Liquid Hydrogen (LH$_2$)	Liquid Hydrogen (LH$_2$)
Engine Cycle:	Staged Combustion	Gas Generator
Average Thrust:	1,856 kN SL	907,624 N SL
	(418,130 lbf SL)	(204,420 lbf SL)
	2,275 kN vacuum	1,182 kN vacuum
	(512,410 lbf vacuum)	(266,230 lbf vacuum)
Chamber Pressure:	22,615 N/m^2	5,909 N/m^2
	(3,280 psia)	(857 psia)
Mixture Ratio:	6.0 : 1	5.5 : 1
Specific Impulse, I_{SP}:	454.4 sec vacuum	339 sec SL
Nozzle Area Ratio:	77.5 : 1	58 : 1
Engine Thrust to Weight	73.3	N/A
Throttle Range: (%)	65 to 109%	40 to 119%
Restart Capability:	No	No
Engine Size:		
Length:	14.0 ft / 8.0 ft	11.0 (max) / 7.3 ft
Width:	4.3 m / 2.4 m	3.4 (max) / 2.2 m

[‡] These are the initial X-33 prototype specifications. Some of these values have changed since the program started.

APPENDIX C   ASCENT MAIN ENGINE CUT OFF
CONDITIONS

The vehicle explodes, literally explodes, off the pad.
The simulator shakes you a little bit,
but the actual liftoff shakes your entire body and soul.

— *Mike McCulley* [52]

ENDO-ATMOSPHERIC ascent flight times indicated here refer to the time from after clearing the tower to MECO point; therefore, add the 5 seconds it took from time of ignition (TIG) to clear off the tower to each flight time.

C.1   Nominal Ascent

Please refer to Section 4.5 starting on page 52 for the discussions of nominal ascent.

Table C.1   MECO for nominal case without q and m_f constraints and
$J = \min t_f$

flight time =	320.99 sec	# of engines =	2
$x =$	6,498,478.57 m	$i =$	51.60°
$y =$	54,354.32 m	yaw $(\psi) =$	5.74°
$z =$	917,835.78 m	pitch $(\theta) =$	−121.10°
$V_x =$	−1,089.38 m/s	roll $(\phi) =$	−2.68°
$V_y =$	−64.50 m/s	mass $(m) =$	38,476.15 kg
$V_z =$	7,716.88 m/s	throttle setting $(\eta) =$	65.50%
range traveled =	903.72 km	$\gamma_f^* =$	0.00°
$r_f^* =$	185.07 km	$V_f^* =$	7,793.66 m/s

Table C.2 MECO for nominal case with q but no m_f constraints and
$J = \min t_f$

flight time =	323.14 sec	# of engines =	2
$x =$	6,499,415.22 m	$i =$	51.60°
$y =$	54,583.82 m	yaw $(\psi) =$	5.66°
$z =$	911,165.71 m	pitch $(\theta) =$	−121.00°
$V_x =$	−1,081.45 m/s	roll $(\phi) =$	−3.08°
$V_y =$	−64.64 m/s	mass $(m) =$	38,298.15 kg
$V_z =$	7,717.99 m/s	throttle setting $(\eta) =$	65.20%
range traveled =	898.70 km	$\gamma_f^* =$	0.00°
$r_f^* =$	185.07 km	$V_f^* =$	7,793.66 m/s

Table C.3 MECO for nominal case with q but no m_f constraints and
$J = \min t_f$

flight time =	320.24 sec	# of engines =	2
$x =$	6,497,470.08 m	$i =$	28.50°
$y =$	−668.36 m	yaw $(\psi) =$	0.42°
$z =$	92,6543.45 m	pitch $(\theta) =$	−121.83°
$V_x =$	−1,100.24 m/s	roll $(\phi) =$	−0.56°
$V_y =$	−38.70 m/s	mass $(m) =$	38,828.59 kg
$V_z =$	7,715.51 m/s	throttle setting $(\eta) =$	66.10%
range traveled =	902.29 km	$\gamma_f^* =$	0.00°
$r_f^* =$	185.07 km	$V_f^* =$	7,793.66 m/s

Table C.4 MECO for nominal case with q and m_f constraints and
$J = \max \mathscr{E}_f$

flight time =	326.99 sec	# of engines =	2
$x =$	6,461,136.33 m	$i =$	51.60°
$y =$	55,553.93 m	yaw $(\psi) =$	5.95°
$z =$	954,520.76 m	pitch $(\theta) =$	−119.34°
$V_x =$	−1,180.31 m/s	roll $(\phi) =$	−0.02°
$V_y =$	−51.79 m/s	mass $(m) =$	37,600.00 kg
$V_z =$	7,792.48 m/s	throttle setting $(\eta) =$	64.10%
range traveled =	946.26 km	$\gamma_f^* =$	0.00°
$r_f^* =$	158.12 km	$V_f^* =$	8,079.33 m/s

Table C.5   MECO for nominal case with q constraint and J = max m_f

flight time =	403.86 sec	# of engines =	2
$x =$	6,424,921.22 m	$i =$	51.60°
$y =$	56,314.15 m	yaw $(\psi) =$	7.27°
$z =$	1,338,961.05 m	pitch $(\theta) =$	−113.19°
$V_x =$	−1,589.33 m/s	roll $(\phi) =$	6.89°
$V_y =$	−76.08 m/s	mass $(m) =$	39146.88 kg
$V_z =$	7,629.50 m/s	throttle setting $(\eta) =$	64.00%
range traveled =	1,320.01 km	$\gamma_f^* =$	0.00°
$r_f^* =$	185.07 km	$V_f^* =$	7,793.66 m/s

Table C.6   MECO for nominal case with q and m_f constraints and J = max V_f

flight time =	411.16 sec	# of engines =	2
$x =$	6,409,216.56 m	$i =$	51.60°
$y =$	56,867.07 m	yaw $(\psi) =$	6.85°
$z =$	1,412,200.38 m	pitch $(\theta) =$	−113.69°
$V_x =$	−1,750.32 m/s	roll $(\phi) =$	5.28°
$V_y =$	−82.07 m/s	mass $(m) =$	37,600.00 kg
$V_z =$	7,947.07 m/s	throttle setting $(\eta) =$	64.00%
range traveled =	1,392.90 km	$\gamma_f^* =$	0.00°
$r_f^* =$	185.07 km	$V_f^* =$	8,137.95 m/s

Table C.7   MECO for nominal case with q and m_f constraints and J = min t_f

flight time =	326.99 sec	# of engines =	2
$x =$	6,501,931.42 m	$i =$	51.60°
$y =$	54,927.24 m	yaw $(\psi) =$	5.81°
$z =$	893,012.53 m	pitch $(\theta) =$	−119.94°
$V_x =$	−1,059.89 m/s	roll $(\phi) =$	−0.27°
$V_y =$	−64.68 m/s	mass $(m) =$	37,600.00 kg
$V_z =$	7,720.98 m/s	throttle setting $(\eta) =$	64.00%
range traveled =	882.22 km	$\gamma_f^* =$	0.00°
$r_f^* =$	185.07 km	$V_f^* =$	7,793.66 m/s

C.2 Abort to Orbit

Please refer to Section 4.6 starting on page 72 for the discussions of ATO.

Table C.8   MECO for ATO case and $J = \min t_f$

flight time =	511.67 sec	# of engines =	1
$x =$	6,365,297.22 m	$i =$	51.60°
$y =$	104,695.81 m	yaw (ψ) =	3.35°
$z =$	1,596,129.91 m	pitch (θ) =	−110.50°
$V_x =$	−1,969.96 m/s	roll (ϕ) =	0.00°
$V_y =$	82.63 m/s	mass (m) =	36,665.65 kg
$V_z =$	7,850.69 m/s	throttle setting (η) =	100.00%
range traveled =	1,511.57 km	$\gamma_f^* =$	0.00°
$r_f^* =$	185.07 km	$V_f^* =$	7,793.66 m/s

C.3 Transoceanic Abort Landing

Please refer to Section 4.7 starting on page 80 for the discussions of TAL. All TAL cases have $J = \min t_f$.

Table C.9   MECO for TAL case inbound Banjul with BCB

flight time =	738.67 sec	# of engines =	1
$x =$	5,843,257.46 m	$i =$	51.60°
$y =$	1,712,706.94 m	yaw (ψ) =	88.88°
$z =$	2,141,537.47 m	pitch (θ) =	−50.53°
$V_x =$	−3,121.19 m/s	roll (ϕ) =	N/A
$V_y =$	5,011.53 m/s	mass (m) =	37,600.00 kg
$V_z =$	4,165.20 m/s	throttle setting (η) =	60.00%
range traveled =	2,781.36 km	range-to-go =	3,997.53 km
$r_f^* =$	76.57 km	$V_f^* =$	7,225.39 m/s
$\gamma_f^* =$	−0.46°	—	—

Table C.10   MECO for TAL case inbound Banjul with BC

flight time =	707.22 sec	# of engines =	1
$x =$	5,911,090.01 m	$i =$	51.60°
$y =$	1,630,875.39 m	yaw $(\psi) =$	14.76°
$z =$	2,018,058.45 m	pitch $(\theta) =$	−88.37°
$V_x =$	−2,988.26 m/s	roll $(\phi) =$	N/A
$V_y =$	4,272.22 m/s	mass $(m) =$	37,600.00 kg
$V_z =$	5,099.50 m/s	throttle setting $(\eta) =$	0.00%
range traveled =	2,621.58 km	range-to-go =	4,152.73 km
$r_f^* =$	77.35 km	$V_f^* =$	7,292.63 m/s
$\gamma_f^* =$	−0.49°	—	—

Table C.11   MECO for TAL case inbound Ben Guerir with BCB

flight time =	744.62 sec	# of engines =	1
$x =$	5,824,592.72 m	$i =$	51.60°
$y =$	996,307.66 m	yaw $(\psi) =$	−10.00°
$z =$	2,597,296.66 m	pitch $(\theta) =$	−93.87°
$V_x =$	−3,169.57 m/s	roll $(\phi) =$	N/A
$V_y =$	2,169.85 m/s	mass $(m) =$	37,600.00 kg
$V_z =$	6,130.71 m/s	throttle setting $(\eta) =$	60.00%
range traveled =	2,828.07 km	range-to-go =	4,018.52 km
$r_f^* =$	76.66 km	$V_f^* =$	7,234.64 m/s
$\gamma_f^* =$	−0.46°	—	—

Table C.12   MECO for TAL case inbound Ben Guerir with BC

flight time =	712.77 sec	# of engines =	1
$x =$	5,892,921.71 m	$i =$	51.60°
$y =$	1,058,008.63 m	yaw $(\psi) =$	12.66°
$z =$	2,414,378.59 m	pitch $(\theta) =$	−90.15°
$V_x =$	−3,040.23 m/s	roll $(\phi) =$	N/A
$V_y =$	2,624.50 m/s	mass $(m) =$	37,600.00 kg
$V_z =$	6,100.24m/s	throttle setting $(\eta) =$	0.00%
range traveled =	2,667.62 km	range-to-go =	3,738.79 km
$r_f^* =$	77.50 km	$V_f^* =$	7,303.69 m/s
$\gamma_f^* =$	−0.40°	—	—

Table C.13 MECO for TAL case inbound Lajes with BCB

flight time =	556.61 sec	# of engines =	1
$x =$	6,288,348.21 m	$i =$	51.60°
$y =$	361,636.62 m	yaw $(\psi) =$	−0.91°
$z =$	1,403,482.63 m	pitch $(\theta) =$	−115.15°
$V_x =$	−1,610.67 m/s	roll $(\phi) =$	N/A
$V_y =$	901.86 m/s	mass $(m) =$	37,600.00 kg
$V_z =$	6,783.63 m/s	throttle setting $(\eta) =$	60.00%
range traveled =	1,444.51 km	range-to-go =	3,579.87 km
$r_f^* =$	75.07 km	$V_f^* =$	7,030.31 m/s
$\gamma_f^* =$	−0.36°	—	—

Table C.14 MECO for TAL case inbound Lajes with BC

flight time =	540.61 sec	# of engines =	1
$x =$	6,308,616.62 m	$i =$	51.60°
$y =$	338,198.65 m	yaw $(\psi) =$	−4.82°
$z =$	1,316,911.50 m	pitch $(\theta) =$	−122.46°
$V_x =$	−1,524.33 m/s	roll $(\phi) =$	N/A
$V_y =$	845.47 m/s	mass $(m) =$	37,600.00 kg
$V_z =$	6,856.43 m/s	throttle setting $(\eta) =$	0.00%
range traveled =	1,352.36 km	range-to-go =	3,670.47 km
$r_f^* =$	75.34 km	$V_f^* =$	7,074.53 m/s
$\gamma_f^* =$	−0.38°	—	—

Table C.15 MECO for TAL case inbound Lajes in 1 stage

flight time =	530.81 sec	# of engines =	1
$x =$	6,314,892.57 m	$i =$	51.60°
$y =$	310,009.95 m	yaw $(\psi) =$	31.31°
$z =$	1,294,043.37 m	pitch $(\theta) =$	−116.44°
$V_x =$	−1,494.15 m/s	roll $(\phi) =$	N/A
$V_y =$	638.27 m/s	mass $(m) =$	37,600.00 kg
$V_z =$	6,900.61 m/s	throttle setting $(\eta) =$	100.00%
range traveled =	1,321.48 km	range-to-go =	3,738.79 km
$r_f^* =$	75.55 km	$V_f^* =$	7,107.14 m/s
$\gamma_f^* =$	−0.40°	—	—

Table C.16   MECO for TAL case inbound Morón with BCB

flight time =	750.92 sec	# of engines =	1
$x =$	5,807,270.70 m	$i =$	51.60°
$y =$	877,258.24 m	yaw $(\psi) =$	65.09°
$z =$	2,677,744.76 m	pitch $(\theta) =$	−75.13°
$V_x =$	−3,209.65 m/s	roll $(\phi) =$	N/A
$V_y =$	1,922.37 m/s	mass $(m) =$	37,600.00 kg
$V_z =$	6,190.72 m/s	throttle setting $(\eta) =$	60.00%
range traveled =	2,869.04 km	range-to-go =	4,015.75 km
$r_f^* =$	76.65 km	$V_f^* =$	7,233.42 m/s
$\gamma_f^* =$	−0.46°	—	—

Table C.17   MECO for TAL case inbound Morón with BC

flight time =	742.99 sec	# of engines =	1
$x =$	5,811,246.62 m	$i =$	51.60°
$y =$	493,263.41 m	yaw $(\psi) =$	8.51°
$z =$	2,766,210.75 m	pitch $(\theta) =$	−90.89°
$V_x =$	−3,203.92 m/s	roll $(\phi) =$	N/A
$V_y =$	848.37 m/s	mass $(m) =$	37,600.00 kg
$V_z =$	6,441.73 m/s	throttle setting $(\eta) =$	0.00%
range traveled =	2,867.84 km	range-to-go =	4,033.86 km
$r_f^* =$	76.74 km	$V_f^* =$	7,241.37 m/s
$\gamma_f^* =$	−0.47°	—	—

Table C.18   MECO for TAL case inbound Zaragoza with BCB

flight time =	805.95 sec	# of engines =	1
$x =$	5,635,125.85 m	$i =$	51.60°
$y =$	744,176.33 m	yaw $(\psi) =$	22.93°
$z =$	3,057,686.42 m	pitch $(\theta) =$	−80.59°
$V_x =$	−3,548.73 m/s	roll $(\phi) =$	N/A
$V_y =$	1,329.66 m/s	mass $(m) =$	37,600.00 kg
$V_z =$	6,101.61 m/s	throttle setting $(\eta) =$	60.00%
range traveled =	3,239.17 km	range-to-go =	3,902.10 km
$r_f^* =$	76.16 km	$V_f^* =$	7,182.69 m/s
$\gamma_f^* =$	−0.43°	—	—

Table C.19   MECO for TAL case inbound Zaragoza with BC

flight time =	775.57 sec	# of engines =	1
$x =$	5,704,303.86 m	$i =$	51.60°
$y =$	439,826.59 m	yaw $(\psi) =$	6.24°
$z =$	2,988,789.93 m	pitch $(\theta) =$	−91.89°
$V_x =$	−3,438.65 m/s	roll $(\phi) =$	N/A
$V_y =$	664.06 m/s	mass $(m) =$	37,600.00 kg
$V_z =$	6,338.15 m/s	throttle setting $(\eta) =$	0.00%
range traveled =	3,103.00 km	range-to-go =	4,033.86 km
$r_f^* =$	76.74 km	$V_f^* =$	7,241.37 m/s
$\gamma_f^* =$	−0.47°	—	—

C.4   Return to Launch Site

Please refer to Section 4.8 starting on page 96 for the discussions of RTLS. All RTLS cases have $J = \min t_f$.

Table C.20   MECO for RTLS case with 2 phases

flight time =	518.29 sec	# of engines =	1
$x =$	6,414,427.70 m	$i =$	51.60°
$y =$	90,039.73 m	yaw $(\psi) =$	−10.00°
$z =$	381,747.32 m	pitch $(\theta) =$	69.38°
$V_x =$	150.12 m/s	roll $(\phi) =$	0.00
$V_y =$	−521.79 m/s	mass $(m) =$	37,600.00 kg
$V_z =$	−2,395.21 m/s	throttle setting $(\eta) =$	100.00%
range traveled =	670.95 km	range-to-go =	444 km
$r_f^* =$	53.94 km	$V_f^* =$	2,463.103m/s
$\gamma_f^* =$	−1.86°	—	—

Table C.21   MECO for RTLS case with 3 phases

flight time =	567.61 sec	# of engines =	1
$x =$	6,415,621.01 m	$i =$	51.60°
$y =$	146,595.31 m	yaw $(\psi) =$	−9.78°
$z =$	472,778.25 m	pitch $(\theta) =$	73.95°
$V_x =$	279.49 m/s	roll $(\phi) =$	−40.79
$V_y =$	−823.44 m/s	mass $(m) =$	37,600.00 kg
$V_z =$	−2,668.95 m/s	throttle setting $(\eta) =$	100.00%
range traveled =	727.52 km	range-to-go =	444 km
$r_f^* =$	56.34 km	$V_f^* =$	2,806.64 m/s
$\gamma_f^* =$	1.08°	—	—

APPENDIX D   ENTRY TERMINAL AREA ENERGY

MANAGEMENT CONDITIONS

[Entry vehicles are] near perfect,
all they lack is the ability to forgive.

— Richard Collins [52]

ENTRY analyses of EG13-21 cases are discussed in Chapter 5 starting on page 107. Tables D.1 through D.9 are the conditions at the end of entry flight at TAEM. The range traveled here refers to a combination of downrange and crossrange.

Table D.1   TAEM conditions for EG13 with $J = \min \int \dot{Q} \, dt$

flight time =	1,161.583 sec	$i =$	51.60°
$r_c =$	6,408,615.000 m	$\gamma =$	−7.360°
$\Theta =$	−81.069 deg	$\Psi =$	109.635°
$\Phi =$	28.611 deg	$\alpha =$	15.003°
$V_r =$	908.150 m/s	$\beta =$	0.167°
range traveled =	6,592.95 km	—	—

Table D.2   TAEM conditions for EG14 with $J = \min \int \dot{Q} \, dt$

flight time =	1,203.430 sec	$i =$	51.60°
$r_c =$	6,408,615.000 m	$\gamma =$	−7.360°
$\Theta =$	−80.890 deg	$\Psi =$	39.212°
$\Phi =$	28.063 deg	$\alpha =$	15.003°
$V_r =$	908.150 m/s	$\beta =$	4.654°
range traveled =	6,592.48 km	—	—

Table D.3   TAEM conditions for EG15 with $J = \min \int \dot{Q} \, dt$

flight time =	1,222.711 sec	$i =$	51.60°
$r_c =$	6,408,615.000 m	$\gamma =$	−7.360°
$\Theta =$	−80.980 deg	$\Psi =$	53.276°
$\Phi =$	28.145 deg	$\alpha =$	15.003°
$V_r =$	908.150 m/s	$\beta =$	−5.000°
range traveled =	6,690.57 km	—	—

Table D.4   TAEM conditions for EG16 with $J = \min \int \dot{Q} \, dt$

flight time =	1,390.780 sec	$i =$	51.60°
$r_c =$	6,407,566.000 m	$\gamma =$	−7.360°
$\Theta =$	−81.046 deg	$\Psi =$	114.794°
$\Phi =$	28.660 deg	$\alpha =$	15.329°
$V_r =$	916.860 m/s	$\beta =$	4.993°
range traveled =	8,248.37 km	—	—

Table D.5   TAEM conditions for EG17 with $J = \min \int \dot{Q} \, dt$

flight time =	1,418.623 sec	$i =$	51.60°
$r_c =$	6,407,566.000 m	$\gamma =$	−7.360°
$\Theta =$	−80.925 deg	$\Psi =$	44.676°
$\Phi =$	28.091 deg	$\alpha =$	15.329°
$V_r =$	916.860 m/s	$\beta =$	4.949°
range traveled =	8,223.75 km	—	—

Table D.6 TAEM conditions for EG18 with $J = \min \int \dot{Q} \, dt$

flight time =	1,433.944 sec	$i =$	51.60°
$r_c =$	6,407,566.000 m	$\gamma =$	−7.360°
$\Theta =$	−80.953 deg	$\Psi =$	47.116°
$\Phi =$	28.117 deg	$\alpha =$	15.329°
$V_r =$	916.860 m/s	$\beta =$	−3.457°
range traveled =	8,262.76 km	—	—

Table D.7 TAEM conditions for EG19 with $J = \min \int \dot{Q} \, dt$

flight time =	1,288.218 sec	$i =$	28.50°
$r_c =$	6,407,566.000 m	$\gamma =$	−7.360°
$\Theta =$	−80.968 deg	$\Psi =$	128.604°
$\Phi =$	28.769 deg	$\alpha =$	15.329°
$V_r =$	916.860 m/s	$\beta =$	4.831°
range traveled =	7,394.29 km	—	—

Table D.8 TAEM conditions for EG20 with $J = \min \int \dot{Q} \, dt$

flight time =	1,312.837 sec	$i =$	28.50°
$r_c =$	6,407,566.000 m	$\gamma =$	−7.360°
$\Theta =$	−80.949 deg	$\Psi =$	47.338°
$\Phi =$	28.112 deg	$\alpha =$	15.329°
$V_r =$	916.860 m/s	$\beta =$	0.000°
range traveled =	7,465.36 km	—	—

Table D.9 TAEM conditions for EG21 with $J = \min \int \dot{Q} \, dt$

flight time =	1,354.082 sec	$i =$	28.50°
$r_c =$	6,407,566.000 m	$\gamma =$	−7.360°
$\Theta =$	−81.050 deg	$\Psi =$	113.959°
$\Phi =$	28.654 deg	$\alpha =$	15.329°
$V_r =$	916.860 m/s	$\beta =$	4.391°
range traveled =	7,658.30 km	—	—

Table D.10   TAEM conditions for EG15 with $J = \min \dot{Q}_{max}$

flight time =	1,204.992 sec	$i =$	51.60°
$r_c =$	6408615.000 m	$\gamma =$	−7.360°
$\Theta =$	−80.937 deg	$\Psi =$	74.876°
$\Phi =$	28.800 deg	$\alpha =$	14.162°
$V_r =$	908.150 m/s	$\beta =$	0.302°
range traveled =	6,795.20 km	—	—

Table D.11   TAEM conditions for EG18 with $J = \min \dot{Q}_{max}$

flight time =	1,449.449 sec	$i =$	51.60°
$r_c =$	6407566.000 m	$\gamma =$	−7.360°
$\Theta =$	−81.096 deg	$\Psi =$	64.848°
$\Phi =$	28.407 deg	$\alpha =$	14.147°
$V_r =$	916.860 m/s	$\beta =$	2.197°
range traveled =	8,257.86 km	—	—

Table D.12   TAEM conditions for EG21 with $J = \min \dot{Q}_{max}$

flight time =	1,352.376 sec	$i =$	28.50°
$r_c =$	6,407,566.000 m	$\gamma =$	−7.360°
$\Theta =$	−80.944 deg	$\Psi =$	46.851°
$\Phi =$	28.108 deg	$\alpha =$	9.419°
$V_r =$	916.860 m/s	$\beta =$	1.704°
range traveled =	7,742.80 km	—	—

APPENDIX E SYSTEM ENGINEERING EXTRAS

Our two greatest problems are gravity and paper work.
We can lick gravity, but sometimes the paperwork is overwhelming.

— Dr. Werner von Braun [52]

RIGOROUS, executable models (what things to do) and structure (how things are to be done) means a system engineering management plan (SEMP) includes technical program planning and control that identifies organizational responsibilities. This includes methods for design and technical program reviews, control of documentation, and CALS transfer of information from paper to electronic media. This appendix includes various forms that pertain to the SEMP for the G&C Project. Please refer to Chapter 7 starting on page 201 for detailed discussions on the SEMP for G&C Project.

E.1 Configuration Management Forms

Please refer to Section 7.4 starting on page 220 for the discussions of configuration management.

MIL-STD-100G entitled "Standard Practice for Engineering Drawings" [181] was used as a guideline to create the basic template for all of the specifications.
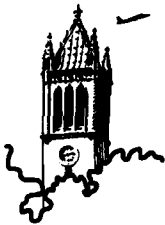
Engineering Change Proposal (ECP)
Page 1 of 1

ECP Number: ISU- _____ - ECP - _____

(Please obtain the number from CML)

Originator Name: _____   Date: _____

Configuration Item: _____

Classification (please check the appropriate category):

____ Priority 1: Prevents accomplishment of an essential capability; immediate attention is required.

____ Priority 2: Adversely affects performance of an essential capability; need to be solved ASAP.

____ Priority 3: Adversely affects performance of an essential capability; a known solution is available.

Short description of problem (including troubleshooting documentation that has been tried):

_____

_____

_____

_____

Impact of problem (short term and long term):

_____

_____

_____

Recommended Solution:

_____

_____

_____

CCB Approval: _____ Disapproval: _____   Date: _____

Date Received: _____   Date Completed: _____

Figure E.1   Engineering change proposal form

Design Activity: Guidance Project	Description: Ascent guidance interface input/output	DWG #: ISU-N830-DWG-001c
Drafter/Engineer: Ping Lu	Scale: N/A Unit: N/A Date: Sept. 7, 2002	Superseding DWG#: ISU-N830-DWG-001b
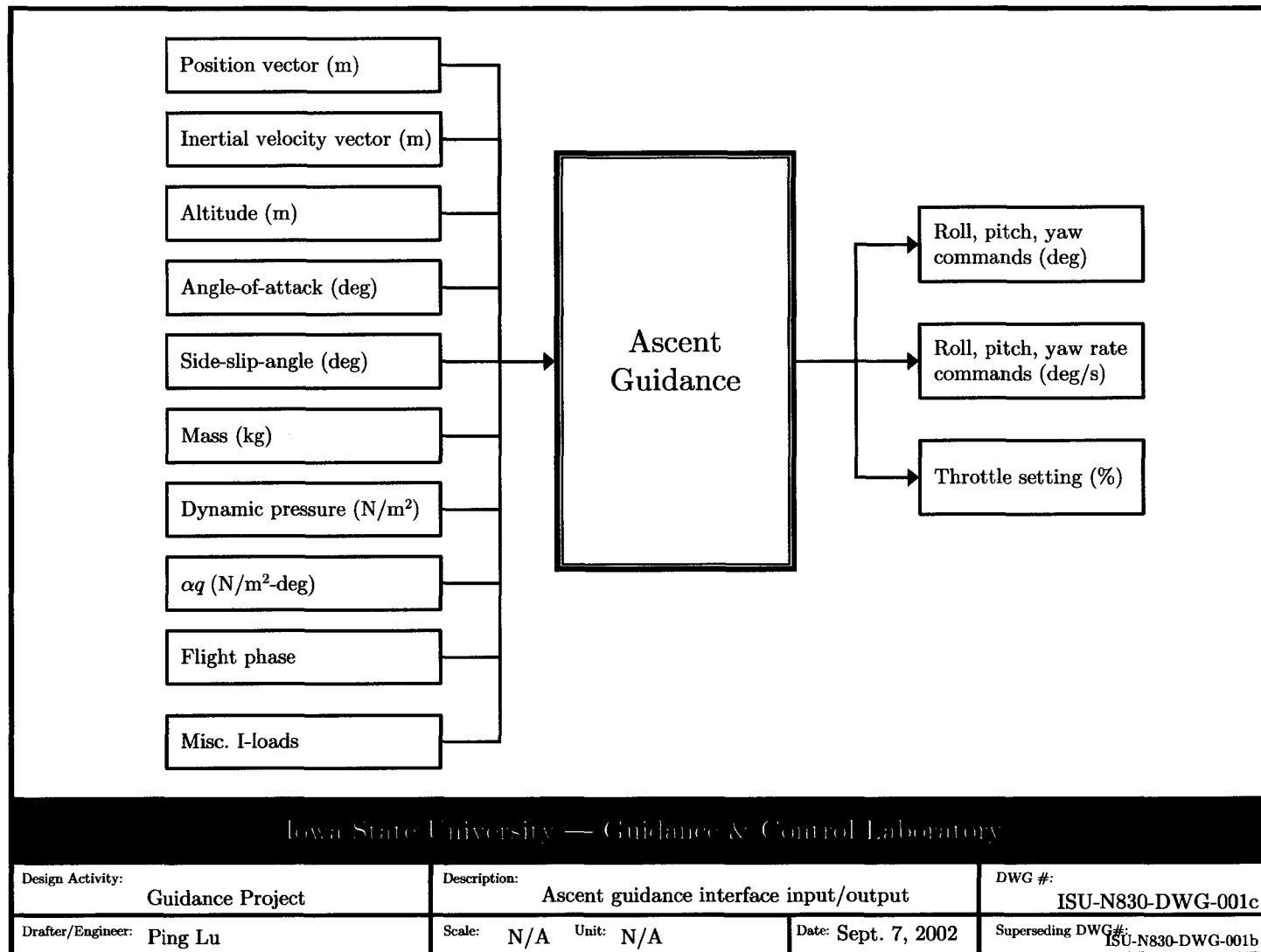
Figure E.2   Ascent guidance interface input/output specification
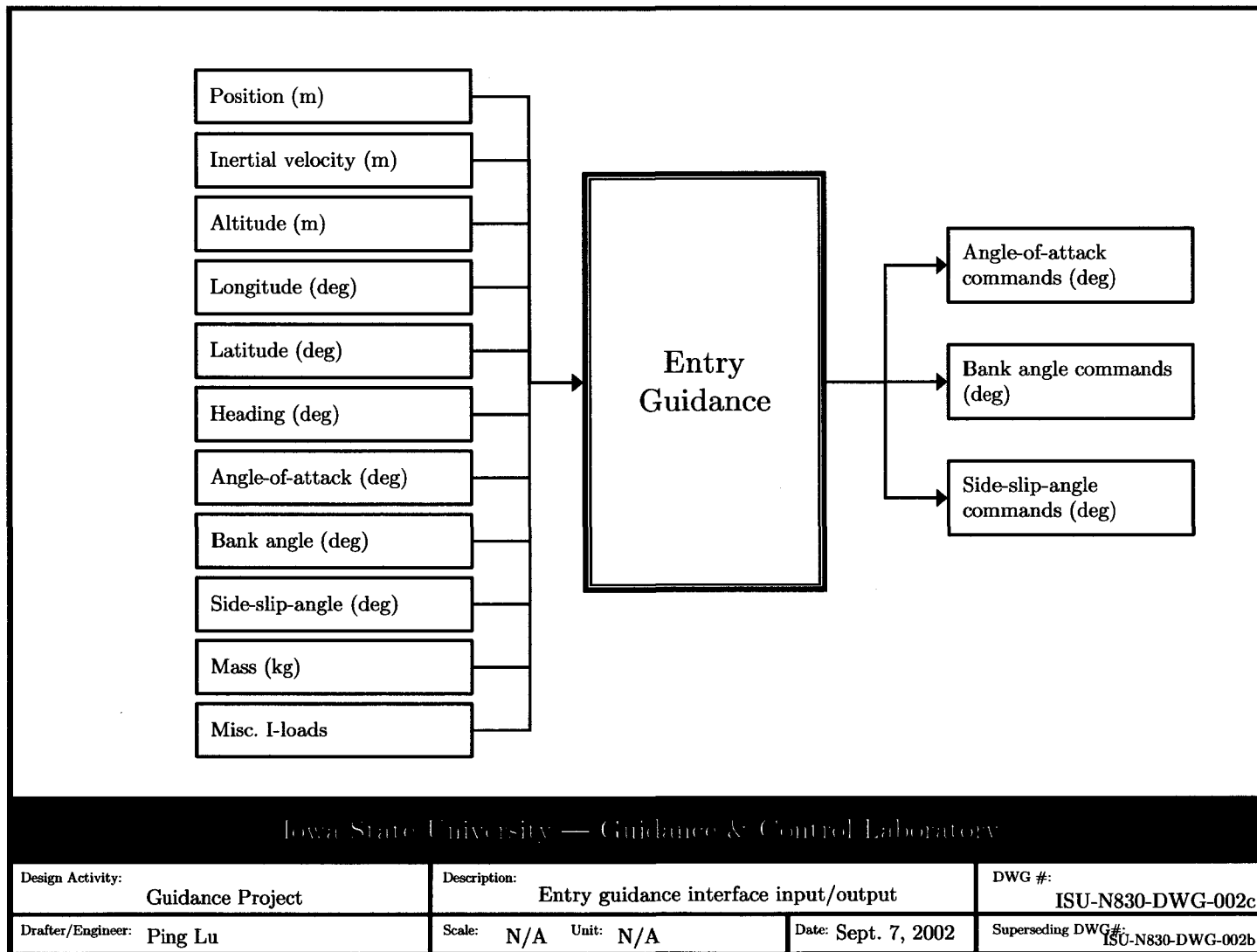
Figure E.3   Entry guidance interface input/output specification

E.2 Work Breakdown Structure

Please refer to Section 7.6 starting on page 235 for the discussions of WBS.
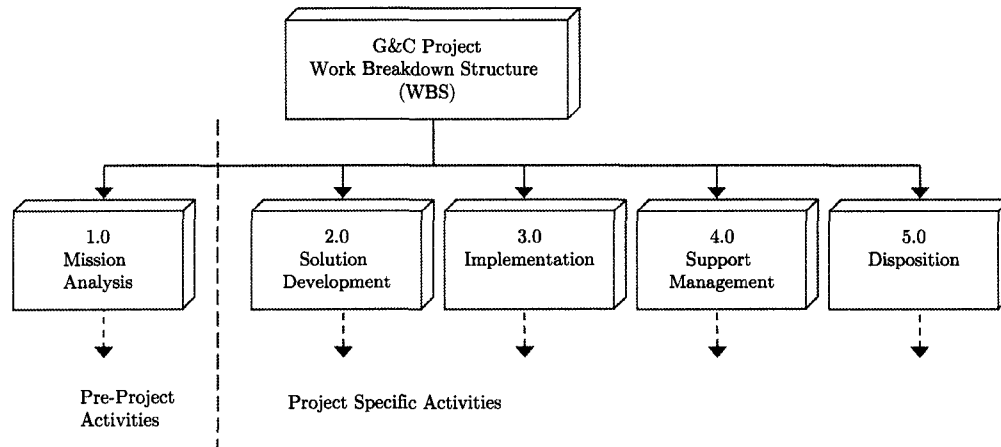
Figure E.4   Level 1 WBS for the G&C Project
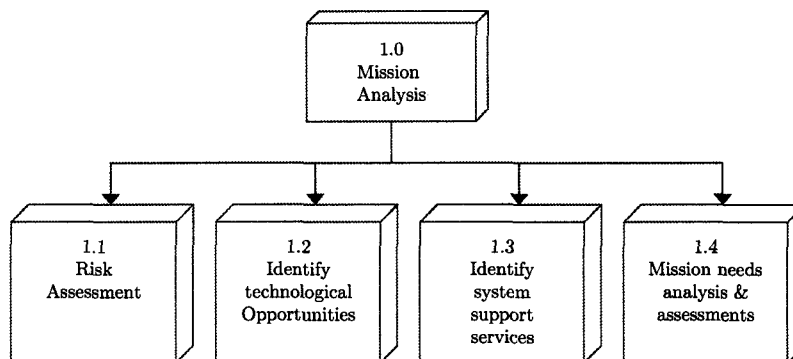
Figure E.5   Level 2: mission analysis WBS
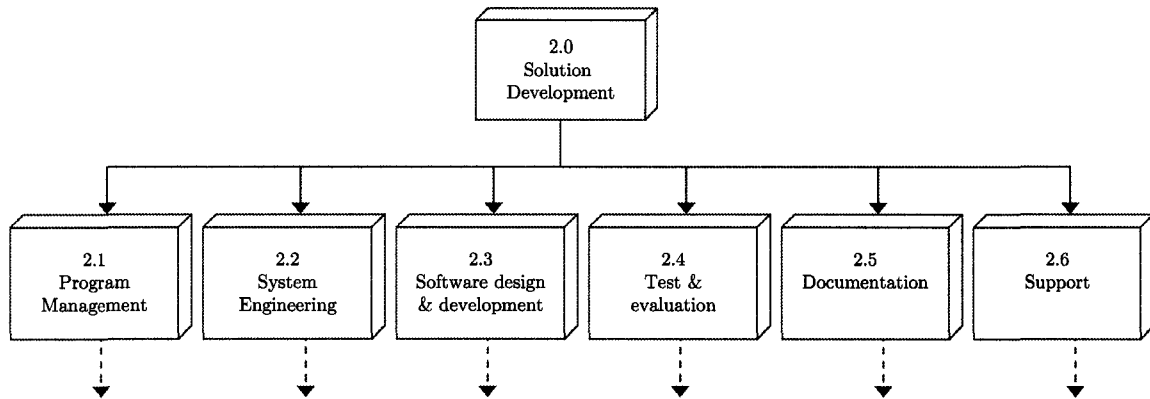
Figure E.6   Level 2: solution development WBS
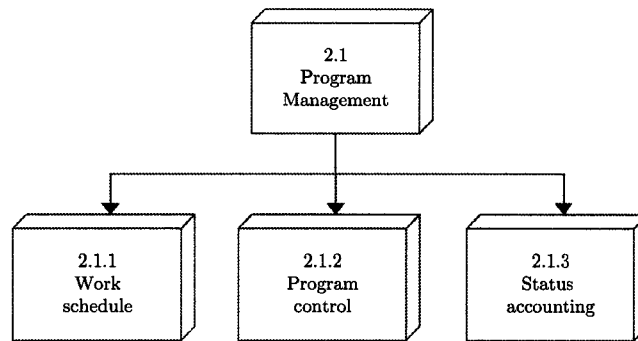
Figure E.7   Level 3: program management WBS
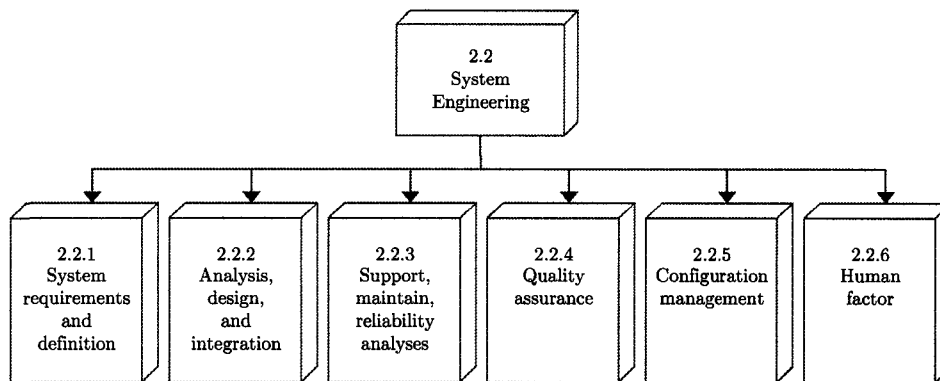
Figure E.8   Level 3: system engineering WBS
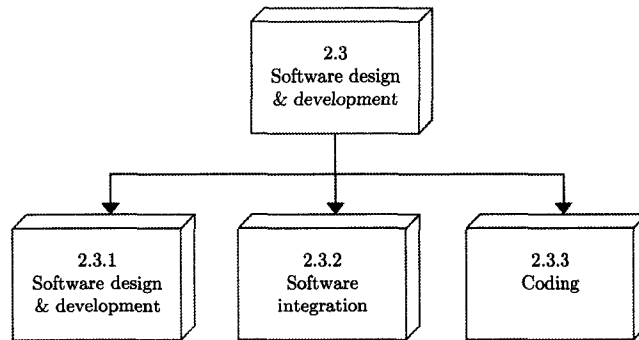
Figure E.9   Level 3: software design & development WBS
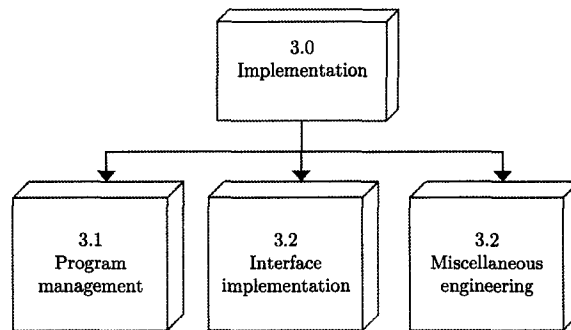
Figure E.10   Level 2: implementation WBS
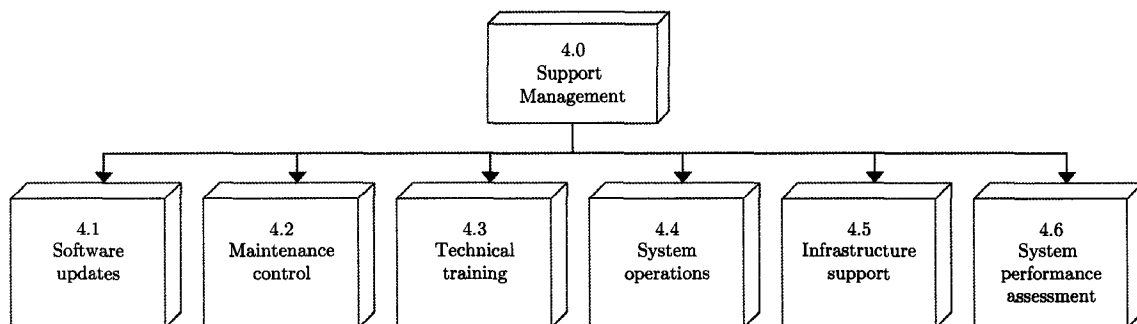
Figure E.11   Level 2: support management WBS
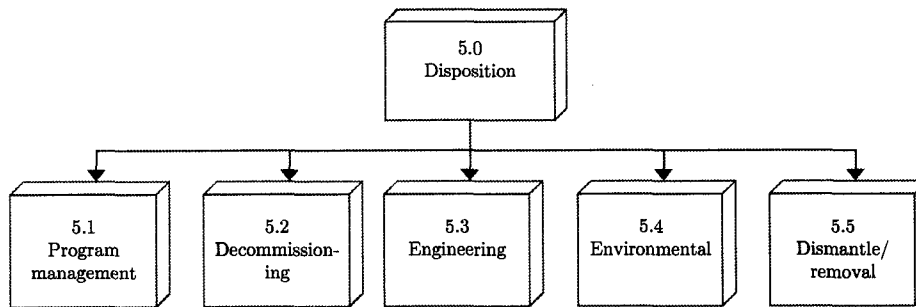
Figure E.12 Level 2: disposition WBS

E.3 Failure Mode, Effects, and Criticality Analysis Worksheet

Please refer to Section 7.7 starting on page 240 for the discussions of reliability analysis.
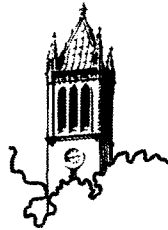
IOWA STATE UNIVERSITY
OF SCIENCE AND TECHNOLOGY

G&C Laboratory

Failure Mode, Effects, and Criticality Analysis (FMECA) Worksheet

	2.	3.	4.	5.	6.	7.
ID number	List all potential failure modes	Severity of effect	Probability of failure effect	Criticality	Risk priority number	Rank

Prepared by: _____ Date: _____   Approved by: _____

Figure E.13   Failure mode, effects, and criticality analysis worksheet

E.4 Story Tree

Please refer to Subsection 7.9.5 starting on page 254 for the discussions of the story tree in the context of documentations.

A story tree (sometimes called "storyboard") is a popular method for preparing group reports in industry. The fundamental idea behind the story tree methodology is similar to the work breakdown structure presented in Section E.2 — a methodical top down approach to write a technical report. The skeleton of the report is first developed to establish a general flow of the paper, i.e., at the chapter level. The responsible group for a particular chapter will decide what information, graphics and tables should be included. In other words, the idea behind a story tree is to develop a table of content, a list of figures and a list of tables before writing a paper. After reviewing each group's ideas, a detail story tree (section level) will be instituted to maintain a level of consistency throughout the paper. This technique will make certain that each chapter has the same type of information even though each chapter is written by a different group. Depending on the size of the report, further specific details at subsection level can be developed to be given out to team members. It is the author's experience both in industry and academia that the further a story tree is developed, the easier and faster it is to finish a report. Moreover, further development of a story tree also allows an overview of the paper flow (logic and order). The top two levels of the story tree used to develop this dissertation is displayed in Figure E.14.
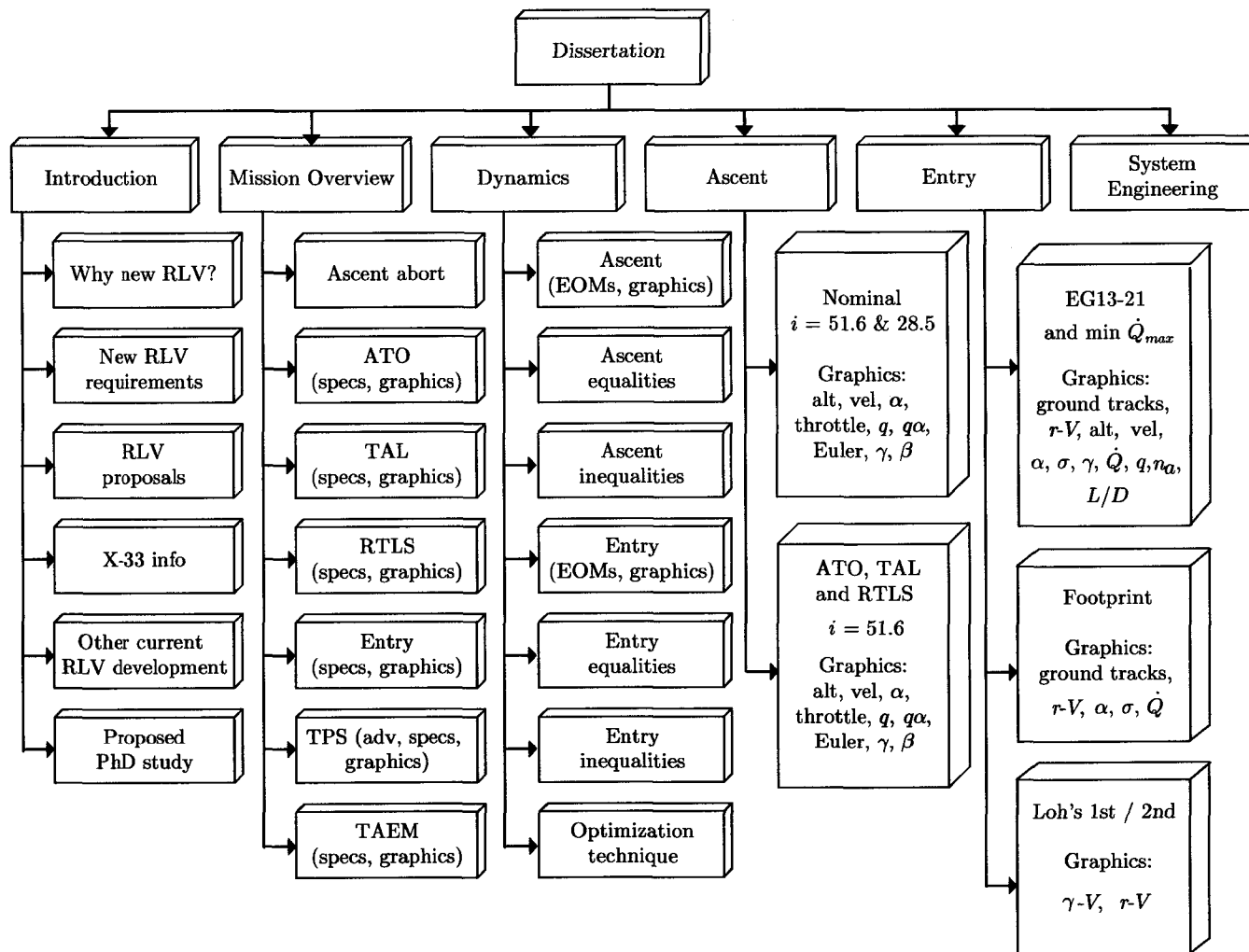
Figure E.14   Story tree for this dissertation

BIBLIOGRAPHY

[1] A. Calaprice. The Quotable Einstein. Princeton University Press, Princeton, New Jersey, 1996.

[2] R. T. Azuma. So Long, and Thanks for the Ph.D.! University of North Carolina, Chapel Hill, North Carolina, 2003. http://www.cs.unc.edu/~azuma/hitch4.html. Date retrieved: July 29, 2003.

[3] Famous Quotes and Quotations at BrainyQuote. http://http://www.brainyquote. com. Date retrieved: July 29, 2003.

[4] Statement on National Space Transportation Policy. The White House. Washington, DC, 1994.

[5] NSTS 1998 News Reference Manual. NASA Johnson Space Center, Houston, Texas, 2000. http://www.ksc.nasa.gov/shuttle/technology/sts-newsref/stsref-toc. html. Date retrieved: July 29, 2003.

[6] 2003 Aerospace Source Book. Aviation Week & Space Technology, 158(2):140–149, January 2003.

[7] VentureStar Specs. Andrews Space & Technology, Seattle, Washington, 2001. http://www.spaceandtech.com/spacedata/rlvs/venturestar_specs.shtml. Date retrieved: July 29, 2003.

[8] X-33 Specs. Andrews Space & Technology, Seattle, Washington, 2001. http://www.spaceandtech.com/spacedata/rlvs/x33_specs.shtml. Date retrieved: July 29, 2003.

[9] R. K. Weegar and R. R. Smiljanic. A System Effectiveness Approach to Developing a Fully-Reusable and Affordable RLV Main Engine. AIAA Paper 97-3125, 1997.

[10] Access to Space: The Future of U.S. Space Transportation Systems. U.S. Congress: Office of Technology Assessment, Washington, DC, 1990. OTA-ISC-415.

[11] Reusable Launch Vehicle Technology Development and Test Program. National Research Council. Washington, DC, 1995.

[12] Lockheed Martin Space Transportation Architecture Study. Lockheed Martin Corporation. Denver, Colorado, 1999.

[13] NASA In-House Space Transportation Architecture Architecture Study Final Briefing. NASA Kennedy Space Center. Cape Canaveral, Florida, 1999.

[14] Space Transportation Architecture Studies Final Review. Orbital Sciences Corporation. Dulles, Virginia, 1999.

[15] Space Transportation Architecture Study. Kelly Space & Technology. San Bernardino, California, 1999.

[16] Space Transportation Architecture Study. Kistler Aerospace Corporation. Kirkland, Washington, 1999.

[17] Space Transportation Architecture Study (STAS) Executive Summary. The Boeing Company. Seattle, Washington, 1999.

[18] M. H. Kaplan. The Next Generation of Launch Vehicles for America. AIAA Paper 96-4425, Huntsville, Alabama, September 1996.

[19] M. K. Lockwood. Overview of Conceptual Design of Early VentureStar Configurations. AIAA Paper 2000-1042, Reno, Nevada, January 2000.

[20] D. Quayle. Final Report to the President on the U.S. Space Program. Office of the Vice President. Washington, DC, 1993.

[21] A National Security Strategy for a New Century. The White House. Washington, DC, 1999.

[22] Introduction to NASA's Integrated Space Transportation Plan and Space Launch Initiative. NASA Marshall Space Flight Center. Huntsville, Alabama, 2001.

[23] D. O. Stanley and W. M. Piland. Technology Requirements for Affordable Single-Stage Rocket Launch Vehicles. IAF Paper 93-627, October 1993.

[24] D. M. Anderson. NASA's Integrated Space Transportation Plan. In 36th AIAA/ASME/SAE/ASEE Joint Propulsion Conference & Exhibit, Huntsville, Alabama, July 2000.

[25] S. Cook and D. Dumbacher. NASA's Integrated Space Transportation Plan. Acta Astronautica, 48(5-12):869–883, 2001.

[26] D. C. Freeman, T. A. Talay, and R. E. Austin. Single-Stage-to-Orbit — Meeting the Challenge. Acta Astronautica, 38(4-8):323–331, 1996.

[27] D. C. Freeman, T. A. Talay, and R. E. Austin. Reusable Launch Vehicle Technology Program. Acta Astronautica, 41(11):777–790, 1997.

[28] X-33 VentureStar. Federation of American Scientists, Washington, DC, 1999. http://www.fas.org/spp/guide/usa/launch/x-33.htm. Date retrieved: July 29, 2003.

[29] 96-04-02 X-33 Cooperative Agreement. NASA Headquarters, Washington, DC, 1996. Release: 96-62.

[30] North American History Chronology. The Boeing Company, Chicago, Illinois. http://www.boeing.com/history/bna/chron.html. Date retrieved: July 29, 2003.

[31] McDonnell Douglas History Chronology. The Boeing Company, Chicago, Illinois. http://www.boeing.com/history/mdc/chron.htm. Date retrieved: July 29, 2003.

[32] Lockheed Martin Selected to Build X-33. NASA Headquarters, Washington, DC, 1996. Press Release: 96-128.

[33] Fact Sheets: X-33 Fact Sheet. NASA Marshall Space Flight Center, Huntsville, Alabama, 1999. http://www1.msfc.nasa.gov/NEWSROOM/background/facts/x33.html. Date retrieved: July 29, 2003.

[34] C. J. Mead. X-33 Lessons Learned. In AIAA/IAF Symposium on Future RLVs, Huntsville, Alabama, April 2002.

[35] NASA Dryden X-33 Photo Collection. NASA Dryden Flight Research Center, Edwards, California, 1999. http://www.dfrc.nasa.gov/gallery/photo/X-33/index.html. Date retrieved: July 29, 2003.

[36] Fact Sheets: X-33 Flight Operations Center. NASA Marshall Space Flight Center, Huntsville, Alabama, 1999. http://www1.msfc.nasa.gov/NEWSROOM/background/facts/x33_site.html. Date retrieved: July 29, 2003.

[37] Lockheed Martin X-33 Reusable Launch Vehicle Prototype. AircraftMuseum.com, 2001. http://www.aerospaceweb.org/aircraft/research/x33/index.shtml. Date retrieved: July 29, 2003.

[38] NASA Fact: The Space Launch Initiative: Technology to Pioneer the Space Frontier. NASA Marshall Space Flight Center, Huntsville, Alabama, 2001. FS-2001-04-74-MSFC.

[39] The X-33 History Project Home Page. NASA Headquarters, Washington, DC, 2001. http://www.hq.nasa.gov/office/pao/History/x-33/home.htm. Date retrieved: July 29, 2003.

[40] Fact Sheets: NASA's Space Launch Initiative: The Next Generation Launch Technology Program. NASA Marshall Space Flight Center, Huntsville, Alabama, 2003. FS-2003-05-63-MSFC.

[41] Next Generation Launch Technology. NASA Marshall Flight Research Center, Huntsville, Alabama, 2003. http://slinews.com/nglt1.html. Date retrieved: July 29, 2003.

[42] J. C. Naftel and R. W. Powell. Analysis of Staging Maneuver and Booster Glideback Guidance for a Two-Stage, Winged, Fully Reusable Launch Vehicle. Technical Report NASA/TP 3335, NASA Langley Research Center, Hampton, Virginia, 1993.

[43] What is the X PRIZE? The X PRIZE Foundation, St. Louis, Missouri, 2002. http://www.xprize.org/press/what.html. Date retrieved: July 29, 2003.

[44] Reusable Launch Vehicles & Spaceports: Programs and Concepts for 2001. Department of Transportation. Federal Aviation Administration, Washington, DC, 2001.

[45] C. Dujarric. Possible Future European Launchers — A Process of Convergence. In Third European Symposium on Aerothermodynamics for Space Vehicles, The Netherlands, November 1998.

[46] F. Morring, Jr. Europe and Japan Have RLV Research Plans. Aviation Week & Space Technology, 155(16):46, October 2001.

[47] J. E. Ward. Reusable Launch Vehicles and Space Operations. Occasional Paper No. 12, Center for Strategy and Technology, Maxwell Air Force Base, Alabama, 2000.

[48] Quarterly Launch Special Report: U.S. Advanced Launch Vehicle Technology Programs. Department of Transportation. Federal Aviation Administration, Washington, DC. 2nd Quarter 1996.

[49] J. M. Hanson, M. W. Shrader, and A. Cruzen. Ascent Guidance Comparisons. In Proceedings of the AIAA Guidance, Navigation and Control Conference, Scottsdale, Arizona, August 1994.

[50] R. L. McHenry, T. J. Brand, A. D. Long, B. F. Cockrell, and J. R. Thibodeau II. Space Shuttle Ascent Guidance, Navigation, and Control. The Journal of the Astronautical Sciences, XXVII(1):1–38, January-March 1979.

[51] A. J. Calise and N. Brandt. Generation of Launch Vehicle Abort Trajectories Using a Hybrid Optimization Method. AIAA Paper 2002-4560, Monterey, California, August 2002.

[52] D. English. The Air Up There: More Great Quotations on Flight. McGraw-Hill, New York, 2003.

[53] The Shuttle Mission Profile. NASA Johnson Space Center, Houston, Texas, 2002. http://spaceflight.nasa.gov/shuttle/reference/shutref/sts/profile.html. Date retrieved: July 29, 2003.

[54] J. Crow. Finite-State Analysis of Space Shuttle Contingency Guidance Requirements. Contractor Report NASA/CR-4741, SRI International, Menlo Park, California, 1996.

[55] J. M. Hanson, D. J. Coughlin, G. A. Dukeman, J. A. Mulqueen, and J. W. Mc-Carter. Ascent, Transition, Entry, and Abort Guidance Algorithm Design for the X-33 Vehicle. AIAA Paper 98-4490, Boston, Massachusetts, August 1998.

[56] Shuttle Orbiter Operational Level C, Functional Subsystem Software Requirements, Guidance, Navigation Control, Part A, Guidance Ascent/RTLS. The Boeing Company, Houston, Texas, 2000. STS 83-0002-30.

[57] Space Transportation System. NASA Kennedy Space Center, Cape Canaveral, Florida, 2000. http://www.ksc.nasa.gov/shuttle/technology/sts-newsref/sts_overview.html. Date retrieved: July 29, 2003.

[58] Mission Events Summary. NASA Johnson Space Center, Houston, Texas, 2002. http://spaceflight.nasa.gov/shuttle/reference/shutref/events. Date retrieved: July 29, 2003.

[59] ATO/AOA/TAL Training. NASA Lyndon B. Johnson Space Center, Houston, Texas, 1995. Manual 2102.

[60] RTLS Abort Training Manual. NASA Lyndon B. Johnson Space Center, Houston, Texas, 1992. RTLS 2102.

[61] STS-107 MCC Status Report #19. NASA Johnson Space Center, Houston, Texas, 2003. http://www.jsc.nasa.gov/news/shuttle/sts-107/sts-107-19.html. Date retrieved: July 29, 2003.

[62] Space Shuttle Orbiter Operational Level C, Functional Subsystem Software Requirements, Guidance, Navigation Control, Part A, Entry Through Landing Guidance. The Boeing Company, Houston, Texas, 2000. STS 83-0001-30.

[63] Computers in the Space Shuttle Avionics System. NASA Headquarters, Washington, DC, 1998. http://www.hq.nasa.gov/office/pao/History/computers/Ch4-3. html. Date retrieved: July 29, 2003.

[64] Intel Architecture Software Developer's Manual. Intel Corporation, Mt. Prospect, Illinois, 1997. Volume 1: Basic Architecture. Order Number 243190.

[65] D. E. Myers, C. J. Martin, and M. L. Blosser. Parametric Weight Comparison of Current and Proposed Thermal Protection System (TPS) Concepts. AIAA Paper 99-3459, Norfolk, Virginia, June 1999.

[66] D. Olynick. Trajectory Based TPS Sizing for an X-33 Winged Vehicle Concept. Journal of Spacecraft and Rockets, 35(3):249–257, May-June 1998.

[67] T. Tam and D. Olynick. An Investigation of Possible Shuttle Upgrades Using Advanced TPS Concepts. AIAA Paper 97-0277, Reno, Nevada, January 1997.

[68] R. A. Thompson. Review of X-33 Hypersonic Aerodynamic and Aerothermodynamic Development. In 22nd Congress of the International Council of the Aeronautical Sciences, Harrogate, United Kingdom, August 2000.

[69] R. Windhorst, M. Ardema, and J. Bowles. Minimum Heating Re-entry Trajectories for Advanced Hypersonic Launch Vehicles. AIAA Paper 97-3535, 1997.

[70] P. V. Tartabini, R. A. Lepsch, J. J. Korte, and K. E. Wurster. A Multidisciplinary Performance Analysis of a Lifting-Body Single-Stage-to-Orbit Vehicle. AIAA Paper 2000-1045, Reno, Nevada, January 2000.

[71] C. C. Poteet, H. Abu-Khajeel, and S. Hsu. Preliminary Thermal-Mechanical Sizing of Metallic TPS: Process Development and Sensitivity Studies. AIAA Paper 2002-0505, Reno, Nevada, January 2002.

[72] G. Palmer, D. Kontinos, and B. Sherman. Surface Heating Effects of X-33 Vehicle Thermal-Protection-System Panel Bowing. *Journal of Spacecraft and Rockets*, 36 (6):536–541, November-December 1999.

[73] Z. Shen and P. Lu. Onboard Generation of Three-Dimensional Constrained Entry Trajectories. *Journal of Guidance, Control, and Dynamics*, 26(1):111–121, January-February 2003.

[74] C. Covault. Astronaut Skills Honed Flying Steep STA Dives. *Aviation Week & Space Technology*, 157(2):56–59, July 2002.

[75] *Terminal Area Energy Management*. NASA Lyndon B. Johnson Space Center, Houston, Texas, 1989. TAEM 2102.

[76] J. C. Harpold and D. E. Gavert. Space Shuttle Entry Guidance Performance Results. *Journal of Guidance, Control and Dynamics*, 6(6):442–447, 1983.

[77] J. C. Harpold and C. A. Graves. Shuttle Entry Guidance. *The Journal of the Astronautical Sciences*, XXXVII(3):239–268, 1979.

[78] N. X. Vinh. *Optimal Trajectories in Atmospheric Flight*. Elsevier Scientific Publishing Company, New York, 1981.

[79] A. E. Bryson, Jr. *Dynamic Optimization*. Addison-Wesley Longman, Menlo Park, California, 1999.

[80] A. E. Bryson, Jr. and Y. C. Ho. *Applied Optimal Control*. John Wiley & Sons, New York, 1975.

[81] J. T. Betts. *Practical Methods for Optimal Control Using Nonlinear Programming*. SIAM, Philadelphia, Pennsylvania, 2000.

[82] E. D. Dickmanns. Efficient Convergence and Mesh Refinement Strategies for Solving General Ordinary Two-Point Boundary Value Problems by Collocated Hermite Approximation. In 2nd IFAC Workshop on Optimization, Oberpfaffenhofen, Germany, September 1980.

[83] R. Bulirsch, D. Kraft, and B. Verlag, editors. Computational Optimal Control, volume 115, pages 8–13. Springer-Verlag, New York, 1994.

[84] J. T. Betts and W. P. Huffman. Path Constrained Trajectory Optimization Using Sparse Sequential Quadratic Programming. Journal of Guidance, Control and Dynamics, 16(1):59–68, January-February 1993.

[85] C. T. Keller and E. W. Sachs. A Pointwise Quasi-Newton Method for Unconstrained Optimal Control Problems. Numerische Mathematik, 55:159–176, 1989.

[86] J. T. Betts and W. P. Huffman. Exploiting Sparsity in the Direct Transcription Method for Optimal Control. Computational Optimization and Applications, 14 (2):179–201, September 1999.

[87] J. T. Betts and W. P. Huffman. Sparse Optimal Control Software: Version 5.0. Library Report MEA-LR-085-R1, The Boeing Company, Seattle, Washington, 2000.

[88] A. R. Curtis, M. J. D. Powell, and J. K. Reid. On the Estimation of Sparse Jacobian Matrices. Journal of the Institute of Mathematics and Applications, 13: 117–120, 1974.

[89] T. F. Coleman and J. J. Moré. Estimation of Sparse Jacobian Matrices and Graph Coloring Problems. SIAM Journal on Numerical Analysis, 20:187–209, 1983.

[90] P. E. Gill, W. Murray, M. A. Saunders, and M. H. Wright. Some Theoretical Properties of an Augmented Lagrangian Merit Function. Technical Report SOL 86-6, Stanford University, Stanford, California, 1986.

[91] J. T. Betts, M. J. Carter, and W. P. Huffman. Software for Nonlinear Optimization. Library Report MEA-LR-083 R2, The Boeing Company, Seattle, Washington, 2000.

[92] A. J. Calise, N. Melamed, and S. Lee. Design and Evaluation of a Three-Dimensional Optimal Ascent Guidance Algorithm. Journal of Guidance, Control and Dynamics, 21(6):867–875, November-December 1998.

[93] P. Lu, H. Sun, and B. Tsai. Closed-Loop Endo-Atmospheric Ascent Guidance. Journal of Guidance, Control and Dynamics, 26(2):283–294, March-April 2003.

[94] R. R. Bate, D. D. Mueller, and J. E. White. Fundamentals of Astrodynamics. Dover Publications, New York, 1971.

[95] P. V. Tartabini, K. E. Wurster, J. J. Korte, and R. A. Lepsch. Multidisciplinary Analysis of a Lifting Body Launch Vehicle. Journal of Spacecraft and Rockets, 39 (5):788–795, September-October 2002.

[96] XRS-2200 Linear Aerospike Engine. The Boeing Company, Chicago, Illinois. http://www.boeing.com/defense-space/space/propul/XRS2200.html. Date retrieved: July 29, 2003.

[97] Director: Ron Howard. With Tom Hanks, Kevin Bacon, and Bill Paxton. Apollo 13. Universal Studios, Hollywood, California, 1995. Motion Picture.

[98] F. J. Regan. Re-Entry Vehicle Dynamics. American Institute of Aeronautics and Astronautics, Washington, DC, 1984.

[99] N. X. Vinh, A. Busemann, and R. D. Culp. Hypersonic and Planetary Entry Flight Mechanics. The University of Michigan Press, Ann Arbor, Michigan, 1980.

[100] C. Jänsch and A. Markl. Trajectory Optimization and Guidance for a Hermes-Type Reentry Vehicle. AIAA Paper 91-2659-CP, 1991.

[101] M. D. Griffin and J. R. French. Space Vehicle Design. American Institute of Aeronautics and Astronautics, Washington, DC, 1991.

[102] W. L. Handkey. Re-Entry Aerodynamics. American Institute of Aeronautics and Astronautics, Washington, DC, 1988.

[103] GN and C Entry Operations, Guidance and Navigation. NASA Lyndon B. Johnson Space Center, Houston, Texas, 1979. GNC ENT 2102.

[104] Entry Guidance Workbook. NASA Lyndon B. Johnson Space Center, Houston, Texas, 1996. ENT GUID 2102.

[105] W. E. Hammond. Design Methodologies for Space Transportation Systems. American Institute of Aeronautics and Astronautics, Washington, DC, 2001.

[106] K. J. Murphy, R. J. Nowak, R. A. Thompson, B. R. Hollis, and R. Prabhu. X-33 Hypersonic Aerodynamic Characteristics. Journal of Spacecraft and Rockets, 38 (5):670–783, September-October 2001.

[107] M. A. Tigges. Deorbit/Entry Flight Profile with Landing Site Precision. Technical Report Preliminary V-201, X-38 Flight Dynamics Team, NASA Johnson Space Center, Houston, Texas, 2001.

[108] A. D. Ngo and D. B. Doman. Footprint Determination of Reusable Launch Vehicles Experiencing Control Effector Failures. AIAA Paper 2002-4775, Monterey, California, August 2002.

[109] D. Sheu and Y. Chen. Optimal Three-Dimensional Glide for Maximum Reachable Domain. AIAA Paper 99-4245, 1999.

[110] D. Sheu, Y. Chen, Y. Chang, and J. Chern. Optimal Glide for Maximum Range. AIAA Paper 98-4462, 1998.

[111] P. Lu, Z. Shen, G. A. Dukeman, and J. M. Hanson. Entry Guidance by Trajectory Regulation. AIAA Paper 2000-3958, Denver, Colorado, August 2000.

[112] W. H. T. Loh. Dynamics and Thermodynamics of Planetary Entry. Prentice Hall, Englewood Cliffs, New Jersey, 1963.

[113] G. Cho, H. Jerrell, and W. Landay. Program Management 2000: Know the Way, How Knowledge Management Can Improve DoD Acquisition. Defense Systems Management College Press. Fort Belvoir, Virginia, 2000.

[114] D. L. Christensen. Advances in the Application of Systems Engineering Procedures. AIAA Paper 96-4433, Huntsville, Alabama, September 1996.

[115] W. E. Hammond. Space Transportation: A Systems Approach to Analysis and Design. American Institute of Aeronautics and Astronautics, Washington, DC, 1999.

[116] Fact Sheets: NASA's Space Launch Initiative: Expanding Access to the Space Frontier. NASA Marshall Space Flight Center, Huntsville, Alabama, 2002. FS-2002-04-88-MSFC.

[117] The Space Launch Initiative: Technology to Pioneer the Space Frontier. 2001. NASA Marshall Space Flight Center, Huntsville, Alabama. FS-2001-06-122-MSFC.

[118] A Blueprint for New Beginnings. Office of Management and Budget. U.S. Government Printing Office, Washington, DC, 2001.

[119] S. Venneri. Statement of Mr. Sam Venneri, Associate Administrator, Office of Aerospace Technology, Before the Subcommittee on Space and Aeronautics Committee on Science House of Representatives. Office of Aerospace Technology. Washington, DC, 2002.

[120] NRA8-30 2nd Generation RLV Systems Engineering and Risk Reduction Phase I. NASA Marshall Space Flight Center, Huntsville, Alabama, 2000. 083261-SOL-001-001.

[121] NRA8-30 Common Instructions 2nd Generation RLV Systems Engineering and Risk Reduction Phase I. NASA Marshall Space Flight Center, Huntsville, Alabama, 2000. 083261-SOL-001-002.

[122] NASA Systems Engineering Handbook. NASA Headquarters, Washington, DC, 1995. SP-610S.

[123] B. S. Blanchard. Systems Engineering Management. John Wiley & Sons, New York, 1991.

[124] A. Ertas and J. C. Jones. The Engineering Design Process. John Wiley & Sone, New York, 1993.

[125] J. C. Blair, R. S. Ryan, L. A. Schutzenhofer, and W. R. Humphries. Launch Vehicle Design Process: Characterization, Technical Integration, and Lessons Learned. Technical Publication NASA/TP-2001-210992, NASA Marshall Space Flight Center, Huntsville, Alabama, 2001.

[126] 2nd Generation Reusable Launch Vehicle Program — Level 1 Requirements. NASA Marshall Space Flight Center, Huntsville, Alabama, 2001. MSFC-RQMT-3221.

[127] Project Management and System Engineering Handbook. NASA Marshall Space Flight Center, Huntsville, Alabama, 2001. MSFC-HDBK-3173.

[128] NASA Program and Project Management Processes and Requirements. NASA Headquarters, Washington, DC, 2002. NPG 7120.5B.

[129] Program/Project Planning. NASA Marshall Space Flight Center, Huntsville, Alabama, 2000. MPG 7120.1, Revision B.

[130] System Engineering Management Plan (SEMP). Department of Defense. Defense
Acquisition University Press, Fort Belvoir, Virginia, 1990. DI-MGMT-81024.

[131] Configuration Management. Department of Defense. Defense Acquisition Univer-
sity Press, Fort Belvoir, Virginia, 1992. MIL-STD-973.

[132] NRA8-30, Part III, Flight Mechanics Risk Reduction Appendix G — Technology
Area 7 (TA-7). NASA Marshall Space Flight Center, Huntsville, Alabama, 2000.
083261-SOL-001-010.

[133] IEEE Standard for Application and Management of the Systems Engineering
Process. The Institute of Electrical and Electronics Engineers, New York, 1998.
IEEE Std 1220-1998.

[134] Systems Engineering Fundamentals. Department of Defense. Defense Acquisition
University Press, Fort Belvoir, Virginia, 2001.

[135] Configuration Management Guidance. Department of Defense. Defense Acquisition
University Press, Fort Belvoir, Virginia, 1997. MIL-HDBK-61.

[136] Configuration Management, MSFC Programs/Projects. NASA Marshall Space
Flight Center, Huntsville, Alabama, 2001. MPG 8040.1, Revision C.

[137] Configuration Management, MSFC Programs/Projects. NASA Marshall Space
Flight Center, Huntsville, Alabama, 2002. MWI 8040.1, Revision E.

[138] Product Identification. NASA Marshall Space Flight Center, Huntsville, Alabama,
2000. MPG 8040.2, Revision B.

[139] Product Traceability. NASA Marshall Space Flight Center, Huntsville, Alabama,
2000. MPG 8040.3, Revision B.

[140] Automated Interchange of Information. Department of Defense. Defense Acquisition University Press, Fort Belvoir, Virginia, 1997. MIL-STD-1840C.

[141] Documentation and Data Control. NASA Headquarters, Washington, DC, 2002. HCP 1400-1D.

[142] J. M. Hanson. New Guidance for New Launchers. Aerospace America, 41(3): 36–41, March 2003.

[143] J. M. Hanson. Advanced Guidance and Control Project for Reusable Launch Vehicles. AIAA Paper 99-4614, Denver, Colorado, August 2000.

[144] E. M. Goldratt. Production — The TOC Way — Work Book. North River Press, Great Barrington, Massachusetts, 1996.

[145] MSFC Records Management Program. NASA Marshall Space Flight Center, Huntsville, Alabama, 2003. MPG 1440.2, Revision J.

[146] H. B. Tsai. A System Engineering Overview of a Parafoil Based Autonomous Recovery Guidance System at Iowa State University. Master of Engineering creative component, Iowa State University, Ames, Iowa, 2000.

[147] Configuration Management Audits, MSFC Programs/Projects. NASA Marshall Space Flight Center, Huntsville, Alabama, 2001. MWI 8040.7.

[148] Flight Systems Design/Development Control. NASA Marshall Space Flight Center, Huntsville, Alabama, 2002. MPG 8060.1, Revision E.

[149] Work Breakdown Structure. Department of Defense. Defense Acquisition University Press, Fort Belvoir, Virginia, 1993. MIL-HDBK-881.

[150] W. R. Humphries, W. Holland, and R. Bishop. Information Flow in the Launch Vehicle Design/Analysis Process. Technical Memorandum NASA/TM-1999-209877, NASA Marshall Space Flight Center, Huntsville, Alabama, 1999.

[151] B. S. Blanchard and W. J. Fabrycky. Systems Engineering and Analysis. Prentice Hall, Englewood Cliffs, New Jersey, 3rd edition, 1998.

[152] Reliability Test. Department of Defense. Defense Acquisition University Press, Fort Belvoir, Virginia, 1986. MIL-HDBK-781D.

[153] Procedure to Perform a Failure Mode, Effect and Criticality Analysis. Department of Defense. Defense Acquisition University Press, Fort Belvoir, Virginia, 1980. MIL-STD-1629A.

[154] C. W. Johnson. Safety Critical Systems Development. University of Glasgow. Glasgow, Scotland, 2001.

[155] Reliability Growth Management. Department of Defense. Defense Acquisition University Press, Fort Belvoir, Virginia, 1981. MIL-HDBK-189.

[156] Test and Evaluation Program Plan. Department of Defense. Defense Acquisition University Press, Fort Belvoir, Virginia, 1992. DI-NDTI-81284.

[157] Electronic Reliability Design Handbook. Department of Defense. Defense Acquisition University Press, Fort Belvoir, Virginia, 1998. MIL-HDBK-338B.

[158] Continuous Acquisition and Life-Cycle (CALS) Support Implementation Guide. Department of Defense. Defense Acquisition University Press, Fort Belvoir, Virginia, 1994. MIL-HDBK-59B.

[159] NATO Concept of Operations. North Atlantic Treaty Organization, Belgium, 1998. Version 2.6.

[160] NATO CALS Handbook. North Atlantic Treaty Organization, Belgium, 2000. Version 2.

[161] Configuration Management Data Interface. Department of Defense. Defense Acquisition University Press, Fort Belvoir, Virginia, 1997. MIL-STD-2549.

[162] Managing Defence Systems in the Information Age. North Atlantic Treaty Organization, Belgium, 1999.

[163] Data Management Plans, Programs/Projects. NASA Marshall Space Flight Center, Huntsville, Alabama, 2000. MWI 7120.5, Revision B.

[164] Data Item Descriptions (DIDs). Department of Defense. Defense Acquisition University Press, Fort Belvoir, Virginia, 1986. MIL-STD-963A.

[165] Evaluation of Commercial Off-the-Shelf Manuals. Department of Defense. Defense Acquisition University Press, Fort Belvoir, Virginia, 1995. MIL-HDBK-1221.

[166] Standard Practice for Manuals, Technical: General Style and Format Requirements. Department of Defense. Defense Acquisition University Press, Fort Belvoir, Virginia, 2000. MIL-HDBK-38754.

[167] Documentation, Preparation Programs/Projects. NASA Marshall Space Flight Center, Huntsville, Alabama, 2002. MWI 7120.4, Revision B.

[168] Human Engineering. Department of Defense. Defense Acquisition University Press, Fort Belvoir, Virginia, 1999. MIL-STD-1472F.

[169] Human Engineering Program Process and Procedures. Department of Defense. Defense Acquisition University Press, Fort Belvoir, Virginia, 1999. MIL-HDBK-46855A.

[170] Lean Aerospace Initiative. Massachusetts Institute of Technology, Cambridge, Massachusetts. http://lean.mit.edu. Date retrieved: July 29, 2003.

[171] S. Shingo. A Study of the Toyota Production System From an Industrial Engineering Viewpoint. Productivity Press, Portland, Oregon, 1989.

[172] K. Bozdogan, R. Milauskas, J. Mize, D. Nightingale, A. Taneja, and D. Tonaszuck. Transitioning to a Lean Enterprise: A Guide for Leaders, Volume I: Executive Overview. Massachusetts Institute of Technology. Cambridge, Massachusetts, 2000.

[173] E. M. Murman, T. J. Allen, and J. Cutcher-Gershenfeld. Lean Enterprise Value: Insights from MIT's Lean Aerospace Initiative. Palgrave Macmilliam, Houndmills, United Kingdom, 2002.

[174] A Guide for the Design of Highly Reusable Space Transportation. NASA Marshall Space Flight Center, Huntsville, Alabama, August 1997.

[175] G. Rabadi, M. Mollaghasemi, G. Cates, and M. Steele. A Discrete-Event Simulation Model for the Space Shuttle Ground Processing Operations at Kennedy Space Center. In 2001 SMART Conference Presentation, Orlando, Florida, April 2001.

[176] Fact Sheets: Linear Aerospike Engine — Propulsion for the X-33 Vehicle. NASA Marshall Space Flight Center, Huntsville, Alabama, 2000. FS-2000-09-174-MSFC.

[177] Aerospike — Specifications. Andrews Space & Technology, Seattle, Washington, 2000. http://www.spaceandtech.com/spacedata/engines/aerospike_specs.shtml. Date retrieved: July 29, 2003.

[178] Fact Sheet: Linear Aerospike Engine — Propulsion for the X-33 Vehicle. NASA Marshall Space Flight Center, Huntsville, Alabama, 2000. http://www1.msfc.

nasa.gov/NEWSROOM/background/facts/aerospike.html. Date retrieved: July 29, 2003.

[179] NASA Dryden X-33 Graphics Collection. NASA Dryden Flight Research Center, Edwards, California, 1999. http://www.dfrc.nasa.gov/gallery/graphics/X-33/index.html. Date retrieved: July 29, 2003.

[180] SSME — Specifications. Andrews Space & Technology, Seattle, Washington, 2001. http://www.spaceandtech.com/spacedata/engines/ssme_specs.shtml. Date retrieved: July 29, 2003.

[181] Standard Practice for Engineering Drawings. Department of Defense. Defense Acquisition University Press, Fort Belvoir, Virginia, 1997. MIL-STD-100G.

[182] G. R. Marek. Beethoven; Biography of a Genius. Funk & Wagnalls, New York, 1969.

EPILOGUE
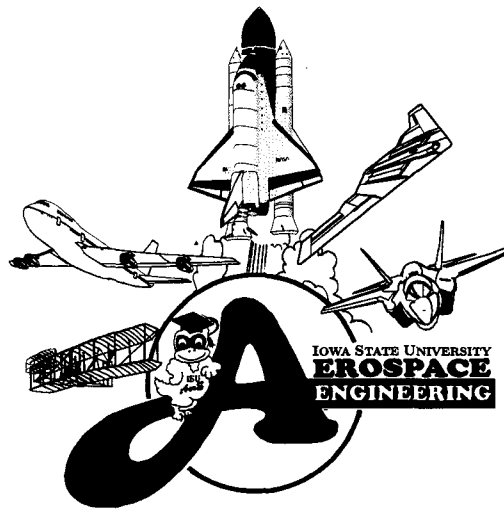
Celebrating the 100th Anniversary
of Power Flight
1903 - 2003

Plaudite, amici, comœdia finita est!
(Applaud, friends, the comedy/drama is over!)

— Ludwig van Beethoven ♫
(final words, March 23, 1827) [182]

Add up all the "dropwords" from "Nomenclature" to "Appendix E" will spell out...